University of Bath

PHD

Design, Synthesis and Evaluation of Fluorescent Sensors for the Detection of Saccharide and Reactive Oxygen Species

Sun, Xiaolong

Award date:
2015

Awarding institution:
University of Bath

Link to publication

Alternative formats
If you require this document in an alternative format, please contact:
openaccess@bath.ac.uk

Copyright of this thesis rests with the author. Access is subject to the above licence, if given. If no licence is specified above, original content in this thesis is licensed under the terms of the Creative Commons Attribution-NonCommercial 4.0 International (CC BY-NC-ND 4.0) Licence (https://creativecommons.org/licenses/by-nc-nd/4.0/). Any third-party copyright material present remains the property of its respective owner(s) and is licensed under its existing terms.

Take down policy
If you consider content within Bath's Research Portal to be in breach of UK law, please contact: openaccess@bath.ac.uk with the details. Your claim will be investigated and, where appropriate, the item will be removed from public view as soon as possible.

Download date: 05. May. 2023

Design, Synthesis and Evaluation of Fluorescent Sensors for the Detection of Saccharide and Reactive Oxygen Species

Xiaolong Sun

A thesis submitted for the degree of Doctor of Philosophy

University of Bath

Department of Chemistry

January 2015

COPYRIGHT

Attention is drawn to the fact that copyright of this thesis rests with its author. This copy of the thesis has been supplied on condition that anyone who consults it is understood to recognise that its copyright rests with its author and that no quotation from the thesis and no information derived from it may be published without the prior written consent of the author.

This thesis may not be consulted, photocopied or lent to other libraries without the permission of the author for three years from the date of acceptance of the thesis.

Signature Date

ABSTRACT

Reactive oxygen species (ROS) and reactive nitrogen species (RNS), saccharide (i.e. monosaccharide, disaccharide and polysaccharide), are continuously generated, transformed and consumed in the living systems. As a consequence of their significant value towards human health in aerobic life, it is very important and has drawn much attention in the chemical and biological sensing of the species. It is our long-standing interest in the recognition of monosaccharide (e.g. glucose) through exploration of various boronate-based fluorescence probes, thus, based on the previous work, we started on the design, synthesis and evaluation of novel fluorescent chemosensors for breakthrough discoveries in the detection of saccharide and ROS selectively and specifically, which are made up of different receptors and diverse singaling fluorophores, e.g. anthracene, coumarin, fluorescein, naphthalimine.

Firstly, "integrated" and "insulated" boronate-based fluorescent probes (2-naphthylboronic acid and *N*-Methyl-*o*-(aminomethyl)phenylboronic acid) have been evaluated for the detection of hydrogen peroxide in the presence of saccharides (i.e. D-fructose). In the presence of D-fructose the initial fluorescence intensity of the "insulated" system is much higher and produces a blue visible fluorescence.

Based on the experimental observation above in the boronate-based systems (i.e. B-N bond protection), a new water-soluble boronate-based fluorescent probe was designed and evaluated for the detection of peroxynitrite (much stronger oxidant) in the presence of D-fructose. The enhanced fluorescence of probe when bound with D-fructose was switched off in the presence of peroxynitrite. While, other reactive oxygen/nitrogen species led to only slight fluorescence decreases due to protection by the internal N-B interaction. The interaction of probe with D-fructose not only strengthens the fluorescence signal, but also protects the boronic acid to oxidation by other ROS/RNS. Therefore, under conditions generating various ROS/RNS, the boronate-based sugar complex preferentially reacts with peroxynitrite ($ONOO^-$). The sensor displays good "on-off" response towards peroxynitrite both in RAW 264.7 cells and HeLa cells. A new ICT (internal charge transfer) sensing system was developed for the detection of hydrogen peroxide and peroxynitrite. The probe displayed an enhanced fluorescence change when bound with D-fructose due to the prolonged N-B distance. The fluorescence intensity of the probe dropped down both in the detection of H_2O_2 and

$ONOO^-$ which was attributed to the oxidation of arylboronic acid even though in the presence of D-fructose.

Using the self-assembly of aromatic boronic acids with Alizarin Red S (ARS), we developed a new chemo/biosensor for the selective detection of peroxynitrite. Phenylboronic acid, benzoboroxole and 2-(N, N-dimethylaminomethyl) phenylboronic acid were employed to bind with ARS to form the complex probes. In particular the ARS-NBA system with a high binding affinity can preferably react with peroxynitrite over hydrogen peroxide and hypochlorite due to the protection of the boron via the solvent-insertion B-N interaction. Our simple system produces a visible naked-eye colorimetric change and on-off fluorescence response towards peroxynitrite. By coupling a chemical reaction that leads to an indicator displacement, we have developed a new sensing strategy, referred to herein as RIA (Reaction-based Indicator displacement Assay).

Next, we developed a novel class of simple materials for sensing monosaccharides by the functionalization of graphene oxide (GO) with boronate-based fluorescence probes. The composite materials were characterized by atomic force microscopy, Raman spectroscopy, and UV-vis/fluorescence spectroscopy. The strong fluorescence of the fluorescence probes is quenched in the presence of GO through fluorescence resonance energy transfer (FRET). The BA@GO composite sensors formed provide a useful platform for fluorogenic detection of monosaccharides based on the strong affinity between the boronic acid receptor and monosaccharides. The BA@GO composite sensor displayed a “turn-on” fluorescence response with a good linear relationship towards fructose over a range of other saccharides.

Next, new water-soluble copper (II) complex fluorescence probes were developed and evaluated for the detection of nitric oxide and nitroxyl in a physiological condition. A significant fluorescence “off-on” response displayed by using the copper (II) complex for the detection of NO and HNO ($Na_2N_2O_3$ as a donor). Under pathological conditions generating various ROS/RNS, the copper (II) complex fluorescent probe preferentially reacts with NO/HNO over other reactive oxygen species. The dual-analyte recognitions of the simple, sensitive probe were further applied in living cell for the exogenous NO/HNO.

In the following work, we synthesised a phosphorous-based compound for the detection of HNO which derived from Angeli's salt in a biological condition. Significantly, it displayed a high sensitivity and selectivity toward HNO over other various ROS species, especially NO since they have a similar chemical property. The underlying mechanism was attributed to the cleavage of C-O bond induced by Staudinger Ligation.

CONTENTS

ACKNOWLEDGEMENTS

There are a lot of people I should be grateful for overthrough my PhD study. First and foremost, I would like to thank Prof. Tony D. James for all the guidance and suggestions that I have ever been offered. In 2012, I joined chemosensor group leading by him and started my PhD. At the early stage of my research project, I got a lot of inspirational ideas from him which helped me out of the darkness. In the past years, we together undertook challenges and conqured them successfully, thus, we were rewarded in a return by publishing good papers, applying patents and getting posters prizes.

Next, I should give my thanks to my second supervisor - Dr. Steven D. Bull which assisted me in solving experimental problem and encouraging me in academia. Especially, through discussion with him, we got a real breakthrough in the discovery of N-B interaction in the selective detection of peroxynitrite. We are very excited since it is a new exploration for the application of boronate-based fluorescence probe. Dr. Stephen E. Flower should be thanked for the big help in the problems-solving, particulary in organic synthesis and daily maintance of the lab running.

I also appreciate the hand they lent to me in my daily life, all the PhD students, Suying Xu, *et al*. Anneke Lubben, John Lowe should also be thanked for providing the use of instruments such as NMR and mass spectrometry.

I had to express my thankfulness to Dr. John Fossey from University of Birmingham and Professor Xuhong Qian from East China University of Science and Technology for their contribution in the projects. In addition, Professor Juyoung Yong, Dr. Qingling Xu, Dr. Gyoungmi Kim from Department of Chemistry and Nano Science, Ewha Womans University, Korea gave us a great hand in the cell imaging experiments. Dr. Xiao-peng He from ECUST offered a big help in the development of Graphene Oxide and characterization. Professor Eric V. Anslyn from Department of Chemistry and Biochemistry, University of Texas at Austin gave invaluable comments on our work.

Xiaolong Sun is also grateful for financial support from China Scholarship Council (CSC) and University of Bath Full Fees Scholarship. The Catalysis And Sensing for our Environment (CASE) network is thanked for research exchange opportunities.

Beyond academia, I would like to give my biggest thanks to my parents, my elder sister, brother-in-law and my girlfriend who support and encourage me by my side forever.

ABBREVIATIONS

A	absorption
AFM	Atomic Force Microscopy
Ar	aryl
ARS	Alizarin Red S
AS	Angeli's salt
BBA	Benzoboroxole or 2-(hydroxymethyl)phenylboronic acid cyclic
BOD	Biochemical Oxygen Demand
BINOL	1, 1'-bi-2-naphthol
bp	boiling point
br	broad
COD	Chemical Oxygen Demand
°C	Degree Celsius
$CDCl_3$	deuterated chloroform
CDI	1,1'-Carbonyldiimidazole
cm^3	cubic centimetre
cm^{-1}	wavenumbers
CTAB	cetyl trimethylammonium bromide
δ	chemical shift in parts per million
Δ	heat
D	deuterium (^2H)
d	doublet
Da	Dalton
D-A	donor-acceptor
D-B-A	donor-bridge-acceptor
dd	doublet of doublets
DFT	density functional theory

D-fru.	D-fructose
d-PET	donor-photo-induced electron transfer
DPBS	Dulbecco's phosphate-buffered saline
dm^3	cubic decimetre
DMSO	dimethyl sulfoxide
e^-	Negative electron
Ɛ	molar absorptivity
EI	electron impact
eNOS	endothelial Nitric oxide Synthases
EPR	electron paramagnetic resonance
ESR	electron spin resonance
ES+	positive phase electrospray ionisation
ES-	negative phase electrospray ionisation
Et	ethyl
EtOAc	ethyl acetate
EtOH	ethanol
ET	electron transfer
equiv.	equivalent
FL	fluorescence intensity
g	gram
GO	Graphene oxide
GOx	Glucose Oxidise
h	hour(s)
HL-60	Human promyelocytic leukemia cells
HPLC	High Performance Liquid Chromatography
HRMS	High Resolution Mass Spectrometry
I_f	fluorescence intensity

I_f/I_0	relative fluorescence intensity
ICT	Internal Charge Transfer
IFN-γ	Interferon Gamma
INH	inhibit
J	coupling constant
k	rate constant
K	stability constant
K_a	acidity constant
K_a'	acidity constant of complexed boronic acid
λ	Wavelength
λ_{em}	emission wavelength
λ_{ex}	excitation wavelength
L	Litre
LDL	low-density lipoprotein
lit	literature
LPS	lipopolysaccharide
µM	micromolar
µm	micrometre
µmol	micromole
µL	microlitre
m	*meta*
m	unresolved multiplet
min	minutes
M	molar (moles per cubic decimetre) / mega
M^{-1}	cubic decimetres per mole
$[M]^+$	parent molecular ion
Me	methyl

MeOD	deuterated methanol
ML	4-Methylesculetin
mg	milligram
MHz	megahertz
mm	millimetre
mM	millimolar
mmol	millimole
mol	mole
Mp	Melting point
m/z	mass-to-charge ratio
ν	Infrared
NBA	2-(*N*, *N*-dimethylaminomethyl) phenylboronic acid
nm	nanometre
nmol	nanomole
NMR	Nuclear Magnetic Resonance
NOS	nitric oxide synthases
ns	nanosecond
o	*ortho*
p	*para*
PBA	phenylboronic acid
PEG	Polyethylene glycol
PET	Photoinduced Electron Transfer
pK_a	- log K_a
PMA	para-methoxyamphetamine
ppm	parts per million
q	Quartet
R^2	linearly dependent coefficient

R_f	retardation factor
ROS	reactive oxygen species
RNS	reactive nitrogen species
rt	room temperature
s	singlet / second
S_0	singlet electronic ground state
S_1	first singlet electronic excited state
S_2	second singlet electronic excited state
siRNA	small interfering RNA
sm	starting material
SWNTs	single wall nanotubes
t	triplet
T_1	first triplet electronic excited state
T1DM	Diabetes mellitus type 1
T2DM	Diabetes mellitus type 2
TEMPO	(2,2,6,6-Tetramethylpiperidin-1-yl)oxy
TET	Tetracycline-Inducible Expression
TFA	trifluoroacetic acid
THF	tetrahydrofuran
TICT	Twisted Internal Charge Transfer
TLC	Thin Layer Chromatography
TMS	tetramethylsilane
UV-vis	ultra-violet
wt%	weight percent

Chapter one

Introduction

1. INTRODUCTION

1.1 OVERVIEW OF INTRODUCTION

The natural world is made up of fundamental elements, ions and molecules which continuously interact with each other through a series of chemical reactions. Thus, it is important to have a molecular level understanding of these processes. Based on this knowledge, scientists wish to carry out research in the areas of chemical, material, physical, biological and medical sciences. These great challenges have attracted many scientists for the creation of effective tools for further exploration.

Molecular recognition and sensor design have a strong and symbiotic relationship which involves the selective interaction between two analytes, often in terms of a host and a guest. Selectivity and sensitivity between the host and guest is often achieved *via* carefully matched electronic, geometric and polar elements. Therefore, we try to design and engineer synthetic receptors with selectivity for any chosen analyte, through the thoughtful choice of functional groups with appropriate three dimensional placement. The Natural world has clearly illustrated the success of this concept. Since, biological systems have clearly evolved to contain exquisitely assembled active binding sites, capable of selectively sequestering the desired target molecule.

Molecular recognition and molecular assembly have been widely explored and employed in the sensing and detection of certain species, such as heavy metals, ions, sugar, amino acid, peptides, explosives or reactive oxygen/nitrogen species, *etc*., in biological systems, supramolecular systems and static/dynamic systems. Traditionally, the term molecular recognition refers to the specific interaction between two or more molecules through non-covalent bonding such as hydrogen bonding, metal coordination, hydrophobic forces, van der Waals forces, π-π interactions, halogen bonding, electrostatic and/or electromagnetic effects.[1] While, the invention of reaction-based chemo-sensors has become an increasingly important branch of research for the substrate sensing and detection using host-guest chemical reactions which is somewhat different from the traditional design principles.

When molecular recognition becomes molecular sensing, it is often results in a chemosensor. Specifically, a molecular sensor or chemosensor is a molecule that

interacts with an analyte to produce a detectable change/signal. To design a chemosensor for the observation of a certain analyte is critical since the host-guest interaction is universe vital natural interaction. Molecular sensors combine molecular recognition with some form of reporter so the presence of the guest can be observed. When it comes to the composition of reporter, the detectable signals can be made up of electrical, optical, structural, and biological change.

Chemical sensing with fluorescence as a signal to report molecular recognition event was first reported during the early 1980s with the synthesis of the first calcium fluorescent indicators by Tsien *et al*.[2-4] Notably, fluorescence sensing has been recognised as a method of choice for the detection of analytes with a very high sensitivity and often has a good selectivity provided the fluorescent molecular sensors are properly designed. Fluorescent probes have been successfully adapted in various notable fields. For example, fluorescent sensors for biomolecules such as glutamate, acetalcholine, glycine, aspartate and dopamine would be very helpful to study the cell chemistry and to further understand the mechanisms involved the the working of cells. In the field of environmental analysis, the early detection of toxic metals, such as mercury, lead and cadmium is desirable for the protection of living organisms. Additionally, accurate, reliable, real-time biological and chemical sensing of explosives and hazardous chemicals is required to detect landmines[5] and chemical warfare agent.[6, 7] Therefore, these many features make fluorescence one of the most powerful transduction mechanisms to report the chemical recognition event.

As a key part of molecular recognition, synthetic fluorescent probes have led researchers to explore the chemical and biological world more precisely based on unique properties of those molecules. In this thesis, we have focused on the introduction of small-molecular fluorescent sensors including the basic structures, design principles, sensing mechanisms and further applications especially for *in vivo* and *in vitro* sensing of reactive oxygen and reactive nitrogen species.

1.2 DESIGN PRINCIPLE

In order to make the fluorescent probes specific for the molecular target and applicable in the complex environment, reasonable imagination and scientific design should follow certain principles. Significantly, the first step in order to choose an approriate reporter or fluorophore is crucial for the whole system. Fluorophores are divided into different classes according to their sensing properties and emission wavelength. A lot of fluorophores can be used as the framework for the chemosensor design strategy, such as anthracene **1**, coumarin **2**, naphthalimine **3**, BODIPY **4**, fluorescein **5**, rhodamine **6** and cyanin **7** (Figure 1). All these fluorophores have been widely employed and applied as reporters in each systematic structure due to the various selection of emission wavelength.

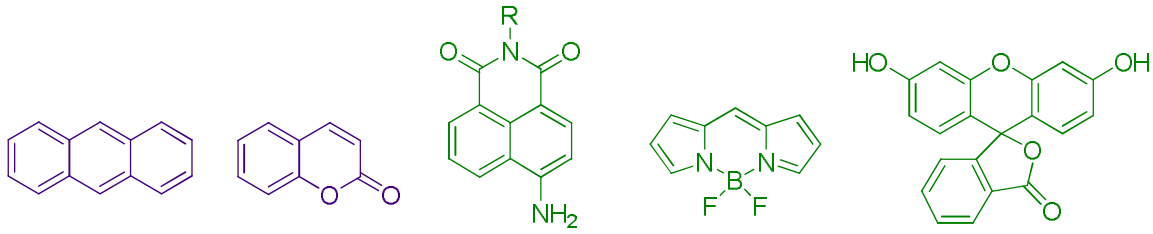

1. Anthracene **2**. Coumarin **3**. Naphthalimine **4**. BODIPY **5**. Fluorescein

6. Rhodamine **7**. Cyanine

Figure 1. *Structures of various luminophores*

In terms of small-molecule fluorescent probes, they are fundamentally composed of a receptor responsible for the molecular recognition of the analyte, a signal reporter (fluorophore in this report) responsible of signalling the recognition event and sometimes a spacer for signal transformation with the target as signal input (Scheme 1). The independent fluorophore is linked covalently or non-covalently with the receptor through spacer and the units are assembled together to form the entire sensing system. In the case when there is interaction between receptor and target molecule, a signal will

be transferred to the reporter, inducing responses such as “off-on”, “on-off”, “colorimetric change” or “assembly”. By using a fluorometer or UV-Vis spectrometer, the spectroscopic signals can be detected or observed automatically or manually which can be used as the reflection of the local environment. Knowing what is happening in the local environment through observing the presence of certain guests is critical for analysing the results, judging the consequence and taking prompt action. For example, in the early stage detection of some cancer diseases, if the typical over-expression or producing of substances which indicate the occurrence of the cancer can be captured quickly and precisely, then early treatment would be possible and provide a powerful tool to prevent the spread and also control the progression of cancer.

Classical design of fluorescent indicators can be divided into three main strategies for chemical sensing in solution. They are “intrinsic fluorescent probes” with a ligand as part of the π-system of the fluorophore; “extrinsic fluorescent probes” with electrical independence of the receptor moiety and the reporter which are covalently linked by a spacer; “chemosensor ensemble” based on the dissociation of receptor-reporter ensemble selectively by the competitive analyte.[8]

In terms of the mechanism for fluorescent probe design, basically, there are PET (photo-induced electron transfer), ICT (internal charge transfer), FRET (Förster resonance energy transfer), and TICT (twisted internal charge transfer). Many reviews have provided a detailed explanation of these kinds of systems; therefore, it is not essential to cover them again in this introduction.

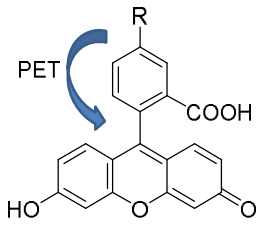

7. R = NO_2
8. R = NH_2

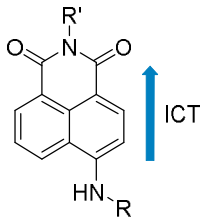

9

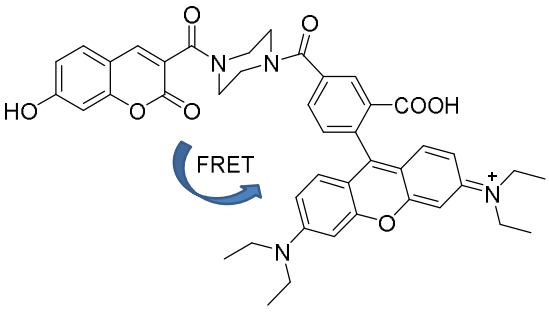

10

Chemical sensors can be grouped as either biosensors, or synthetic sensors. Biosensors make use of existing biological recognition elements. In many cases selective biological receptors already exist for many important analytes, therefore, modification of the

receptor to include a signal transducer produces a biosensor.[9] In addition, effective reaction-based fluorescent probes should be biocompatible and bioorthogonal, which can proceed safely with reasonable kinetics in water under physiological pH, high salt content and large excess of reactive nucleophilic thiols. Additionally, particular attention should be paid to the non-interference to the endogenous cellular and tissue processes, and be non-toxic to living systems.

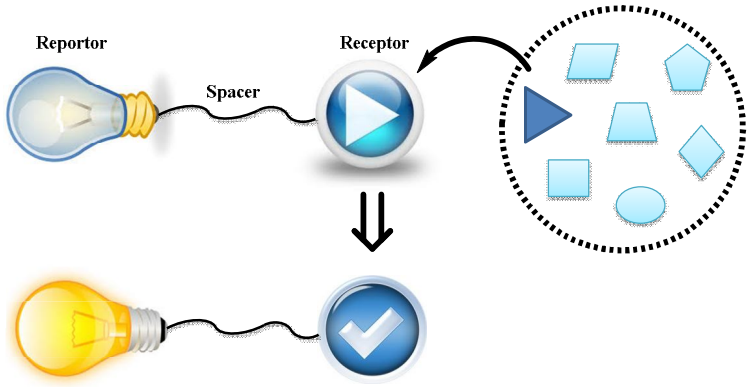

Scheme 1. *The complementary interaction between a guest analyte and a host binding pocket, illustrated here by a triangle guest and switch host, allows selective binding to occur between two elements. Incorporation of a unit capable of generating a physical signal in response to this binding event, converts the receptor into a sensor. In this cartoon an optical "off-on" response is depicted from an appended fluorophore, illustrated in yellow, typical of the systems covered within this introduction.*

Above all, the requirements of success in this sensor design are not only a working knowledge of fundamental organic and organometallic reactivity but also an understanding of the intrinsic reactivity of the target analyte in the biological setting.[10]

1.3 INTRODUCTION OF BORONIC ACIDS

1.3.1 BRIEF INTRODUCTION

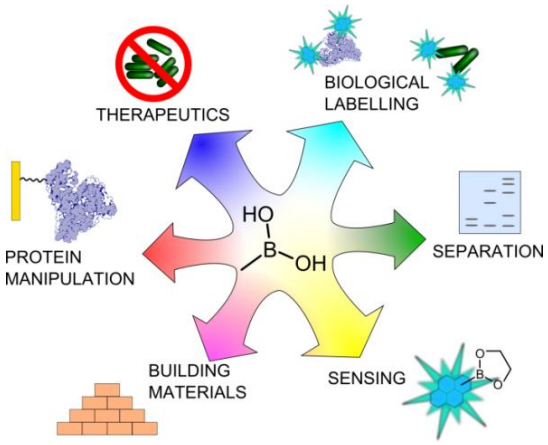

Scheme 2. *Diverse usage and applications of boronic acids.*

Boronic acids both alky and aryl have been available for around 150 years. The most common method used to prepare boronic acids is the reaction of trialkyl borates with Grignard reagents. The interaction of boronic acids with saccharides[11-38] or anions[37, 39-42] has been intensively investigated, and boronic acids have been exploited in a range of applications as diverse as NMR shift reagents,[43-46] functional polymers[47-50] and molecular self-assembled materials.[51-56] Sensors for reactive oxygen and reactive nitrogen species (ROS and RNS) have also been developed based on oxidative removal of the boronic acid group (Scheme 2).[10, 57-65]

1.3.2 BORON–DIOL INTERACTIONS

Both boric and boronic acids have been used to determine the configuration of saccharides for around 50 years. These early investigations determined that cyclic boric and boronic esters are formed when boronic acids are mixed with polyhydroxylated compounds such as sugars. The origins of boronic acid based receptor design can be traced back to the seminal work of Lorand and Edwards.[66] They used the pH drop observed on addition of saccharides to determine the association constants (Scheme 3). The acidity of the boronic acid is enhanced when 1,2-, 1,3- or 1,4-diols react with boronic acids to form cyclic boronic esters (5, 6 or 7 membered rings) in aqueous media.[37, 50] When phenylboronic acid and water react to generate a tetrahedral boronate a hydrated proton is liberated, thereby defining the

acidity constant K_a. Typically, the pK_as of phenylboronic acid range between ~ 8.7 and 8.9, and 8.70 in water at 25 ºC.[67]

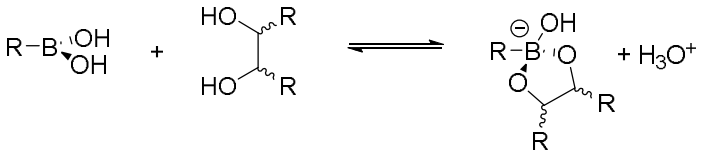

Scheme 3. *The rapid and reversible formation of a cyclic boronate ester.*

The recognition of saccharides through boronic acid complex (or boronic ester) formation often relies on an interaction between a Lewis acidic boronic acid and a proximal tertiary amine (Lewis base). The true nature of the nitrogen-boron (N-B) interaction has been much debated (especially in an aqueous environment), but it is clear that an interaction of some kind exists which offers two advantages.[68] Firstly, this interaction enhances binding at neutral pH, (by facilitating tetrahedral boronate formation) allowing the development of receptors with practical applicability. Secondly, saccharide binding enhances the N-B interaction (due to an increase in Lewis acidity of the boron on saccharide binding) and modulates the fluorescence of nearby fluorophores, (fluorescent photo-induced electron transfer (PET) from the nitrogen is controlled by the strength of the N-B interaction) which is extremely useful in the design and application of chemosensors.[37]

The Lewis acidic nature of boron has also led to the development of anion receptors and sensors (Scheme 4).[37, 39-42]

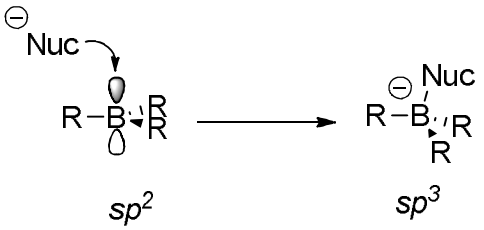

Scheme 4. *Diagram illustrating the change in geometry at the boron centre on interaction with a nucleophile.*

The interaction of boronic acids with Lewis basic species in buffered solutions results in binary (boronate - Lewis base) complexes as well as ternary (boronate - Lewis base - saccharide) complexes.[67] These species persist into acidic solution and under certain stoichiometric conditions can become the dominant component in the

solution. Therefore, when conducting fluorescence experiments in solutions buffered with a Lewis basic component a “medium dependence” related to the formation of these Lewis base adducts will be observed. These complexes reduce the free boronate and boronic acid concentrations, diminishing the observed stability constants (K_{obs}).

From an experimental perspective, the buffer should be chosen so as not to overwhelm the system being investigated. Serendipitously, phosphate buffer (pH 7.5) does not significantly contribute to the observed fluorescence intensity or alter significantly the binding constants of the excited state complex under investigation.

Therefore, so long as one is aware of the conditions observed stability constants (K_{obs}) have been determined under and the effect that is induced by Lewis basic components in solution, these spectrophotometrically determined constants do provide an accessible, useful and valid measure in the development of boronic acid based sensory systems.

The fast and stable bond formation between boronic acids and diols to form boronate esters can also be utilised to build reversible molecular assemblies. In spite of the stability of the boronate esters’ covalent B-O bonds, their formation is reversible under certain conditions or under the action of certain external stimuli.[54-56]

The reversibility of boronate ester formation and Lewis acid-base interactions has also resulted in the development and use of boronic acids within multicomponent systems. The dynamic covalent functionality of boronic acids with structure-directing potential has led researchers to develop a variety of self-organizing systems.[51-56]

1.3.3 AMINE – BORON INTERACTIONS

The N-B interactions in analogous boronic acids and esters have been extensively cited in molecular recognition and chemosensing literature.[69] It is known that the amine-boron interaction has been widely explored in the study of fluorescence/colorimetric sensing with a particular emphasis on the detection of saccharides and anions.[70-73] The strength of the B-N bond depends on the group linked with the boron atom; electron-withdrawing moieties increase the Lewis acidity of boron while electron-donating moieties increase the Lewis basicity. There is a general agreement that the binding of boronic acid with 1,2 or 1,3-diols - a vicinal bifunctionalized, electron-withdrawing substrate - led to the change of hybridization of boron from trigonal planar geometry sp^2 to tetrahedral sp^3. Thus, the formation of boronate ester increased the Lewis acidity of the boron and created a stronger N-B interaction (or solvent insertion).

In the study of N-B interaction, Wulff, Anslyn, Wang and within James group had made a lot of investigations about the binding motif in the case of *N*-methyl-*o*-(phenylboronic acid)-*N*-benzylamine system.[67, 74-76]

Wulff developed a new polymer containing the 2-(dimethylaminoethyl)benzene boronic acid moiety, by utilizing the N-B interaction to reduce the pK_a of boronic acid. Thus, the modified polymer can be performed in the chromatography of diols in a neutral aqueous solution (Scheme 5).

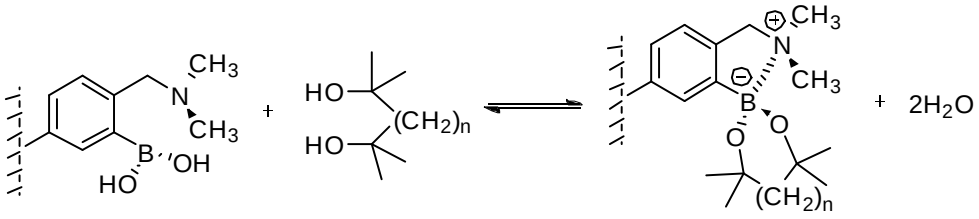

Scheme 5. *Wulff-type boronic acids and reversible interaction with diols.*

Based on the work reported by Wulff, Shinkai and James made a landmark exploration in the study of saccharide sensing by utilizing the fluorescence of boronic acid receptor. Most of the fluorescence probes **11**, **12**, **13** were developed on the basis of reversible interaction between boronic acid and diol, which hampered the PET effect from tertiary

amine (Scheme 6). Thus, the B-N interaction plays an important role in the design of chemosensor for the fluorescence detection of saccharides.

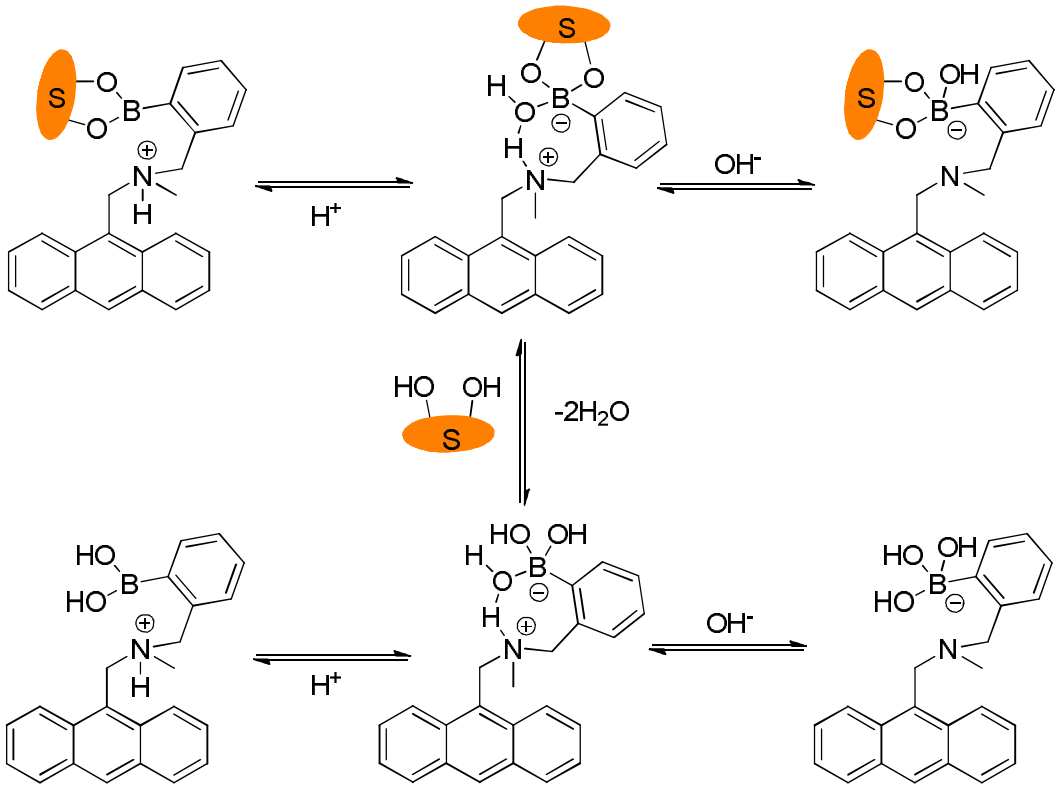

Scheme 6. *The effect of saccharide complexation and pH changes on the fluorescence of monoboronic acid*

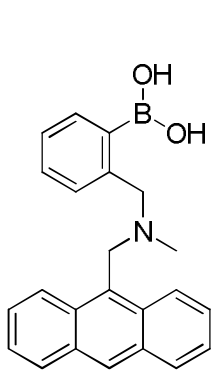

11

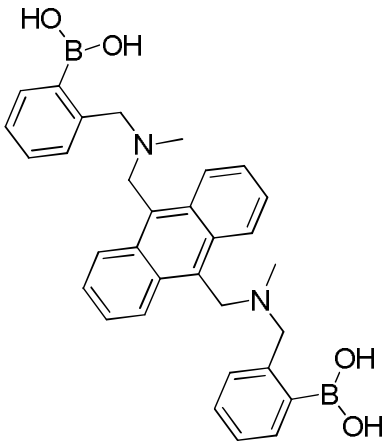

12

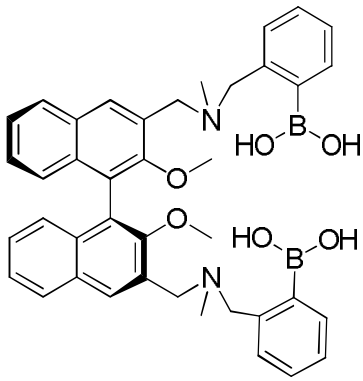

13

Since the revealed importance of N-B interaction in the modulation of PET sensors, it is significant to know the quenching efficiency, which is dependent on the strength of this interaction. The strength of the N-B interaction has been calculated from the stepwise

formation constants of potentiometric titration (i.e. **14**, **15**, **16**). It was estimated that the upper and lower limits of energy between N-B interaction should be bound between ~15 and 25 KJ mol^{-1} in the case of *N*-methyl-*o*-(phenylboronic acid)-*N*-benzylamine.[67]

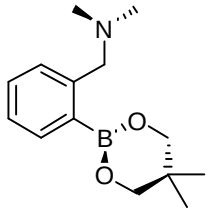

14

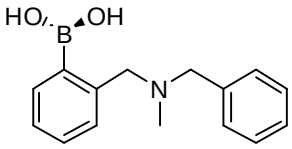

15

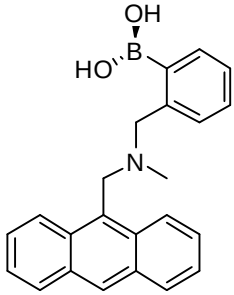

16

Wang has investigated the mechanism of electron-transfer quenching by boron-nitrogen adducts in fluorescent sensors. In the case of *N*-methyl-*o*-(aminomethyl)phenylboronic acid, through density functional theory (DFT) and theoretical model, they found a new mechanism other than B-N bond strength change can be used to explain the fluorescent switching in biosensors that involve interaction of boron and nitrogen affected by boronate ester formation. However, to date the predicted hydrolysis mechanism has not been proven by experimental evidence.

Through structure analysis of ^{11}B-NMR measurement and X-ray data in *o*-(*N*,*N*-dialkyl aminomethyl) arylboronate systems, Anslyn *et al.* concluded the effect of solvent insertion on N-B interaction in the cases of aprotic and protic media (Scheme 7). Results demonstrated that the N-B dative bond is usually present in an aprotic solvent while in a protic media, a hydrogen-bonded zwitterionic species with solvent insertion observed rather than a formal of N-B bound. Also, the N-B coordinated and solvated species are in equilibrium.[69]

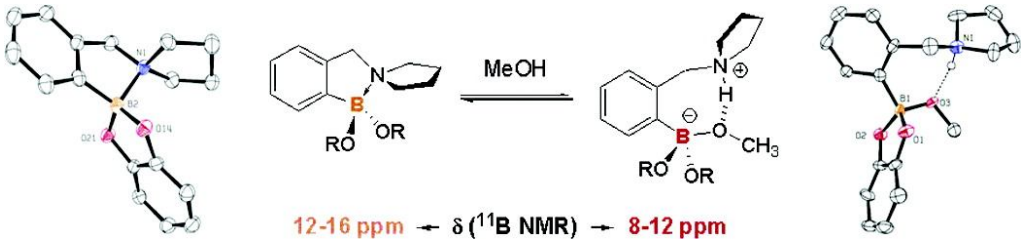

Scheme 7. *Solvent insertion on N-B interaction in the cases of aprotic and protic media. Reproduced with permission from (J. Am. Chem. Soc., 2006, **128**, 1222). Copyright © 2006 American Chemical Society.*

1.3.4 INDICATOR DISPLACEMENT ARRAYS

There is another approach towards boronic acid based sensors, where the receptor and a reporter unit are separate in a competitive assay. A competitive assay requires that the receptor and reporter (typically a commercial dye) to associate under the measurement conditions. The receptor-reporter complex is then selectively dissociated by the addition of the appropriate guests. When the reporter dissociates from the receptor, a measurable response is produced (Scheme 8).

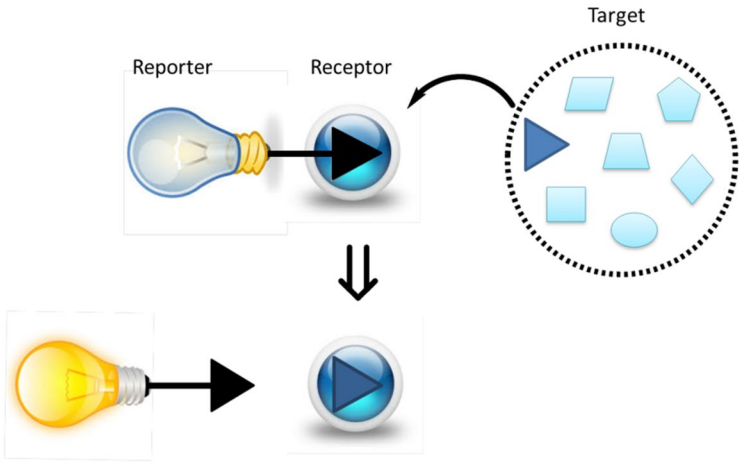

Scheme 8. *Cartoon depicting the function of an assay system*

An indicator displacement assay is primarily a colorimetric competitive binding sensor system where an analyte displaces a dye from a receptor, this displacement results in some absorbance shift (colour change) which can be related to the amount of analyte present. Pioneering reports in this arena include the influential protocols of Anslyn,[77-83] Severin[84] and Singaram[85-92] all of which may be broadly described as "Supramolecular Sensing".[93]

Wang has shown that Alizarin Red S (ARS) and phenyl boronic acid (PBA) could be used in competitive assays for saccharides.[94-96] The system is D-fructose selective, which is the expected selectivity for a monoboronic acid system.[66] This system takes advantage of the known interaction of alizarin red S with boronic acids.[97] The observed stability constants (K_{obs}) for the PBA-alizarin red S assay were 160 M^{-1} for D-fructose and 4.6 M^{-1} for D-glucose in water at pH 7.4 (phosphate buffer). Developing this elegant system, Hu employed 3-pyridinylboronic acid and pyrocatechol violet in a competitive assay for D-glucose.[98] The observed stability constants (K_{obs}) for assay were 272 M^{-1} for

D-glucose in water at pH 7.4 (phosphate buffer). Therefore this very simple system can be used to detect millimolar D-glucose. The fluorescence response of these displacement systems can be improved by using surfactants (e.g. cetyltrimethylammonium bromide CTAB). Since the fluorescence intensity can be enhanced in the hydrophobic core of micelles.[99]

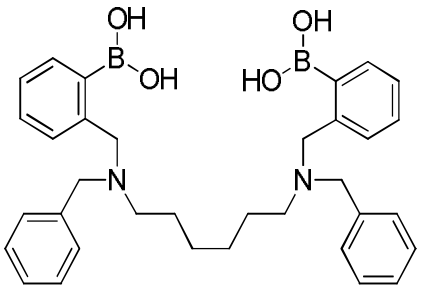

17

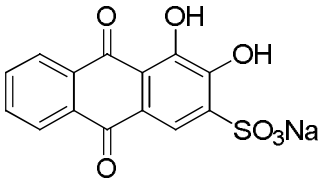

Alizarin Red S

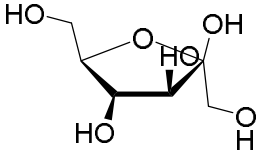

D-fructose

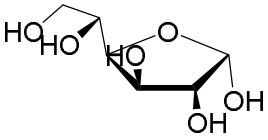

D-glucose

Alizarin Red S has been used in the design of a D-glucose selective fluorescent assay.[100] Sensor **17** and ARS shows a six-fold enhancement over PBA for D-glucose. Sensor **17** can also be used at a concentration ten times lower than PBA. The observed stability constants (K_{obs}) for **17** were 140 M^{-1} for D-fructose and 66 M^{-1} for D-glucose in 52.1 wt% methanol/water at pH 8.21 (phosphate buffer). Alizarin Red S has also been used by Basu with a number of commercial monoboronic acids, and found that 3-methoxycarbonyl-5-nitrophenyl boronic acid, was much more efficient than PBA in competitive assays.[101]

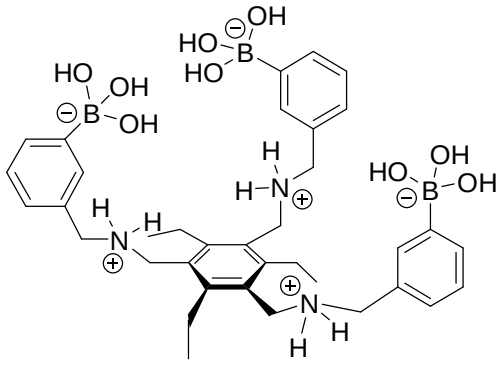

18

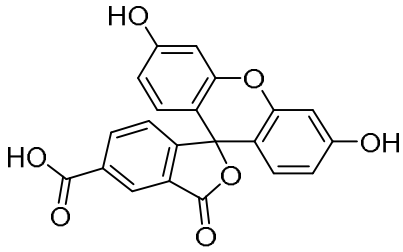

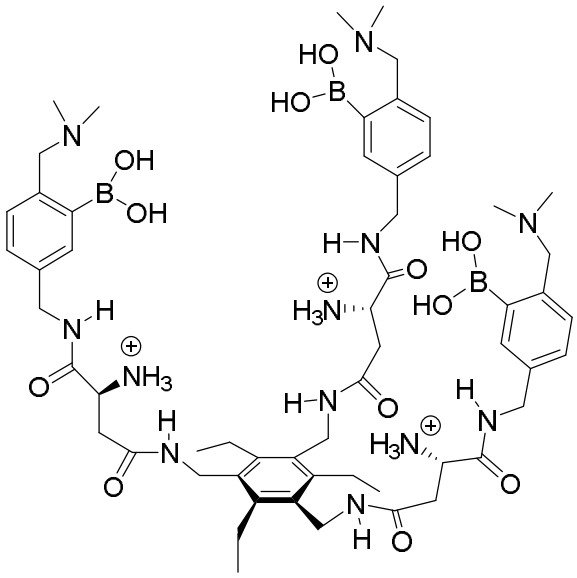

19

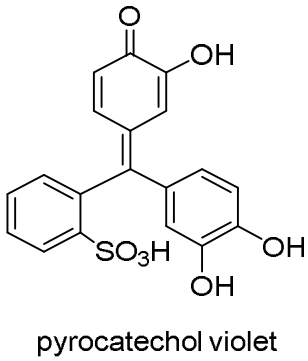

Anslyn reported two very elegant systems based on boronic acid receptors. The C_3 symmetric tri-podal boronic acid is a selective receptor for D-glucose-6-phosphate.[102] The binding of D-glucose-6-phosphate is measured through the competitive displacement of 5-carboxyfluorescein. Addition of the D-glucose-6-phosphate caused a decrease in the absorption of light at 494 nm allowing the concentration of the guest to be monitored directly within the visible spectrum. Anslyn has also prepared more elaborate C_3 symmetric tri-podal boronic acid receptors. The binding of heparin and **19**, is monitored through displacement of pyrocatechol violet.[103]

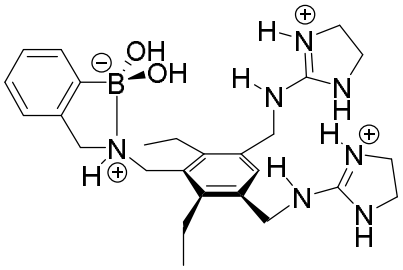

20

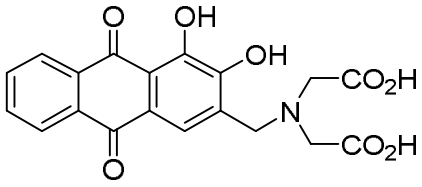

Alizarin complexone

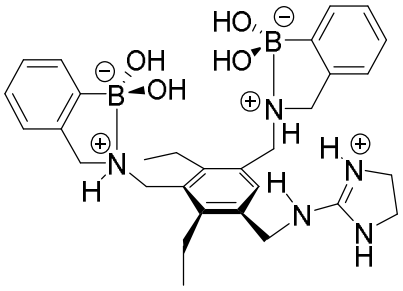

21

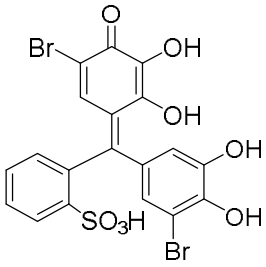

bromopyrogallol red

With sensor **20** the binding of the tartrate or malate anions can be detected through the competitive displacement of alizarin complexone. The same sensor system was used for the analysis of malate in pinot noir grapes.[104] When **21** was paired with pyrocatechol violet an assay suitable for the detection of gallic acid in Scotch whiskies was developed. An increase in the concentration of gallic acid correlated with the age of the whiskies.[105] A combination of **20** and **21** and two indicators pyrocatechol violet and bromopyrogallol red can be used to detect the concentrations of tartrate and malate in mixtures.[106] Using **21** and pyrocatechol violet the reaction kinetics for the formation of tartaric acid by the dihydroxylation of malic acid could be followed.[107] Anslyn has also elegantly paired chiral boronic acids with a variety of indicators to develop enantioselective assays for α-hydroxyl carboxylates and diols.[108, 109]

1.3.5 BORON-H_2O_2/$ONOO^-$ INTERACTIONS

In addition to serving as fluorescent sensors for carbohydrate and anions, boronic acids or esters also can be used as chemical probes and antioxidants for the detection and detoxification of ROS/RNS (i.e. H_2O_2, $ONOO^-$, ClO^-) generated in biological and cellular systems, which is due to the electron-deficiency of the boron atom with the open shell which confers its acidic character. Resulting in boronates as mild organic

Lewis acids that can coordinate basic molecules and nucleophilic species. Thus, nucleophilic addition of reactive species to electron-deficient boronate probes is a facile reaction. This unique chemical property of boronates has propelled their use as effective traps of ROS and RNS in biological systems.[110]

The reaction-based approach has been employed in the study and detection of ROS/RNS selectively based on the inherent chemical reactivity of a specific species. Chang and co-workers have developed a series of boronate-based derivatives for the fluorescent detection of H_2O_2 in living systems.[60, 64, 111-115] They have focused on the use of H_2O_2-mediated boronate oxidation as a bioorthogonal reaction-based approach to detection since hydrogen peroxide reacts with arylboronic acids under neutral or mild alkaline conditions to generate phenols,[116] aryl boronates were identified as species with complementary ambiphilic reactivity towards H_2O_2 by taking advantage of these characteristic molecular features.

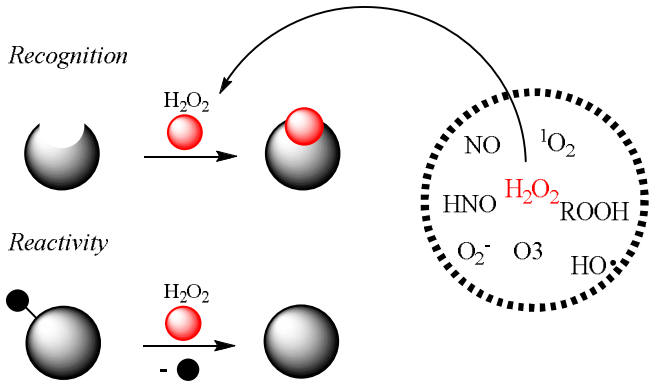

Scheme 9. *Design of a bioorthogonal reactivity approach for selective H_2O_2 detection via boronate oxidation.*

However, using stopped-flow kinetic techniques in the case of **22**, **23**, **24**, **25**, Kalyanaraman *et al*. measured the second–order rate constants for the reaction with peroxynitrite ($ONOO^-$), hypochlorous acid (HOCl), and hydrogen peroxide (H_2O_2) and found that $ONOO^-$ reacts with 4-acetylphenylboronic acid nearly a million times (k = 1.6×10^6 $M^{-1}s^{-1}$) faster than H_2O_2 (k = 2.2 $M^{-1}s^{-1}$) and over 200 times faster than HOCl (k = 6.2×10^3 $M^{-1}s^{-1}$).[117] Thus, the boronate probes can be employed as diagnostic tools for real time monitoring of peroxynitrite and hydroperoxides.

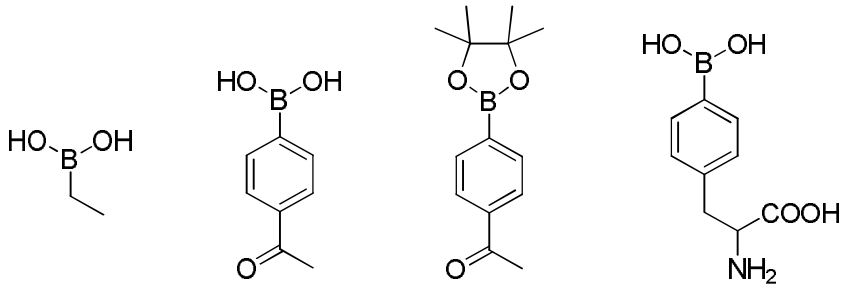

22 **23** **24** **25**

Since the oxidation-reduction reaction of boronates can occur with peroxynitrite and hydrogen peroxide, it has become a challenge to distinguish them using fluorescence tools.

1.3.6 STABILITY CONSTANTS

A stability constant (formation constant, binding constant) is an equilibrium constant for the formation of a complex in solution. It reflects the strength of the binding between the receptor and substrate. The significance of the index can be frequently used in the two main kinds of complexes, including interaction of a metal ion with a ligand (**26**) and supramolecular complex (**27**). To affect the stability constant, there are intrinsic and extrinsic factors, which are ionic strength dependence and temperature dependence, respectively. It should be noted that the chelate effect, macrocyclic effect, geometrical factors and effect of ionic radius would play an important role for the modulation of the stability in the formation of the complexes.

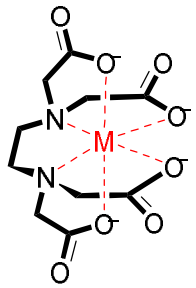

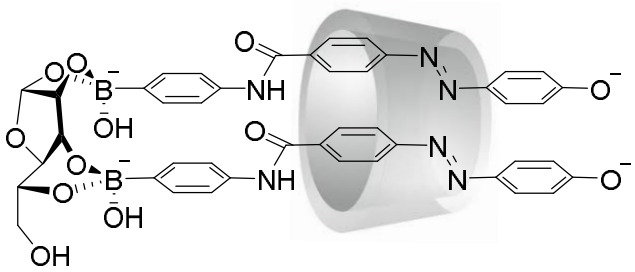

26. Metal-EDTA interaction **27.** Boron-diol interaction.

Basically, the interaction of the reagents (two componets) is reversible, so there are two different constants, K_a and K_d, which are for association constant and dissociation constant, respectively.

$$A + B \rightleftarrows AB$$

$$K_a = \frac{[AB]}{[A][B]}$$

$$K_d = \frac{[A][B]}{[AB]}$$

The following is one of the examples in the calculation of binding constant through the fitting equation (Figure 1S).

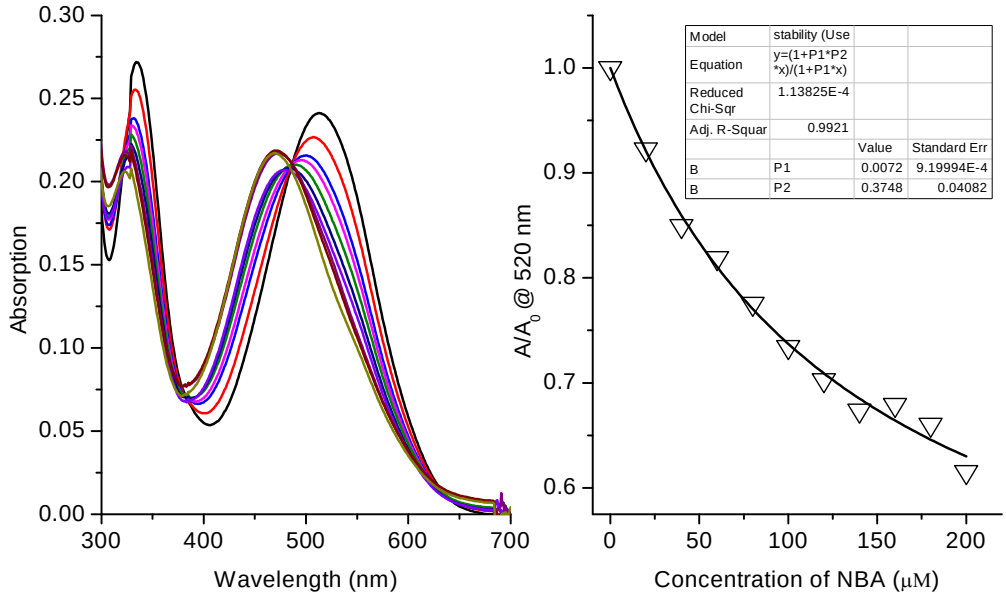

Figure 1S. *(a) UV-Vis absorption titration spectra of ARS (50 μM) and addition of various concentrations of NBA (0 – 200 μM). (b) Curve fitting and binding constant calculation between ARS and NBA. The data were taken in 52.1% MeOH/H_2O PBS buffer（pH 8.10）at 25 °C.*

$$A/A_0 = (1 + A_{lim}K[Guest])/(1 + K\,[Guest])$$

A is the absorbance for a particular concentration of guest; A_0 is the initial absorbance; A_{lim} is the limiting (final) absorbance; K is the stability constant of the receptor with the guest; [guest] is the concentration of of the guest.

By fitting the relationship curve between absorption intensity at A/A_0 = 520 nm and concentration of NBA (0 – 200 μM) using equation above, we resulted the binding constant and limitation of absorption in the case:

$$k = 7200 \pm 92\ M^{-1}$$

$$A_{lim} = 0.37 \pm 0.04$$

In chemistry, biochemistry, and pharmacology, stability constant values are exploited in a wide variety of applications. Significantly, chelation therapy is medical process by using a strong ligand to selective bind and then remove the heavy metals from the body. Similarly, we and other researchers have designed and synthesized kinds of chemosensors for the detection and separation of toxic trace-metals in the govenance of Chinese medicine, effluent. Among them, stability constant can be managed properly for the selective and sensitive binding of the target. In terms of supramolecular complexes, a typical application in molecular recognition involved the determination of formation constants for complexes formed between a tripodal substituted urea molecule and various saccharides.

1.4 INTRODUCTION OF ROS/RNS SPECIES

1.4.1 DEFINITION AND CLASSIFICATION

Free radicals and related species have captured great attention in recent years. They are mainly derived from oxygen and nitrogen and generated in our body by different endogenous systems. Free radicals and oxidants play a dual role as both toxic and beneficial compounds, since they can be either harmful or helpful to the body (Scheme 10). Notably, reactive oxygen species (ROS) and reactive nitrogen species (RNS) are chemically reactive radicals containing oxygen or nitrogen. They include superoxide ($O_2^{\bullet-}$), hydroxyl ($HO^{\bullet}$), peroxyl radical ($ROO^{\bullet}$), hydrogen peroxide (H_2O_2), singlet oxygen ($^1O_2$), ozone (O_3), hypochlorous acid (HOCl) - normally defined as ROS and nitric oxide (NO), nitroxyl (HNO), peroxynitrite ($ONOO^-$) - normally defined as RNS. ROS/RNS are formed as natural by-products of the normal metabolism of oxygen or nitrogen and play an important role in cell signalling. Specifically, during times of environmental stress (e.g. heat exposure or UV); ROS/RNS levels can increase dramatically. They are also generated by exogenous sources such as ionizing radiation.

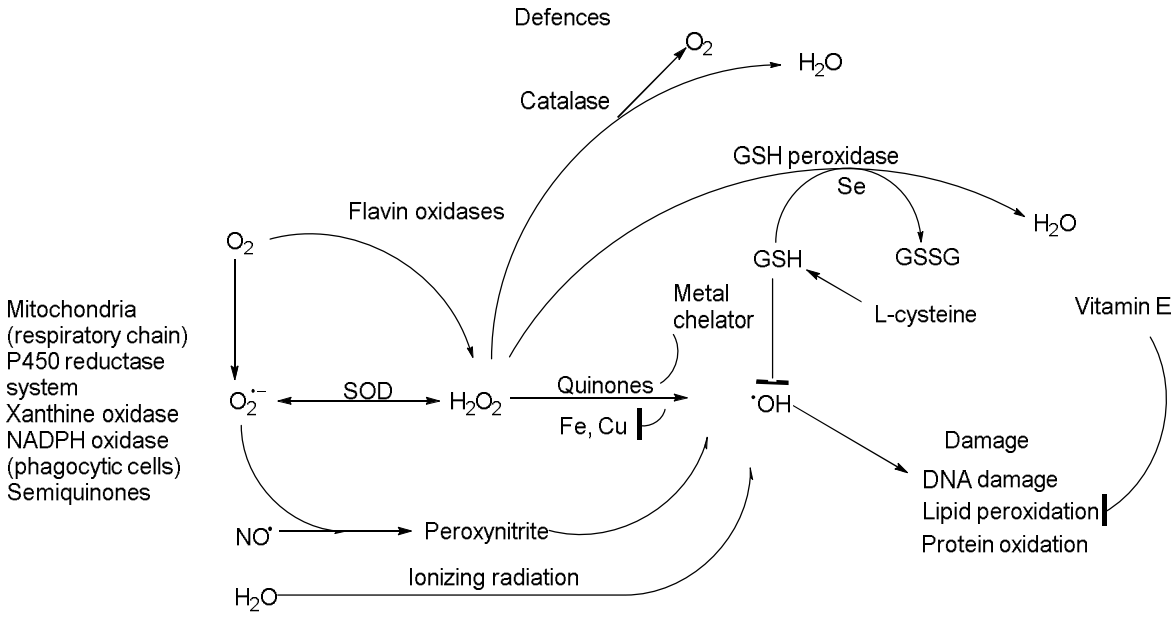

Scheme 10. *Main ROS pathways and antioxidant defences.*

1.4.2 THE PROPERTIES OF ROS/RNS

A variety of documentary sources exist on the effects of ROS/RNS on cell metabolism. ROS/RNS are not only involved in apoptosis (programmed cell death) but also beneficial effects such as the induction of host defence[118, 119] genes and mobilisation of ion transport systems. The evidence implicates them in control of cellular function. In particular, platelets involved in wound repair and blood homeostasis, release ROS to recruit additional platelets to sites of injury. These also provide a link to the adaptive immune system *via* the recruitment of leukocytes. There are also a range of harmful effects that ROS and RNS have on the human body. Many diseases, such as stroke and heart attack, are caused by reactive oxygen or nitrogen species in mediation of apoptosis or programmed cell death and ischaemic injury.

From a negative perspective on the cell damage, what researchers have discovered and explored can be divided into the following areas: [120]

(1) Damage of DNA

(2) Oxidation of polyunsaturated fatty acids in lipids

(3) Oxidation of amino acids in proteins

(4) Oxidatively inactivate specific enzymes by oxidation of co-factors

1.5 THE MOLECULAR RECOGNITION OF ROS/RNS

1.5.1 MOLECULAR RECOGNITION

The broad physiological and pathological consequences of ROS/RNS biology and the chemical complexities associated with these reactive small molecules require a need for new and better methods to monitor the origins and fates of ROS, particularly those that can be used in intact living specimens and give real-time information.[59] Molecular recognition is a particularly useful way of monitoring and sensing the presence of the certain species instantly and also can be taken as a powerful tool to reflect the living environment. In the various methodologies of molecular recognition, such as electrochemistry, fluorescence-based techniques, EPR, and chemiluminescence, small-molecular fluorescence probes could be considered as the most powerful weapon in the detection of ROS/RNS due to their high sensitivity, simple manipulation and easy instrumentation.

1.5.2 REACTION-BASED FLUORESCENT PROBES FOR ROS/RNS

Over the past decades, a large amount of work has been done for the exploration of reaction-based fluorescent probes. They were developed for the specific detection of ROS/RNS species as a primary need due to the result of the distinct reactivity of each ROS/RNS molecule in terms of selectivity and kinetics. Also, different species have been involved with good reactivity under mild conditions for the typically reported chemical reactions. In addition, some of the probes have been used for bio-imaging experiments and achieved great success, in order to meet the needs of chemo-selectivity and bioorthogonality. Based on the great success of the reaction-based fluorescent probes, there is a great potential for the development of higher-performance sensors and further application in real-time monitoring of these species. Thus, it is important in the design of useful reaction-based probes for ROS/RNS to use a selective reaction trigger and a suitable fluorophore platform.

1.6 FLUORESCENT PROBES TO DETECT ROS

Chemical tools for studying ROS biology were developed due to the broad physiological and pathological consequences of ROS biology and the chemical complexities associated with these reactive molecules. To meet the requirement of selectivity and kinetics towards each type of ROS, a growing number of small molecules and protein-based probes have been introduced instead of the traditional probes such as dichlorodihydrofluorescein.

In the following, different kinds of small molecule fluorescent probes for the detection of hydrogen peroxide (H_2O_2), hydroxyl radical (HO•), singlet oxygen ($^1O_2$), hypochlorous acid/hypochlorite ($HClO/ClO^-$) [121] will be explored.

1.6.1 PROBES FOR HYDROGEN PEROXIDE

Hydrogen peroxide (H_2O_2) is the simplest peroxide (a compound with an oxygen-oxygen single bond) and it is a strong oxidizing agent, which has been widely employed as bleach and as a cleaning reagent to reduce BOD[122] and COD[123] from industrial wastewater. Hydrogen peroxide, one of reactive oxygen species (ROS), also plays an important role as a signalling molecule in the regulation of a variety of biological processes, such as immune response, cell signalling,[124] Alzheimer's diseases[125] and cancer.[126] However, when misregulated and accumulated, the presence of excess hydrogen peroxide can cause oxidative stress and damage to cellular proteins, nucleic acids, and lipid molecules, thereby leading to aging and age-related diseases. Therefore, the importance of H_2O_2 has led to researchers seeking effective and applicable approaches for its detection. Among the powerful tools available for H_2O_2 detection are synthetic fluorescent probes. They provide the advantages in the chemoselectivity and bioorthogonality in the molecular imaging of this oxygen metabolite, which is a powerful method for real-time and non-invasive monitoring of hydrogen peroxide chemistry in biological world.[62]

Over the last decade, several groups introduced different fluorescent probes for the detection of hydrogen peroxide. Chang and co-workers have developed ratiometric, targetable, near-IR, and lanthanide-based luminescent probes in targeting subcellular domains (Figure 2). As can be seen from the structures, they are fluorescein, naphthalimine, and rhodamine, resorufin-based derivatives with boronic acids moiety

modified and designed by using turn-on signal transformation. The fusion of factors was to make the probes suitable for the chemoselectivity and bioorthogonality. Above all, the probes were designed skilfully to meet the requirement of the functionality in a specific environment.

Turn-on H_2O_2 probe

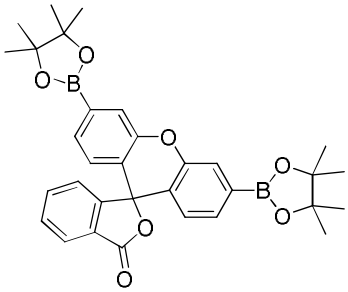

28. PF1

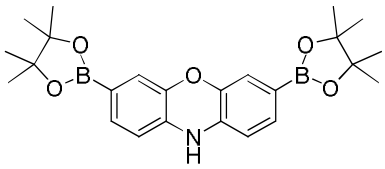

29. PR1

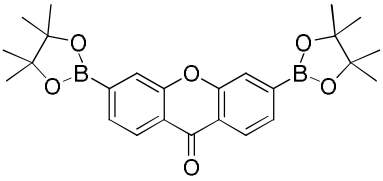

30. PX1

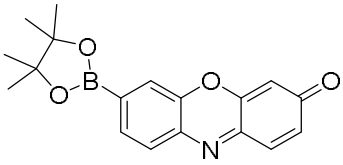

32. PC1

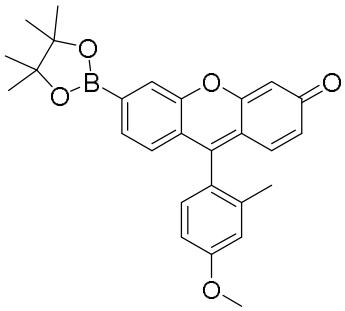

32. PF2

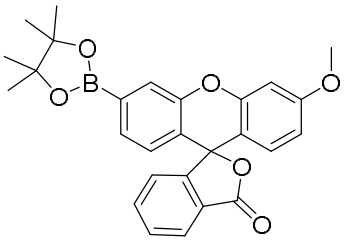

33. PF2

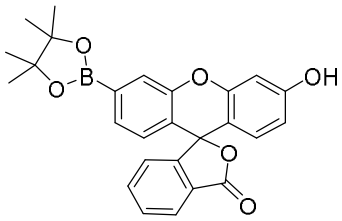

34. PF3

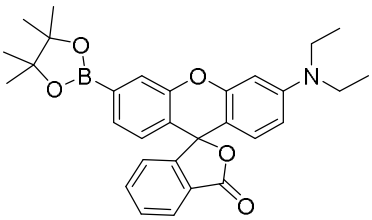

35. PY1

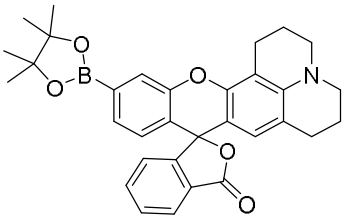

36. PO1

Ratiometric H_2O_2 probe

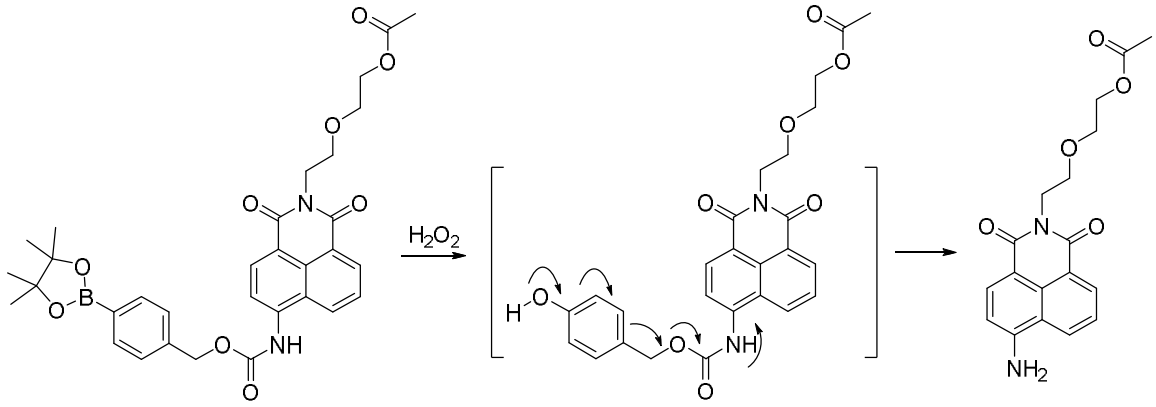

37

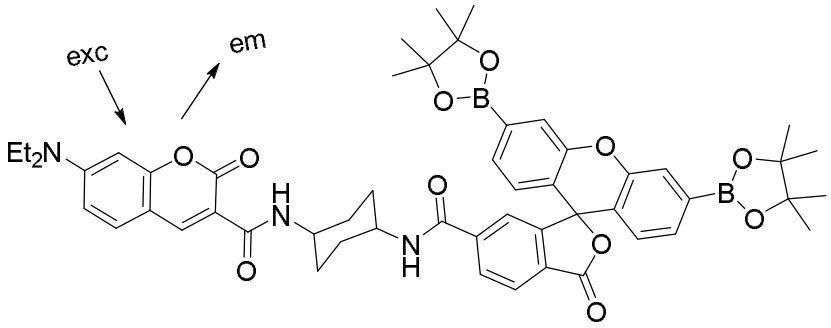

38

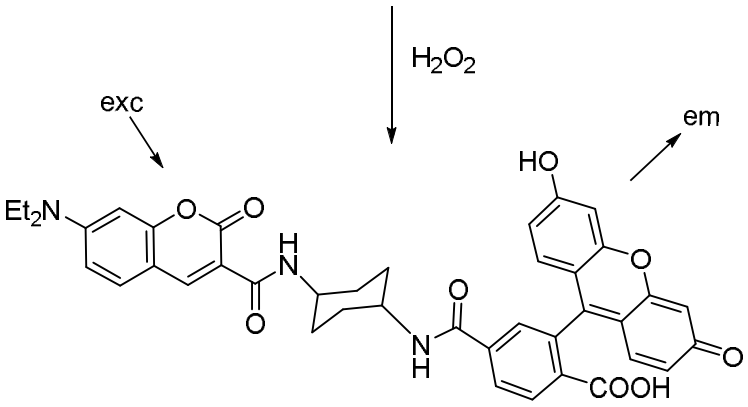

Target and trappable H_2O_2 probes

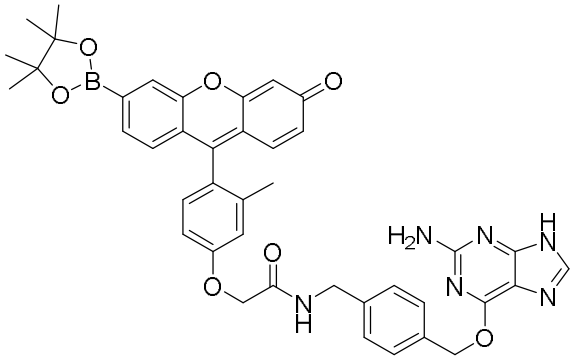

39. SPG1

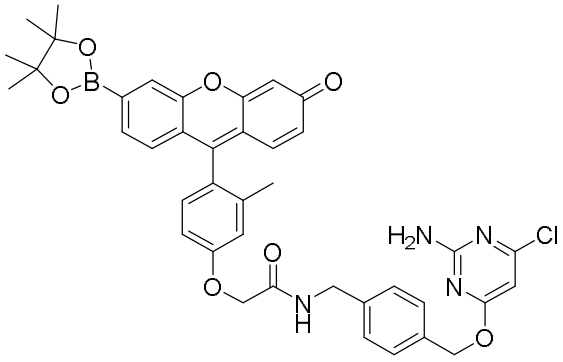

40. SPG2

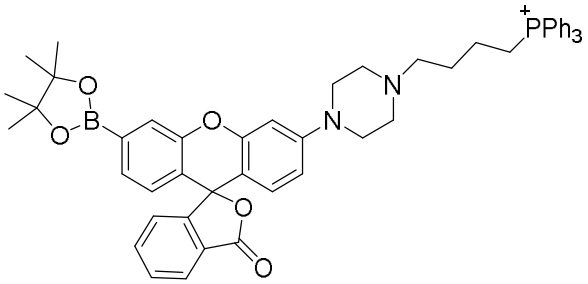

41. MitoPY1

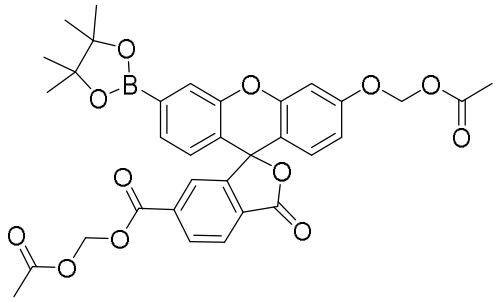

42. PF6AM

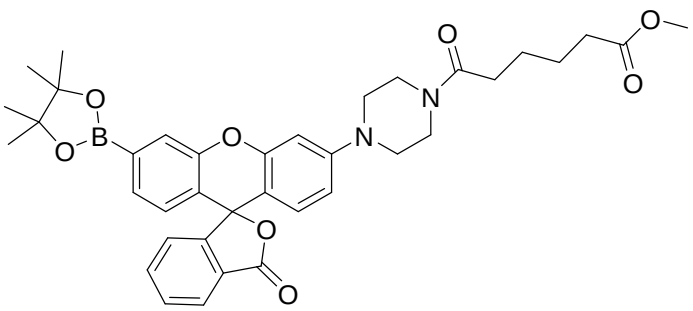

43. PY1ME

Figure 2. *Boronate-based identification system probes*

Tomapatanaget *et al*. used the H_2O_2 generated from glucose by the action of glucose oxidase to convert boronic acids to phenols in their glucose sensing system.[127] The sensory molecule has exhibited the specific–glucose sensing *via* GOx enzymatic reaction and very low determination limit of the glucose concentration (Scheme 11).

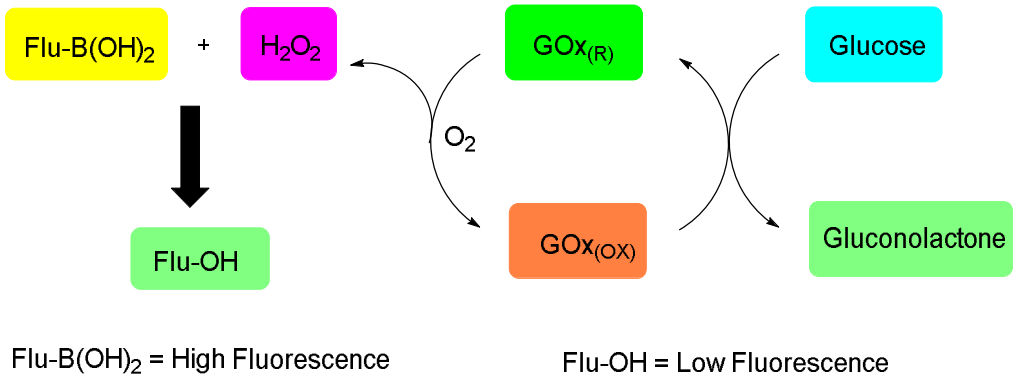

Scheme 11. *Schematic illustration of the GOx enzymatic mechanism for glucose detection using boronic-based fluorescent sensors.*

Recently, Tetsuo Nagano *et al.* designed 5-benzoylcarbonylfluorescein derivatives as candidate fluorescence probes **44. NBzF** for the specific detection of hydrogen peroxide by utilizing the unique chemical reactivity of benzil and hydrogen peroxide. In this approach, d-PET mechanism was employed to control the "off-on" fluorescence change. More importantly, the model molecule NBzF was practically used to detect endogenous hydrogen peroxide generation in living RAW 264.7 macrophages and A431 human epidermoid carcinoma cells (Scheme 12).[128] It was also predicated this alternative methodology with ease of use and high selectivity could be employed for cell-based high-throughput screening of inhibitors of ROS-producing enzymes.

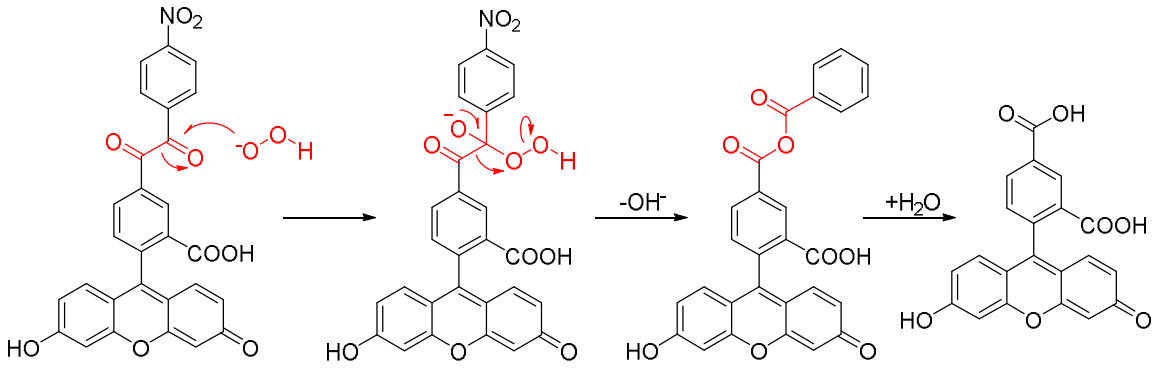

44. NBzF

Scheme 12. *Sensing mechanism between benzil and hydrogen peroxide*

1.6.2 PROBES FOR HYDROXYL RADICAL

Hydroxyl radical (HO•) is the neutral form of hydroxide ion (HO^-). In 1963, Weinreb *et al*. discovered the existence of HO•, the experimental evidence for the presence of 18 cm absorption lines of the HO• in the radio absorption spectrum of Cassiopeia A.[129] Since then, there were a series of important subsequent reports on HO• astronomical and biological detections. In particular, the involvement in the degradation of biomolecules, such as DNA, proteins, lipids, in cells and tissues, they are recognized as key roles in radiation therapy for cancer treatment. The biological importance of HO• led researchers to explore applicable detection methods, such as electron spin resonance (ESR) spectroscopy, real-time visualization and synthetic fluorescent probes have been widely used.

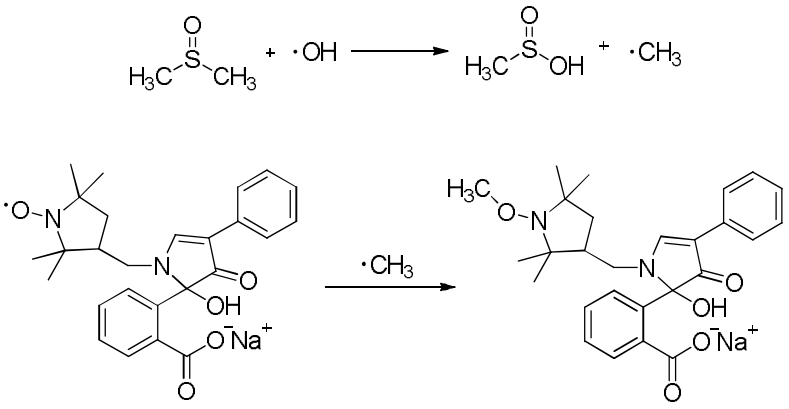

45

Scheme 13. *Mechanism of hydroxyl radical detection by fluorophore-nitroxide.*

Carbon-centered radicals have been determined in aqueous solution by liquid chromatography with fluorescence detection, as reported in 1990 by Blough and co-authors.[130] Since carbon-centered radicals can be formed by reaction between hydroxyl radical and DMSO (Scheme 13). Pou and co-authors have developed **45** (fluorophore-nitroxides) as a reporter for the detection of hydroxyl radical, *via* the derived methyl (Scheme 13).[131] Since then, several research groups used the nitroxide functional group to monitor hydroxyl radical production based on different fluophores (**46**, **47**, **48**, **49**), such as naphthalene, anthracene,[132] BODIPY,[133] and perylenebisimide.[134] Among them, the BODOPY-based fluorescent probe was notable for the high selectivity and sensitivity in the fluorescence imaging of living cells.

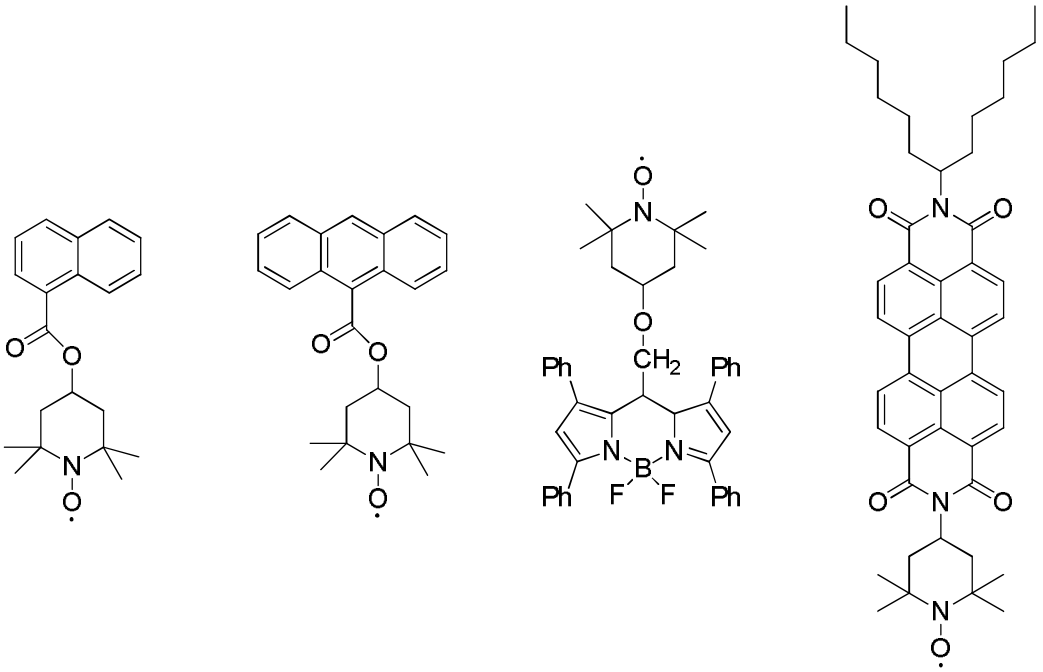

46 **47** **48** **49**

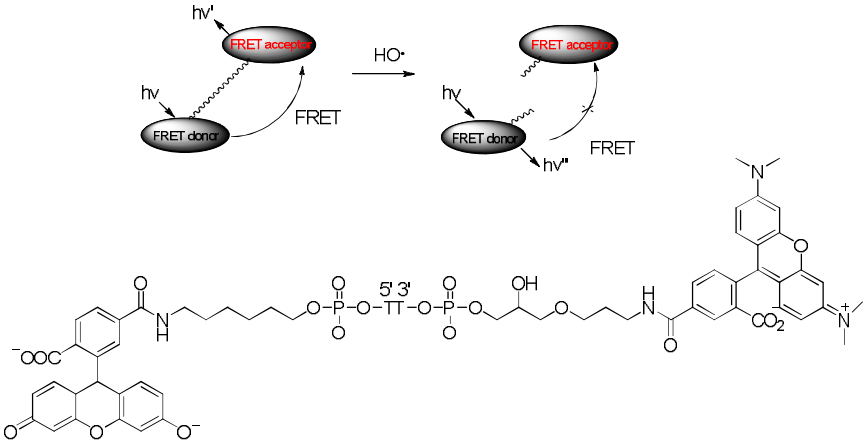

50

Scheme 14. *FRET-based hydroxyl radical probes.*

In other types of hydroxyl radical probes, the FRET-based strategy has been employed by using FRET donors and acceptors linked by single stranded DNA (Scheme 14, probe **50**). The fluorescence change was attributed to the cleavage of DNA linker caused by HO•.[135, 136]

1.6.3 PROBES FOR SINGLET OXYGEN

Singlet oxygen ($^1O_2$) is the common name used for an electronically excited state of molecular oxygen. The generation of singlet oxygen is usually achieved using

photosensitiser pigment. The damaging effects of sunlight on many organic materials (polymers, etc.) are often attributed to the effects of singlet oxygen. Furthermore, singlet oxygen has been widely used to kill cancer cells in photodynamic therapy. As one of the reactive oxygen species, it is linked to oxidation of LDL cholesterol and resultant cardiovascular effects in mammalian biology.

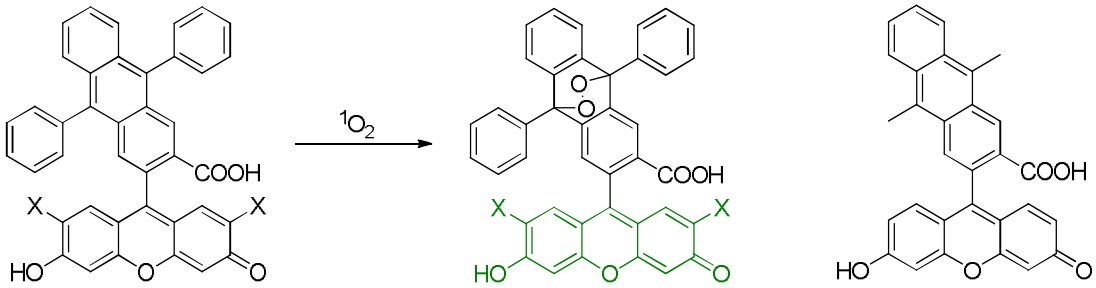

X = H: **51**a
Cl: **51**b
F: **51**c

52

Scheme 15. *Sensing mechanism of anthracene-fluorescein fused probes.*

In the past few years, a range of fluorescent probes for the detection of singlet oxygen have been reported. They are designed on the basis of the reaction between singlet oxygen and an anthracene moiety. Nagano and co-workers have introduced various structures **51a**, **51b**, **51c**, **52** which linked an anthracene group with fluorescein body in different position using a fluorescence PET mechanism.[137, 138] In the presence of $^1O_2$, the anthracene moiety was converted to the corresponding endoperoxide, which hampered the PET process and led to the efficient emission from the fluorophores (Scheme 15). Most notably, a commercially available probe **53** was developed for the selective and sensitive $^1O_2$ detection. Meanwhile, this probe has been utilized to monitor $^1O_2$ production during photo-oxidative stress, pathogen attack and wounding (Scheme 16).[139]

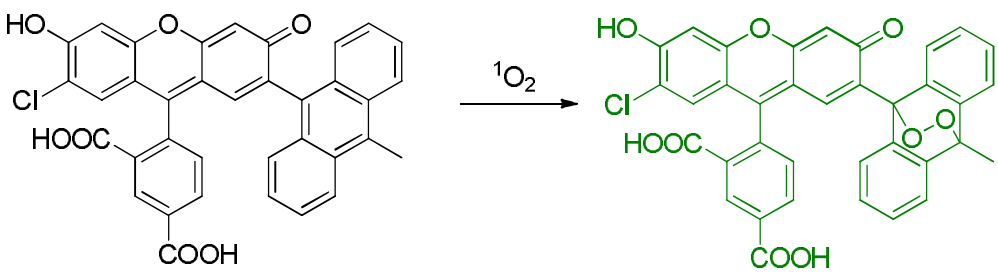

53

Scheme 16. *Sensing mechanism of probe by singlet oxygen*

1.6.4 PROBES FOR HYPOCHLOROUS ACID/ HYPOCHLORITE

Hypochlorous acid (HClO) is a weak acid and can be formed by adding chlorine into water. In terms of its uses, the most common things in our daily life are its sodium salts, such as sodium hypochlorite (NaClO), or its calcium salt calcium hypochlorite ($Ca(ClO)_2$), which are often used as bleach, deodorant and disinfectant. In organic synthesis, people use it as a reagent to convert alkenes to chlorohydrins. In the family of ROS, hypochlorous acid (HOCl) plays as a powerful microbicidal agent in the innate immune system.

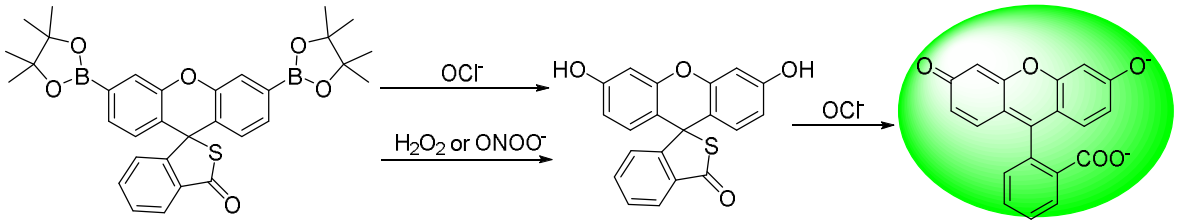

54

Scheme 17. *"Dual-lock" structure of the fluorescent probe for the specific detection of HClO*

Because of its biological value, significant efforts have been made for the development of fluorescent probes towards the selective detection of HClO over the past few years. Based on Chang's work, Yong *et al*. explored a highly specific fluorescent probe **54** for hypochlorous acid using boronic esters and thiolactone (Scheme 17). The probe displayed a high selectivity towards HOCl over other ROS, especially H_2O_2 and $ONOO^-$ since reaction can only happen between the intermediate and hypochlorous acid. The importance of the result is the ability to distinguish between HOCl and H_2O_2 or $ONOO^-$. The presence of thiolactone plays a key role due to the reaction with HOCl exclusively and led to the fluorescence recovery in the system. The "dual-lock" probe was further employed in the application of visualizing microbe-induced HOCl production.

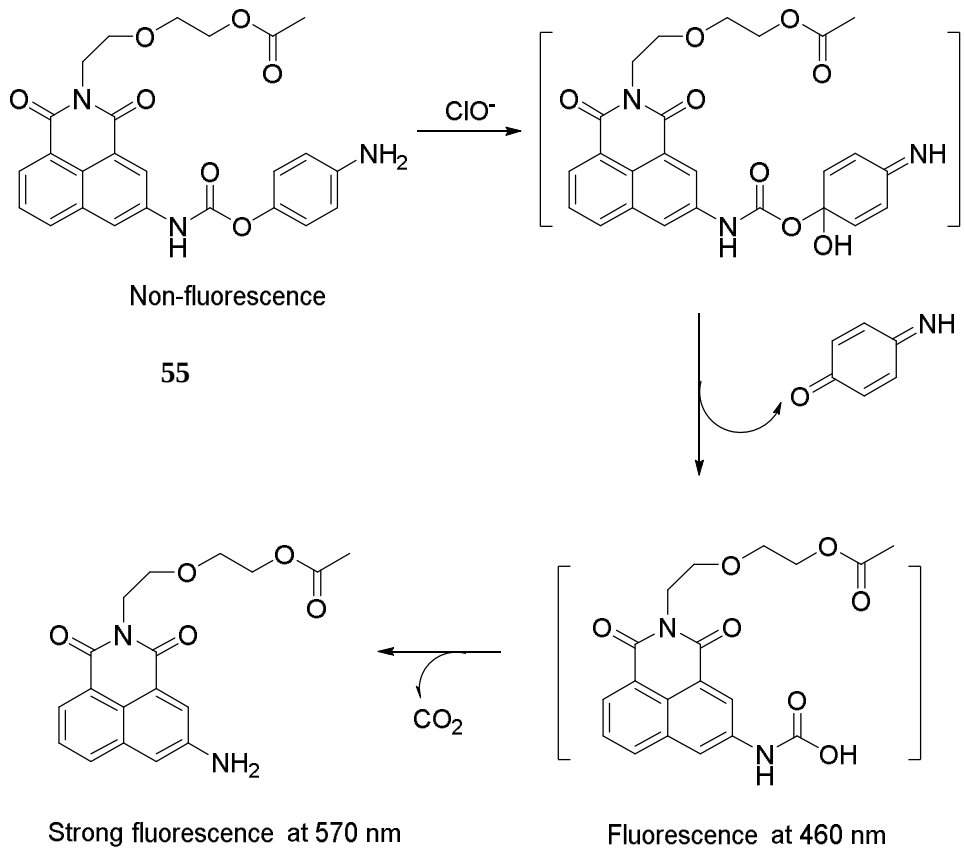

Scheme 18. *Proposed mechanism for the detection of HClO.*

Recently, Qian and co-workers have demonstrated a novel dual-emission fluorescence probe **55** for specific and sensitive detection of hypochlorite (ClO^-).[140] The chemo-sensor is constructed by tethering 4-aminophenoxyl to 1,8-naphthalimide *via* a carbamate linkage and showed a dual-channel emission while only a single channel enhancement for $ONOO^-$. The bio-imaging application of the probe was also investigated to selectively and quantitatively detect ClO^- in live cells (Scheme 18).

1.7 FLUORESCENT PROBES TO DETECT RNS

Reactive nitrogen species (RNS) are a family of antimicrobial molecules derived from nitric oxide radical, generally, such as nitric oxide, nitroxyl and peroxynitrite. Together with reactive oxygen species (ROS), RNS usually acts to damage cells, causing nitrosative stress. They are also continuously produced in plants as by-products of aerobic metabolism or in response to stress.[141] It should be noted as well for the fluorescent detection of reactive nitrogen species both *in vivo* and *in vitro*.

1.7.1 PROBES FOR NITRIC OXIDE

Nitric oxide (NO) is widely recognized as one of the indispensable parts of many physiological events, such as neurodegenerative injury, vasodilation, cancer and inflammation.[121] There have been a number of methodologies[142] for detecting NO, including electrochemical,[143] EPR,[144] chemiluminescence,[145] and fluorescence-based techniques. Yet, the most powerful tool for the detection of analysts is synthetic fluorescent probes.[146]

In the past decade, a range of fluorescent probes for *in vivo* and *in vitro* NO detection has been reported. The group led by Nagano and co-workers first demonstrated the use of *o*-phenylenediamine moiety for NO detection and constructed a list of fluorescent probes based on photoinduced electron transfer (PET) mechanism (Figure 3).[147-152] The formation of a triazole through the N-nitrosation reaction between *o*-phenylenediamine and nitric oxide caused the fluorescence turn-on response. For the small organic nitric oxide probes, they are pH-independent, highly sensitive and applicable to both *in vivo* and *ex vivo* imaging of NO. However, the sensing reaction towards NO can only happen in the presence of oxygen under aerobic conditions which makes measurements of intracellular NO concentrations possibly inaccurate.

a. Reaction-based NO fluorescent probes

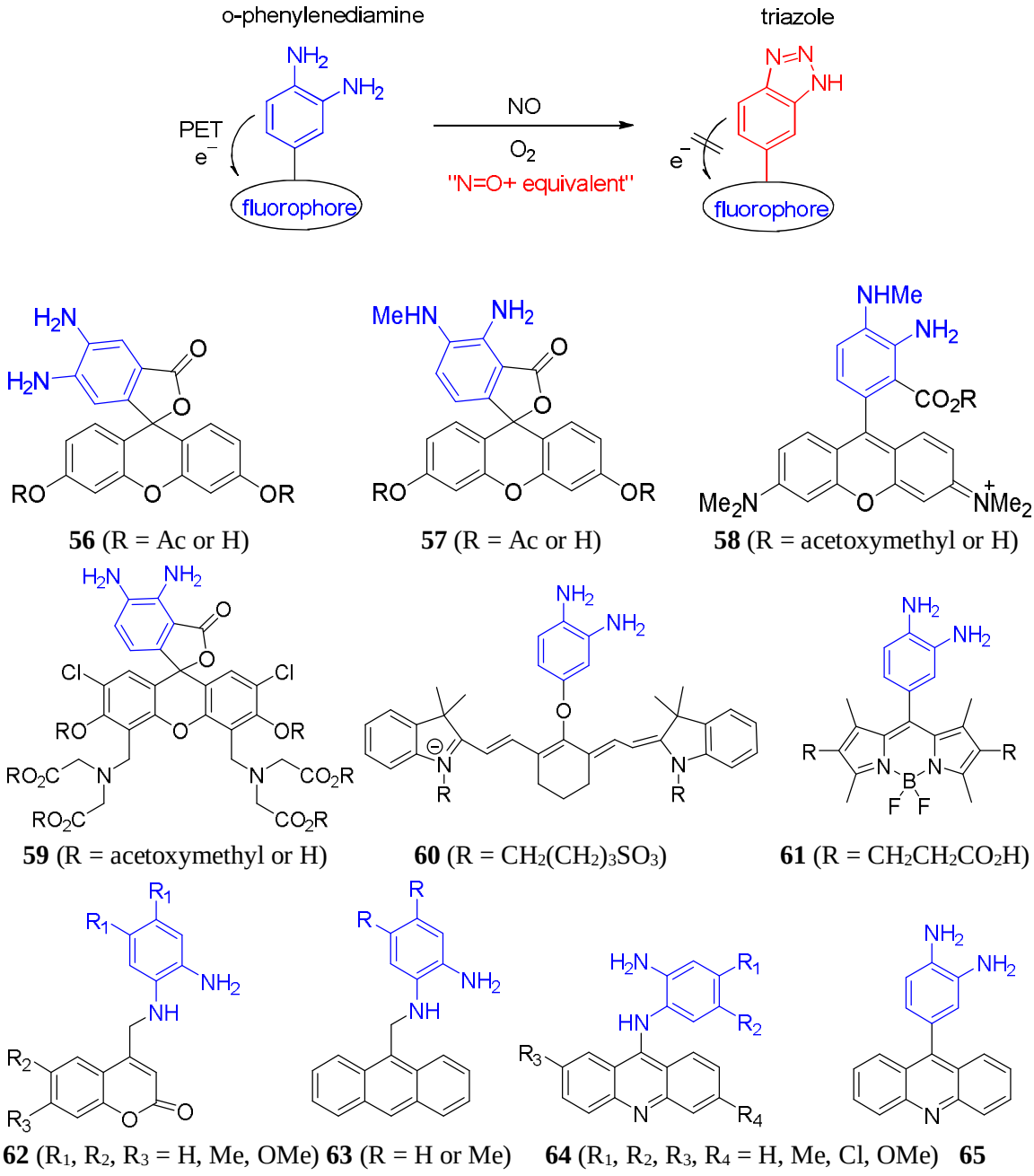

Figure 3. *o-Phenylenediamine-based fluorescent probes to monitor NO in vitro and in vivo.*

Lippard *et al.* has developed transition metal based nitric oxide probes based on paramagnetic quenching of the fluorescence.[153-159] Among them, copper complex-based fluorescent probes for monitoring nitric oxide in aqueous solutions is very promising (Scheme 21, 22) because it overcomes the limitations of the cobalt **66**, ruthenium **67** and dirhodium-based fluorescent NO probes, such as low sensitivity and water-incompatibility (Scheme 19, 20).[160-163]

b. Metal-based NO fluorescent probes

I. Fluorophore displacement

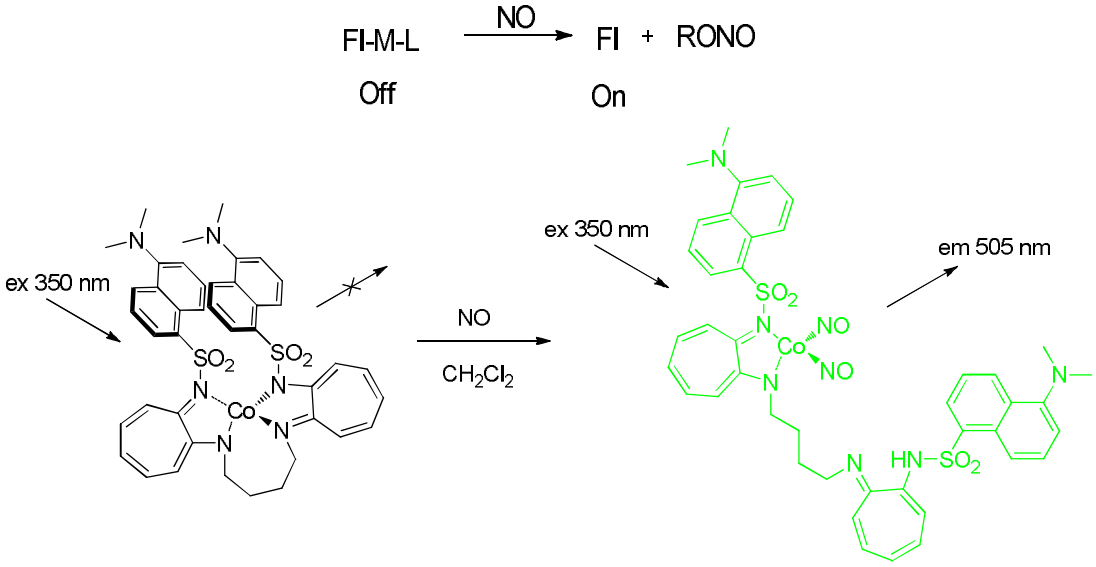

66

Scheme 19. *NO fluorescent probes based on Co complex. Reproduced with permission from (Angew. Chem. Int. Ed., 2000, **39**, 2120.)*

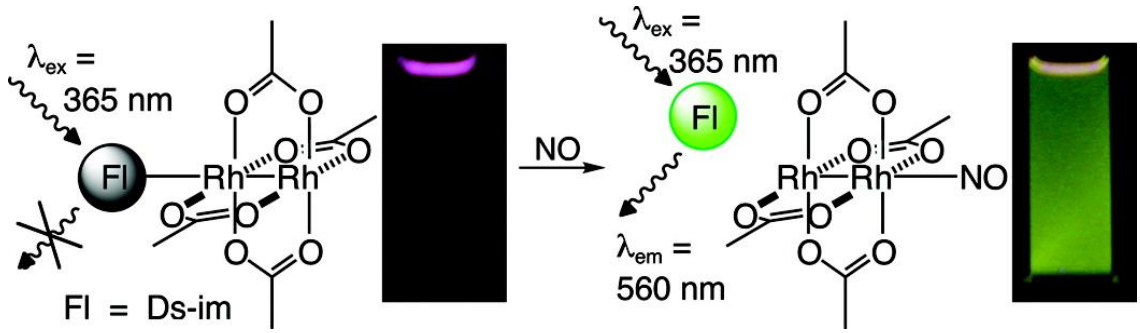

67

Scheme 20. *NO fluorescent probes based on Rh complex[156] Reproduced with permission from (J. Am. Chem. Soc., 2004, **126**, 4972.). Copyright © 2004 American Chemical Society.*

II. Method of metal-reduction

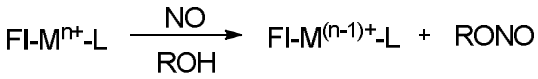

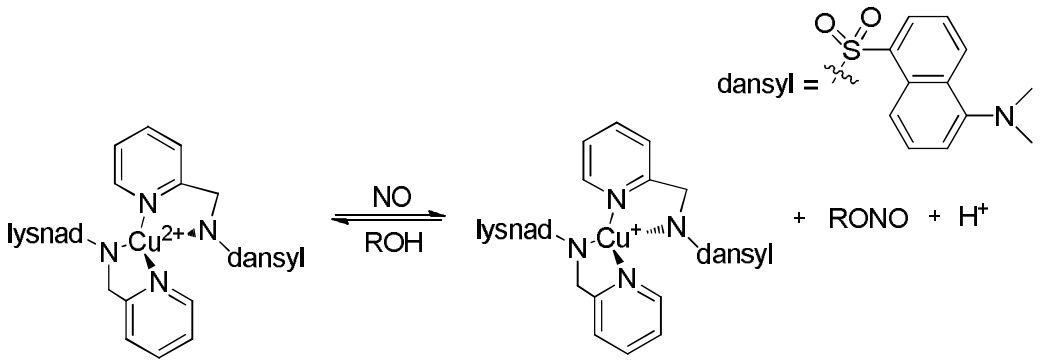

68

Scheme 21. *NO fluorescent probe based on copper-complex*[164]

III. Method of metal-reduction and ligand nitrolyation[163]

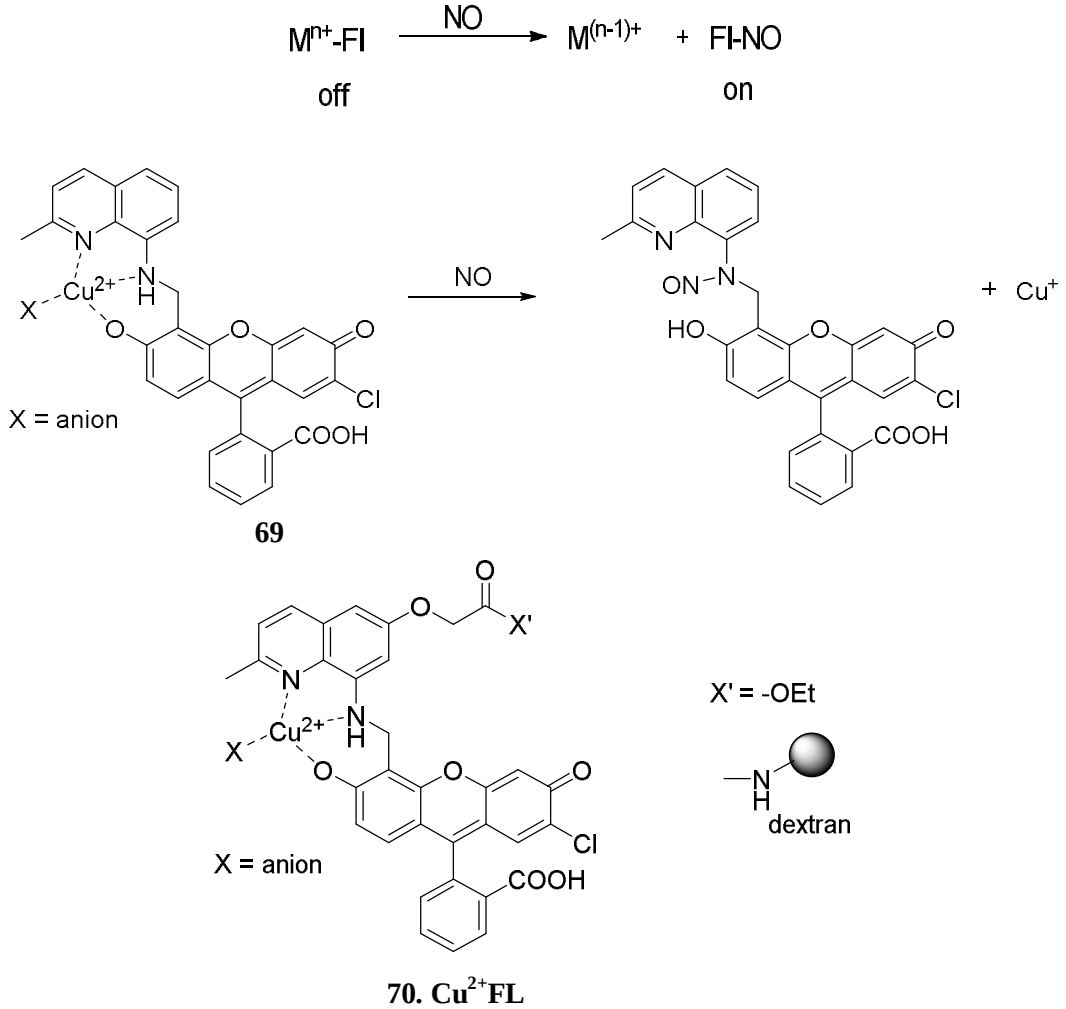

69

70. Cu^{2+}FL

Scheme 22. *NO probes based on copper-complex in vivo*[162]

Qian synthesized a new *o*-phenylenediamine-based fluorescent molecule **71** as chromogenic and fluorogenic NO probe using Cu^{2+} as a promoter (Scheme 23).[165] The

Cu^{2+}[FS] generated through combining FS with Cu^{2+} exhibited a significant fluorescent increase and a large blue shift of 200 nm upon addition of nitric oxide in neutral buffer solution. The fluorescence response toward nitric oxide is highly selective and sensitive over other biologically ROS and RNS. The analytical detection limit (ADL) was 30 nM. This is a novel copper-promoted nitric oxide fluorescent probe based on *o*-phenylenediamine, and opens up new possibilities for the construction of colorimetric and fluorescent sensors for nitric oxide.

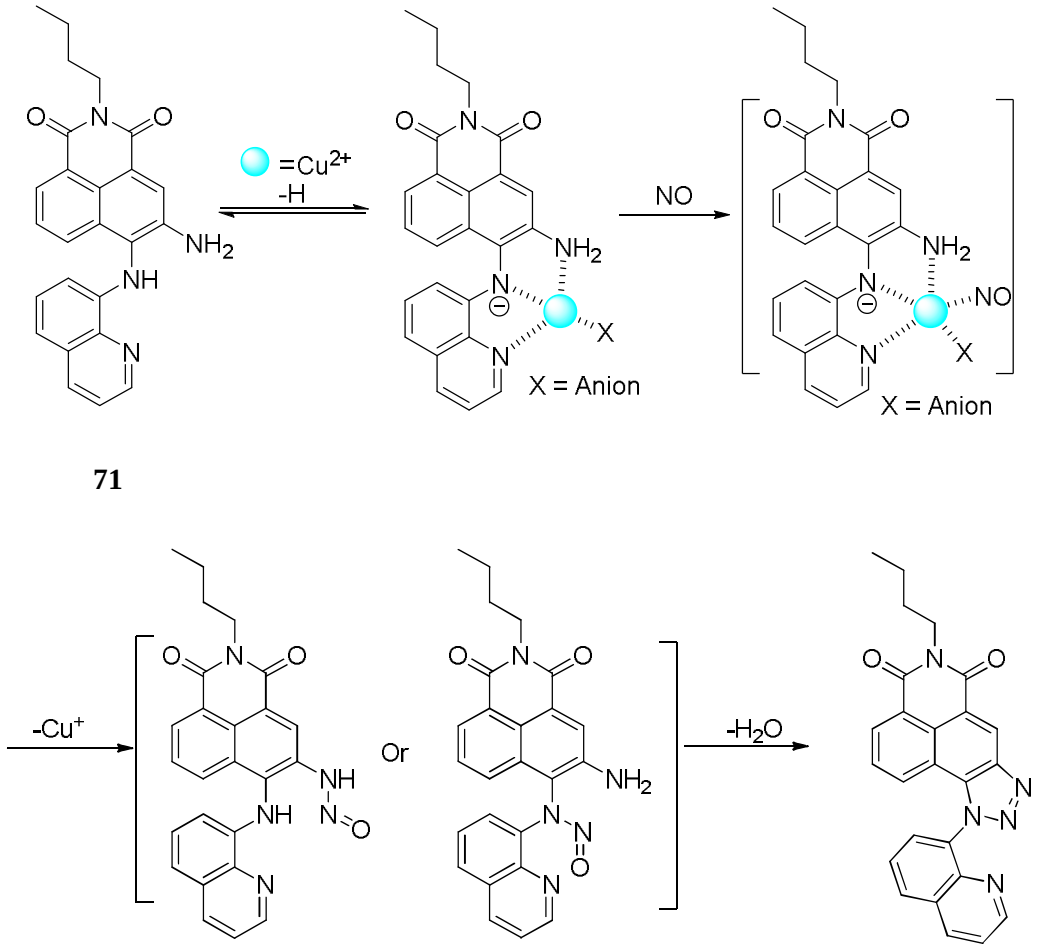

71

Scheme 23. *Possible mechanism of metal complex with NO in a neutral buffer solution.*

Anslyn *et al.*[166] reported a new fluorescence probe **67** for NO on the basis of an *N*-nitrosation reaction. It introduced a novel sensing mechanism and showed excellent selectivity for intra- and extracellular NO imaging (Scheme 24). However, what participates in the reaction is the oxidation product (N_2O_3) of nitric oxide under aerobic conditions. Therefore, it is also inaccurate in the measurement of intracellular nitric oxide concentrations.

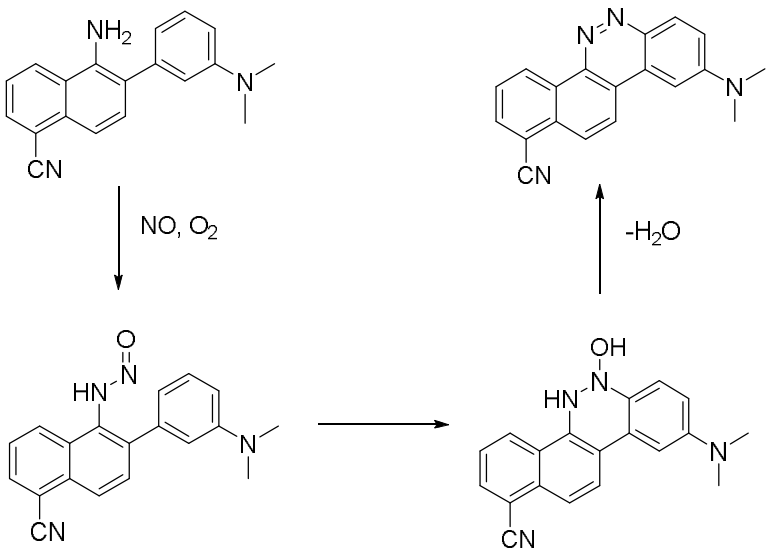

Scheme 24. *NO probe based on N-nitrosation reaction.*

1.7.2 PROBES FOR NITROXYL

Nitroxyl (HNO/NO^-), the one-electron reduction product of nitric oxide, was studied as an intermediate in the thermal and photochemical reactions dating back to early 1900s.[167, 168] Nowadays, it has been widely recognized as one of the important reactive oxygen species in the biological world. In the past decade, a series of studies has outlined the potential important biological and pharmacological activity of HNO.[169] For example, it is a potent, positive inotropic agent endowed with preferential venous dilatative properties;[170] HNO enhanced cardiac inotropy and lusitropy while also unloading a failing heart both at baseline and notably during β-stimulation;[171] Nitroxyl improved cellular heart function by directly enhancing cardiac sarcoplasmic reticulum Ca^{2+} cycling;[172] HNO can target cardiac sarcoplasmic ryanodine receptors to increase myocardial contractility.[173] While, nitroxyl frequently functions as an electrophile, and is very reactive toward thiols,[174] oxidized metals,[175, 176] oxygen molecule[177] and amines.

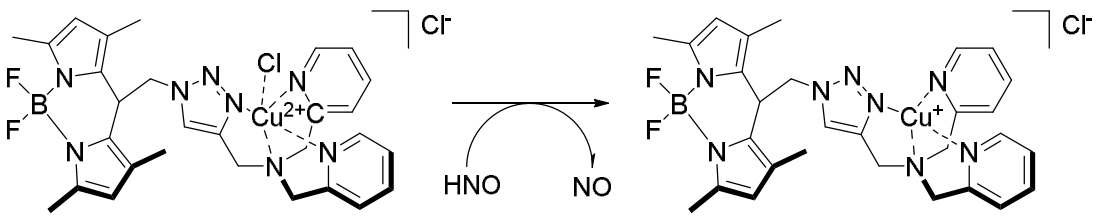

73. Cu^{II}[BOT1] **74.** Cu^{I} [BOT1]

Scheme 25. *Proposed mechanism of interaction with HNO based on BODIPY*

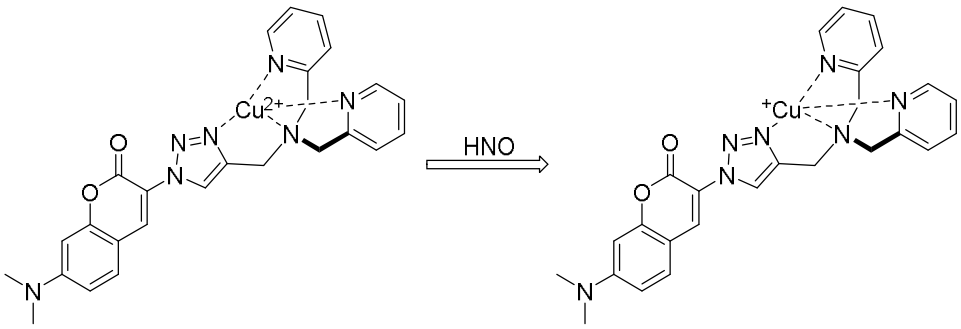

75. OFF- nonemissive **76.** ON- fluorescent

Scheme 26. *Proposed mechanism of interaction with HNO based on coumarin.*

Due to the co-existence and similarity of nitric oxide and nitroxyl in the biological system, one big challenge for its detection is to discriminate HNO from NO. In the last decade, several specialised techniques were used to specifically detect HNO, such as EPR,[178] transition metal complexes,[179] MIMS[180] and fluorescent probes. In the reported fluorescent methods for the detection of HNO, copper-based fluorescent complexes, Cu^{2+}[BODIPY] (Scheme 25, probe **73**) and Cu^{2+}[coumarin] (Scheme 26, probe **75**) have been used to distinguish HNO from NO *in vivo* and *in vitro*.[175, 176] However, the reagents were not applicable for live cell imaging due to small fluorescence changes and could generate certain amounts of NO upon Cu^{2+} reduction. Additionally, the use of the pre-fluorescent probe TEMPO-9-AC was complicated by intermolecular fluorescence quenching and competitive HNO trapping by other reactive oxygen species.[181] Therefore, it is essential to develop powerful tools for the specific detection of HNO for the application to both *in vitro* and *in vivo* systems.

King and co-workers investigated the use of phosphines as selective and efficient agents for the detection and quantitation of HNO (Scheme 27).[182] The aza-ylide **78** formed from the reaction between phosphine derivative **77** and HNO undergoes a Staudinger ligation to generate the amide and the reporter with free hydroxyl is released from the whole body. These results demonstrate progress toward the development of reaction-based probes for rapid *in vitro* and *in vivo* measurements of HNO.

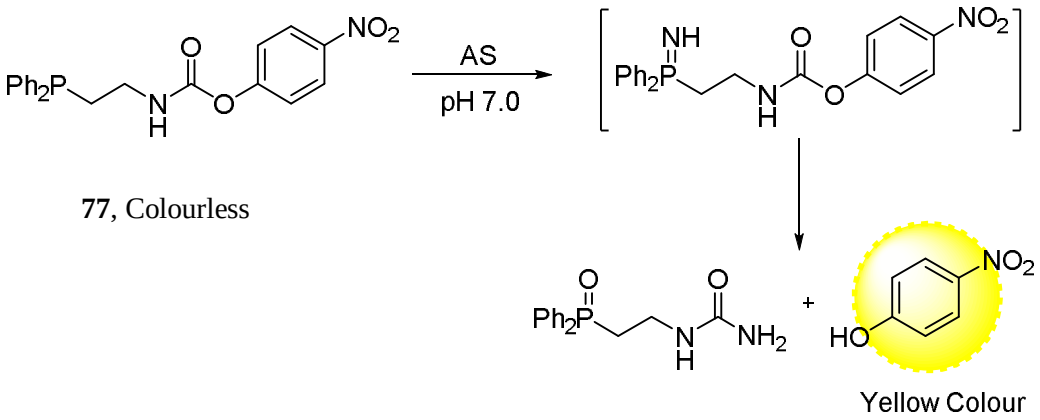

Scheme 27. *Sensing mechanism of probe 77 for HNO in neutral buffer.*

In light of the reaction between HNO and triarylphosphines, Nakagawa *et al.* reported the first metal-free and reductant-resistant HNO imaging probe **79** available for use in living cells.[183] As shown in Scheme 28, the system consists of rhodol acylated at its amino moiety, coupled to a triphenylphosphine moiety *via* an ester linker. In the presence of HNO (Angeli's salt as donor), the reaction of triarylphosphine with HNO leads to the formation of an aza-ylide and subsequently the open−closed tautomerism of rhodol fluorophore **80**. Probe **79** could successfully image the HNO intracellularly released from AS, with excellent selectivity over other ROS and RNS.

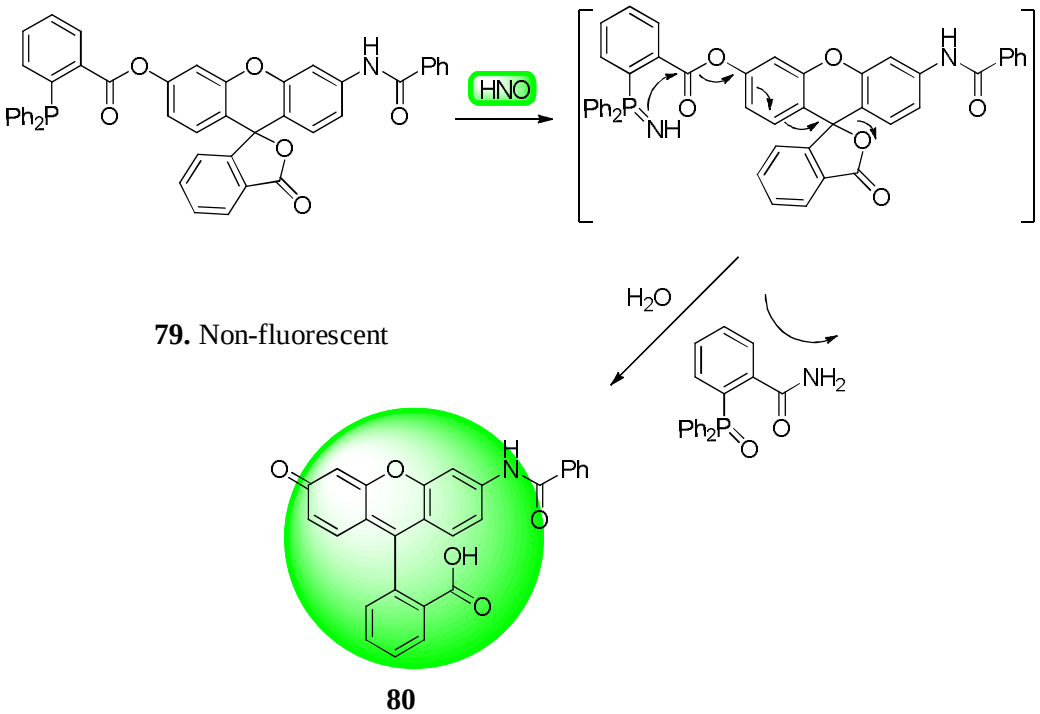

Scheme 28. *Proposed mechanisms of the reaction of probe 79 with HNO (2 eq.).*

By using the similar mechanism, Zhu and Zhang evaluated a fast-response, highly sensitive and selective fluorescent probe for the ratiometric imaging of nitroxyl in living cells (Scheme 29). The ICT-based ratiometric fluorescent probe **81** for HNO was designed with carbonyl protected 4-hydroxynaphthalimide. As reported, the probe displayed a 104 nm red-shift of absorption spectra and the colour changes from colorless to yellow, and 128 nm red-shifted emissions with excellent sensitivity among the various ROS/RNS.

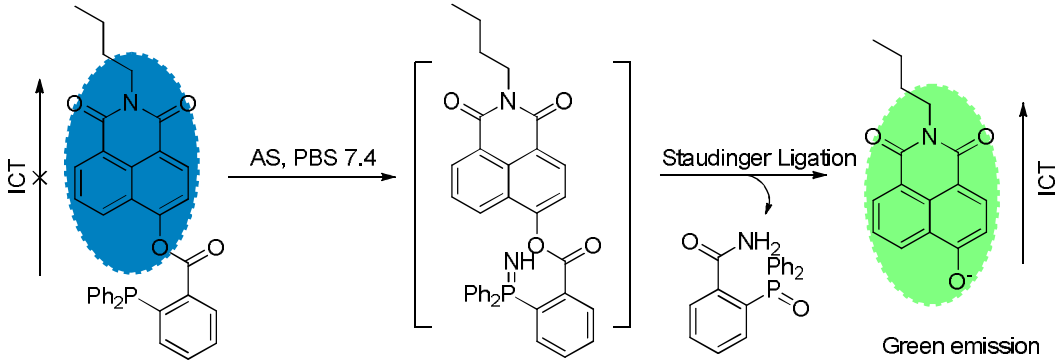

81

Scheme 29. *Proposed reaction mechanism between **81** and HNO.*

1.7.3 PROBES FOR PEROXYNITRITE

Peroxynitrite is a product from the reaction of free radical nitric oxide with free radical superoxide in human's body at diffusion-controlled rates (~ 1×10^{10} $M^{-1}S^{-1}$, Scheme 30). $ONOO^-$ acts as a strong oxidizing agent in physiological and pathological processes. Because of its oxidising properties, peroxynitrite can damage a wide array of molecules in cells, including DNA and proteins. Endogenous peroxynitrite formation and/or protein nitration in cardiac and vascular diseases has been implicated in Alzheimer's disease, Parkinson's disease, Huntington's disease, amyotrophic lateral sclerosis, viral myocarditis, septic shock, cardiac allograft, transplant coronary artery disease, idiopathic dilated cardiomyopathy, atrial fibrillation, hypercholesterolemia, atherosclerosis, hypertension, diabetes (T2DM, T1DM), diabetic nephropathy, and traumatic brain injury. Thus, the importance of peroxynitrite has led to researchers to seek effective approaches for its detection.

$$NO^{\cdot} + O_2^{\cdot -} \longrightarrow ONOO^-$$

Scheme 30. *Production of peroxynitrite in physiological condition*

Peroxynitrite (pK_a = 6.8) also can be prepared by the reaction of hydrogen peroxide with sodium nitrite and stable in alkaline solution (Scheme 31), which is frequently used for *in vitro* experiments.[184]

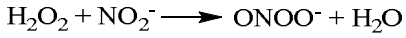

Scheme 31. *Production of peroxynitrite in basic condition*

In the work for the fluorescent detection of peroxynitrite, Yang *et al.* has designed a range of chemo-sensors which contain a ketone unit linked to different fluorophores through aryl ether moiety.[185-187] The presence of peroxynitrite oxidizes the ketone group to a dioxirane intermediate, which subsequently oxidizes the phenyl ring resulting in cleavage of the ether, to afford the strongly fluorescent product (Scheme 32). In this case, the "off-on" response of the probes **82**, **83**, **84** was developed for the detection of $ONOO^-$ over other ROS/RNS.

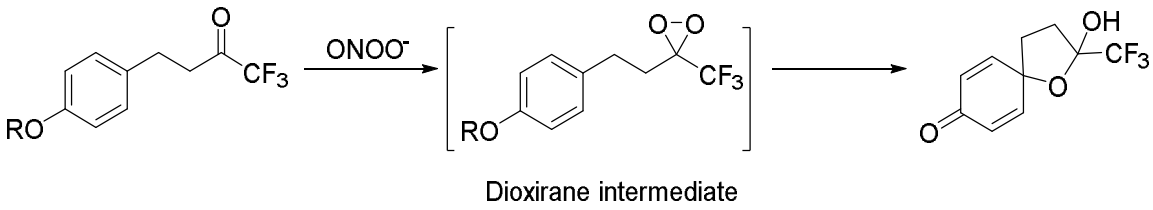

Scheme 32. *Peroxynitrite-mediated oxidation of an anisole-derived ketone via dioxirane intermediate.*

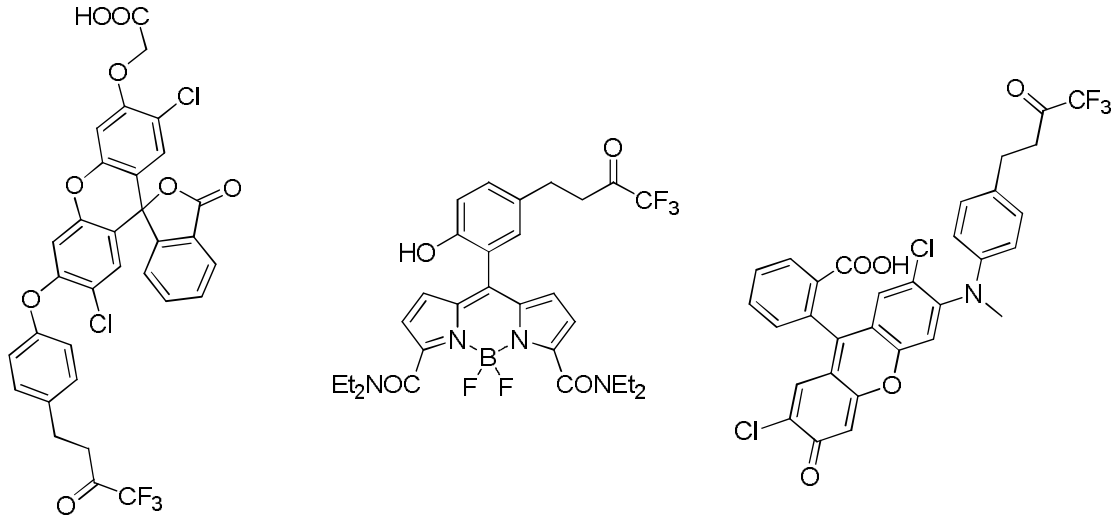

82 **83** **84**

Figure 4. *Different structures of $ONOO^-$ probes*

On the basis of a unique fluorophore assembly approach, Qian and Yang have rationally designed a green-emitting coumarin derivative **85** which is redox-active, low-molecular weight for the fluorescent imaging of peroxynitrite.[188] Importantly, it produces a three-channel fluorescence signal able to differentiate peroxynitrite from other reactive oxygen and nitrogen species, including hypochlorite and hydroxyl radical (Scheme 33).

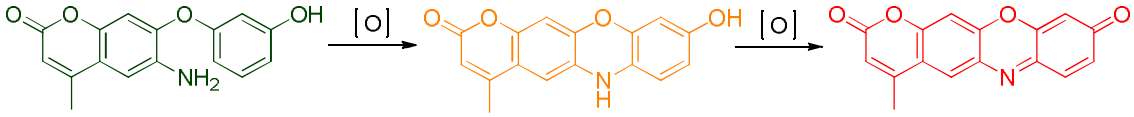

85. PN_{600}

Scheme 33. *Detection scheme of* PN_{600}

In the design of fluorescent probes, the use of near-IR (NIR) wavelength (650-900 nm) is essential and promising, which allows deep penetration into tissues and avoids the influence of bio-autofluorescence. Han *et al.* developed two distinct near-IR reversible fluorescent probes **86**, **87** containing organoselenium and telluroenzyme mimics functional groups in different systems which can be used for the highly sensitive and selective monitoring of peroxynitrite oxidation and reduction events under physiological conditions (Scheme 34).[189, 190] The Cy-NTe and Cy-PSe systems use the PET fluorescence signalling mechanism and use $ONOO^-$/GSH to trigger the fluorescent response cycles.

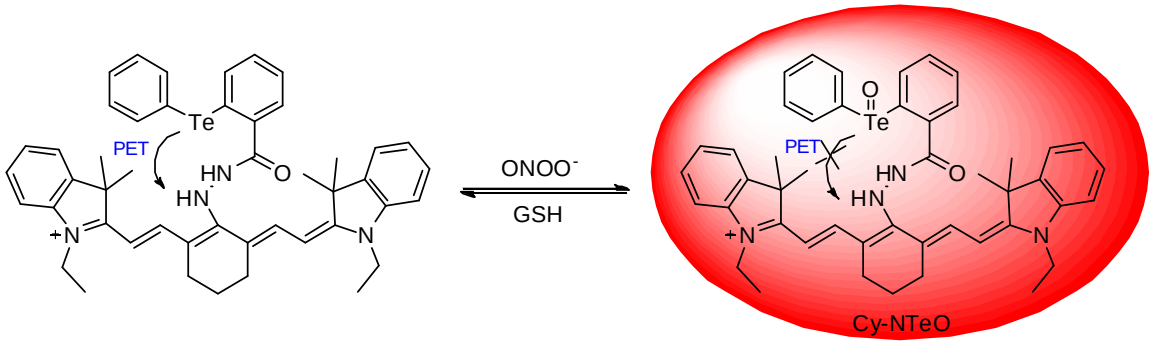

86. Cy-NTe

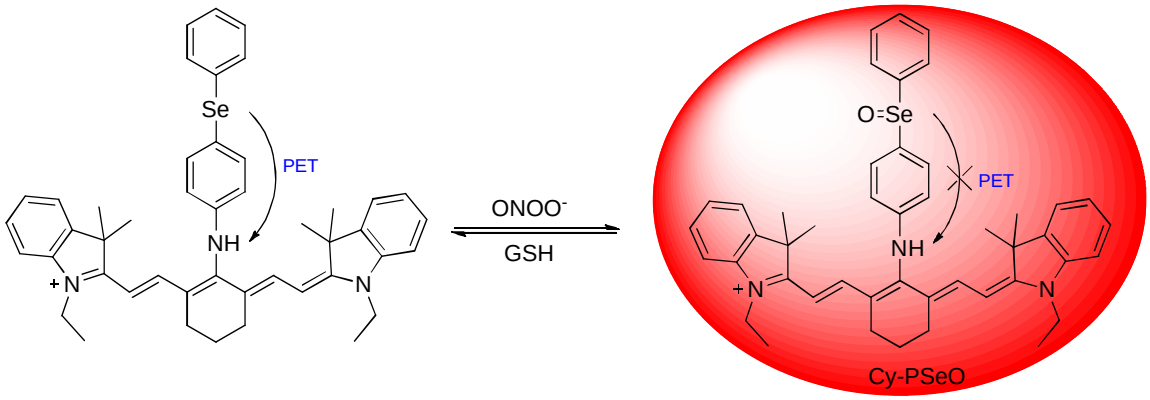

87. Cy-PSe

Scheme 34. *Reversible fluorescent probes based on Cy fluorophore.*

Recently, Ai *et al.* report a novel genetically encoded probe, **pnGFP**, which can selectively sense peroxynitrite to other common cellular redox signalling molecules (Scheme 35). Under physiological conditions, it is possible to directly measure $ONOO^-$ in cell or tissue samples. In order to distinguish $ONOO^-$ from H_2O_2, a site-directed random mutagenesis strategy was undertaken. The designed **pnGFP** showed a much higher response to $ONOO^-$ (20 μM) but did not respond to H_2O_2 at a 50-fold higher concentration (1 mM). The probe has also been genetically introduced into mammalian cells to image peroxynitrite at physiologically relevant concentrations.[191]

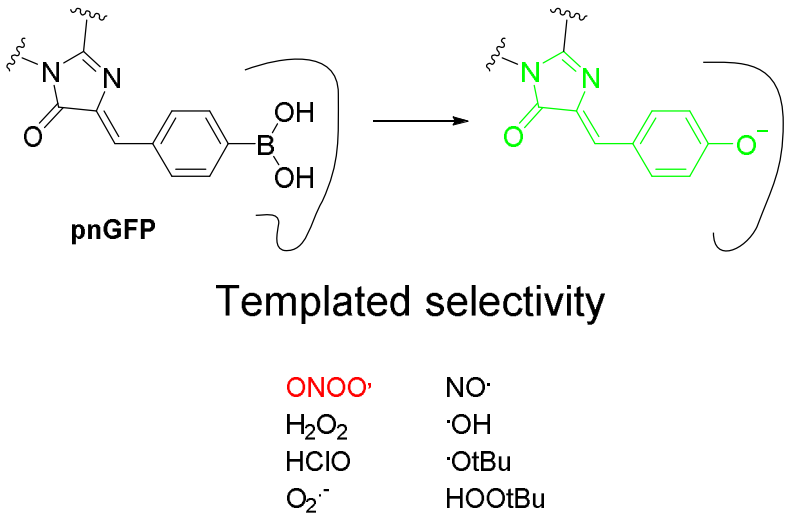

Scheme 35. *Design of genetically encoded fluorescence probe.*

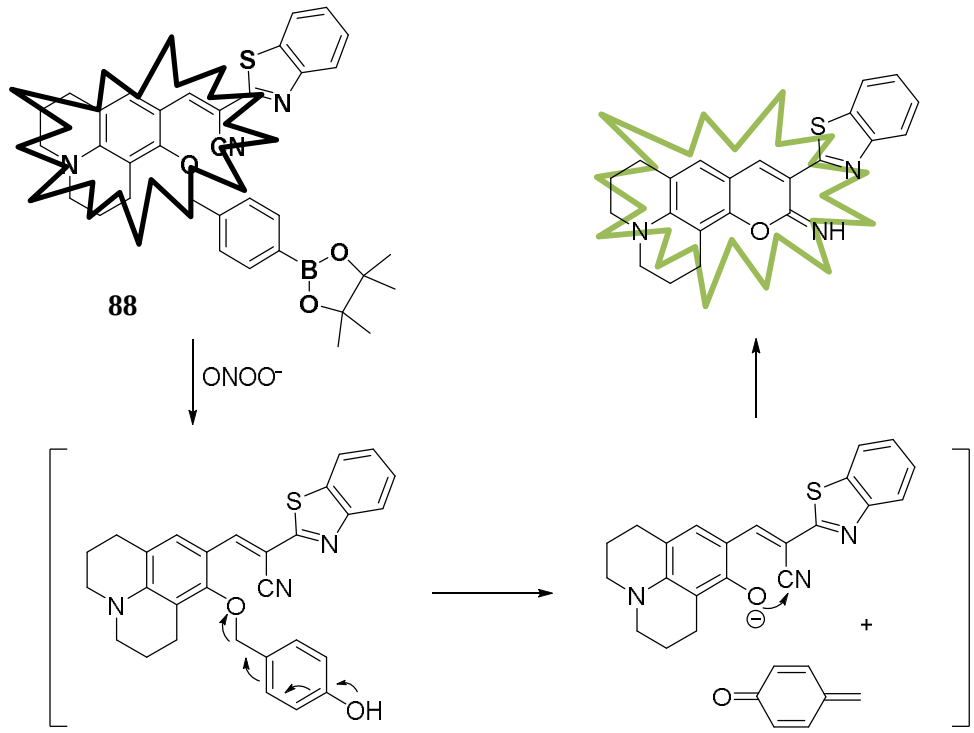

Scheme 36. *Chemical structure of probe and reaction mechanism with ONOO⁻.*

Choi and Kim reported a new fluorescence probe based on the arylboronate-derived structure **88** which can be selective detection of peroxynitrite over other ROS with a fast response and large fluorescence turn-on signal (Scheme 36). In the work, benzothiazolyl iminocoumarin scaffold was employed as the basic fluorophore and the probe was designed by masking a phenol moiety with a *p*-dihydroxyborylbenzyloxy group. In the presence of $ONOO^-$, oxidative hydrolysis of the arylboronate group to generate the corresponding phenol and then the elimination of *p*-quinomethane to produce the final highly fluorescent benzothiazolyl iminocoumarin.

However, it has been reported several times before that similar structures like the *p*-dihydroxyborylbenzyloxy group also can be oxidised by hydrogen peroxide over a prolonged time period. Thus, even the examples above will be challenged to distinguish $ONOO^-$ under high concentrations of H_2O_2.

1.8 SUMMARY OF INTRODUCTION

The phenomenon of molecular recognition and its motivation for the man-made tools in the detection of distinct substances has been introduced. Furthermore, the fundamental structure and relevant mechanism of fluorescent probes have been demonstrated, that meet the requirements of specific species recognition in a complex environment. The biological and medicinal significance of reactive oxygen and nitrogen species were described briefly. The importance for the development of useful methods for the measurement and detection of ROS and RNS both *in vivo* and *in vitro* was introduced. Synthetic fluorescent probes, especially reaction-based small molecules, have received great attention and achieved great success in the tracking and detecting of certain molecule selectively and sensitively.

Since we are mainly focused on the development of boronate-based chemosensors in the recognition of saccharides, ROS/RNS, the applicable introduction of various boronic acid-based probes has been made in terms of boron-diol interaction, amine-boron interaction and boron-H_2O_2/$ONOO^-$ reaction. It should be noted that it is still a big challenge using traditional boronate-based chemosensors to distinguish between H_2O_2 and $ONOO^-$.

We then classified and summarized the recent fluorescent compounds, developed, for superoxide ($O_2^{\bullet-}$), hydroxyl ($HO^{\bullet}$), hydrogen peroxide (H_2O_2), singlet oxygen ($^1O_2$), hypochlorous acid (HOCl), nitric oxide (NO), nitroxyl (HNO), peroxynitrite ($ONOO^-$). Fluorescent probes for the detection of ROS and RNS are increasingly important in the discipline of molecular recognition. So far, there are still a lot of challenges in the search for more effective fluorescent probes, such as chemoselectivity, biocompatibility and bioorthogonality. Thus, we are convinced in the near future more and more practical probes will be developed and reported to overcome the present disadvantages.

Chapter Two:
Results and Discussion I

[Image removed for copyright reasons]

2. RESULTS AND DISCUSSION I

2.1 BACKGROUND

Hydrogen peroxide (H_2O_2) was first described in 1818 by Louis Jacques Thénard, who produced it by treating barium peroxide with nitric acid.[192] It is the simplest peroxide with an oxygen-oxygen single bond and also it is a strong oxidizer, which has been widely used as a bleaching agent and disinfectant. In the biological and physiological process, hydrogen peroxide is an essential oxygen metabolite in living systems, and mounting evidence supports its role as a messenger in cellular signal transduction. In particular, hydrogen peroxide, as one of reactive oxygen species (ROS), has important roles as a signalling molecule in the regulation of a wide variety of biological processes, such as immune response, cell signalling,[124] Alzheimer's diseases[125] and cancer.[126]

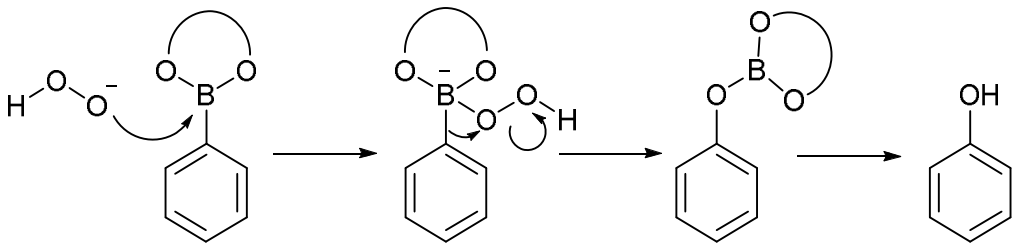

Scheme 37. *The reaction mechanism between a generic aryl boronic acid/ester and H_2O_2*

Among the powerful tools available for H_2O_2 detection are synthetic fluorescent probes. Given its high sensitivity and selectivity, small molecular fluorescent probes are becoming increasingly important in the recognition of certain substrate. Additionally, it has been reported that hydrogen peroxide reacts with arylboronic acids under neutral and mild alkaline conditions to generate phenols (Scheme 37).[116] Over the last decade, several groups introduced different fluorescent probes for the detection of hydrogen peroxide by utilising this mechanism. Chang and co-workers have developed a series of boronate-based derivatives for the fluorescent detection of H_2O_2 in living systems,[60, 64, 111-115] and Tomapatanaget *et al.* used the H_2O_2 generated from glucose by the action of glucose oxidase to convert boronic acids to phenols in their glucose sensing system.[127] Both the examples indicated the possibilities of further development of boronate-based chemical compounds for the detection of H_2O_2.

2.2 BORON-BASED PROBES

In our research group, we have a long-standing interest in boronic acids for saccharide and anion detection,[40, 145, 193, 194] boronic acid derivatives rapidly and reversibly interact with saccharides in aqueous media.[195, 196] Due to its unique high affinity and reversible interactions with diols, the boronic acid functional group is routinely incorporated into synthetic receptors for the complexation of saccharides and other guests that possess the 1,2- or 1,3-diol group.[76] In addition, since the development of the first fluorescent sensor for fluoride,[73] fluorescence of a series of simple aromatic boronic acids was observed to be quenched in buffered aqueous methanol solution at pH 5.5 upon addition of KF. Also, boronic acid derivatives have played a part in other area, such as chiral sensor, dye displacement assay, cation-π interactions, and electrochemical methods.[197-200]

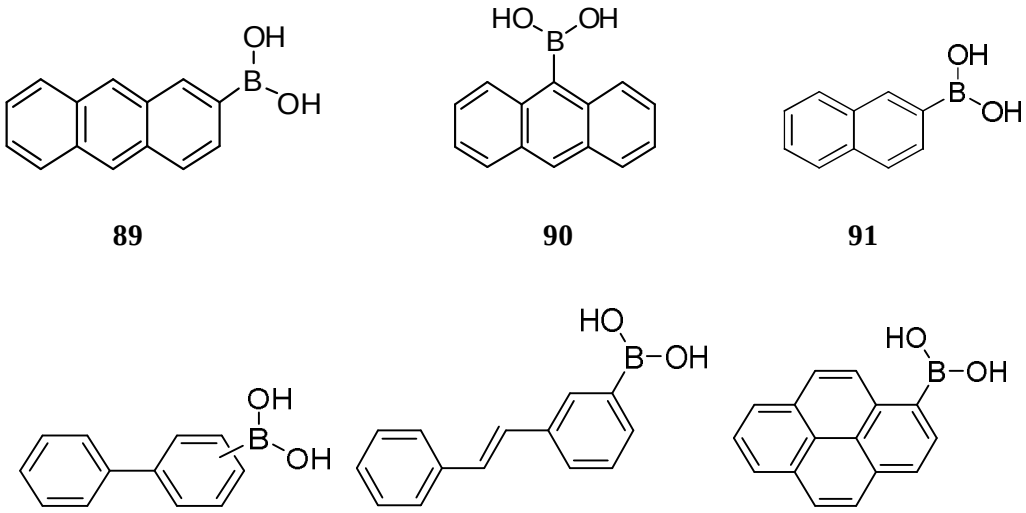

89 **90** **91**

92a: 2-$B(OH)_2$
92b: 3-$B(OH)_2$
92c: 4-$B(OH)_2$

93 **94**

Figure 5. *"Integrated" system of boronic acid derivatives*[201]

During the course of our investigations, we and others have employed boronic acids as sensors where the boron atom is directly attached to a fluorphore (integrated) (Figure 5) and separated by a Lewis basic spacer (insulated) (Figure 6). In the "integrated" system, the binding of boronic acid with diols led to the change of the fluorescence which mainly ascribed to the formation of the cyclic boronate ester and the inhibition of dynamic protons. While in the insulated system, the enhanced N-B interaction after bound with saccharide is the main reason to cause the change of the

signal on account of PET effect.

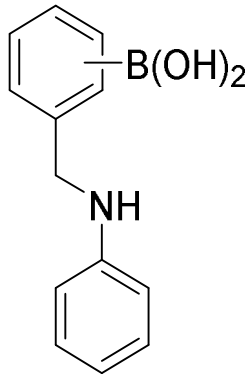

95a: 2-$B(OH)_2$

95b: 3-$B(OH)_2$

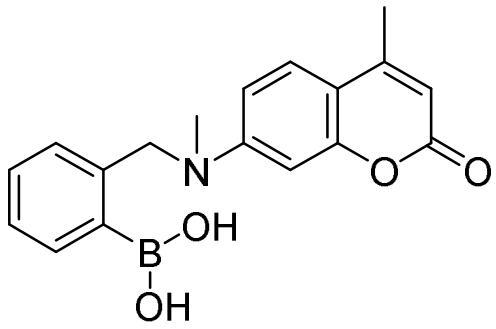

96

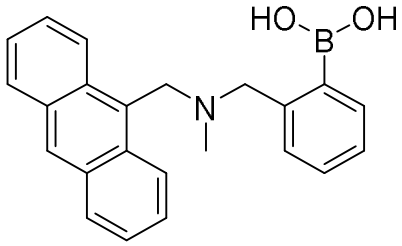

97

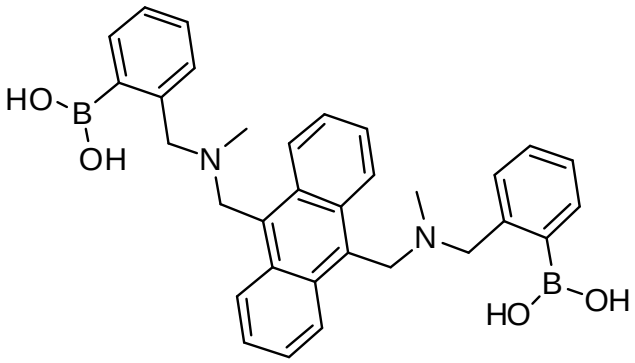

98

Figure 6. *"Insulated" system of boronic acid derivatives*.

2.3 DESIGN STRATEGY

Bearing these in mind, as a motivation from Chang's work[62] in the exploration of boronate-based fluorescent probes for the detection of H_2O_2, we decided to evaluated the sensing property between H_2O_2 and arylboronic acids in the presence of monosaccharide (Scheme 38).

As a model integrated boronate-based fluorescent probe we chose 2-naphthylboronic acid **99**. 2-Naphthylboronic acid **99** can be employed to detect saccharides *via* fluorescence intensity changes on addition of saccharides at constant pH resulting in an "on-off" or "off-on" fluorescence switch. Shinkai *et al.* reported it was an excellent fluorescent probe for sugar sensing among the various "integrated" system of boronic acid derivatives due to its strong fluorescence intensity, large pH-dependent change in I_{max}.[201]

While as a model insulated boronate-based fluorescent probe we chose *N*-methyl-*o*-(aminomethyl)phenylboronic acid **100**. *N*-Methyl-*o*-(aminomethyl)phenylboronic acid **100** has been previously demonstrated as an "off-on" fluorescent switch on saccharide binding, operating *via* a PET mechanism.[202]

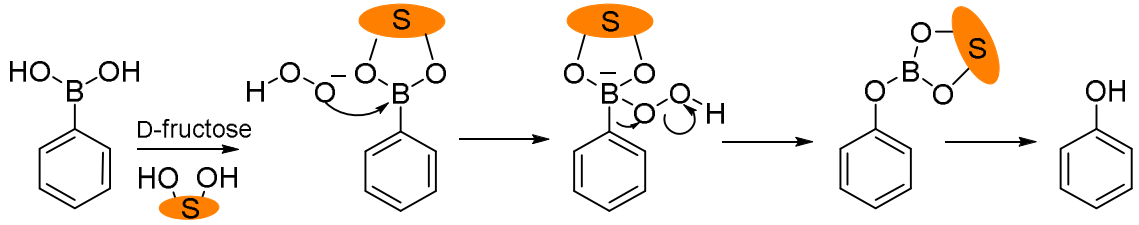

Scheme 38. *The reaction mechanism between a generic aryl boronic acid/ester and H_2O_2*

To the best of our knowledge, the reaction between arylboronic acids and hydrogen peroxide through modulating by the saccharides has never been reported. Bearing this in mind, we decided to investigate how the reaction of H_2O_2 with two classes of boronic acid (integrated and insulated) fluorescent probes changes in the presence of saccharides. This is conceptually similar to the inspirational work by Jiang into the effect of saccharides on Suzuki homocoupling reactions.[133] Understanding the effect of saccharides on this reaction and fluorescence may be important in developing advanced intracellular probes to accurately map H_2O_2 concentrations in living systems. Probes **99** and **100** (Figure 7) and their saccharide (D-fructose was chosen as a model

saccharide since it has a high binding constant) complexes were evaluated as fluorescent indicators for hydrogen peroxide both in neutral and alkaline aqueous solutions.

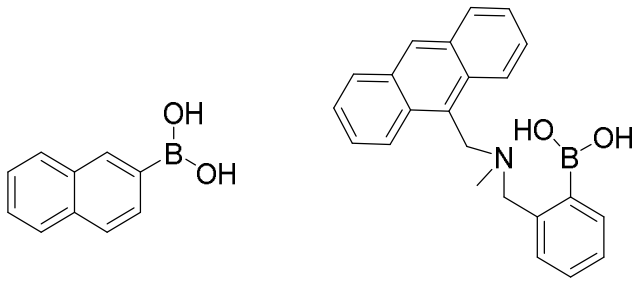

"Integrated" "Insulated"

99 **100**

Figure 7. *Chemical structures of probe **99** and **100**.*

2.4 RESULTS AND DISCUSSION

2.4.1 "INTEGRATED" SYSTEM OF 2-NAPHTHYLBORONIC ACID

Through a series of experiments, we found binding D-fructose to 2-naphthylboronic acid **99**, in the absence of H_2O_2, causes a decrease and an increase in fluorescence intensity at pH 7.20 and pH 9.70, respectively.

As can be seen from Figure 8, in the presence of D-fructose (100 mM), plot of I (in the presence of saccharide) /I_0 (in the absence of saccharide) for 2-naphthylboronic acid at the maximum wavelength of 340 nm dropped down to a level of F/F_0 = *ca.* 0.35 over 10 min and it was stable over the next 160 min in a pH 7.20 PBS buffer. In contrast, the fluorescence of naphthalene increased up to F/F_0 = *ca.* 2.70 when adding D-fructose (100 mM) into the sensing system in a pH 9.70 buffer solution. These results are in accordance with the work reported by Shinkai to prove that 2-naphthylboronic acid was one of the good candidates for sugar sensing.[201]

Furthermore in our research, we tested the reaction of 2-naphthylboronic acid with hydrogen peroxide in the absence and presence of D-fructose (Figure 8, Figure 9). In pH 7.2 phosphate buffer, free boronic acid probe **99** (10 μM) showed a gradual decrease in fluorescence intensity ratio F_T (in the presence of H_2O_2) /F_0 (in the absence of H_2O_2) = *ca.* 0.3 over 3 h in the presence of H_2O_2 (1.0 mM). When D-fructose (100 mM) was linked to the probe **99** (10 μM) to form a complex, the addition of H_2O_2 (1 mM) led to even greater reduction in the fluorescence intensity with a ratio F_T/F_0 = *ca.* 0.2 in the first 10 min (Figure 8). In the meanwhile, the blank test presents that 2-naphthylboronic acid as a fluorescent probe is stable in the neutral condition.

Next, in a pH 9.7 sodium carbonate buffer, the fluorescence intensity of free boronic acid probe **99** (10 μM) dropped down to F_T/F_0 = *ca.* 0.5 in the presence of H_2O_2 (0.10 mM). In the same condition, the high emission intensity of **99**-D-fructose complex was caused to drop from F_T/F_0 = *ca.* 2.7 to F_T/F_0 = *ca.* 0.8 after reaction with H_2O_2 (0.10 mM).

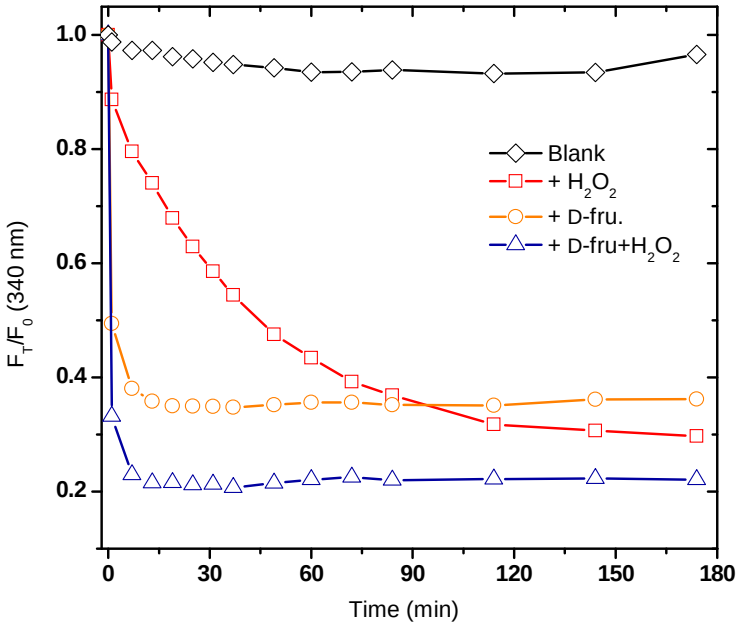

Figure 8. *Plots of F_T/F_0 for probe **99** (10 μM) with input of D-fructose (100 mM) and H_2O_2 (1 mM). Diamond– Blank; Square– (+ H_2O_2); Round– (+ D-fructose); Triangle– (+ D-fructose + H_2O_2). The mixture was incubated in pH 7.20 PBS bufferat 25 ºC. Fluorescence intensities at 340 nm were measured with excitation at 290 nm.*

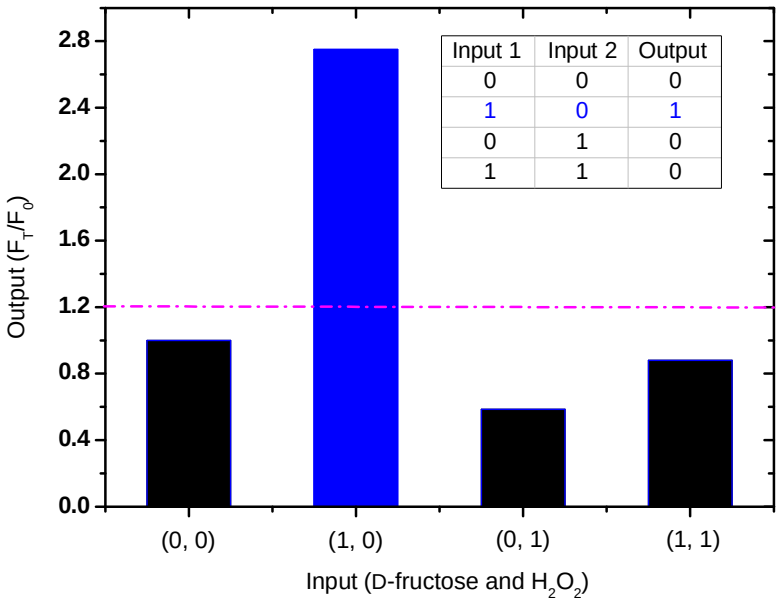

Figure 9. *Column spectra and truth table of probe **99** with D-fructose (100 mM) and H_2O_2 (0.10 mM) as inputs. The mixture was incubated in pH 9.70 $Na_2CO_3/NaHCO_3$ buffer at 25 ºC. Fluorescence intensities at 340 nm were measured with excitation at 290 nm.*

For the unbound 2-naphthylboronic acid probe, we also studied its sensing properties of reaction speed in the presence of various concentrations of H_2O_2 under neutral condition.

Four sorts of H_2O_2 concentration solutions were used, which are 0.10 mM, 0.50 mM, and 1.00 mM, respectively. As can be revealed from Figure 10, the ratio of fluorescence intensity of probe **99** (10 μM) showed different reaction rate constant with *k*' = 0.0029 min^{-1}, 0.010 min^{-1} and 0.0122 min^{-2}, separately, on exposing to the selected concentration of H_2O_2 solutions over the observed time (80 min). Apparently, with the increasing concentration of H_2O_2 aqueous solution, the boronic acid moiety can be oxidized to phenol faster in the reaction between probe **99** and hydrogen peroxide

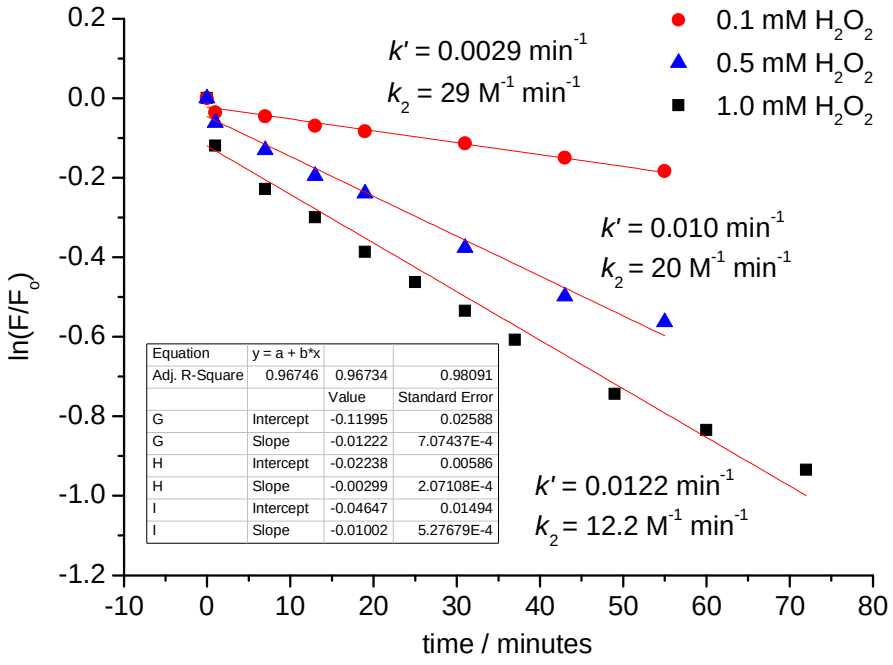

Figure 10. *Time curve of fluorescent spectra changes for probe **99** (10 μM) in various concentrations of H_2O_2 (Round - 0.10 mM, Up triangle - 0.50 mM, Square - 1.00 mM). The mixture was incubated in pH 7.20 PBS buffer at 25 ºC. Fluorescence intensities at 340 nm were measured with excitation at 290 nm.*

In order to testify how the saccharide affects the reaction between boron and H_2O_2, it is worth making a comparison from a perspective of reaction speed for the free boronic acid and saccharide-bound boronic ester with H_2O_2.

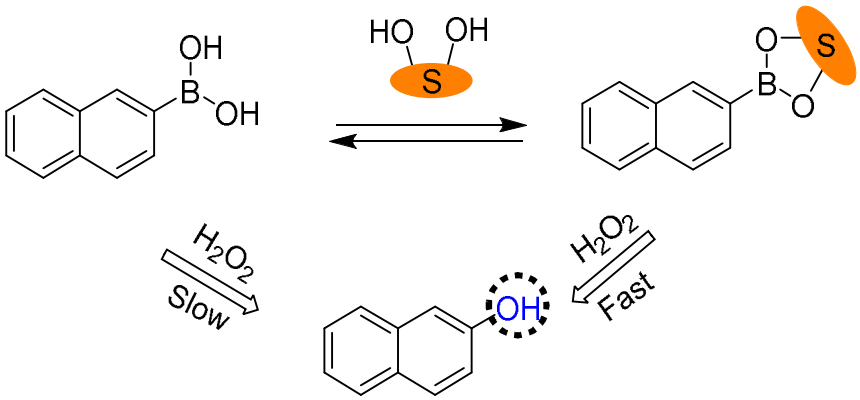

(a)

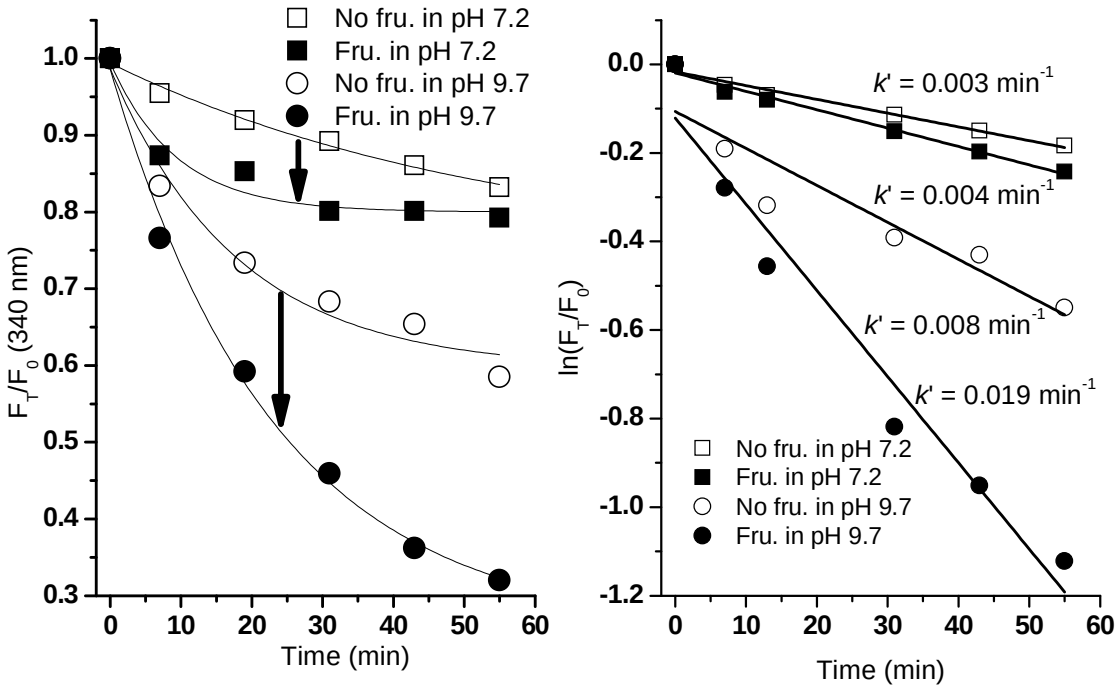

(b)

Scheme 39. *(a) Proposed strategy of probe **99** and **99**-D-fructose complex for sensing of H_2O_2; (b) Time curve of fluorescence intensity changes with probe **99** (10 μM) and D-fructose (100 mM) in aqueous H_2O_2 (0.10 mM) at different pH values. (Empty square - **99** and Solid square – **99**-D-fructose in pH 7.20; Empty circle - **99** and Solid circle – **99**-D-fructose in pH 9.70). The mixture was incubated in pH 7.20 PBS buffer and pH 9.70 $Na_2CO_3/NaHCO_3$ buffer at 25 ºC, respectively. Fluorescence intensities at 340 nm were measured with excitation at 290 nm.*

Scheme 39 summarises the reaction scheme and the fluorescence intensity changes for fluorescent probe **99** and the **99**-D-fructose complex in pH 7.20 and 9.70 buffer. It is known that on saccharide binding and formation of a cyclic boronate ester, the pK_a of

the boronic acid is enhanced, or in other words the 'ester' is more acidic than the 'acid'.[203] Therefore**,** binding with D-fructose increases the electrophilicity of boron in probe **99**, making it more easily oxidised by H_2O_2. This observation was borne out by our experiments.

As was shown in Scheme 39b, the fluorescence decreased over the observed time (55 min) of probe **99** (10 μM) was F_T/F_0 = *ca*. 0.85 (*k*' = 0.003 min^{-1}) while there was a larger change for the **99**-D-fructose complex, F_T/F_0 = *ca*. 0.80 (*k*' = 0.004 min^{-1}) upon expose to H_2O_2 (0.10 mM) over the same period in a neutral buffer solution. Under alkaline conditions, the **99**-D-fructose boronate ester complex reacted even faster with H_2O_2 (0.10 mM) (F_T/F_0 = *ca*. 0.30, *k*' = 0.019 min^{-1}) than the unbound boronic acid **99** (F_T/F_0 = *ca*. 0.60, *k*' = 0.008 min^{-1}). The responses of **99** and the **99**-D-fructose complex towards H_2O_2 became more rapid at high pH because the binding between boronic acid and saccharide has enhanced and also H_2O_2 is more reactive at higher pH.

When H_2O_2 is present, 2-naphthylboronic acid is oxidatively converted to 2-naphthol (Scheme 39a), and the fluorescence is reduced at 340 nm and red-shifted to 410 nm from pH 7.2 to 9.7, when excited at 290 nm (Figure 11).

Fluorescence was confirmed to be due to the generation of 2-napthol by comparison with spectroscopic properties of an authentic sample. *i.e.* The emission maxima for 2-naphthol (10 μM, pK_a = 9.51) was found at 340 nm in pH 7.20 PBS buffer while the maxima shifted to 410 nm in pH 9.70 alkaline buffer (Figure 11). These results demonstrate the proton-induced fluorescence switching of 2-naphthol[204] at pH 7.20 and the electron donation of the negative oxygen to the fluorophore causing the red-shift at pH 9.70.

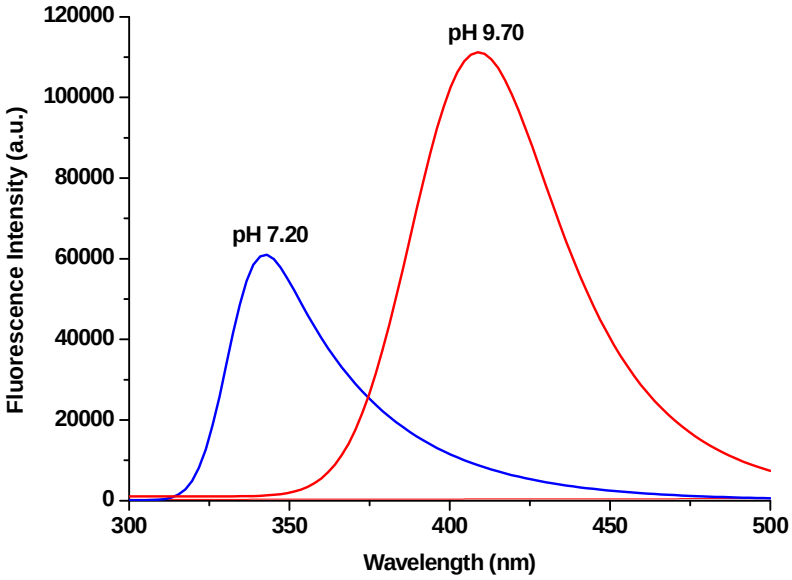

Figure 11. *Fluorescence spectra of 2-naphthol (10 μM) with excitation at 290 nm. The mixture was incubated in pH 7.20 PBS buffer and pH 9.70 $NaCO_3$/$NaHCO_3$ buffer at 25 ºC.*

2.4.2 "INSULATED" SYSTEM OF *N*-METHYL-*O* -(AMINOMETHYL)PHENYLBORONIC ACID

In 1994, Shinkai and James reported a novel photoinduced electron-transfer fluorescence sensor for saccharide detection on the interaction of boronic acid and amine. As observed, the boronic acid derivative *N*-methyl-*o*-(aminomethyl) phenylboronic acid displays a remarkable fluorescence enhancement over a large pH range in aqueous media upon saccharide connection. As can be seen from Figure 12a, addition of saccharide (D-fructose was chosen, 100 mM) led to fluorescence increase of probe **100** (10 μM) to I (in the presence of saccharide)/I_0 (in the absence of saccharide) = *ca.* 2.2 at the maxima emission 410 nm. While in the pH 9.7 media from Figure 12b, the value of I/I_0 was grown up to *ca.* 4.2 since there is a much stronger association between boronic acid and D-fructose in a higher pH condition. Also, we can observe the lower fluorescence intensity of free boronic acid **100** (FL = 150000 in pH 7.2 while FL = 50000 in pH 9.7) and **100**-D-fructose (FL = 330000 in pH 7.2 while FL = 210000 in pH 9.7) in the same concentration due to stronger PET with increasing of pH.

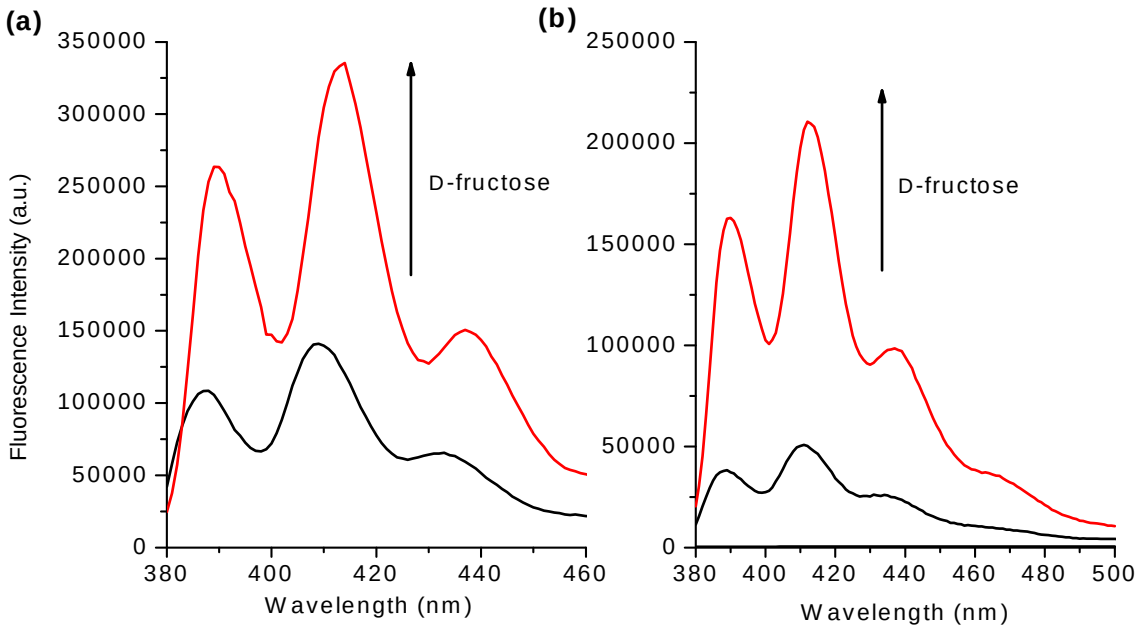

Figure 12. *(a) Fluorescent spectra changes for probe **100** (10 μM) and **100**-D-fructose (100 mM) complex. The mixture was incubated in pH 7.20 PBS buffer at 25 ºC with excitation at 370 nm; (b) Fluorescent spectra changes for probe **100** (10 μM) and **100**-D-fructose (100 mM) complex. The mixture was incubated in pH 9.70 Na_2CO_3/$NaHCO_3$ buffer at 25 ºC with excitation at 370 nm.*

Next, we investigated the sensing property of *N*-methyl-*o*-(aminomethyl) phenylboronic acid towards H_2O_2 in the absence of saccharide. When aromatic boronic acid was oxidized into phenol, the PET from amine would become much stronger which inhibited the emission of the anthracene fluorophore. This is most probably due to the broken of weaker N-B interaction after reaction with H_2O_2 in the system.

As can be revealed by Figure 13, presence of H_2O_2 (0.5 mM) led to almost 4-fold fluorescence drop down of the probe **100** (10 μM) over through 3 h in a neutral buffer. For the unbound *N*-methyl-*o*-(aminomethyl) phenylboronic acid probe, we also studied its properties of reaction speed in various concentrations of H_2O_2 under neutral condition (Figure 13b). Three sorts of H_2O_2 concentration solutions were selected, which are 0.05 mM, 0.10 mM, 0.50 mM, respectively. As can be revealed from Figure 13, the fluorescence intensity of probe **100** (10 μM) dropped down to different levels F_T/F_0 = *ca.* 0.55 (k' = 0.023 min^{-1}), *ca.* 0.40 (k' = 0.007 min^{-1}), *ca.* 0.25 (k' = 0.004 min^{-1}), separately, on expose to the selected concentration of H_2O_2 solutions over the observed time (180 min). Apparently, with the increasing concentration of H_2O_2, the boronic acid moiety can be oxidized even faster for the reaction between probe **100** and hydrogen peroxide.

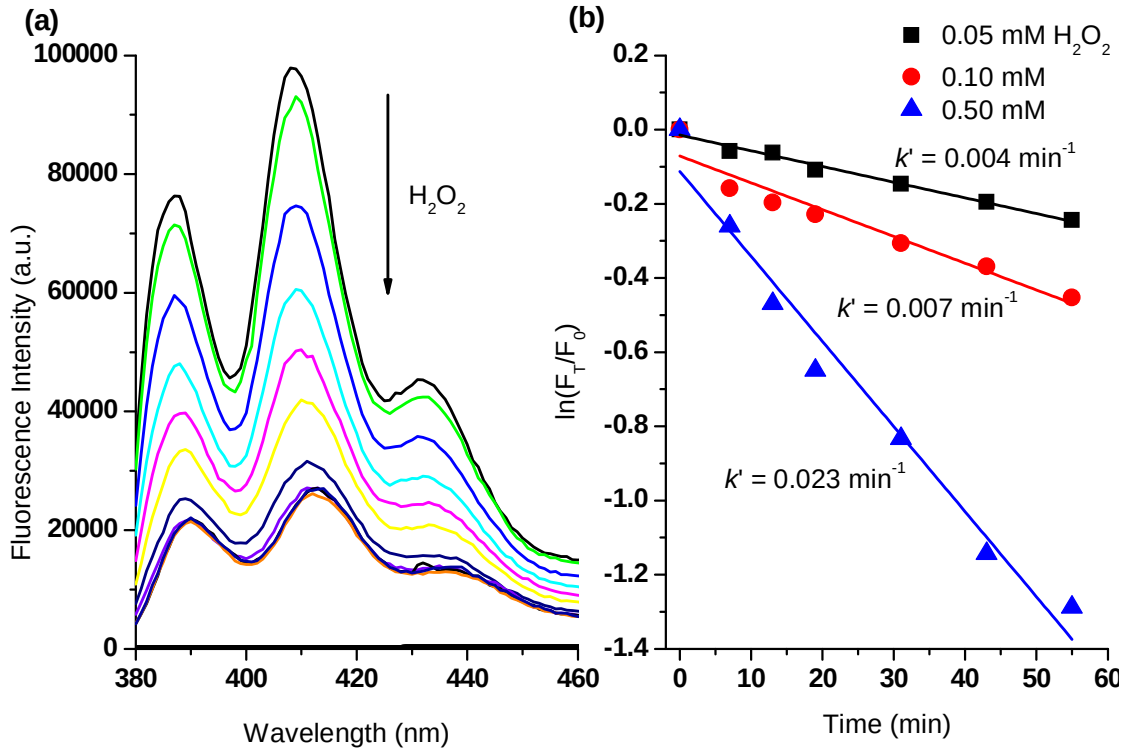

Figure 13. *(a) Time curve of fluorescent spectra changes for probe **100** (10 μM) upon adding H_2O_2 (0.50 mM, 0, 1, 6, 12, 18, 30, 42, 54, 84, 114, 144, 174 min); (b) Plots of F_T/F_0 upon addition of H_2O_2 (Square - 0.05 mM, Round - 0.10 mM, Up triangle - 0.50 mM). The mixture was incubated in pH 7.20 PBS buffer at 25 ºC. Fluorescence intensities at 410 nm were measured with excitation at 370 nm.*

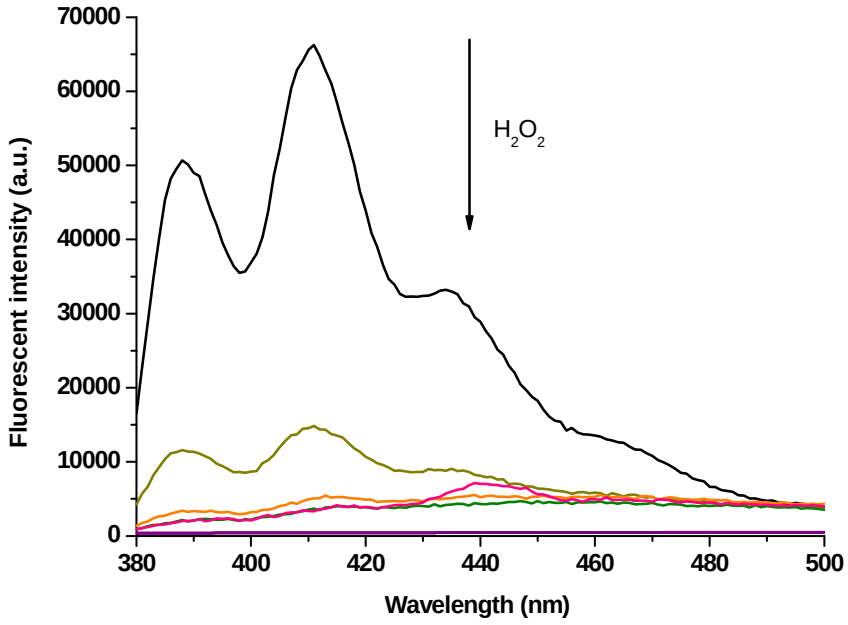

Figure 14. *Time curve of fluorescent spectra changes for probe **100** (10 μM) with addition of H_2O_2 (0.02 mM, 0, 0.5, 1, 6, 10 min). The mixture was incubated in pH 9.70 $Na_2CO_3/NaHCO_3$bufferat 25 ºC with excitation at 370 nm.*

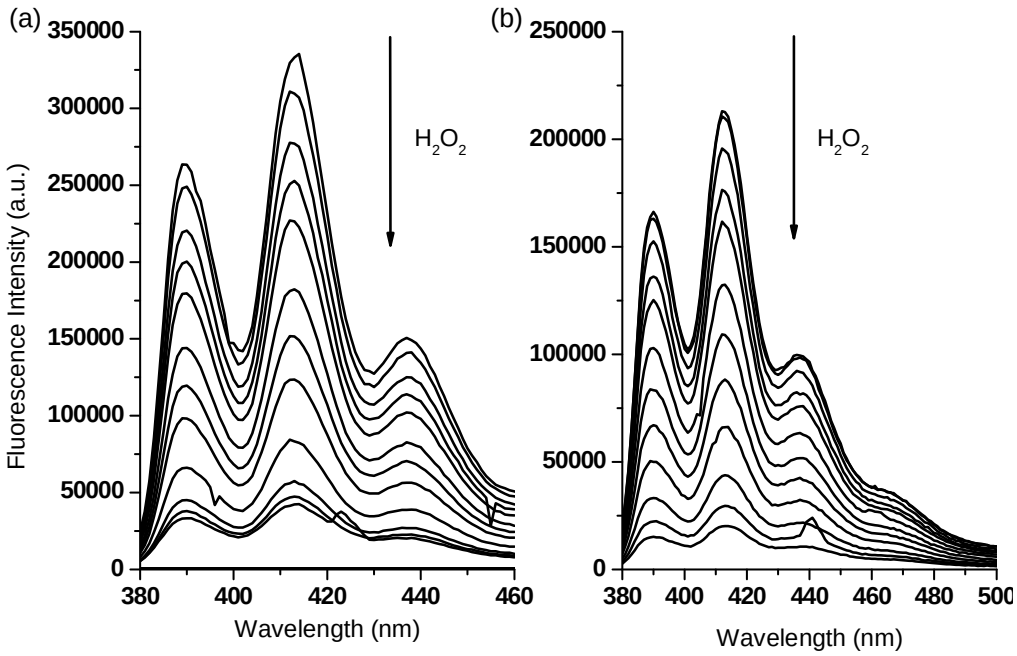

Figure 15. *(a) Time curves of fluorescent spectra changes for **100**-D-fructose complex with addition of H_2O_2 (0.50 mM, 0, 1, 6, 12, 18, 30, 42, 54, 84, 114, 144, 174 min). The mixture was incubated in pH 7.20 PBS buffer at 25 ºC with excitation at 370 nm. (b) Time curves of fluorescent spectra changes for **95**-D-fructose complex with addition of H_2O_2 (0.05 mM, 0, 1, 6, 12, 18, 30, 42, 54, 84, 114, 144, 174 min). The mixture was incubated in pH 9.70 Na_2CO_3/$NaHCO_3$ buffer at 25 ºC with excitation at 370 nm.*

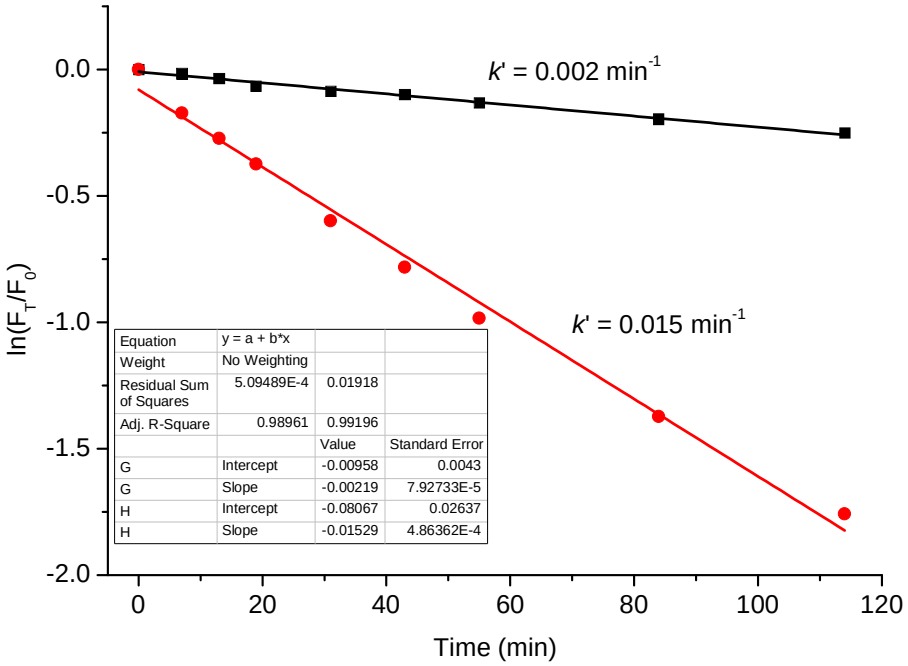

Figure 16. *Time curve of fluorescent spectra changes for **100**-D-fructose complex in various concentrations of H_2O_2 (Square - 0.05 mM, Round - 0.50 mM). The mixture was incubated in pH 7.20 PBS buffer at 25 ºC. Fluorescence intensities at 410 nm were measured with excitation at 370 nm.*

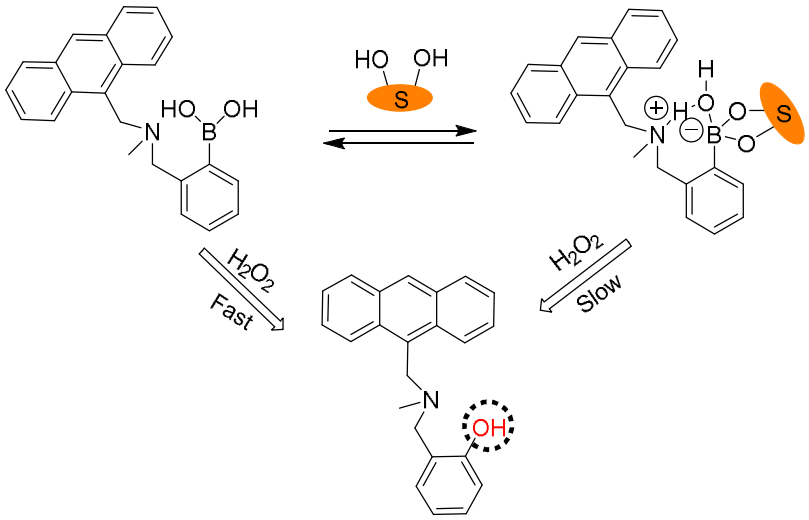

(a)

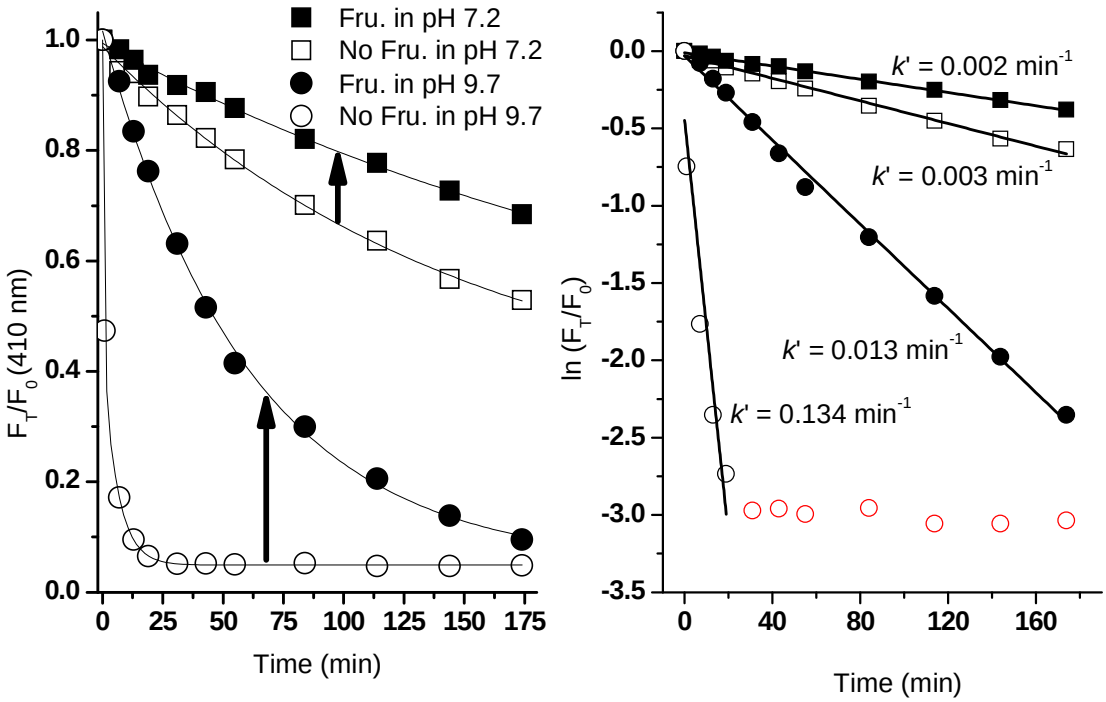

(b)

Figure 17. *(a) Proposed strategy of probe **100** and **100**-D-fructose complex for sensing of H_2O_2; (b) Time curve of fluorescence intensity changes with probe **95** (10 μM) and D-fructose (100 mM) in aqueous H_2O_2 (0.05 mM for the first three samples and 0.02 mM for last sample). (Solid Square - **100**-D-fructose and Empty Square - **100** in pH 7.20; Solid circle - **100**-D-fructose and Empty circle - **100** in pH 9.70). The mixture was incubated in pH 7.20 PBS buffer and pH 9.70 $Na_2CO_3/NaHCO_3$ buffer at 25 ºC. Fluorescence intensities at 410 nm were measured with excitation at 370nm.*

To summarize, in the case of *N*-methyl-*o*-(aminomethyl) phenylboronic acid (**100**), a significant "off-on" signal response has been seen on binding with D-fructose (Figure 12)

due to a PET mechanism.[71] However, when the arylboronic acid moiety of probe **100** was transformed into a phenol upon adding H_2O_2, the fluorescence was further reduced due to the stronger PET from the amine in the boron free system both in neutral and alkaline condition (Figure 13, 14, 15, 16).

The reaction scheme and fluorescence intensity changes for fluorescent probe **100** and the **100**-D-fructose complex in pH 7.20 and 9.70 buffer are given in Figure 17. From Figure 17b, it can be seen that the fluorescence intensity ratios with time (F_T/F_0) of **100**-D-fructose complex slowly change to *ca*. 0.72 (*k*' = 0.002 min^{-1}), while for the saccharide free system a bigger change F_T/F_0 = *ca*. 0.55 (*k*' = 0.003 min^{-1}) on addition of 0.05 mM H_2O_2 over three hours in pH 7.20 PBS buffer (probe **100**, 10 μM). The difference between **100** and the **100**-D-fructose (*k*' = 0.013 min^{-1}) complex towards H_2O_2 became much larger in pH 9.70 buffer solution with F_T/F_0 = *ca*. 0.05 (*k*' = 0.134 min^{-1}) within 20 min upon addition of only 0.02 mM H_2O_2 (Figure 14, Figure 17).[205] More importantly, the signal to noise ratio output of probe **100** was enhanced through binding with saccharide, allowing colorimetric detection (bright blue to colourless) in the reaction with H_2O_2 (Figure 18).

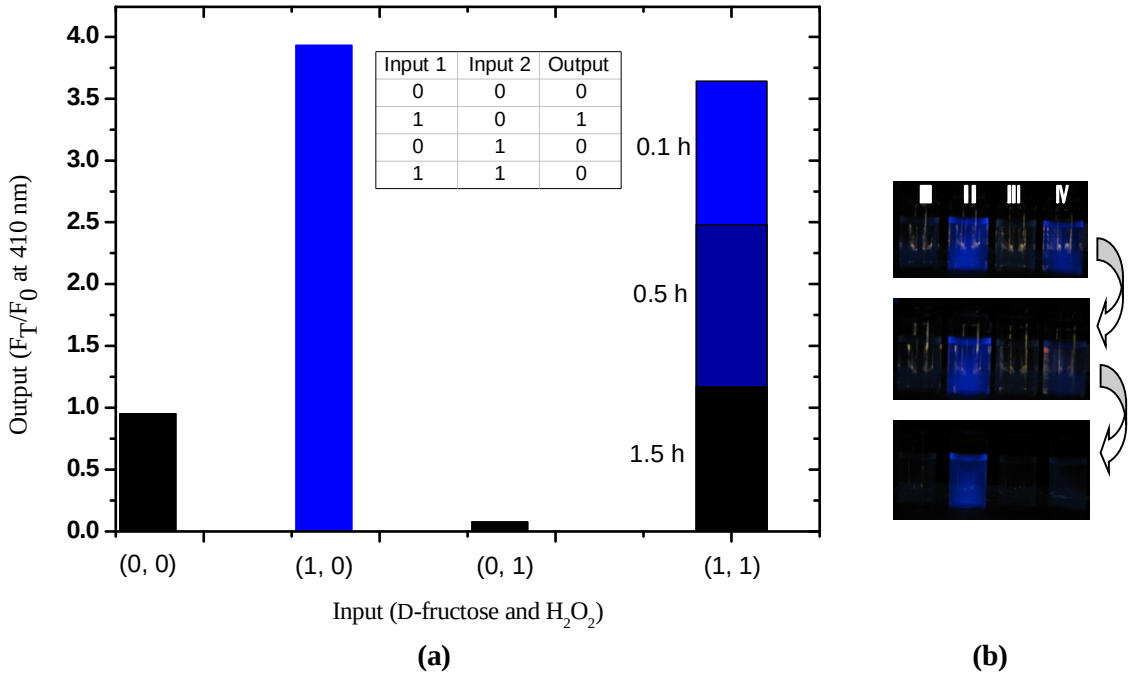

Figure 18. *(**a**) Column spectra and truth table with D-fructose (100 mM) and H_2O_2 (0.05 mM) as inputs; (**b**) Fluorescent colourimetric detection using naked eye with I (probe **100** only); II (+ D-fructose 100 mM); III (+ H_2O_2 0.10 mM); IV (+ D-fructose 100 mM + H_2O_2 0.10 mM) after 0.1 h, 0.5 h, 1.0 h. The mixture was incubated in pH 9.70 $Na_2CO_3/NaHCO_3$ buffer at 25 ºC. Fluorescence intensities at 410 nm were measured with excitation at 370 nm.*

The fluorescence of **100** is turned on by saccharide binding, since boronic ester formation causes an enhanced interaction between the neighbouring amine and the boron atom (mediated *via* an inserted solvent molecule).[69, 194, 76] This N-B interaction hinders the reaction between boron and H_2O_2 in the presence of saccharides resulting in a slower decrease in fluorescence. (*cf.* saccharide free system)

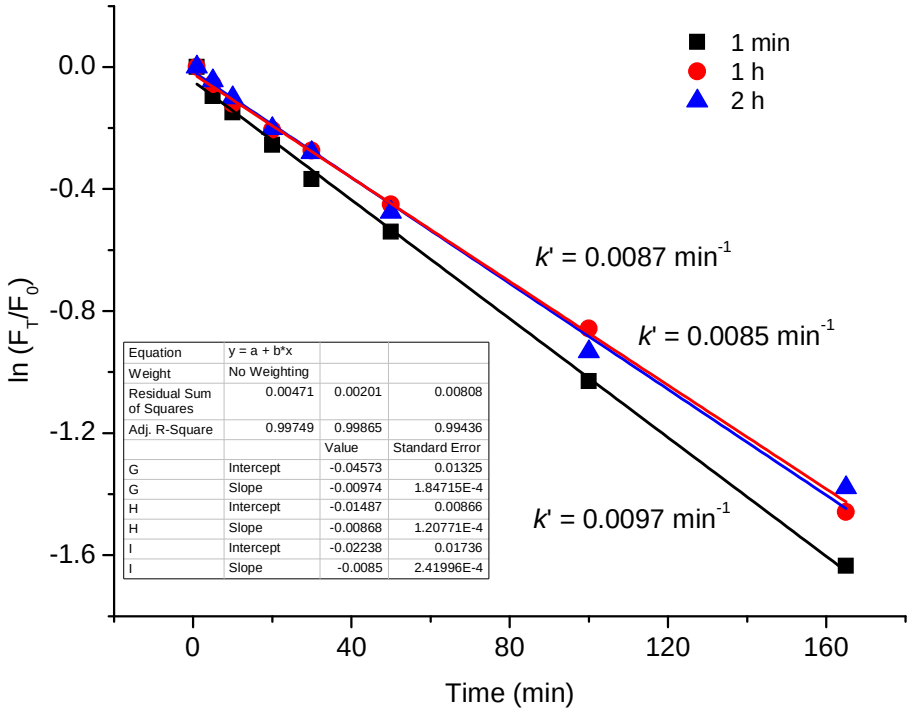

Figure 19. *Time curve of fluorescence intensity changes with probe **100** (10 μM) and D-fructose (100 mM) in aqueous H_2O_2 (0.05 mM). (Black circle – H_2O_2 in pH 9.70 buffer that was left for 1 min before adding probe **100**, Red circle – H_2O_2 in pH 9.70 buffer that was left for 1 h before adding probe **100**, Pinkcircle – H_2O_2 in pH 9.70 buffer that was left for 2 h before adding probe **100**). The mixture was incubated in pH 9.70 Na_2CO_3/$NaHCO_3$ buffer at 25 ºC. Fluorescence intensities at 418 nm were measured with excitation at 370 nm.*

Given that the reactions take time to reach completion we confirmed that H_2O_2 is stable in a higher pH buffer (i.e. pH 9.70) at 25 ºC for two hours (Figure 19). The experiment below verified the outcome through the reaction between boronic acid–D-fructose complex (10 μM) and H_2O_2 (0.05 mM). Firstly, the same concentrations of aqueous H_2O_2 solutions were kept stirring in pH 9.7 buffers for 0 h, 1 h and 2 h, respectively, and it can be seen that the fluorescence intensity ratios (F_T/F_0) of the **100**-D-fructose complexes changed to *ca.* 0.20 (k' = 0.0087 min^{-1}, k' = 0.0085 min^{-1}, k' = 0.0097 min^{-1}) in the three different cases of H_2O_2 (0.05 mM, 0 h, 1 h, 2 h) over through 120 min. That's to say, in alkaline condition, the reactivity of H_2O_2 can be kept stable for at least two hours.

2.4.3 LOGIC GATE SYSTEM

Nowadays, it is of high interest to develop molecular logic gate system through processing input information and generating output signal.[206] In the present work, both D-fructose and H_2O_2 could lead to changes in emission characteristics which makes probe **99** and **100** as potential logic gates.

In the case of 2-naphthylboronic acid, the system follows the combination mode of "fluorophore-receptor" conjugate while D-fructose and H_2O_2 function as input signals and the ratio of F_T/F_0 at 340 nm as output signal. The processed data demonstrated the logic relationships among them. Interestingly, the single molecule showed different logic relationships, a "NOR"[207] gate in neutral buffer and an "INHIBIT" gate in alkaline condition, respectively.

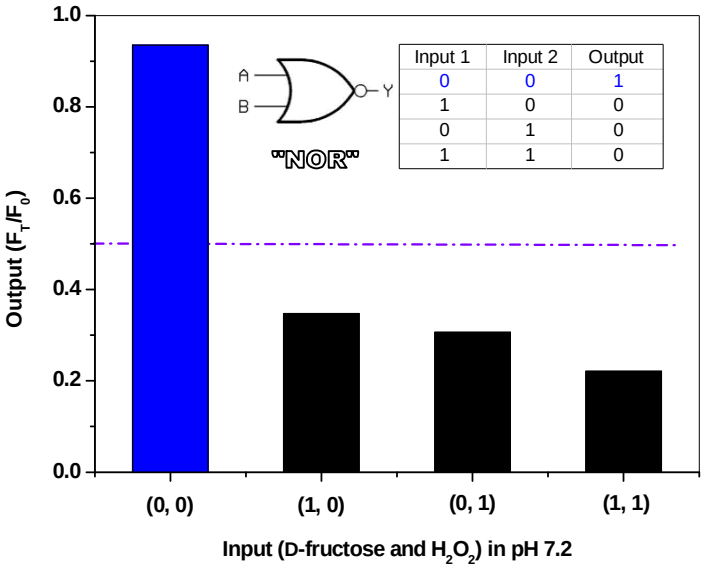

Figure 20. *"NOR" logic gate of probe* **99** *with D-fructose and H_2O_2 as inputs in pH 7.2*

Initially, in the presence of H_2O_2 (1.0 mM) and D-fructose (100 mM), the fluorescence output signals of probe **99** (10 µM) with F_T/F_0 at 340 nm were only *ca.* 0.30 and *ca.* 0.35, respectively in pH 7.20 buffer. Subsequently, the concurrence of them led to much higher fluorescence decrease to *ca.* 0.20. The strong fluorescence of free probe **99** and the low fluorescent signals in the presence of H_2O_2 and D-fructose generate a low output threshold level F_T/F_0 = 0.4 of the highest fluorescent intensity. Figure 20 summarises the performance of the "NOR" gate function and truthtable. (0 = off, 1 =

on). Clearly, only in the absence of D-fructose and H_2O_2, the fluorescence ratio of 2-naphthylboronic acid can be kept at a high level (F_T/F_0 = *ca.* 0.92).

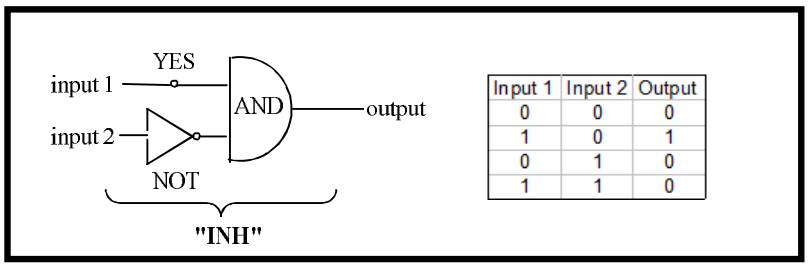

Figure 21. *"INH" logic gate of probe* **99** *with D-fructose and H_2O_2 as inputs in pH 9.7.*

While, in pH 9.70 condition, the logic relationship of probe **99** in the absence and presence of H_2O_2 and D-fructose can be explained in terms of "INHIBIT" gate due to the only induced fluorescence increase by D-fructose. As has been revealed by Figure 21, the signal was enlarged to F_T/F_0 = *ca.* 2.70 when adding D-fructose (100 mM) into the solution of probe **99** (10 μM). Without the input of H_2O_2 and D-fructose, slight fluorescence decreasing can be seen with F_T/F_0 = *ca.* 0.90 over the observed time. In the states of (0, 1) and (1, 1) where H_2O_2 (0.1 mM) was involved in the system, the fluorescence intensities dropped down to *ca.* 0.60 and *ca.* 0.80 (F_T/F_0). Therefore, it is a typical "INHIBIT" logic system with *ca.*1.20 as the threshold level.

In the case of *N*-methyl-*o*-(aminomethyl) phenylboronic acid, the system follows the combination mode of "fluorophore-spacer-receptor" conjugate while D-fructose and H_2O_2 function as input signals and the ratio of F_T/F_0 at 410 nm as output signal. The processed data demonstrated the logic relationships among them.

Like the demonstration of probe **99** in pH 9.70, the logic relationship of probe **100** in the absence and presence of H_2O_2 and D-fructose can be explained in terms of "INHIBIT" gate due to the only induced fluorescence increase by D-fructose both in neutral and alkaline conditions. Herein, we take the logic relationship in alkaline solution as a typical example. As has been revealed by Figure 12, the signal was enlarged to F_T/F_0 = *ca.* 3.8 when adding D-fructose (100 mM) into the solution of probe **100** (10 μM). Without the input of H_2O_2 and D-fructose, slight fluorescence decreasing can be seen with F_T/F_0 = *ca.* 0.95 over the observed time. In the states of (0, 1) and (1, 1) where H_2O_2 (0.1 mM) was involved in the system, the fluorescence intensities dropped down to *ca.* 0.05 and *ca.* 0.10 (F_T/F_0). Therefore, it is a typical "INHIBIT" logic system with *ca.*1.0 as the threshold level.

2.5 CONCLUSION

In conclusion, D-fructose effects the reaction of integrated (compound **99**) and insulated (compound **100**) boronic acid-based fluorescent probes with hydrogen peroxide in opposite directions. Integrated boronic acid fluorophores (compound **99**) display enhanced reactivity with H_2O_2 in the presence of D-fructose. While the PET fluorophore systems (compound **100**) display reduced reactivity with H_2O_2 in the presence of D-fructose. The insulated PET system (compound **100**) are particularly interesting, because in the presence of D-fructose the initial fluorescence intensity is much higher and produces a blue visible fluorescence, which implies that they could be used as temporal fluorescent probes to map both intracellular H_2O_2 and saccharide concentrations. The insulated systems also produce a larger fluorescence response in low concentrations of H_2O_2. Therefore, we believe that insulated (PET) systems are the fluorescent probes of choice for use as imaging agents and sensors for H_2O_2.

Meanwhile, we found the two different systems could also function as different logic gates with D-fructose and H_2O_2 as signal input, “NOR” gate in pH 7.2 and “INH” gate in pH 9.7 for compound **99** while it is “INH” gate for compound **100** both in low and high pH condition.

This work has been published: *X, Sun, S.-Y. Xu, S. E. Flower, J. S. Fossey, X. Qian and T. D. James, "Integrated" and "insulated" boronate-based fluorescent probes for the detection of hydrogen peroxide. Chem. Commun., 2013,* ***49****, 8311-8313 (Front cover, Reported in various scientific media, UK, top 10 paper assessed by Chem.Commun.)*

Chapter Three: RESULTS AND DISCUSSION II

[Image removed for copyright reasons]

3. RESULTS AND DISCUSSION II

3.1 BACKGROUND

Peroxynitrite ($ONOO^-$) – a product combining nitric oxide with superoxide radical anion – has been known as a strong oxidant in physiological and pathological processes. It was first discovered as a biological endogenous oxidant in 1990.[208] Under physiological conditions, peroxynitrite is also a highly reactive molecule with a very short lifetime (~10 ms) involved in cell signal transduction[209] and apoptosis in HL-60 cells,[210] and PC-12 cells.[211] Many biomolecules are oxidized and/or nitrated by peroxynitrite-derived radicals, including DNA, tyrosine residues, thiols, and unsaturated fatty-acid-containing phospholipids.[212] In the last decades, researchers have found many *in vivo* diseases were caused due to peroxynitrite, which included cardiac diseases,[213] vascular diseases,[214] circulatory shock,[215] local inflammation,[216] cancer,[217] stroke,[218] neurodegenerative disorders,[219] diabetes and diabetic complications.[220] Peroxynitrite formation has been implicated in Alzheimer's disease, Parkinson's disease, Huntington's disease, amyotrophic lateral sclerosis, viral myocarditis, septic shock, cardiac allograft, idiopathic dilated cardiomyopathy, atrial fibrillation, hypercholesterolemia, atherosclerosis, hypertension, diabete and traumatic brain injury.[219, 221, 222] Recently, peroxynitrite was found as a key trigger of skeletal muscle hypertrophy *via* activation of calcium signalling.[223]

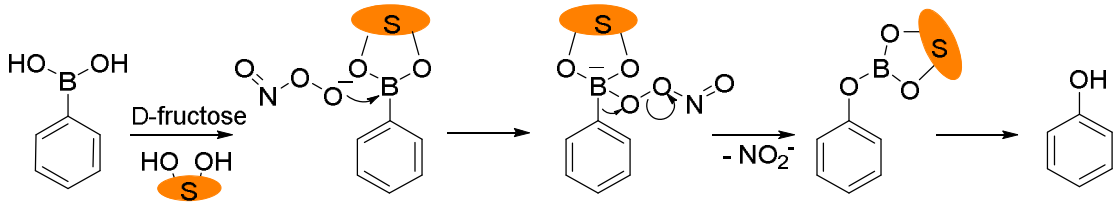

Scheme 40. *The reaction mechanism between a generic aryl boronic acid/ester and* $ONOO^-$.

Synthetic fluorescent probes have the potential to be powerful tools for peroxynitrite detection since they can measure intracellular $ONOO^-$ directly.[121] Working towards the fluorescent detection of peroxynitrite, Yang *et al.* developed a range of chemo-sensors in which $ONOO^-$ reacts with activated ketones to form dioxiranes,[185-187] and Yang and Qian have also designed a three-channel fluorescent probe capable of distinguishing peroxynitrite from hypochlorite.[188] Recently, Ai *et al.* reported a genetically encoded

fluorescent probe for the detection of peroxynitrite.[191] However, it still remains a great challenge using small-molecular fluorescent probes to detect $ONOO^-$ selectively and sensitively amongst the large number of biologically relevant reactive oxygen and nitrogen species (*e.g.* H_2O_2 and ClO^-).

In the fluorescent detection of H_2O_2, Chang and co-workers have also developed a series of boronate-based derivatives for the fluorescent detection of H_2O_2 in living systems.[60-62, 64, 65, 111-115, 224] However, Kalyanaraman *et al.* reported that boronate probes can be taken as diagnostic tools for real time monitoring of peroxynitrite and hydroperoxides.[110, 117] The findings indicate that general boronate-based probes hardly distinguish apart these two species since both of them can react with the boronate moiety to generate the same product. Essentially, this implies that it is crucial to design new fluorescent probes with special structures to break the barrier (Scheme 41).

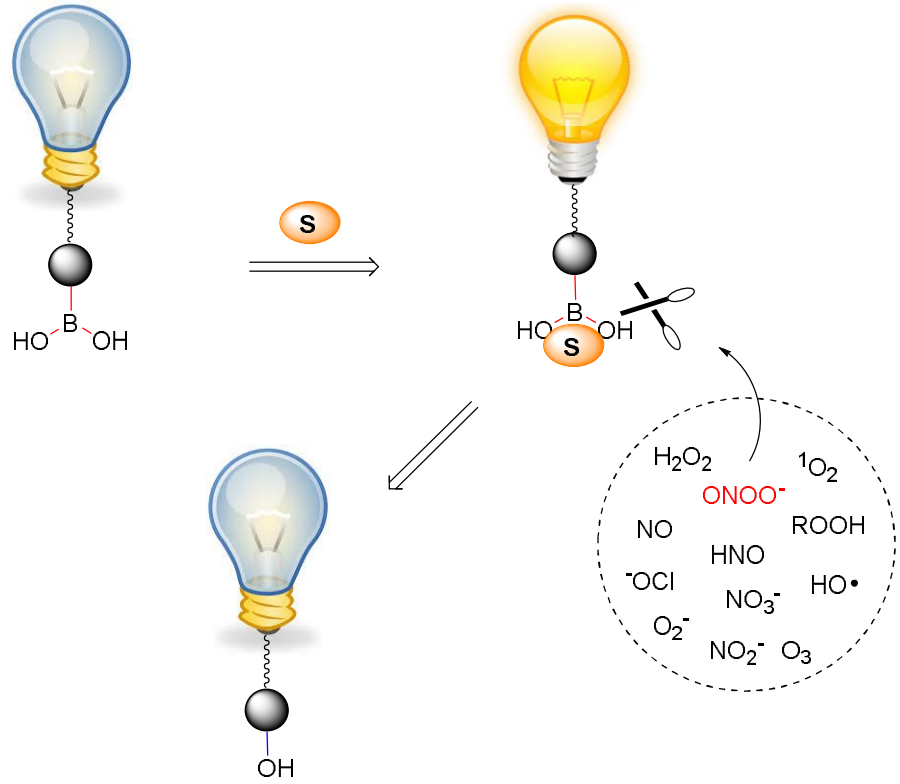

Scheme 41. *Schematic representation of the designed fluorogenic sensors for detection of peroxynitrite.*

We also have a long-standing interest in boronic acids for monosaccharide and anion detection,[40, 193, 194] and have found that boronic acid derivatives rapidly and reversibly interact with saccharides in aqueous media. In the previous work, we investigated the

reaction of "integrated" and "insulated" boronate-based fluorescent probes with hydrogen peroxide (pK_a = 11.6) in the presence of monosaccharide.[225] From the previous research, we found that boronic ester formation causes an enhanced interaction between the neighbouring amine and the boron atom. This N-B interaction[69] (whether direct or *via* solvent insertion) hinders the reaction between boron and H_2O_2 in the presence of saccharides resulting in a much slower decrease in fluorescence intensity. (*cf.* saccharide free system).

It is known that $ONOO^-$ (pK_a = 6.8) - a strong nucleophile - reacts rapidly and stoichiometrically with aromatic boronate derivatives ($K \sim 10^6\ M^{-1}S^{-1}$ at pH 7.4, Scheme 39).[110, 117,226] From this observation and our previous results, we wondered if a powerful nucleophile such as $ONOO^-$ could overcome the protection given to the boron atom by the N-B interaction in the "insulated" probes. Therefore, we reasoned that it would be possible to develop novel boronate-based "insulated" probes for the selective intracellular mapping of peroxynitrite in the presence of monosaccharide (D-fructose was chosen as a model saccharide since it has a high binding affinity, 4400 mol^{-1})[194].

3.2 DESIGN STRATEGY

3.2.1 GENERAL IDEAS

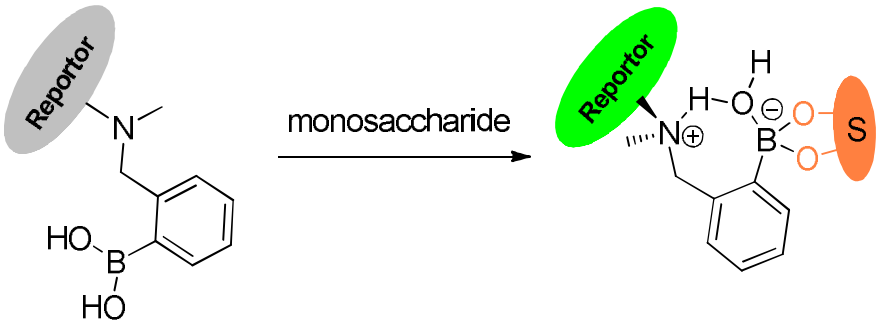

Scheme 42. *Binding mode between monosaccharides and boronic acids in a solvent-inserted N-B interaction.*

In our design strategy, it is a method of detecting peroxynitrite in a sample comprising the steps of

(a) Providing a complex of a saccharide with an aryl boronate compound in a formula (I):

$$F - L_1 - N(R) - L_2 - Ar - B(OH)_2 \qquad (I)$$

Wherein:

F is a fluorophore;

L_1 and L_2 are linker groups;

R is H or optionally substituted alkyl;

Ar is optionally substituted aryl;

(b) Contacting said aryl boronate – saccharide complex with said sample, whereby $ONOO^-$ in said sample cleaves said boronate – saccharide complex to generate a compound in a formula (II):

$$F - L_1 - N(R) - L_2 - Ar - OH \qquad (II)$$

(c) Detecting a decrease in a fluorescence intensity of said fluorophore resulting from said cleavage reaction in step (b).

Wherein, L_1 and L_2 are independently selected from saturated or unsaturated, linear or branched aliphatic chains including 1-6 carbon atoms, preferably 0, 1 or 2 carbon atoms;

Wherein, R is optionally substituted C1 - C7 alkyl, preferably methyl; Wherein, said Ar group is optionally substituted phenyl, and said L_2 and -$B(OH)_2$ groups are *ortho* positioned on said phenyl group.

Said step (a) comprises reacting said arylboronate of Formula (I) with a saccharide in solution to form a solution of said complex, and said step (b) comprises mixing said solution with said sample.

A kit for detecting peroxynitrite by a method according to any preceding claim, comprising either (i) an arylboronate of Formula (I) and a saccharide in separately packaged form, or (ii) a complex of an arylboronate of Formula (I) and a saccharide in packaged form.

3.2.2 PET-BASED PROBES DESIGN

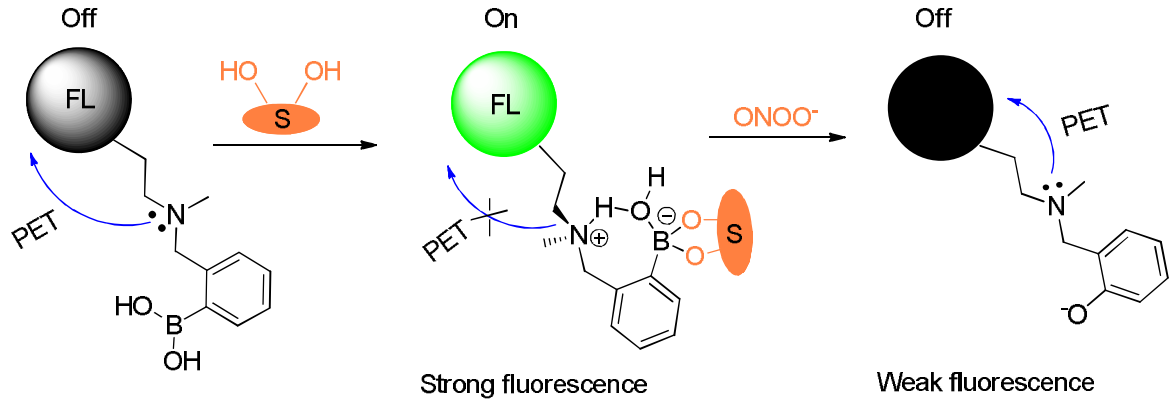

Scheme 43. *Schematic design of the B-N model compounds.*

Probe **101** (λ_{abs} = 440 nm, ε = 9500 $M^{-1}cm^{-1}$, Scheme 44) was designed based on PET mechanism and the introduction of hydroxyethoxyl side chain not only improves its water-solubility, but also provides a potential route to develop polymer bound receptor.[227] Probe **101** was synthesised in three steps starting from 4-bromo-1, 8-naphthalic anhydride in 24% overall yield.[227]

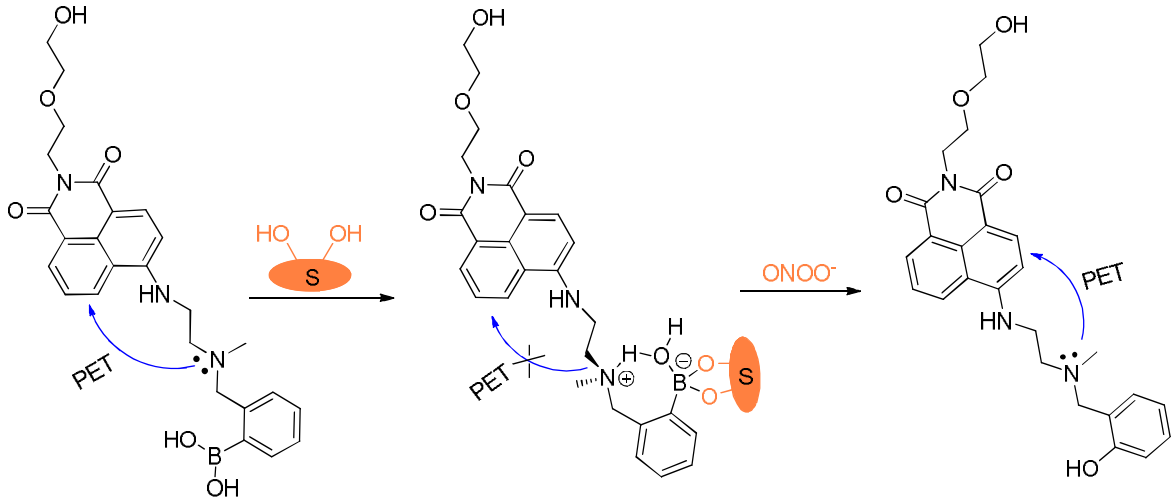

101 **101**-D-fructose Weak fluorescence

Scheme 44. *Design strategy of probe **101** for the detection of peroxynitrite in the presence of D-fructose.*

In addition, functional *N*-substituted-1,8-naphthalimide derivatives have been successfully employed as DNA targeting, anticancer and cellular imaging agents.[228, 229] Due to its good photophysical and photochemical properties, *N*-substituted-1,8-naphthalimide is widely recognizable as an excellent D-π-A chromophore with which herein can be a promising reporter in the design of fluorescence probes. Thus, they have been employed as versatile platforms to develop sensors due to its advantageous optical properties, including strong absorption and emission in the visible region, large Stokes shifts, and high photostability *etc.*[230] In addition, they have relatively simple structures for which facile and straightforward syntheses can be realized.

The boronic acid moiety is widely recognized as an excellent binding node able to connect monosaccharides with fluorescent probe. Notably, boronic acids are an excellent molecular receptor for monosaccharides since boronic acid derivatives rapidly and reversibly interact with saccharides in aqueous media, thus consuming no analytes. The chemical and biological significance of the interaction between boronic acid and saccharides has been used widely for the study of saccharides detection *via* fluorescence tools.[194, 231] In our case, the signal of the fluorophore *N*-substituted-1, 8-naphthalimide can be modulated through N-B interaction when binding with monosaccharide. The "insulated" system displays an "off-on" response towards D-fructose due to the enhanced N-B interaction (Scheme 44).[71]

The formed monosaccharide complex shows a stronger fluorescence signal than the original system, which can be used a novel fluorescence sensing probe towards other substrates, such as ROS/RNS, fluoride and sulfenic acids.

Furthermore, we decided to evaluate the fluorescence property of the monosaccharide complex **101**-D-fructose towards peroxynitrite *in vitro* and also *in vivo* cellular imaging for the endogenous and exogenous produced peroxynitrite.

3.2.3 ICT-BASED PROBES DESIGN

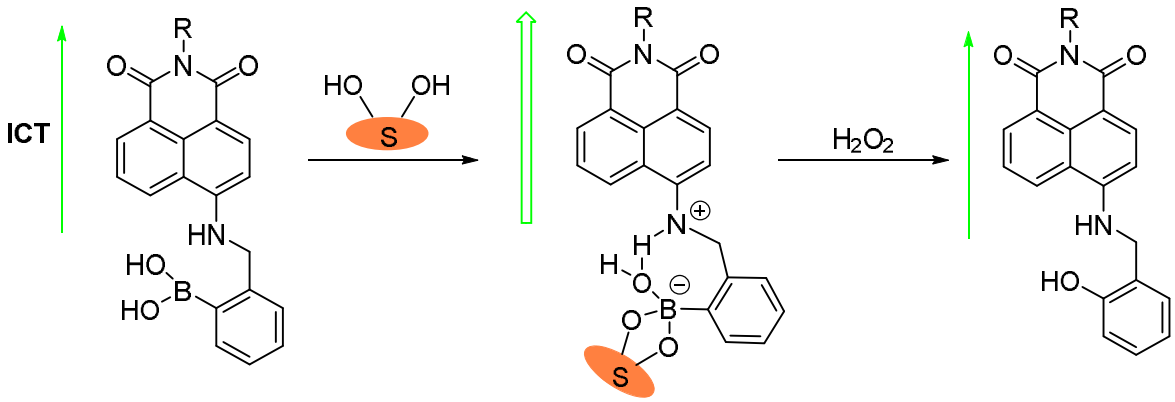

102a: R = Bn
102b: R = *n*-Propyl

Strong FL

Weak FL

Scheme 45. *Mechanism of reaction between probe **102** and hydrogen peroxide in the presence of D-fructose.*

Since the utility of the boron-amine interaction in the design of fluorescent probes, the majority of the systems were developed on the basis of the PET mechanism. The enhanced emission of the fluorophore was caused by the inhibition of PET from amine due to the stronger B-N interaction on account of the saccharide linkage. The discovery of the B-N protection in the selective detection of peroxynitrite has been discussed and proved in the examples above. Therefore, we reasoned that it would be possible to develop new sensing probe by using the strategy. In the series of *N*-substituted-1,8-naphthalimide derivatives, as a key part of the ICT system, amine served as the electron donor and has been functionalized into various sensing system. Bearing this in mind, we developed new boronated-based "insulated" systems with amine as one part of the signal moiety (Scheme 45). The interaction between boron and amine will have an effect on the "donor–acceptor" ICT system in the presence of monosaccharide. Next, we

decided to investigate its sensing property for the detection of hydrogen peroxide and peroxynitrite.

3.3 RESULTS AND DISCUSSION

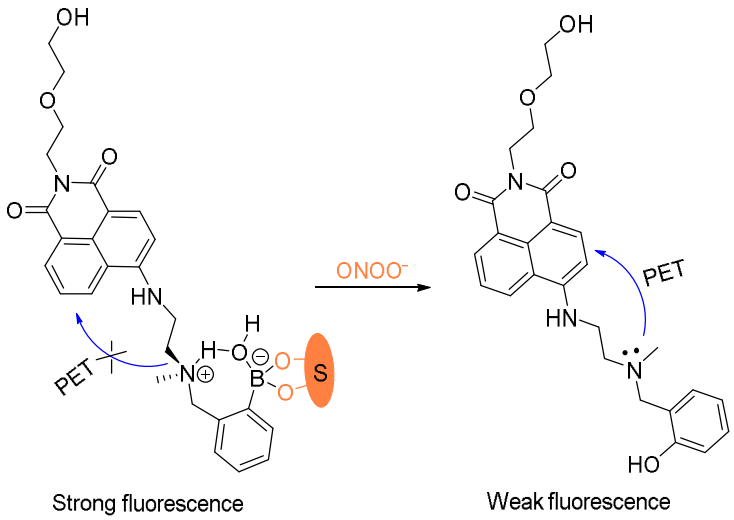

Scheme 46. *Fluorescent detection of peroxynitrite based on PET system.*

3.3.1 pH TITRATION

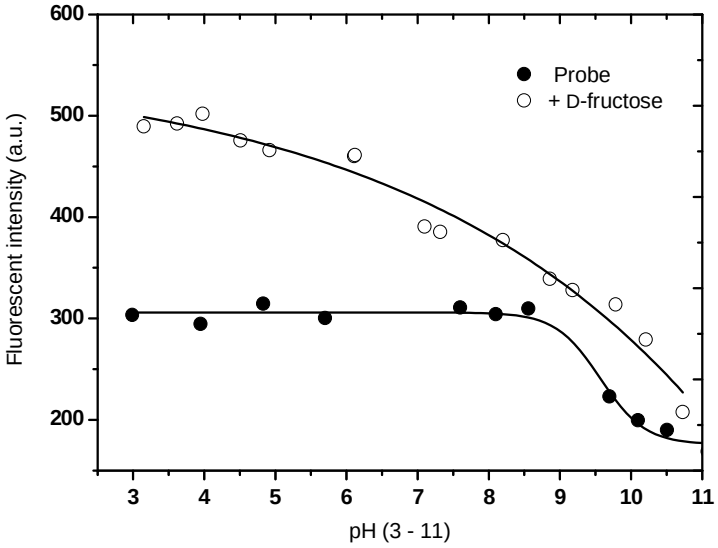

Figure 22. *pH titration of probe **101** (2 µM) and **101**-D-fructose (probe **101**, 2 µM; D-fructose, 100 mM), modulating by utilizing aqueous hydrochloric acid (1.2 N) and sodium hydroxide solution (1 N).*

We carried out a pH titration to evaluate the pH effect on the fluorescence of probe **101** (2 µM). As shown by Figure 22, the fluorescence intensity of the probe **101** decreased at pH values above 8.0. While, in the range between 3.0 and 8.0, the pH change had hardly any effect on the fluorescence intensity. Thus, the probe can be expected to work well

under a physiological condition (pH 7.30, PBS buffer). In the presence of D-fructose (100 mM), the fluorescence of the formed **101**-D-fructose complex increases due to the enhanced N-B interaction at different pH values. The fluorescence of the **101**-D-fructose complex displayed a downwards trend over a pH range of 3-11.

3.3.2 UV-VIS SPECTRA TOWARD $ONOO^-$

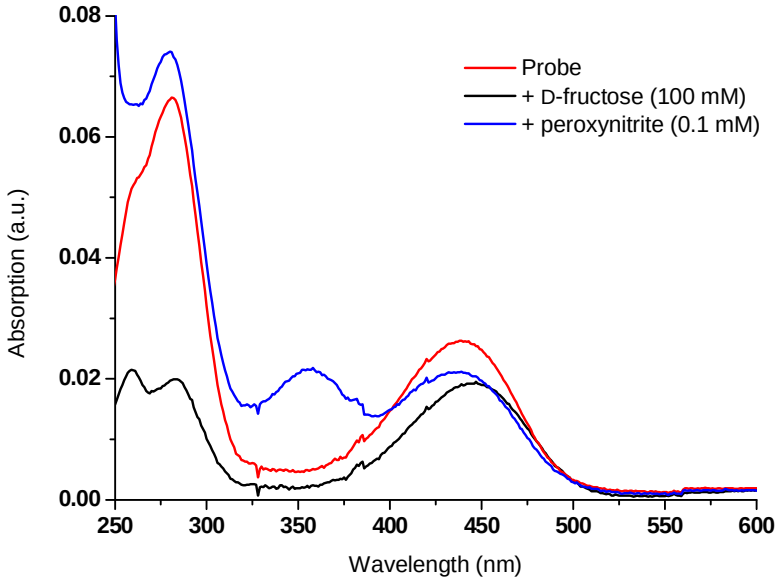

Figure 23. *UV-vis absorption of probe **101** (2 µM, red line), addition of D-fructose (100 mM, black line), addition of peroxynitrite (0.1 mM, blue line). The mixture was stirred for 10 min after addition of D-fructose. The spectra were collected after 5 min in the presence of peroxynitrite.*

In the UV-Vis spectra (Figure 23), the free boronic acid probe **101** (2 µM) displayed a maximum absorption (A = 0.026) at 440 nm while the binding of D-fructose (100 mM) led to a decrease to A = 0.019 at the maximum absorption wavelength. While the presence of $ONOO^-$ (100 µM), a new peak (A = 0.021) at 360 nm was generated due to the formation of phenol.

3.3.3 EMISSION SPECTRA TOWARD $ONOO^-$

In the case of probe **101**, a significant "off-on" signal response is seen on binding with D-fructose due to an inhibition of PET mechanism. From Figure 24, the maximum

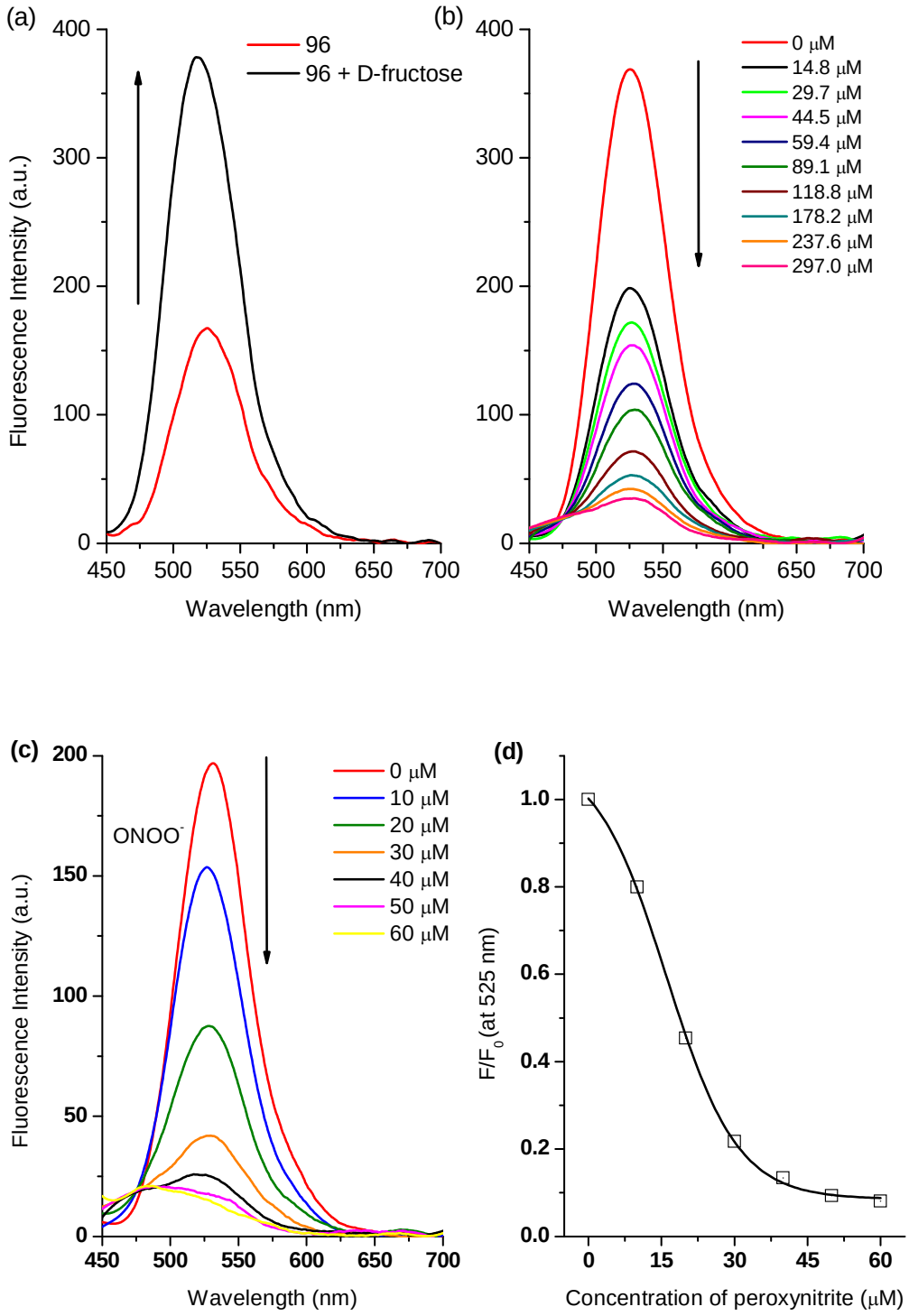

Figure 24. *(a) Fluorescence spectra of probe **101** (2 μM) and then addition of D-fructose (100 mM). After addition of D-fructose, the mixtures were stirred for 10 min; (b) Probe **101**-D-fructose complex (probe **101**, 2 μM; D-fructose, 100 mM) in different concentration of $ONOO^-$. After addition of peroxynitrite, the mixtures were stirred for 5 min. (c) Fluorescence spectra of probe **101** (2 μM) in the presence of various peroxynitrite at pH 7.3 buffer solution; (d) Non-linear relationship between probe **101** (2 μM) and $ONOO^-$ (0 – 60 μM) at pH 7.3 buffer solution. The spectra were collected after 5 min stirring for each dose. The data was collected in PBS buffer (1/15 M, pH 7.30) with excitation at 410 nm (Ex slit: 5 nm, Em slit: 5 nm).*

fluorescence intensity of probe **101** (2 μM, λ_{em} = 525 nm) is increased two-fold in the presence of D-fructose (100 mM) at pH 7.3 buffer solution. However, when the arylboronic ester moiety of probe **101** was transformed into a phenol upon adding peroxynitrite, the fluorescence was further reduced due to the recovered and stronger PET from the amine in the boron free system. As can be seen from dose-dependent titration curve in Figure 24b, the enhanced fluorescence of probe **101**-D-fructose complex was finally reduced to a F (in the presence of $ONOO^-$) /F_0 (in the absence of $ONOO^-$) = *ca.* 0.10 over a concentration range of $ONOO^-$ (0 – 297 μM). While, for the saccharide free system, small amounts of peroxynitrite (60 μM) caused a big change in fluorescence intensity F/F_0 = *ca.* 0.10 (Figure 24c).

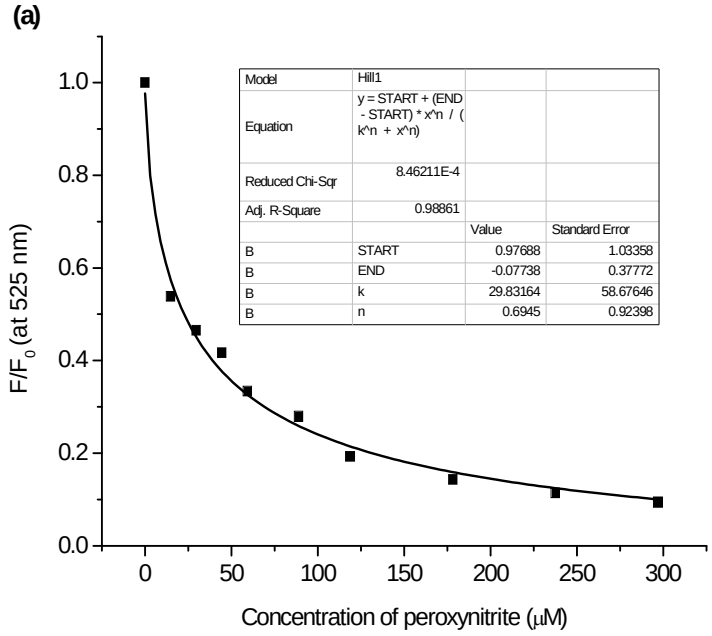

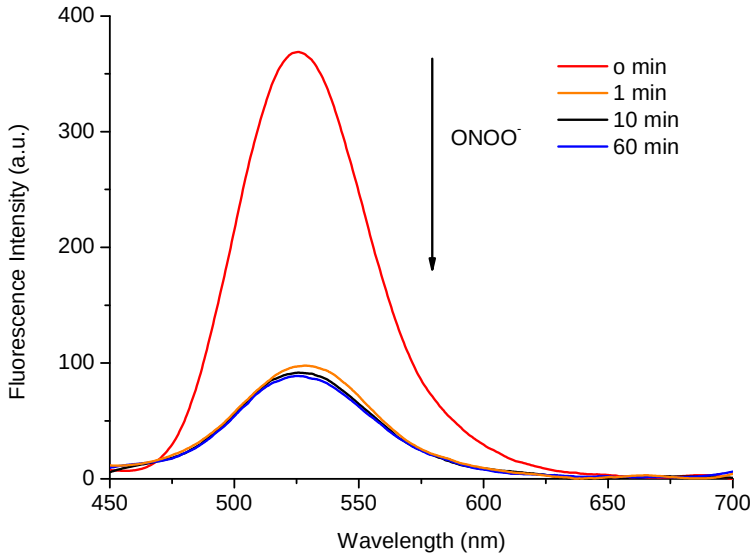

Figure 25. *Non-linear relationship between fluorescence intensity ratio F/F_0 at 525 nm of probe **101**- D-fructose (probe **101**, 2 µM; D-fructose, 100 mM) and concentration of peroxynitrite (0 - 300 µM) at pH 7.30 buffer solution. The mixture was stirred for 5 min for each dose. Time-course kinetic measurement of the fluorescence response of probe **101**-D-fructose (probe **101**, 2 µM; D-fructose, 100 mM) to peroxynitrite (100 µM) at pH 7.30 buffer solution. The spectra were collected with excitation at 410 nm (Ex slit: 5.0, Em slit: 5.0).*

Thus, the fluorescence of probe **101** is turned on by saccharide binding, since boronic ester formation causes an enhanced interaction between the neighbouring amine and the boron atom. This N–B interaction also hampers the reaction between boron and peroxynitrite in the presence of saccharides resulting in a slower decrease in the observed fluorescence.

3.3.4 EMISSION SPECTRA TOWARD H_2O_2

Since boronate-based derivatives can be oxidized to phenol by H_2O_2 and $ONOO^-$, it is very important to discriminate them by fluorescence tools. Independently, we tested the responses of probe **101** and **101**-D-fructose complex towards hydrogen peroxide (Figure 26, Figure 27). With the free boronic acid system, the fluorescence of probe **101** (2 µM) increased to F/F_0 = *ca.* 1.59 in the presence of hydrogen peroxide (100 µM) over 1 h at pH 7.30 buffer solution (Figure 26a). When the solution was adjusted to pH 8.10, the fluorescence decreased most probably due to the decomposition of the intermediate to phenol (Figure 27a). This is different from the process observed for the detection of $ONOO^-$ in which boronic acid was transformed into phenol quickly and directly. While in the case of the **101**-D-fructose complex, the fluorescence showed only a slight drop

F/F_0 = *ca.* 0.75 even after the addition of H_2O_2 (1 mM) over 1 h (Figure 27b, 28). Therefore, the probe **101**-D-fructose complex does not produce a significant response to H_2O_2.

Therefore, the connection of probe **101** with D-fructose not only strengthens the fluorescence signal, but also protects the boronic acid from oxidation by hydrogen peroxide *via* N-B bond. However, with peroxynitrite, the oxidation reaction between boron and peroxynitrite was still very rapid and was complete within 1 min (Figure 25).

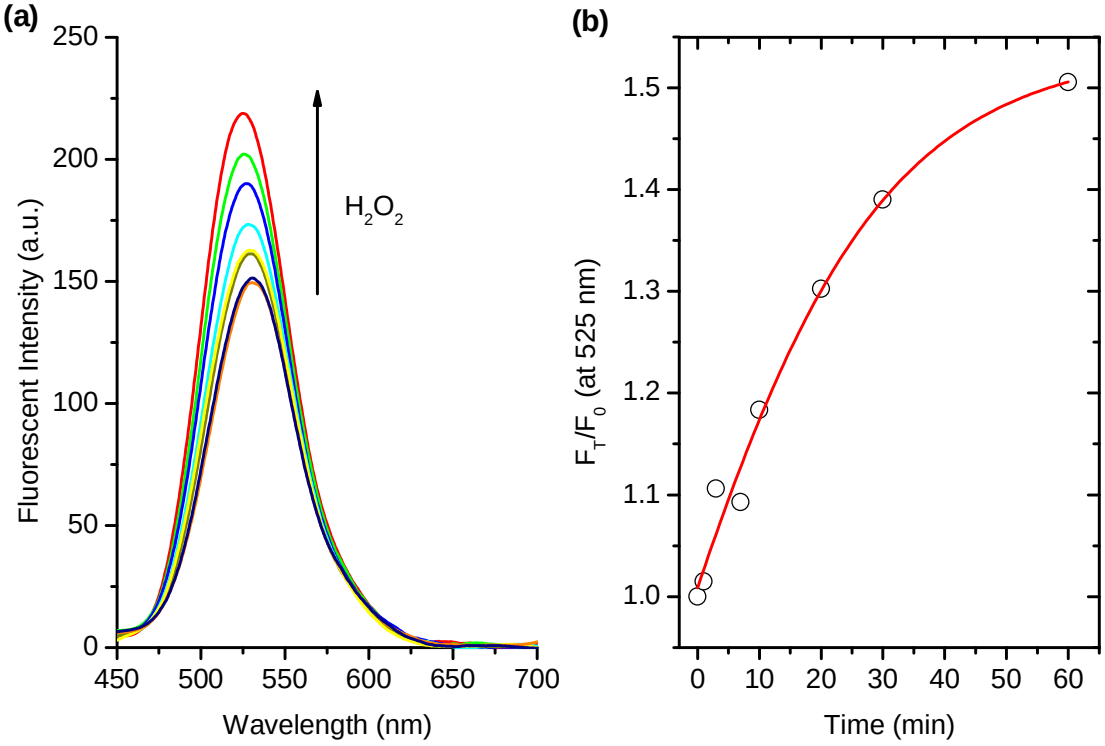

Figure 26. *(a) Fluorescence spectra of probe **101** (2 μM) in the presence of hydrogen peroxide (100 μM) at pH 7.3 buffer solution; (b) Time curve of probe **101** (2 μM) with the fluorescence intensity ratio (F_T/F_0 at 525 nm). The data was collected in PBS buffer (1/15 M, pH 7.30) with excitation at 410 nm (Ex slit: 5 nm, Em slit: 5 nm).*

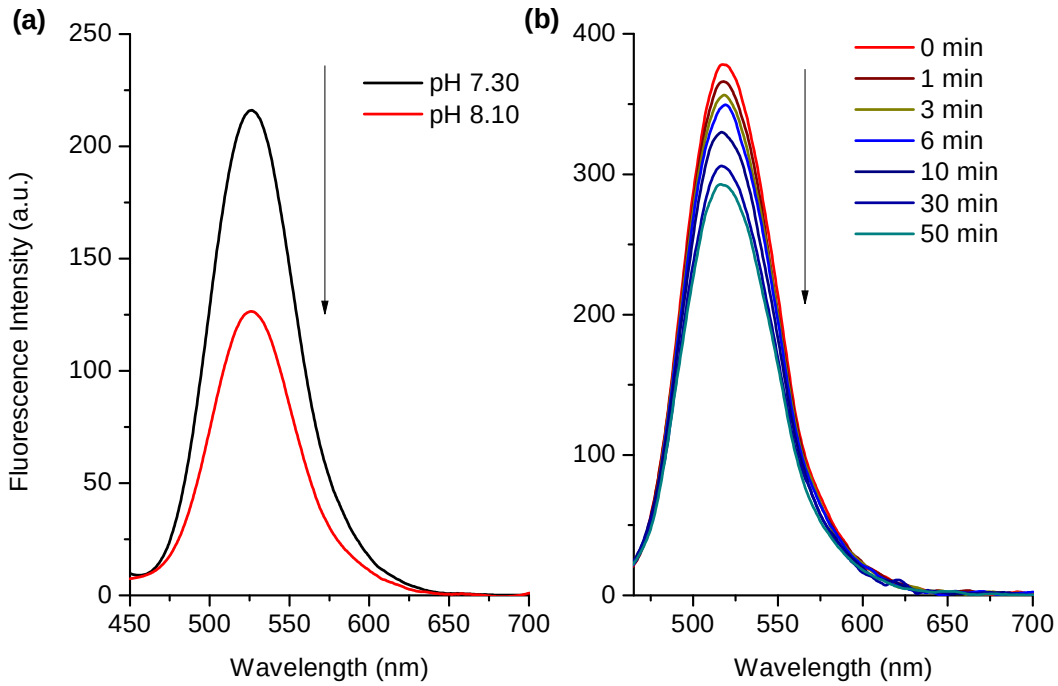

Figure 27. *(a) Fluorescence spectra of probe **101** after reaction with H_2O_2 in pH 7.30 and pH 8.10. The pH was adjusted from 7.30 to 8.10 using aqueous sodium hydroxide (10 N); (b) Fluorescence spectra of probe **101**-D-fructose complex (probe **101**, 2 µM; D-fructose, 100 mM) in the presence of hydrogen peroxide (1 mM) at pH 7.3 buffer solution. The spectra were collected in different time with excitation at 410 nm (Ex slit: 5.0, Em slit: 5.0).*

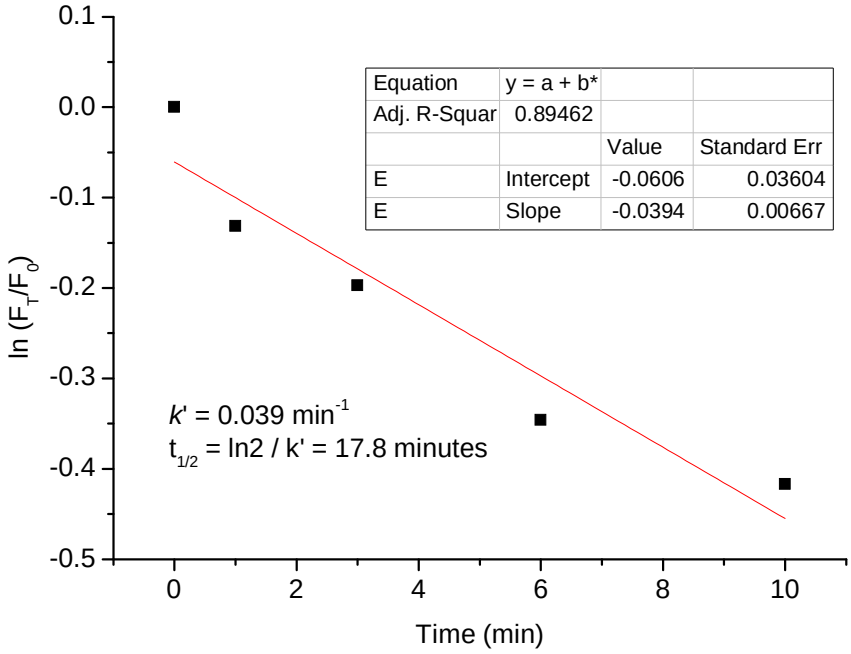

Figure 28. *Time curve of **101**-D-fructose complex (probe **101**, 2 µM; D-fructose, 100 mM) in the presence of hydrogen peroxide (1 mM) with the fluorescence intensity ratio (F_T/F_0 at 525 nm). The data was collected in PBS buffer (1/15 M, pH 7.30) with excitation at 410 nm (Ex slit: 5 nm, Em slit: 5 nm).*

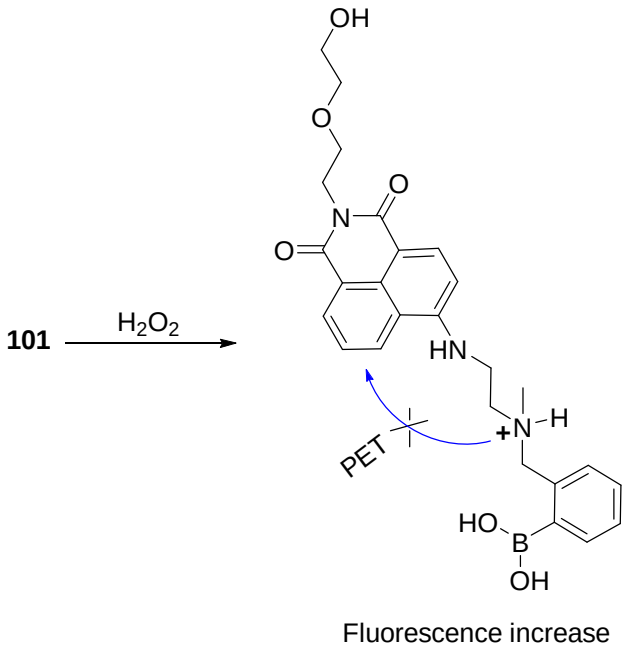

Scheme 47. *Protonation of probe **101** with hydrogen peroxide causes fluorescence enhancement*

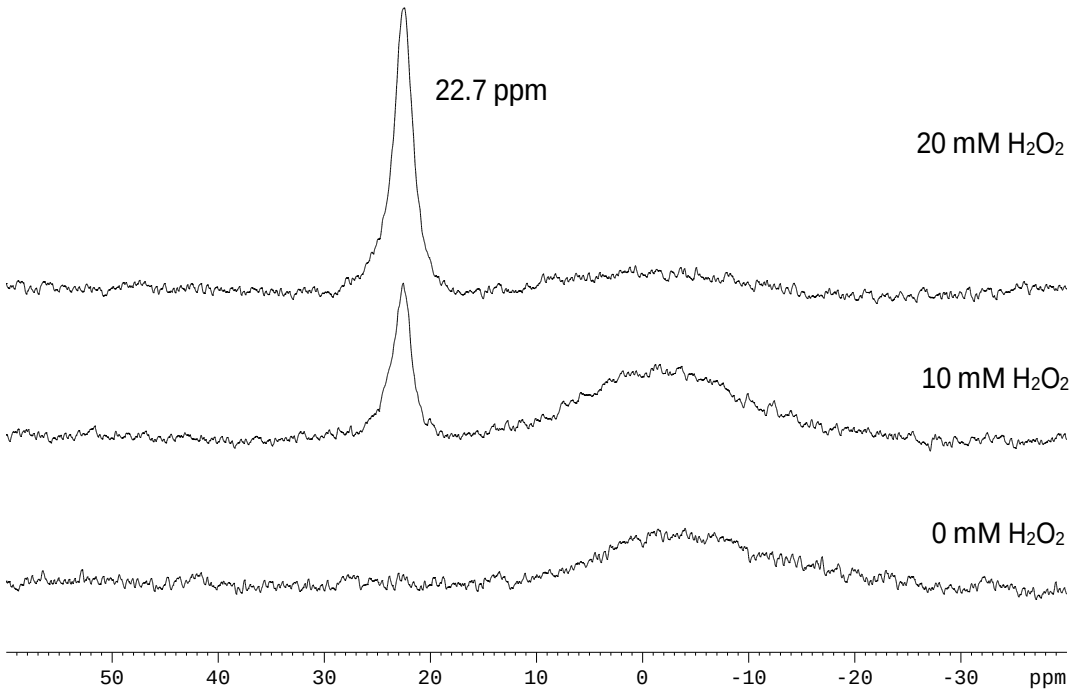

Figure 29. *^{11}B NMR of probe **101** (40 mM) in the presence of various concentrations of hydrogen peroxide (0 - 20 mM). The data was collected in 20% D_2O/MeOD. Acquired at a Bruker AV300 spectrometer operating at 96.3 MHz for ^{11}B, using 128 scans for each spectrum. Spectra were acquired with no proton decoupling, a repetition time of 1.6 seconds, and using composite pulses to help suppress the background signal.*

To explain fluorescence enhancement of probe **101** in the detection of hydrogen peroxide, we assume it might be due to the protonation of tertiary amine rather than oxidation of boronic acid in the presence of H_2O_2 under the aqueous neutral buffer solution (Scheme 47). As can be verified from boron NMR spectrum (Figure 29), no boron peak can be observed in 20% D_2O/MeOD solvent system for **101**-D-fructose complex, while the peak at 22.7 ppm appeared with the increasing concentration of H_2O_2 (10 mM, 20 mM) in the same solvent mixture. Thus, the reaction between boron acid and H_2O_2 was inhibited in this case which is different with the **101**-D-fructose complex since an absolute stronger B-N interaction was formed to against the protonation of tertiary amine and also oxidation of boronic ester.

The sugar complex reacts stoichiometrically and rapidly with $ONOO^-$ to form the phenol product. Therefore, under conditions generating both H_2O_2 and $ONOO^-$, the probe **101**-D-fructose complex preferentially reacts with $ONOO^-$.

3.3.5 SELECTIVITY TESTS TOWARDS ROS/RNS

We also investigated the selectivity of **101**-D-fructose complex towards other reactive oxygen and nitrogen species, such as hypochlorite (^-OCl), nitric oxide (NO), nitrite (NO_2^-), nitrate (NO_3^-), peroxyl radical ($ROO^\cdot$), superoxide ($\bullet O_2^-$), hydroxyl radical (•OH) in pH 7.30 buffer solution (Figure 30, 31). All the ROS/RNS species play important roles in the biological system and physiological process. Through observation, we found that among them, only hypochlorite (100 µM) caused a big fluorescence decrease $(F - F_0)/F$ = *ca.* 0.48 over 1 h (Figure 30b, 31b). As reported previously,[117] aryl boronic acid and ester can be oxidized into phenol by hypochlorite. However, under the same concentration of ^-OCl (100 µM) and $ONOO^-$ (100 µM), peroxynitrite reacts much more with the **101**-D-fructose sensing system ($(F - F_0)/F$ = *ca.* 0.78).

We also tested the fluorescence reaction of **101**-D-fructose complex towards $ONOO^-$ and H_2O_2 at pH 5.0 buffer solution under the consideration of acidic cancer environment in biological condition (Figure 32). Under the same level of H_2O_2 (500 µM) and $ONOO^-$ (500 µM), the fluorescence ratio only decreased to $(F - F_0)/F$ = *ca.* 0.09 for H_2O_2 (Figure 32b) while the value was enlarged to $(F - F_0)/F$ = *ca.* 0.65 for $ONOO^-$ (Figure 32a). Therefore, our fluorescent probe can be employed for the detection of

peroxynitrite selectively and sensitively under physiological and pathological conditions which are either low or have no $^{-}$OCl.

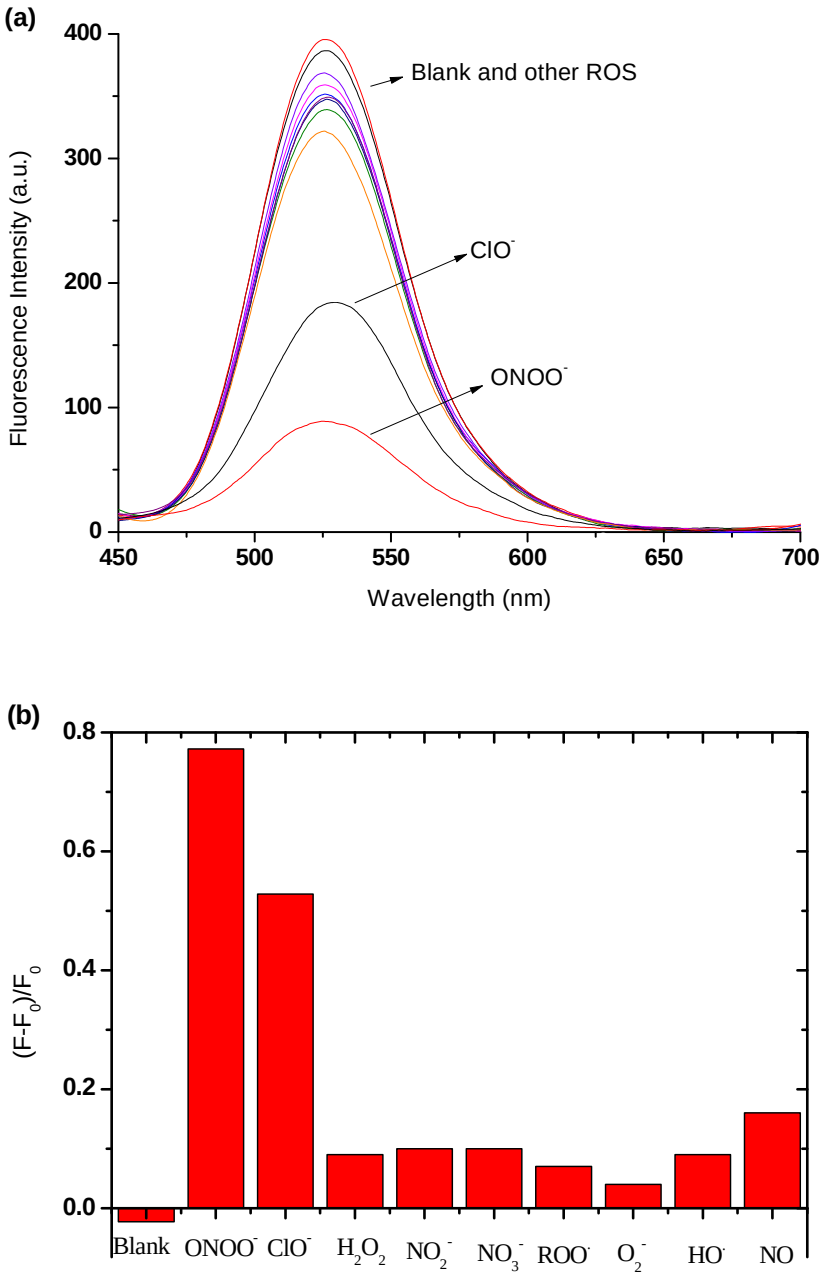

Figure 30. *(a) Fluorescence spectra of probe **101**-D-fructose (probe **101**, 2 μM; D-fructose, 100 mM) in the presence of various ROS/RNS: $ONOO^{-}$ (100 μM, 5 min), ^{-}OCl (100 μM, 5 min), H_2O_2 (100 μM, 5 min), NO_2^{-} (100 μM, 5 min), NO_3^{-} (100 μM, 5 min), ROO• (100 μM, 5 min), $•O_2^{-}$ (100 μM, 5 min), •OH (100 μM, 5 min), NO (100 μM, 5 min) at pH 7.30 buffer solution; (b) Selectivity test of probe **101**-D-fructose complex (probe **101**, 2 μM; D-fructose, 100 mM) in the presence of various ROS/RNS at pH 7.3 buffer solution. The spectra were collected with excitation at 410 nm at 25 ˚C (Ex slit: 5.0, Em slit: 5.0).*

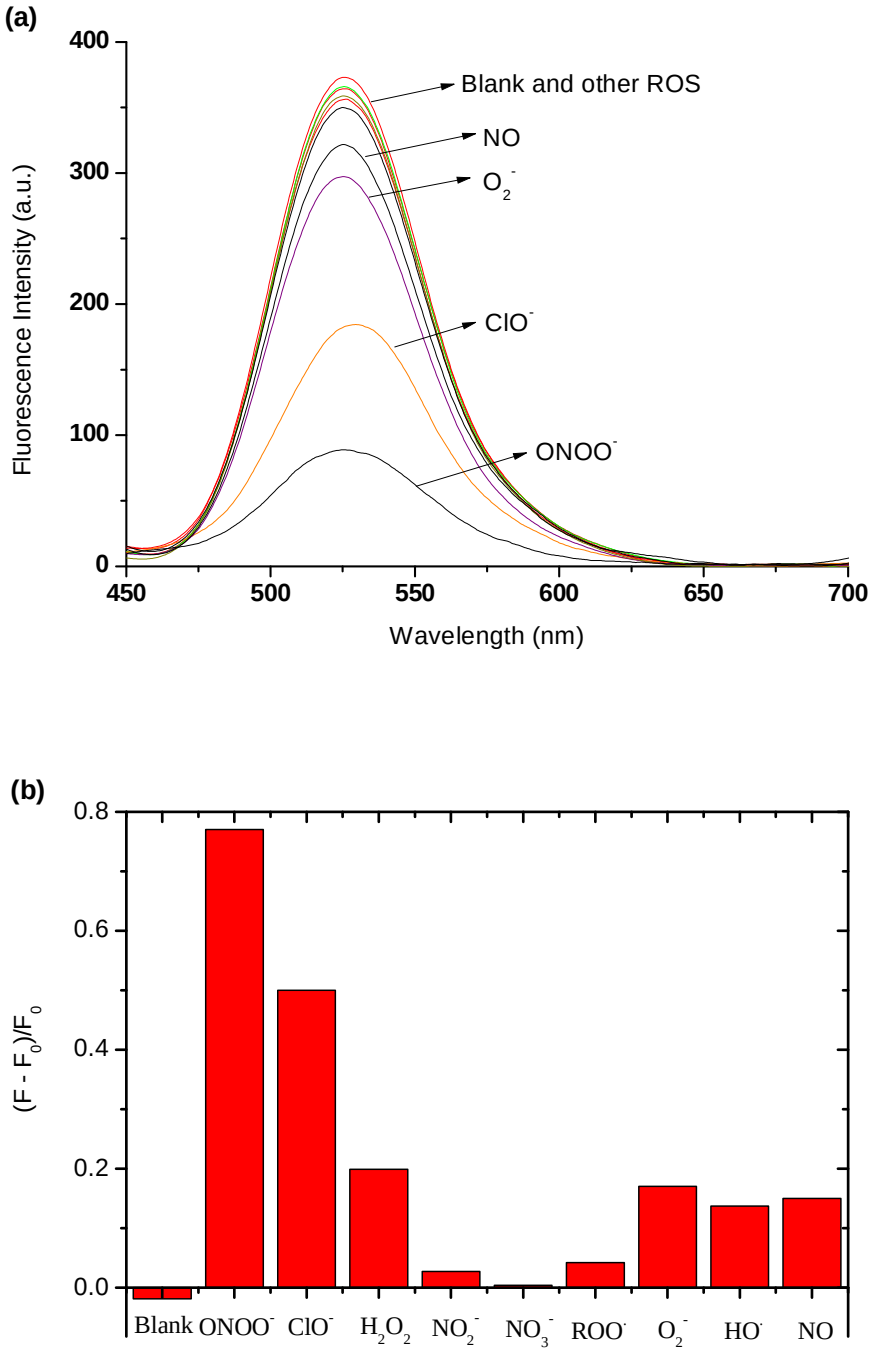

Figure 31. *(a) Fluorescence spectra of probe **101**-D-fructose (probe **101**, 2 μM; D-fructose, 100 mM) in the presence of various ROS/RNS: $ONOO^-$ (100 μM, 5 min), ^-OCl (100 μM, 1 h), H_2O_2 (1 mM, 1 h), NO_2^- (1 mM, 1 h), NO_3^- (1 mM, 1 h), ROO• (1 mM, 1 h), $•O_2^-$ (100 μM, 1 h), •OH (100 μM, 1 h), NO (100 μM, 1 h) at pH 7.30 buffer solution; (**b**) Selectivity test of probe **101**-D-fructose complex (probe **101**, 2 μM; D-fructose, 100 mM) in the presence of various ROS/RNS at pH 7.3 buffer solution. The spectra was collected with excitation at 410 nm at 25 ºC (Ex slit: 5.0, Em slit: 5.0).*

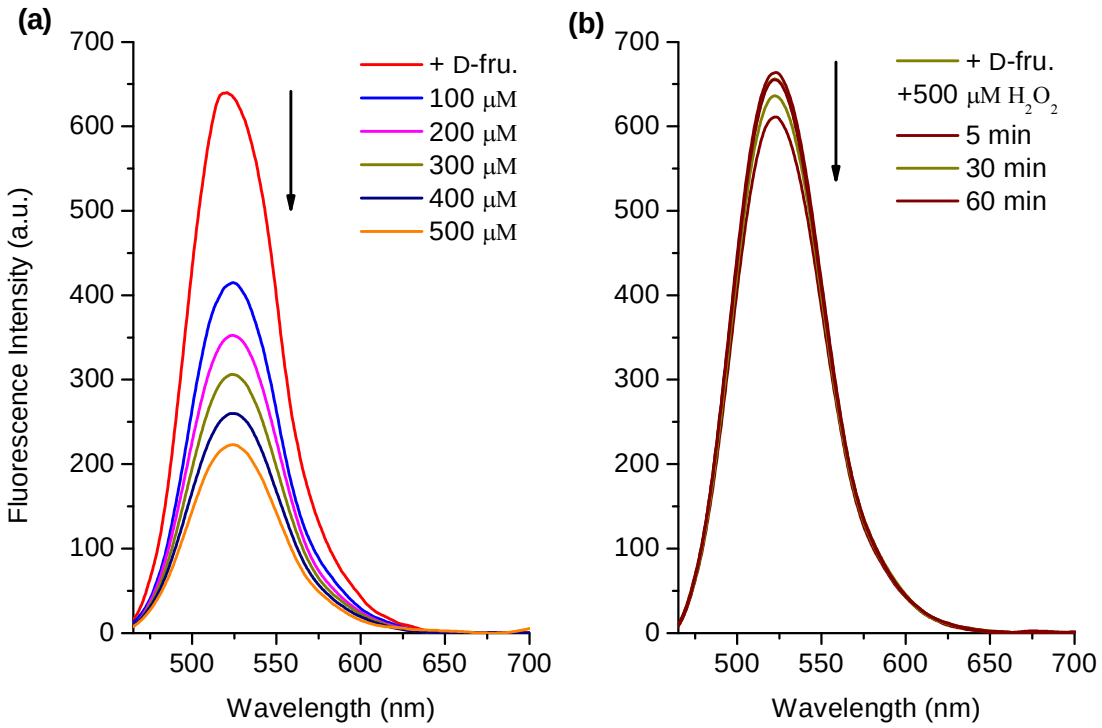

Figure 32. *(**a**) Fluorescence spectra of probe **101**-D-fructose complex (probe **101**, 2 μM; D-fructose, 100 mM) in the presence of various peroxynitrite at pH 5.0 buffer solution. The mixture was stirred for 5 min for each dose; (**b**) Time curve of probe **101**-D-fructose complex (probe **101**, 2 μM; D-fructose, 100 mM) in the presence of hydrogen peroxide (500 μM) at pH 5.0 buffer solution. The spectra were collected with excitation at 410 nm (Ex slit: 5.0, Em slit: 5.0).*

3.3.6 INTROCELLULAR IMAGING FOR EXOGENOUS AND ENDOGENOUS $ONOO^-$

Next, we evaluated the ability of the probe **101**-D-fructose complex to visualize exogenous and endogenous $ONOO^-$ using cell imaging experiments (*Work was performed in Deapartment of Chemistry and Nano Science, Ewha Womans University, Korea*). The HeLa cells were incubated with probe **101** (5 μM) and D-fructose (250 mM) for 30 min at 37 ºC, to which were added 0, 5 μM, 30 μM peroxynitrite/PBS buffer solutions for 10 min at 37 ºC and after washing with DPBS, the cells were observed using the confocal laser scanning microscopy. The probe **101**-D-fructose complex can penetrate into the live cell membrane and displayed strong fluorescence throughout the cytoplasm region (Figure 33. **A:** b). When external peroxynitrites were added into the cells, the fluorescence of the probe **101**-D-fructose complex was quenched in a concentration-dependent manner (Figure 33. **A:** c, **A:** d).

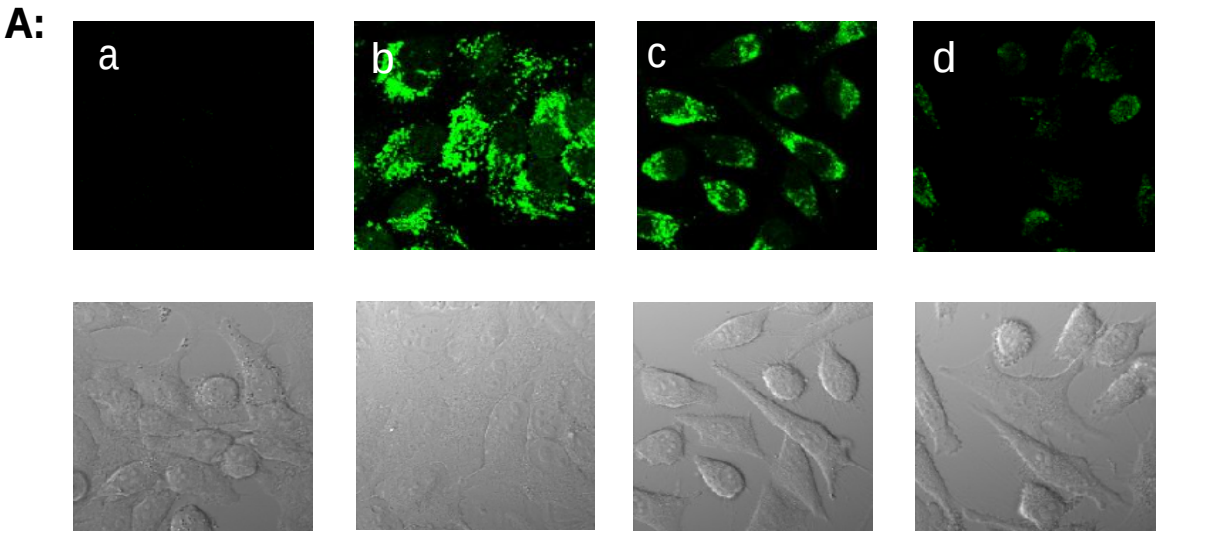

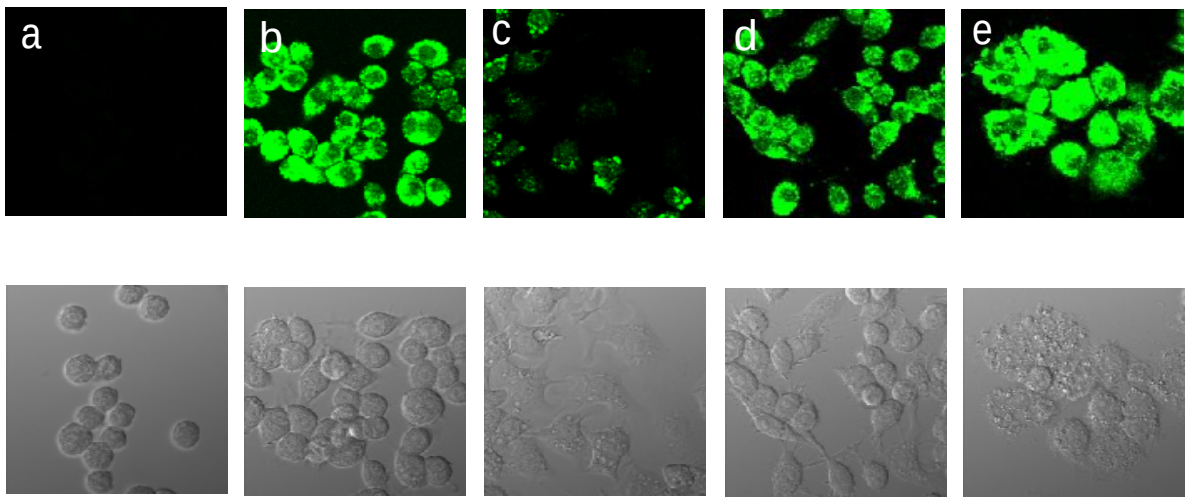

Figure 33. ***A****: Fluorescent imaging for exogenous* $ONOO^-$ *in HeLa cells. The probe* ***101****-D-fructose was formed by mixing probe* ***101*** *(5 μM) and D-fructose (250 mM) in situ.* ***(a)****Blank without probe; (b) Probe* ***101****-D-fructose only; (c) Probe* ***101****-D-fructose and* $ONOO^-$ *(5 μM); (d) Probe* ***101****-D-fructose and* $ONOO^-$ *(30 μM).* ***B****: Fluorescent imaging for endogenous* $ONOO^-$ *in RAW 264.7 cells. The probe* ***101****- D-fructose was formed by mixing probe* ***101*** *(5 μM) and D-fructose (250 mM) in situ. (a) Blank without probe; (b) Probe* ***101****-D-fructose only; (c) Probe* ***101****-D-fructose and LPS, IFN-γ, PMA; (d)* ***c*** *+ aminoguanidine;* ***(e)*** *c + TEMPO.*

Animal macrophage cell lines produce peroxynitrite followed by immunogenic stimuli.[232] To detect the peroxynitrite made from the cell naturally, we used RAW 264.7 cell (mouse macrophage). RAW 264.7 cells were stimulated with 1 μg/ml LPS (lipopolysaccharide, bacterial membrane component) for 16 h at 37 ºC, 50 ng/ml IFN-γ

for 4 h and 2.5 ng/ml PMA for 30 min then incubated with 5 μM sensor for 30 min and they showed weak fluorescence compared to control cells (Figure 33. **B:** b, **B:** c). For the inhibition test of peroxynitrite production, 100 μM TEMPO (superoxide scavenger) and 0.5 mM amino guanidine (nitric oxide synthase inhibitor) was pre-treated with the media for 4 h and in this case strong fluorescence was observed (Figure 33. **B**: d, **B**: e). From these experiments, it is clear that the reaction of the sensor with peroxynitrite can be detected in live cells.

3.3.7 POTENTIAL APPLICATION

The results and discussion above shows the potential utility of the fluorescence probe **101**-D-fructose complex as a powerful tool for diagnosing and/or detecting a disease in a subject. It can be employed to detect peroxynitrite in a living cell and image a spatial distribution of peroxynitrite. The present project will have many applications in the fields of medical research, diagnosis and therapy *via* evaluating peroxynitrite activity in biological systems in pharmacological and biochemical experiments, thereby helping to elucidate the exact role of peroxynitrite in diseases – such as Alzheimer's disease, Parkinson's disease, Huntington's disease, traumatic brain injury, and skeletal muscle hypertrophy etc.

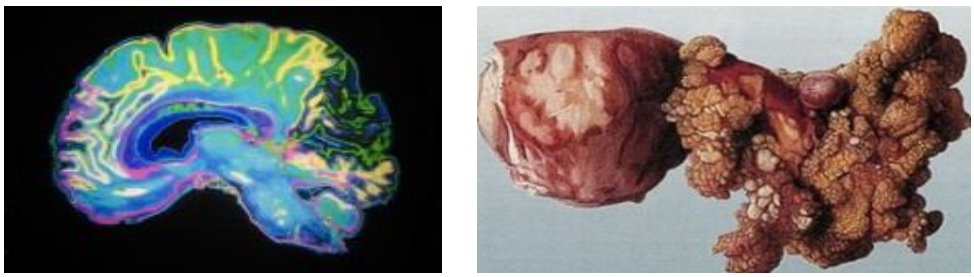

Figure 34. *Alzheimer's and Ovarian tissue*

3.3.8 EMISSION SPECTRA TOWARDS FLUORIDE

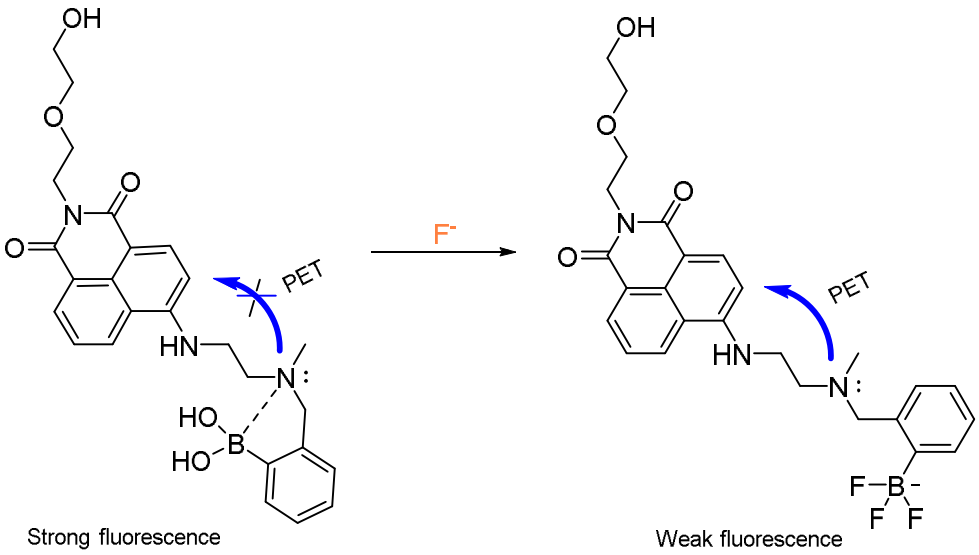

Scheme 48. *Mechanism of reaction between probe **101** and fluoride in MeCN.*

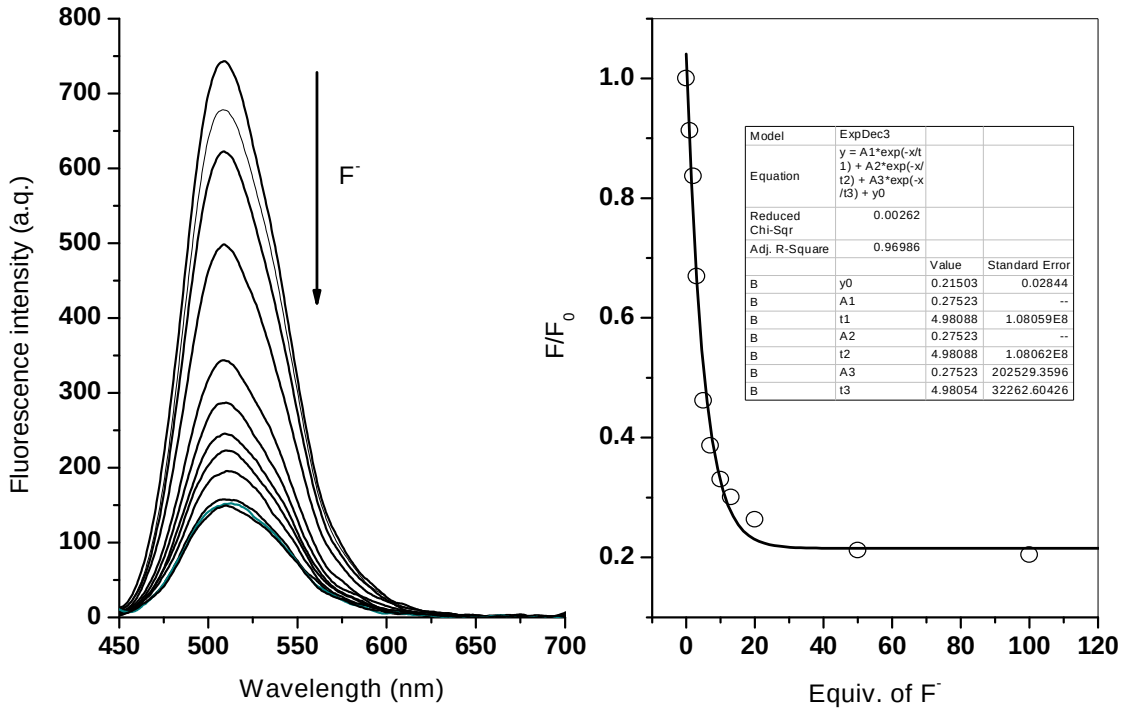

(a) **(b)**

Figure 35. ***(a)*** *Fluorescence spectra of probe **101** (2 µM) with addition of fluoride (0 – 300 µM) in MeCN;* ***(b)*** *Concentration curve of fluorescence intensity changes (F/F_0) with probe **101** (2 µM) and various equivalent of fluoride in MeCN at 25 ˚C. Fluorescence intensities were measured with excitation at 410 nm with Ex slit: 5.0 and Em slit: 5.0.*

Figure 35 demonstrated the fluoride titration experiment for probe **101** (2 µM). To initiate the release of fluoride, various amounts of tetrabuthylammonium fluoride (0 – 0.3 mM) in acetonitrile were added into solution of probe **101** (2 µM) and then the mixtures were kept stirring for 3 min. In the excitation at 410 nm, the data was collected in a fluorescence spectrometer between 465 – 700 nm. Significantly, fluoride led to the decrease of the fluorescence intensity maxima at 510 nm in a dose-dependent manner (Figure 35). The reaction between probe **101 (**2 µM) and tetrabuthylammonium fluoride (0.1 mM) triggered a 5-fold "on-off" fluorescent response (I_F/I_0, in the presence of fluoride/in the absence of fluoride). It is predicated that the binding of fluoride with boronic acid weakened the B-N interaction thus enhancing the PET effect from amine (Scheme 48).

3.3.9 "INSULATED" SYSTEM BASED ON ICT MECHANISM

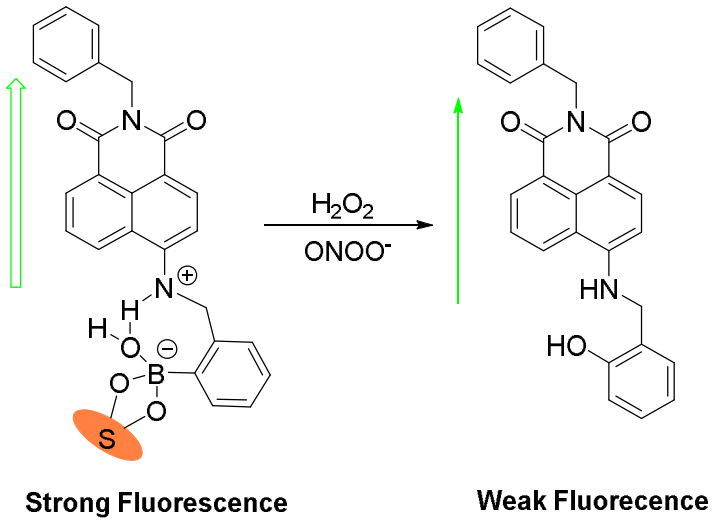

Scheme 49. *Sensing mechanism of probe **102a** with H_2O_2 and $ONOO^-$.*

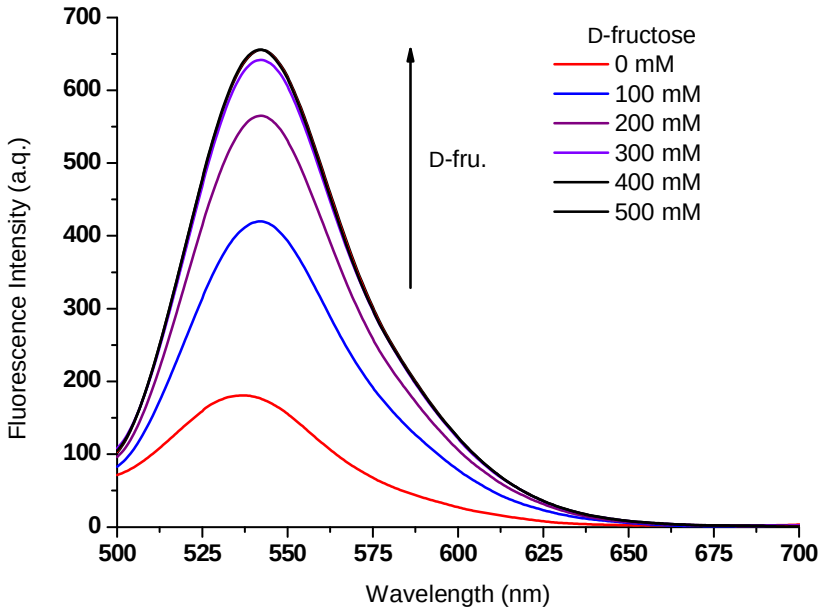

Figure 36. *Fluorescence spectra of probe **102a** (10 μM) in the presence of D-fructose (0 – 500 mM). The data was obtained in pH 7.30 PBS buffer with excitation at 493 nm. Ex slit: 5 nm; Em slit: 5 nm.*

As can be revealed by Figure 36, it has been assumed that the addition of various concentrations of D-fructose (100 – 500 μM) led to the increase of the fluorescence intensity which was attributed to the interaction of N-B bond in the presence of monosaccharide. We observed that 300 mM D-fructose caused 3.7-fold rise to the fluorescence of probe **102a** (10 μM) which was almost the maximum growth of fluorescence intensity. Subsequently, more additional D-fructose only gave subtle rise to the signal. It is predicted that the deprotonation of the amine and the enhanced electron donating ability of the negative nitrogen in the system resulted in the strengthening of fluorescence signal.

Thus, the complex probe formed by attachment of D-fructose (300 mM) with probe **102a** (10 μM) was studied further to testify the effect of boron-amine interaction in the distinguishing of hydrogen peroxide and peroxynitrite. Knowing of this is very important since it might be taken as another strong proof using the N-B protection to detect peroxynitrite selectively and sensitively. In order to make the comparation with the previous system, we evaluated the new sensing probe through keeping the detection condition in constant, under the same buffer solution and temperature.

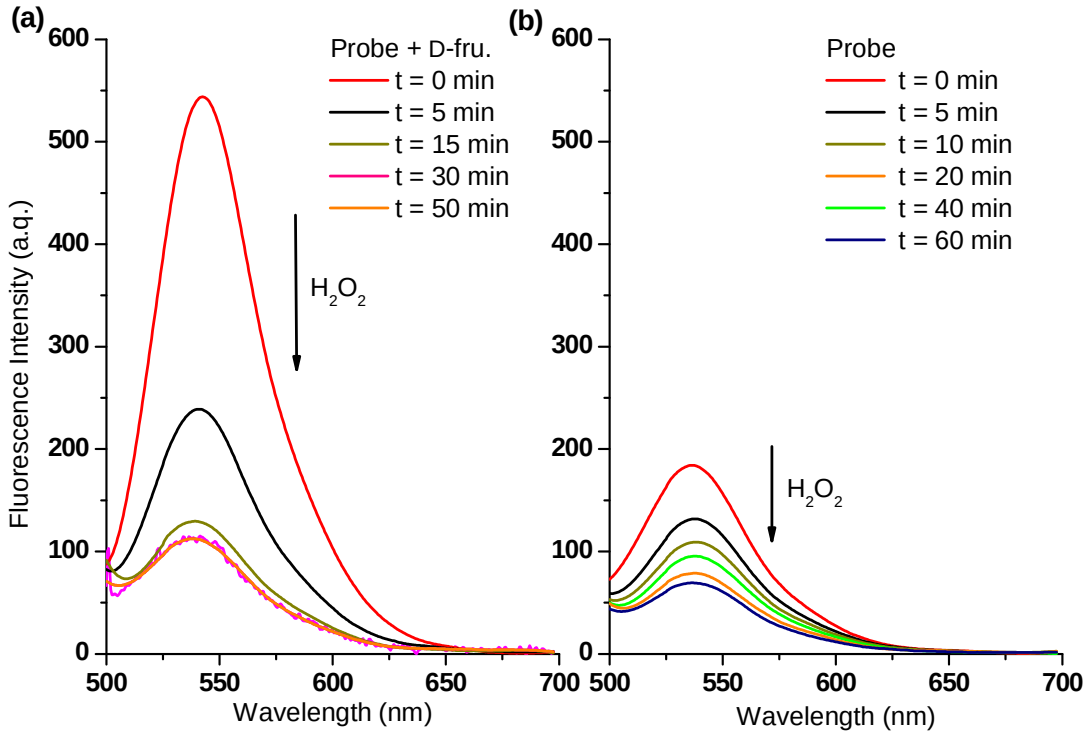

Figure 37. *(a) Time-curve fluorescence spectra of probe **102a**-D-fructose complex (**102a**, 10 μM; D-fructose, 300 mM) in the presence of H_2O_2 (1 mM). (b) Time-curve fluorescence spectra of probe **102a** (10 μM) in the presence of H_2O_2 (1 mM). The data was obtained in pH 7.30 PBS buffer with excitation at 493 nm. Ex slit: 5 nm; Em slit: 5 nm.*

In the boronate-based "insulated" system **101**-D-fructose, we found that the protection of B-N bond hampered the reaction of boronate with H_2O_2 while a much stronger oxidant $ONOO^-$ was employed to break down the interaction. Thus, we decided to evaluate the reactivity of probe **102a** for the detection of H_2O_2 and $ONOO^-$ in the presence and absence of D-fructose. Independently, we tested the responses of probe **102a** and **102a**-D-fructose complex towards hydrogen peroxide (Figure 37). With the free boronic acid system, the fluorescence of probe **102a** (2 μM) decreased to F/F_0 = *ca.* 0.39 in the presence of hydrogen peroxide (1 mM) over 1 h at pH 7.30 buffer solution (Figure 37b). While in the case of the **102a**-D-fructose complex, the fluorescence showed a big drop F/F_0 = *ca.* 0.22 after the addition of H_2O_2 (1 mM) over 1 h (Figure 37a). Therefore, the probe **102a**-D-fructose complex does produce a significant response to H_2O_2. To explain the phenomenon, it is due to the oxidation of boron into phenol which led to the ICT weakening and formation of PET effect.

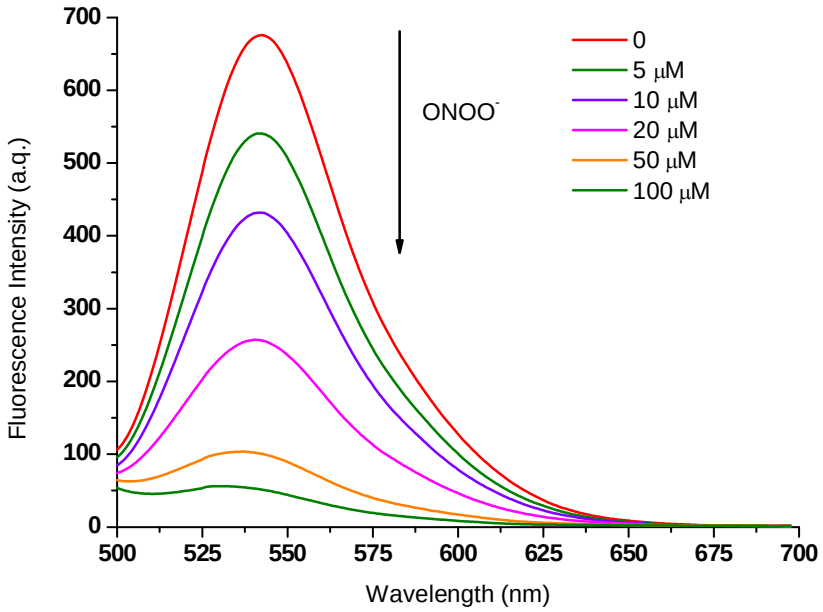

Figure 38. *Dose-dependent fluorescence spectra of probe **102a**-D-fructose complex (**102a**, 10 μM; D-fructose, 300 mM) in the presence of peroxynitrite (0, 5, 10, 20, 50, 100 μM). The data was obtained in pH 7.30 PBS buffer with excitation at 493 nm. Ex slit: 5 nm; Em slit: 5 nm*

In the case of **102a**-D-fructose complex, when the arylboronic ester moiety of probe **102a** was transformed into a phenol upon adding peroxynitrite, the fluorescence was further reduced due to the recovered and stronger protonation of amine in the boron free system. As can be seen from dose-dependent titration curve in Figure 38, the enhanced fluorescence of probe **102a**-D-fructose complex was finally reduced to a F (in the presence of $ONOO^-$) /F_0 (in the absence of $ONOO^-$) = *ca.* 0.07 over a concentration range of $ONOO^-$ (0 – 100 μM).

Above all, the probe displayed an enhanced fluorescence change when bound with D-fructose due to the prolonged N-B distance. Through observation, the N-B protection mechanism was not formed in the linkage of monosaccharide against hydrogen peroxide and the internal N-B interaction was weakened in this case. Subsequently, the fluorescence intensity of the probe dropped down both in the detection of H_2O_2 and $ONOO^-$ which was attributed to the oxidation of arylboronic acid in the presence of D-fructose.

3.4 CONCLUSION

In conclusion, we have developed a new approach for the intracellular detection of $ONOO^-$ through the use of a boronic acid fluorescence probe in the presence of monosaccharide (eg. D-fructose). The reaction between peroxynitrite and boronic ester triggered a significant fluorescence on-off response which is selective over a variety of reactive oxygen and nitrogen species. Notably, from the perspective of a mechanistic explanation, the enhanced interaction between the amine and boron provides a novel strategy to design new fluorescent probes for the detection of peroxynitrite which can distinguish $ONOO^-$ from H_2O_2 and other ROS/RNS. More importantly, the simple, sensitive fluorescent probe was successfully manipulated to visualize exogenous and endogenous $ONOO^-$ in living cells. We believe that our novel system will enable the investigation of diseases states (such as inflamation) in biological systems involving the production of peroxynitrite.[209, 233, 234] We also observed the sensing ability of probe **102** for fluoride in the acetonitrile solvent system.

In the example of ICT-based probe **102a**, it displayed an enhanced fluorescence change when bound with D-fructose due to the prolonged N-B distance. The N-B protection mechanism was not formed in the linkage of monosaccharide against hydrogen peroxide and the internal N-B interaction was weakened in this case. Thus, the fluorescence intensity of the probe dropped down both in the sensing of H_2O_2 and $ONOO^-$ which was attributed to the oxidation of arylboronic acid in the presence of D-fructose.

This work has been published: *Sun, X.; Xu, Q.; Kim, G.; Flower, S. E.; Lowe, J. P.; Yoon, J.; Fossey, J. S.; Qian, X. H.; Bull, S.; James, T. D., A water-soluble boronate-based fluorescence probe for the selective detection of peroxynitrite and imaging in living cells. Chem. Sci. 2014.* ***5****, 3368-3373 (Front cover); Sun, X.; Dull, S.; James, T. D., "Methods (Peroxynitrite)", UK Patent Application No. 1403470.6.*

Chapter Four:

RESULTS AND DISCUSSION III

4. RESULTS AND DISCUSSION III

4.1 BACKGROUND

Phenylboronic acid (PBA, pK_a = 8.83), benzoboroxole (BBA, pK_a = 7.30), and 2-(*N*, *N*-dimethylaminomethyl) phenylboronic acid (NBA, pK_a = 6.70) are three representative receptors among all boronic acid derivatives (Figure 39) which have been applied for monosaccharide sensing,[194, 231, 235] while, Alizarin Red S (ARS) and 4-methylesculetin (ML), had been successfully employed as a general optical reporter for investigating the binding of boronic acids with carbohydrates (Figure 40).[94, 235] Also, some of our previous research has used the binding and analyte-mediated release of Alizarin Red S from hydrogel-bound boronic acids. [198]

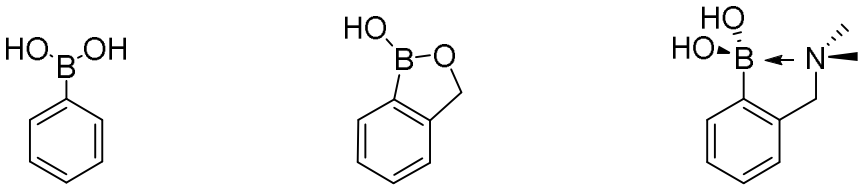

103. **PBA** **104**. **BBA** **105**. **NBA**

Figure 39. *Structures of the three candidates phenylboronic acid (PBA), benzoxaborole (BBA), 2-(N,N-dimethylaminomethyl) phenylboronic acid (NBA).*

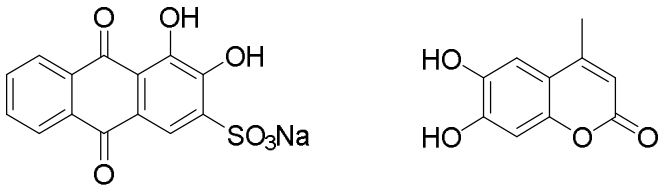

Alizarin Red S 4-Methylesculetin

106 **107**

Figure 40. *Structures of the indicator candidates, Alizarin Red S (ARS), 4-methylesculetin (ML).*

Binding with phenylboronic acids, ARS showed a blue-shift colour change (from pink to orange) and a dramatic increase in fluorescence intensity due to the inhibition of the active protons especially by an assistance of surfactant (e.g. CTAB). Also, the previous research has demonstrated the binding and analyte-mediated release of Alizarin Red-S with hydrogel-bound boronic acid.[198] In the work reported from Benkovic, there are four reactant species involved in the formation of four different adduct species between ARS and phenylboronic acid. The rate of a given complex formation depended on the

combination of the solution pH value and the pK_a's of both ARS and the arylboronic acid. The elucidation of the mechanism indicated the presence of two fluorescent products with the structure of the major contributor. [236]

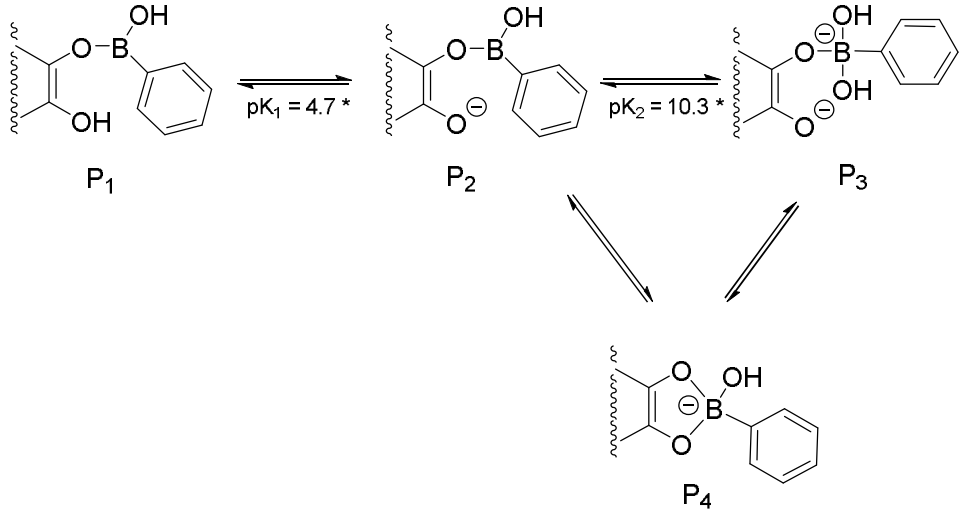

Scheme 50. *Elucidated mechanism for the formation of four reactant species between phenylboronic acid and ARS in aqueous solution in pH ranging from 4 to 10.5*

Hall has taken a different approach to improve the binding efficacy of simple boronic acid units. The design takes its inspiration from the enhanced binding of *o*-benzoboroxoles **104** with 4,6- or *cis*-3,4-diols.[237, 238] The binding constants of *o*-benzoboroxoles with glycopyranosides were obtained by using an ARS UV assay in neutral water. The K_{obs} with D-glucose was 22 M^{-1} while, the binding constant of phenyl boronic acid with glucose was *ca.* 5 M^{-1} under similar conditions.

Besides, a very interesting and popular chemical structure has been studied and deeply explored where neighbouring tertiary amino groups were installed in proximity of boron atoms, in many reported boronic acid receptors, e.g. receptor **105**. In the case, amino groups were postulated to accelerate the association equilibria with their substrates, by serving as proton shufflers or by modulating the thermodynamics of the association as Lewis bases for the boron atoms.[110] The nitrogen atom coordinates with the electron-deficient boron atom to form a relatively rigid five-member-ring structure, particularly in the presence of monosaccharide (e.g. glucose).

4.2 DESIGN STRATEGY

It should be noted that limited work has been carried out in the development of small-molecule probe for the colorimetric sensing of H_2O_2 and $ONOO^-$. Particularly, we are trying to explore a new system in the selective detection of $ONOO^-$ based on our previous observation (i.e. system **100**-D-fructose and **101**-D-fructose). Bearing this in mind, we decided to evaluate the sensing systems (Fluorophore-BAs), which was formed by the attachment of boronic acid derivatives with catechol-based fluorophores *in situ* (Scheme 51), in the detection of hydrogen peroxide and peroxynitrite and distinction of them *via* system based on the N-B protection in an aqueous media.

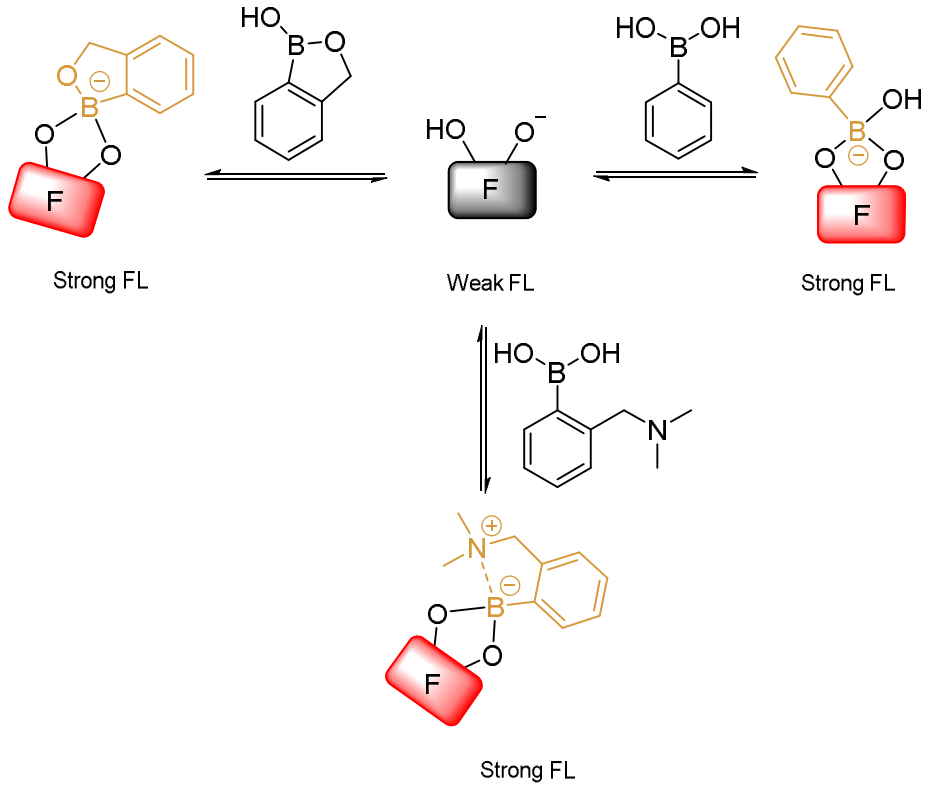

Scheme 51. *The binding mode of the BAs-Fluorophores.*

As illustrated in Scheme 51, three different types of boronic ester complexes are designed and developed for purpose of application in the detection and separation of H_2O_2 and $ONOO^-$. It should be noted that the pK_{a1} of ARS is 6.0* and pK_{a2} is 11.0*, thus the existence form of ARS in pH range 6.0 – 11.0 buffer solution is the deprotonating state with the negative charge.

Firstly, attachment of phenylboronic acid (PBA) with Alizarin Red S (ARS), we assume it should be a good chemo/biosensor for the detection of hydrogen peroxide through

colorimetric, fluorescence, and electrochemical measurements. The reaction-based probe demonstrated H_2O_2-mediated oxidation of aryl boronates to phenols.

Next, benzoboroxole (BBA), with a higher binding affinity with diols, was chosen as a good receptor which binds with ARS to shape a new complex probe. It was predicted that sp2 rehybridised boron might become sp3 when connecting with diols on the surface of ARS, thus, forming a protection system and reducing its reactivity with H_2O_2.[236]

In the case of 2-(*N, N*-dimethylaminomethyl) phenylboronic acid (NBA), linking with the diols-bearing reportors, they have inherently similarity with the previous **100**-D-fructose and **101**-D-fructose complex systems. A significant turn-on fluorescence response can be trigered in the process of complex formation and the interaction between the amine and boron was enhanced so as to protection of boron against H_2O_2 and ClO^- and selective detection of peroxynitrite.[69, 236]

In this strategy, the receptor and reporter unit are separate initially and the combination of them under the measurement of conditions was dissociated by the addition of the target. Colour change and fluorescence on-off, those measurable responses can be produced then. Therefore, novel approach of indicator displacement assay based on chemical reaction can be used in our project firstly in the application of ROS/RNS colourimetric and fluorimetric detection.

4.3 RESULTS AND DISCUSSION

4.3.1 ARS-PBA COMPLEX SYSTEM

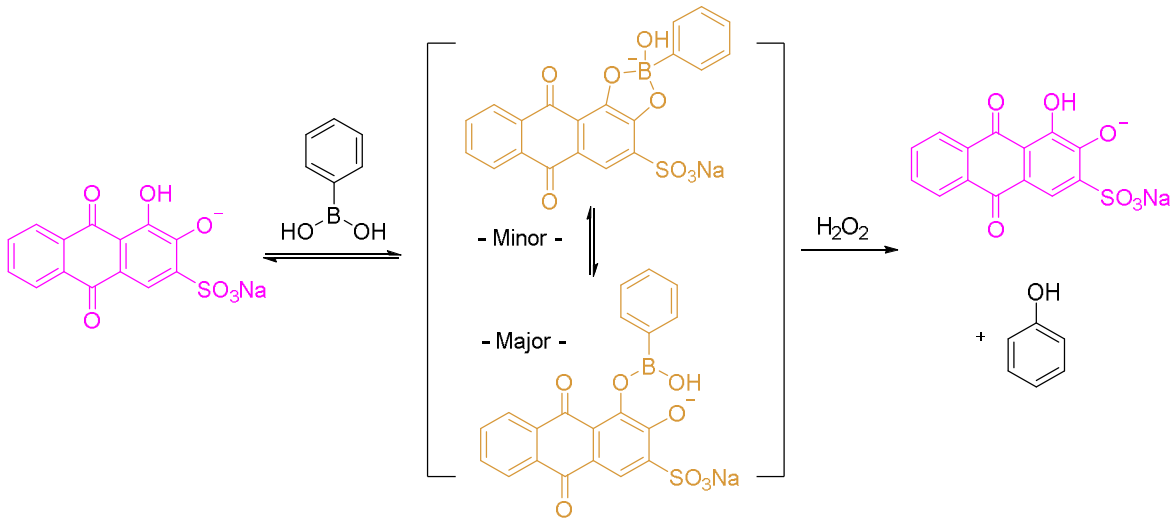

Scheme 52. *Design strategy of probe ARS-PBA complex for H_2O_2.*

Alizarin Red S is a water-soluable compound so we started the detection in an aqueous PBS buffer. Also, cetyl trimethylammonium bromide (CTAB) was employed to improve the signal sensitivity through creating the hydrophobic core of micelles. In the test of the sensing properties of probe ARS-PBA for the detection of H_2O_2, we decided to adopt UV-Vis, fluorescence spectroscopy and electrochemical measurements to study the interaction between boron and H_2O_2.

4.3.1.1 UV-Vis spectra towards H_2O_2

Initially, in the UV-Vis spectroscopy, we observed the maximum absorption for the free ARS (50 μM) is centred at λ_{abs} = 550 nm while the addition of phenylboronic acid (200 μM) caused a blue shift to maxima λ_{abs} = 480 nm which was attributed to the alternation of conjugated structure in pH 7.30 PBS buffer. Therefore, the linking of ARS with PBS led to a significant colour change from pink to orange over through 15 min.

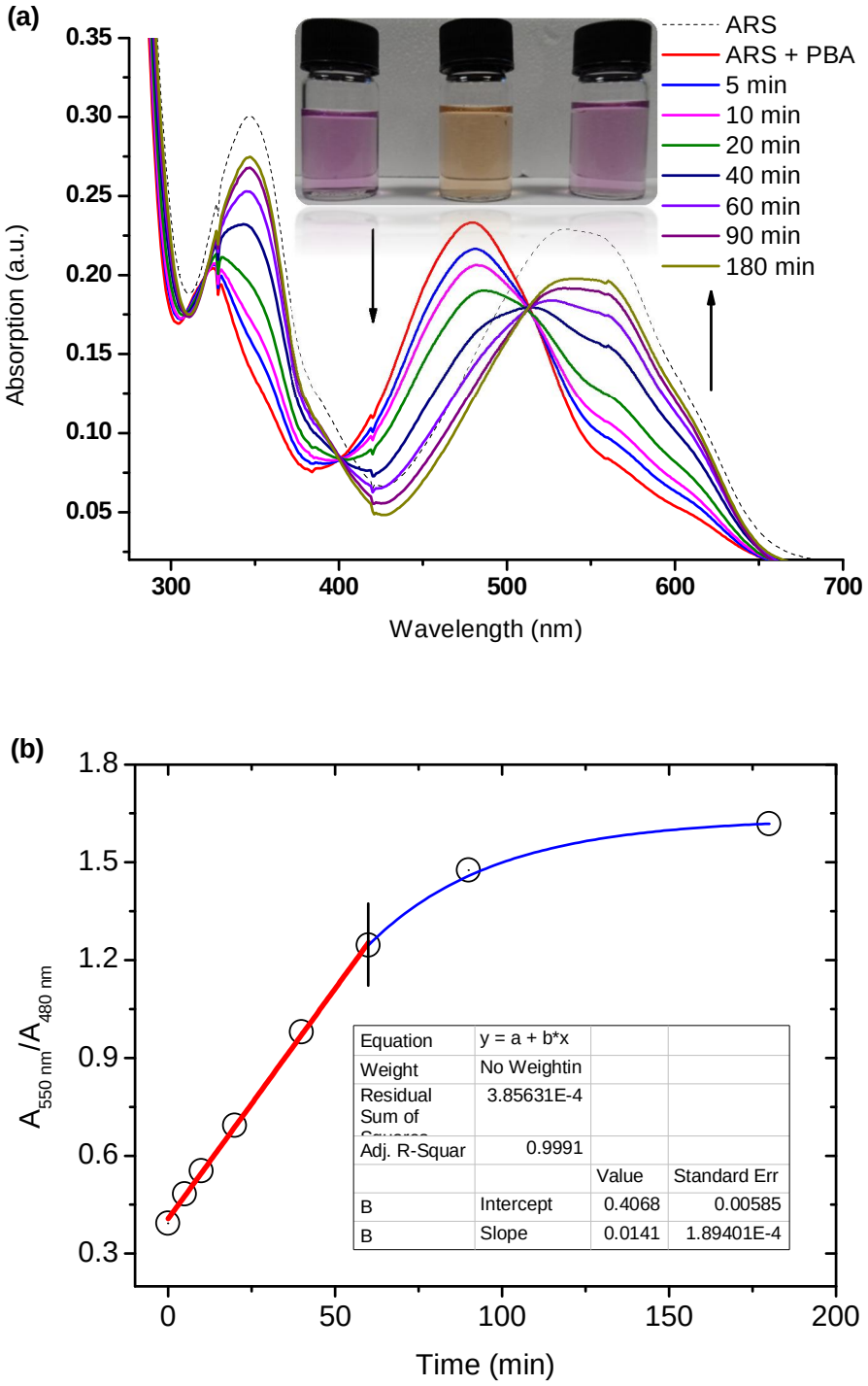

Figure 41. *(a) UV-Vis absorption spectra for ARS only (50 μM), ARS-PBA (ARS, 50 μM; PBA, 200 μM) and then addition of H_2O_2 (500 μM, 5, 10, 20, 40, 60, 90, 180 min). (b) Relationship between absorption ratio ($A_{550\ nm}/A_{480\ nm}$) and reaction time. The data was obtained in 1/15 M PBS buffer with 2.0 mM CTAB in solution at 25 ºC.*

To the formed sensing system, the H_2O_2-mediated oxidation of aryl boronates to phenols and subsequent decomposition of the intermediate induced free of ARS from the complex and then led to the red-shifted wavelength change of the complex probe

(before: λ_{abs} = 480 nm; after: λ_{abs} = 550 nm). As can be revealed from Figure 41a, when H_2O_2 (500 μM) was added to a solution of ARS-PBA (ARS, 50 μM; PBA, 200 μM), a significant decrease in the 480 nm absorption was observed with the appearance of a red-shifted band centred at 550 nm over through 3 h with 2.0 mM CTAB in the system and a clear iso-absorption point can be seen at 510 nm. This is due to the reaction between boron and hydrogen peroxide which led to the release of free ARS and production of phenol. In Figure 41b, there is a good linear relationship (R^2 = 0.9991) which can be seen between absorption ratio ($A_{550\ nm}/A_{480\ nm}$) and reaction time (0 – 60 min) under the concentration of ARS-PBA (ARS, 50 μM; PBA, 200 μM) and H_2O_2 (500 μM). There is an obvious decreasing reaction rate after 60 min which is due to the lower concentration of the reagents inside and huge consumption of H_2O_2. However, the recovered absorption intensity of the complex probe is only 86.9% of the original free ARS during the observing time (3 h) on account of the incomplete reaction or the incomplete decomposition of the intermediate.

4.3.1.2 Emission spectra towards H_2O_2

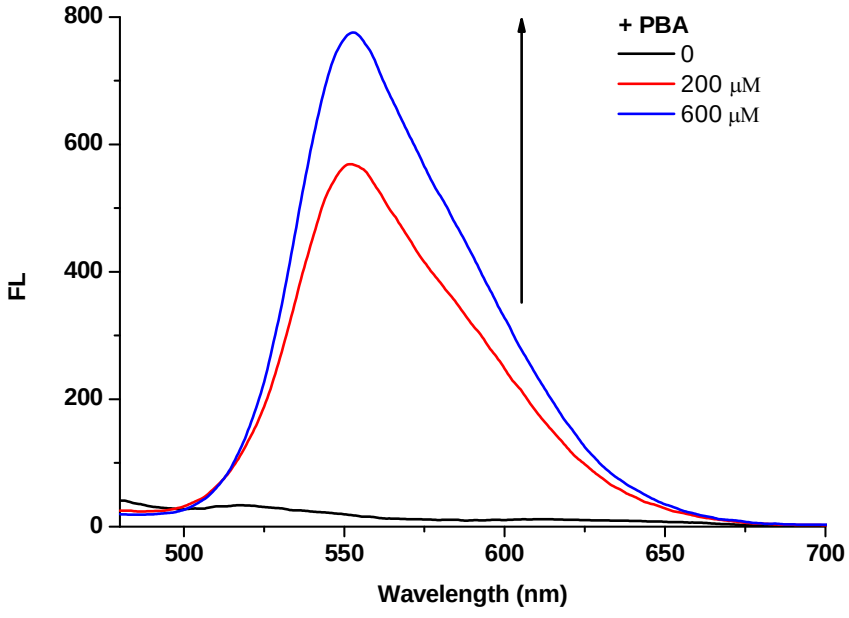

Figure 42. *Fluorescence spectra (λ_{ex} = 460 nm) of ARS (50 μM) in the presence of phenylboronic acid (PBA, 0, 200 μM, 600 μM). The data was obtained in 1/15 M PBS buffer at pH 7.30 with 2.0 mM CTAB solution at 25 ºC.*

In terms of emission spectroscopy, it is almost fluorescence-quenched in the case of free ARS (50 μM) due to the active protons of hydroxyanthraquinone, while the

addition of various concentrations of phenylboronic acid caused the dramatic increase of the fluorescence through the binding of catechol with boronic acid moiety. The formed complex was taken as a new fluorescence sensing system with a very strong emission property (Figure 42, Figure 45).

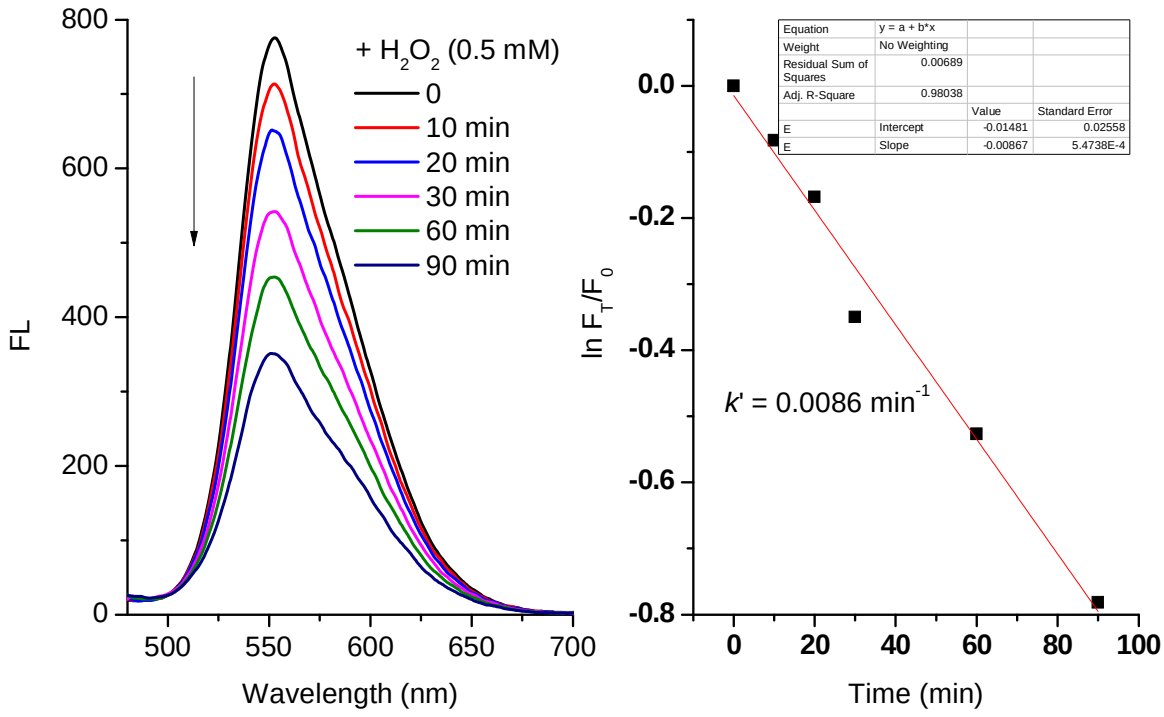

Figure 43. *Fluorescence spectra (λ_{ex} = 460 nm) of ARS-PBA (ARS: 50 μM, PBA: 600 μM) in the presence of hydrogen peroxide (H_2O_2, 500 μM). (a) Emission spectra in different time; (b) Time curve and non-fitting correlation. The data was obtained in 1/15 M PBS buffer with 2.0 mM CTAB solution at 25 ºC.*

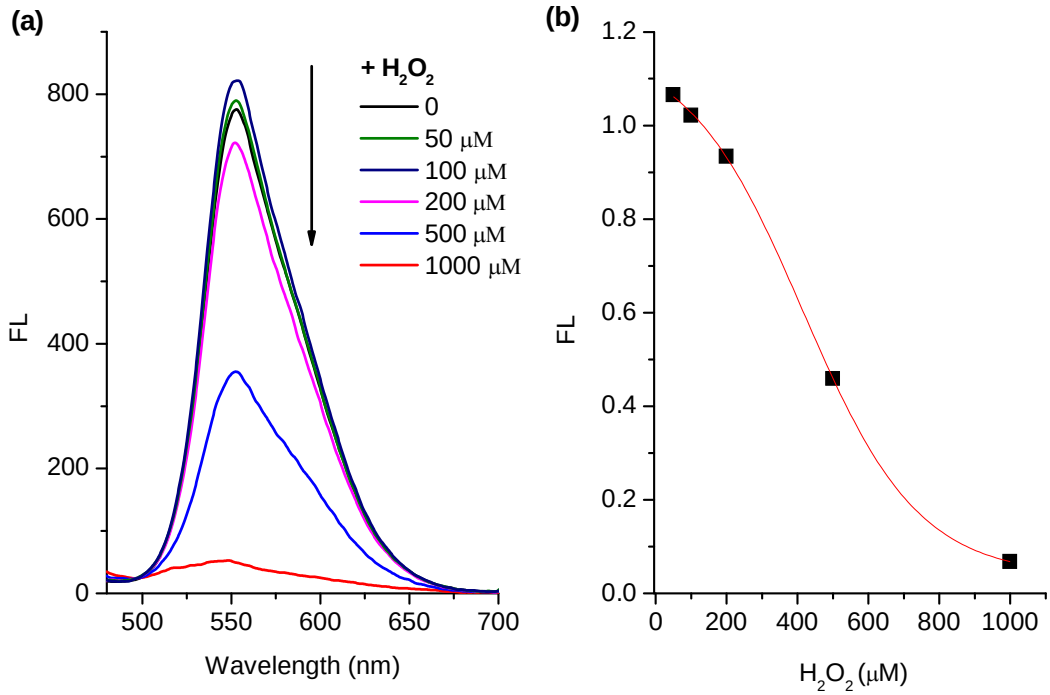

Figure 44. *Fluorescence spectra (λ_{ex} = 460 nm) of ARS-PBA (ARS: 50 μM, PBA: 600 μM) in the presence of hydrogen peroxide (H_2O_2, 0, 50 μM, 100 μM, 200 μM, 500 μM, 1000 μM), then stirred for 60 min. (a) Emission spectra in different dose of H_2O_2; (b) Dose-dependent curve and non-fitting correlation. The data was obtained in 1/15 M PBS buffer with 2.0 mM CTAB solution at 25 ºC.*

Next, we studied its fluorescence sensing property in the presence of H_2O_2. At the early stage, a higher concentration of PBA (600 μM) was used since it triggered larger FL increase (F/F_0 = *ca.* 38.5) in the presence of ARS (50 μM). However, in the time curve (Figure 43) and dose-dependent curve (Figure 44), we observed, in order to quench the FL effectively and completely, a higher concentration of H_2O_2 (approximately 1 mM, Quenching efficiency F_T/F = *ca.* 0.06, *k'* = 0.0086 min^{-1}) was required over a specific time (1 h) in the case of higher PBA. This is attributed to the excess use of phenylboronic acid in the reaction with hydrogen peroxide. Therefore, for the sake of good results with a reducing H_2O_2 utility, we determined to cut down the concentration of PBA in the sensing system (Figure 45).

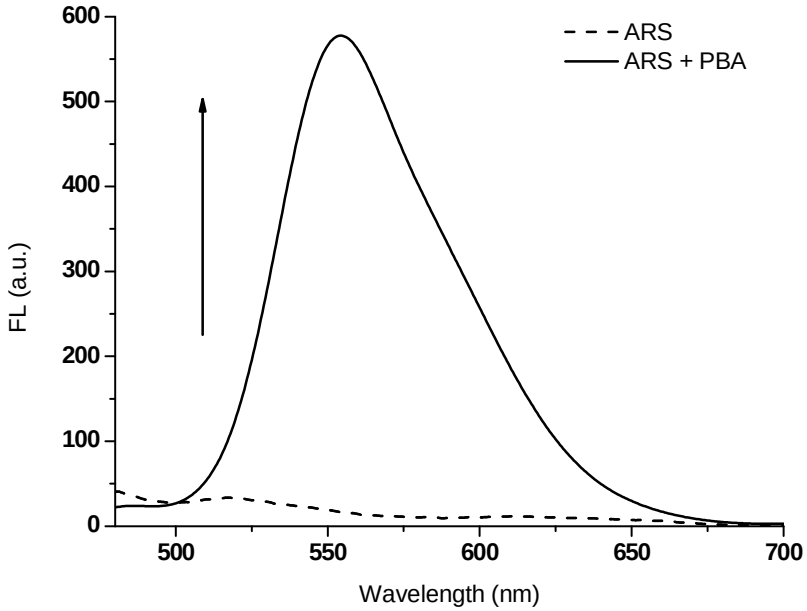

Figure 45. *Fluorescence spectra (λ_{ex} = 460 nm) of ARS only (50 μM), ARS-PBA (ARS, 50 μM; PBA, 200 μM, 15 min). The data was obtained in 1/15 M PBS buffer with 2.0 mM CTAB solution at 25 ºC.*

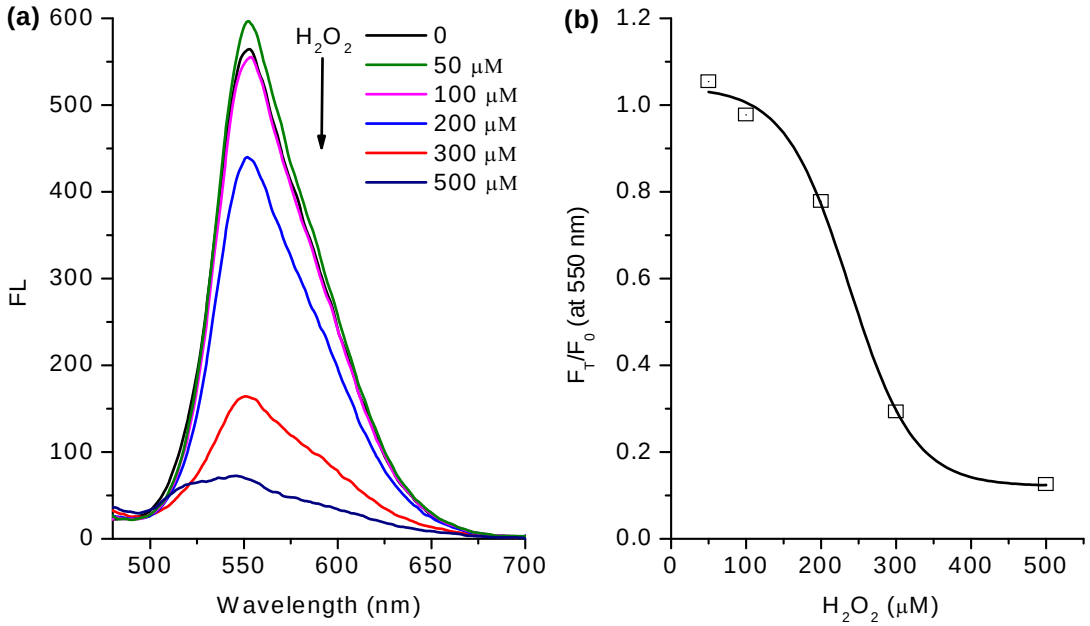

Figure 46. *Fluorescence spectra (λ_{ex} = 460 nm) of ARS-PBA (ARS: 50 μM, PBA: 200 μM) in the presence of hydrogen peroxide (H_2O_2, 0, 50 μM, 100 μM, 200 μM, 500 μM), then stirred for 1 h. (A) Emission spectra in different dose of H_2O_2; (B) Dose-dependent curve and non-fitting correlation. The data was obtained in 1/15 M PBS buffer with 2.0 mM CTAB solution at 25 ºC.*

As can be seen from Figure 45, the fluorescence intensity of ARS (50 μM) was increasing to F/F_0 = *ca.* 28.5 significantly in the presence of PBA (200 μM), while

only 500 μM H_2O_2 resulted in FL decreasing dramatically (Quenching efficiency, F_T/F = *ca.* 0.12) over 1 h (Figure 46). Thus, in the case of reducing PBA concentration to bind with ARS, small amount of H_2O_2 was utilized in this reaction which can release the free ARS and lead to the almost fluorescence quenching.

4.3.1.3 Electrochemical spectra towards H_2O_2

Next, we experimented the sensing procedure and tried to explain the mechanism further using electrochemical method.[239] To the buffer solution of ARS (50 μM), 200 μM of PBA was added. The oxidation signal of free ARS at electrochemical potential of 0.375 V was remarkably decreased due to the hindered oxidation of ARS unit after its complexation with PBA Figure 47a. Similar behaviour was observed in the experiment of the complexation of ARS with another derivative of boronic acid, benzoxaborole.

An effect of ROS on the system consisting of ARS/PBA was studied in time after addition of 300 μM H_2O_2. We can see the reappearance of the peak of the released ARS at 0.375 V and a new peak at 0.585 V which is attributed to the production of phenol, Figure 47b. Both, the oxidation peaks of ARS and phenol were strengthening with the extended response time (0 – 80 min). The inequality of ARS and phenol peaks is caused not only by the different electrochemical activity and mobility of these two molecules but also by equilibrium nature of a boronic acid-diol, i.e. PBA-ARS interaction. It has been already proven that the cleavage of PBA forming borate and phenol is accelerated by the added diol.[225] ARS acts in a catalyst-like manner as it is released unaffected from the cleaved complex and further interacts with another PBA molecule facilitating its cleavage. It has to be said that slow cleavage of PBA occurs spontaneously and contributes thus to the signal of phenol as well.

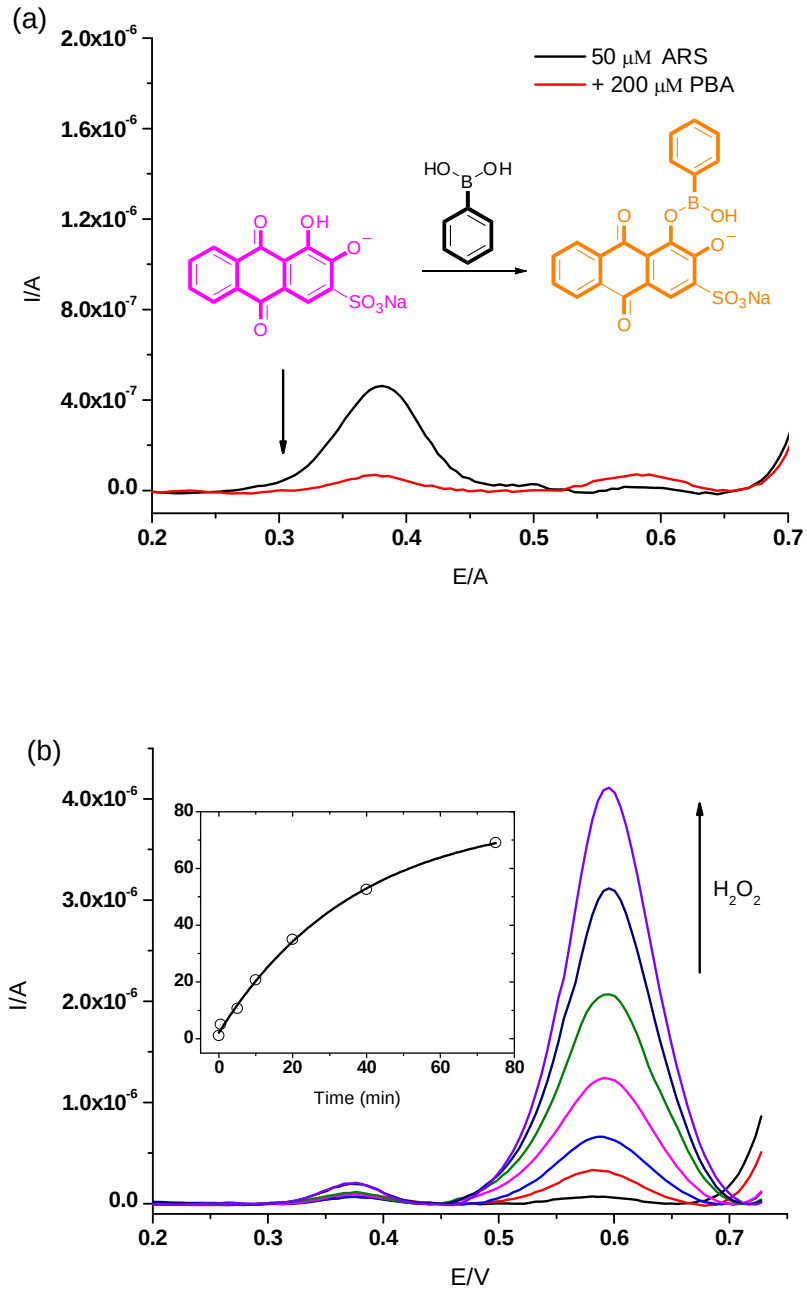

Figure 47. *SW voltammograms for (a) the ARS only (50 μM), ARS-PBA (ARS, 50 μM; PBA, 200 μM); (b) and then addition of H_2O_2 (300 μM, 0 - 75 min).*

4.3.2 ARS-BBA COMPLEX SYSTEM

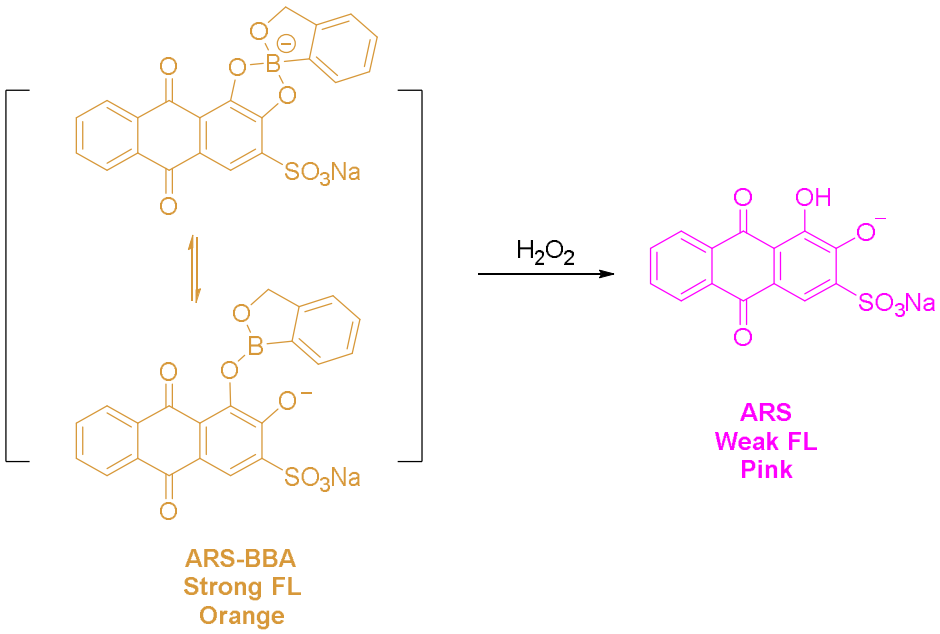

Scheme 53. *Design strategy of probe ARS-BBA complex for H_2O_2.*

Since benzoboroxole has a higher binding constant with diols, we assume its binding with ARS not only can enlarge the absorption and emission signal response, but also change the hybridization mode of boron from sp2 to sp3 then make it less reactive with H_2O_2. If so, this anti-oxidant property might be used in the selective recognition of peroxynitrite which is a much stronger oxidant and more reactive species.

4.3.2.1 UV-Vis spectra towards H_2O_2

In the UV-Vis spectra, the maximum absorption for the free ARS (50 μM) centred at λ_{abs} = 550 nm made a blue shift to maxima λ_{abs} = 470 nm upon addition of phenylboronic acid (200 μM) in pH 7.30 PBS buffer (Figure 47a). Thus, a significant colour change from pink to orange was observed over through 15 mins stirring.

The H_2O_2-mediated oxidation of aryl boronates and subsequent decomposition of the intermediate led to the red-shifted wavelength change of ARS-BBA complex due to the freedom of ARS. When H_2O_2 (500 μM) was added to a solution of ARS-BBA (ARS, 50 μM; PBA, 200 μM), a drop-down at λ = 480 nm absorption was observed with a rising red-shifted band centred at λ_{em} = 535 nm over 2 h with 2.0 mM CTAB and a clear iso-absorption point can be seen at λ_{em} = 500 nm. Figure 49 shows a noticeable colour

change in the formation of the adduct ARS-BBA from pink to orange. In the sensing of H_2O_2 (500 μM), the color of ARS-BBA complex was gradually changed to pink over through 60 min reaction. The big colour difference can be easily noticed by the human's naked eyes.

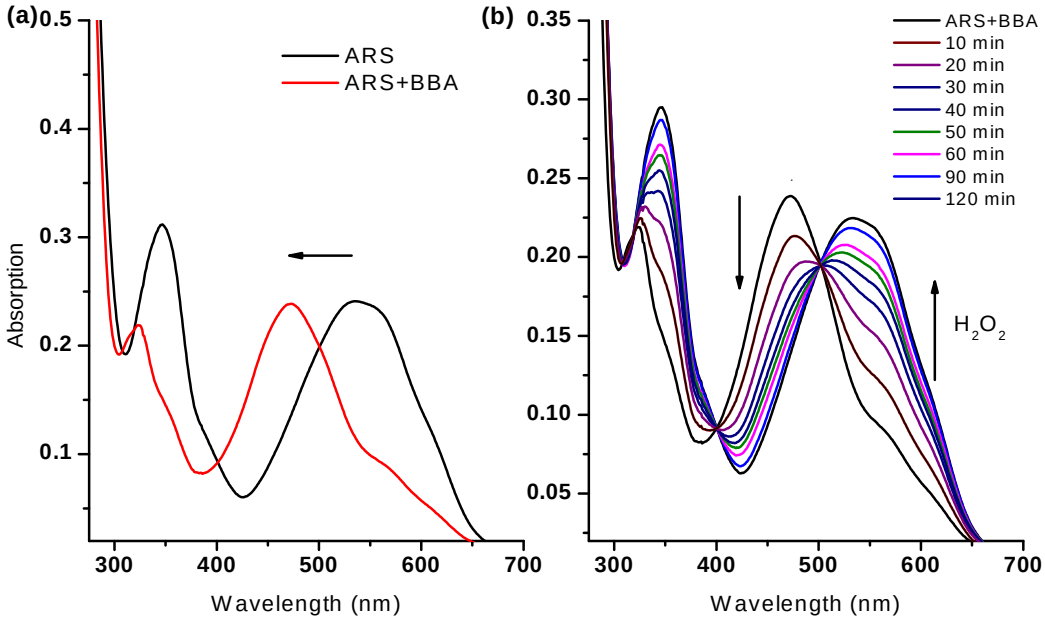

Figure 48. *UV-Vis absorption spectra (a) for ARS only (50 μM), ARS-BBA (ARS, 50 μM; BBA, 200 μM) and (b) then addition of H_2O_2 (500 μM) in the presence of CTAB (2 mM).*

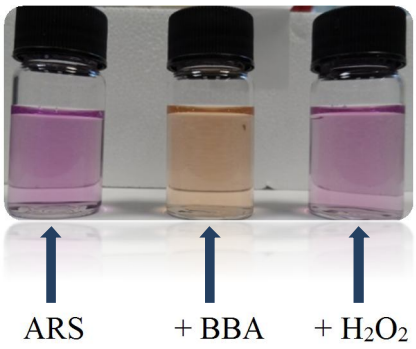

Figure 49. *Color images for ARS (50 μM, left), ARS-BBA (ARS, 50 μM; BBA, 200 μM, middle) and then addition of H_2O_2 (500 μM).*

In Figure 50, there is a good non-linear relationship which can be seen between absorption ratio ($A_{550\ nm}/A_{480\ nm}$) and reaction time (0 – 120 min) under the concentration of ARS-BBA (ARS, 50 μM; BBA, 100 μM) and H_2O_2 (300 μM). The curve was fitted following Equation 2 with a coefficient of determination $R^2 = 0.9988$.

$$y = A1 + (A2-A1)/(1 + 10\text{^}((LOGx0-x)*p)) \qquad \text{Equation 2}$$

Also, the non-100% percent recovery of the absorption intensity from the probe was attributed to incomplete reaction or the incomplete decomposition of the intermediate.

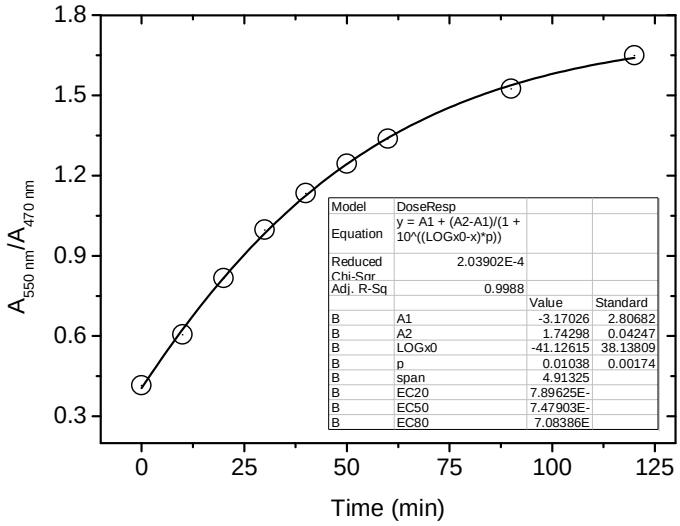

Figure 50. *Relationship between absorption ratio ($A_{550\ nm}/A_{470\ nm}$) and reaction time. The data was obtained in 1/15 M PBS buffer with 2.0 mM CTAB in solution at 25 ºC.*

4.3.2.2 Emission spectra towards H_2O_2

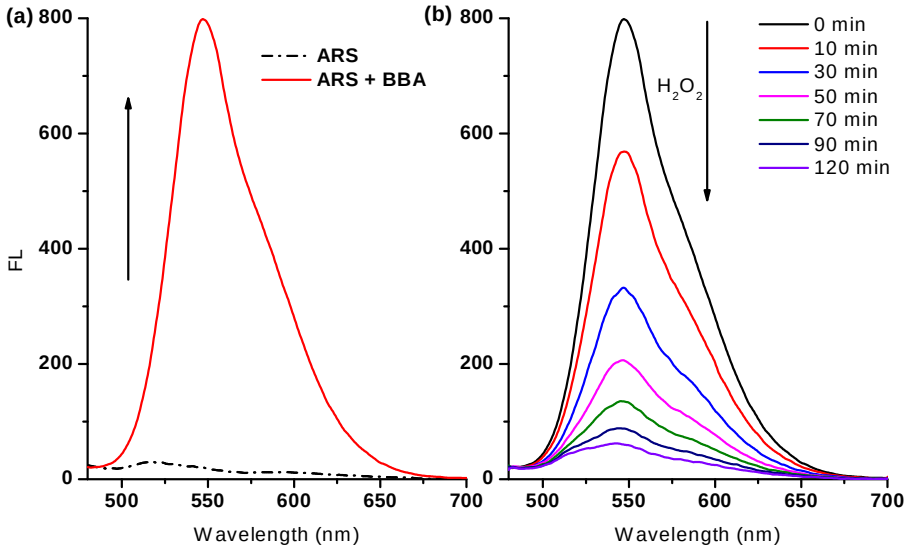

Figure 51. *Fluorescence spectra (λ_{ex} = 460 nm) of (a) ARS only (50 µM), ARS-BBA (ARS, 50 µM; BBA, 100 µM) and (b) addition of H_2O_2 (300 µM).The data was obtained in 1/15 M PBS buffer with 2.0 mM CTAB solution at 25 ºC.*

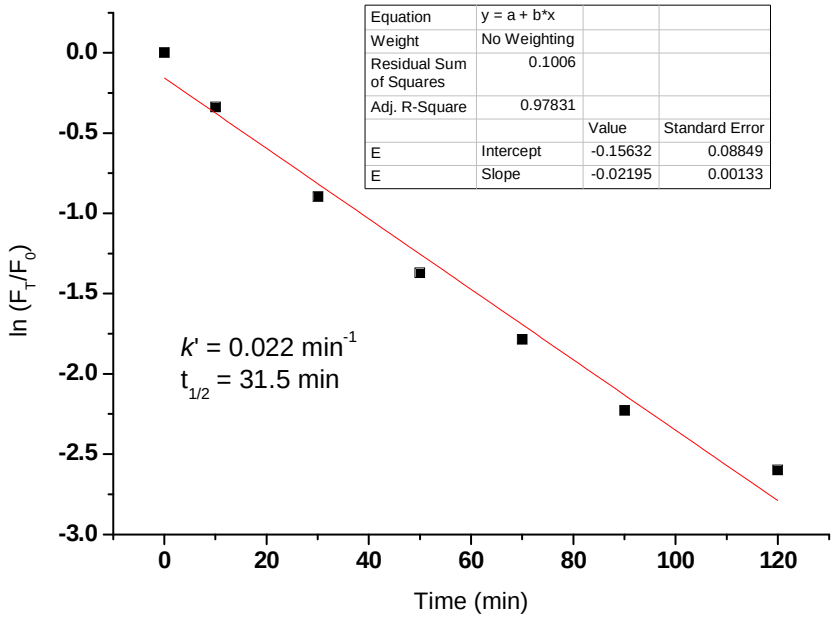

Figure 52. *Time curve and non-fitting correlation of fluorescence spectra (λ_{ex} = 460 nm) for ARS-PBA (ARS: 50 μM, BBA: 100 μM) in the presence of hydrogen peroxide (H_2O_2, 300 μM). The data was obtained in 1/15 M PBS buffer with 2.0 mM CTAB solution at 25 ºC.*

As can be seen from Figure 51a, only presence of 100 μM BBA led to the fluorescence intensity of ARS (50 μM) enlarge to F/F_0 = *ca.* 45.1, while 300 μM H_2O_2 resulted in FL decreasing dramatically (Quenching efficiency, F_T/F = *ca.* 0.07, *k*' = 0.022 min^{-1}) over 2 h (Figure 51b and 52) in pH 7.30 PBS buffer.

4.3.3 COMPARISION BETWEEN ARS-PBA AND ARS-BBA

According to Benkovic's work, it is predicated that there are two fluorescent products for the contribution of the fluorescence increasing in the cases of ARS binding with PBA and BBA, respectively. Considering the reaction in the sensing of hydrogen peroxide, it is reasonable to predicate the boronate binding mode is the minor ingredient to against H_2O_2 while the major product is very reactive to the substrate (Scheme 54).

Given the different performances of ARS-PBA system and ARS-BBA system in the sensing of H_2O_2, it is worth making a comparison from the perspective of binding affinity, optical sensitivity and chemical reactivity between them due to their similar boronate-based structures. Firstly, binding with PBA, it caused a 70 nm blue-shift (λ_{max} from 550 nm to 480 nm) to ARS (Figure 41a) while there is an 80 nm blue-shift (λ_{max} from 550 nm to 470 nm) induced under the case of BBA linking with ARS in the UV-Vis absorption (Figure 48b). The 10 nm longer wavelength change occurring on ARS-

BBA indicated the possibility of a higher binding constant between them as reported. Meanwhile, the data in fluorescence detection demonstrated that it is F/F_0 = *ca.* 28.5 fold increase for ARS (50 μM) in the presence of PBA (200 μM) while the value is *ca.* 45.1 fold fluorescence enlargement on addition of BBA (100 μM). More importantly, quenching efficiency for ARS-BBA system towards H_2O_2 (300 μM) reach up to F_T/F = *ca.* 0.07 while it is a little bit higher for ARS-PBA system with F_T/F = *ca.* 0.12 towards H_2O_2 (500 μM).

The noticeable change and difference in the absorption and emission detection demonstrated that boronic acid receptor BBA is much more competitive in binding with ARS and then sensing of H_2O_2. Thus, it is reasonable to predicate that major hybridization of boron atom on the structure of ARS-BBA is sp2 rather than sp3 (Scheme 54) in neutral aqueous solution and this finding is different with the reported results in terms of BBA-diol interaction.[240-242]

We also verified the deduction *via* ^{11}B NMR spectra (Figure 53) where the peak for the free BBA appears at 35 ppm and with the increasing concentration of ARS (1.6 mM - 6.4 mM) cause no effect on the boron position but enhanced the boron signal. Based on this observation, we can draw the conclusion that the major component in the sensing of H_2O_2 is sp2 hybridized boron under the environment of $-CB(OR)_2$ in the cases of ARS-BBA and the minor structure is boronate mode. Also in the major part of the ARS-BBA species, contraction of the O-B-O bond angle led to the boron atom much more electron-deficiency and stronger eletrophilicity (*ef.* H_2O_2). This advantage belongs to ARS-BBA system which reduced the use of BBA for purpose of sensing lower concentration H_2O_2.

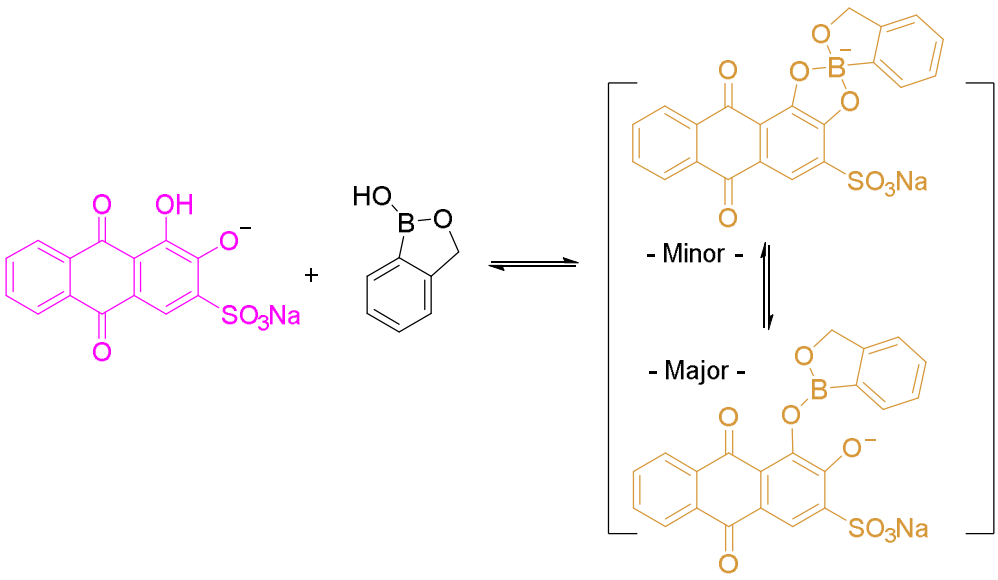

Scheme 54. *Binding mode of ARS and BBA in 1/15 M PBS buffer with 2.0 mM CTAB solution.*

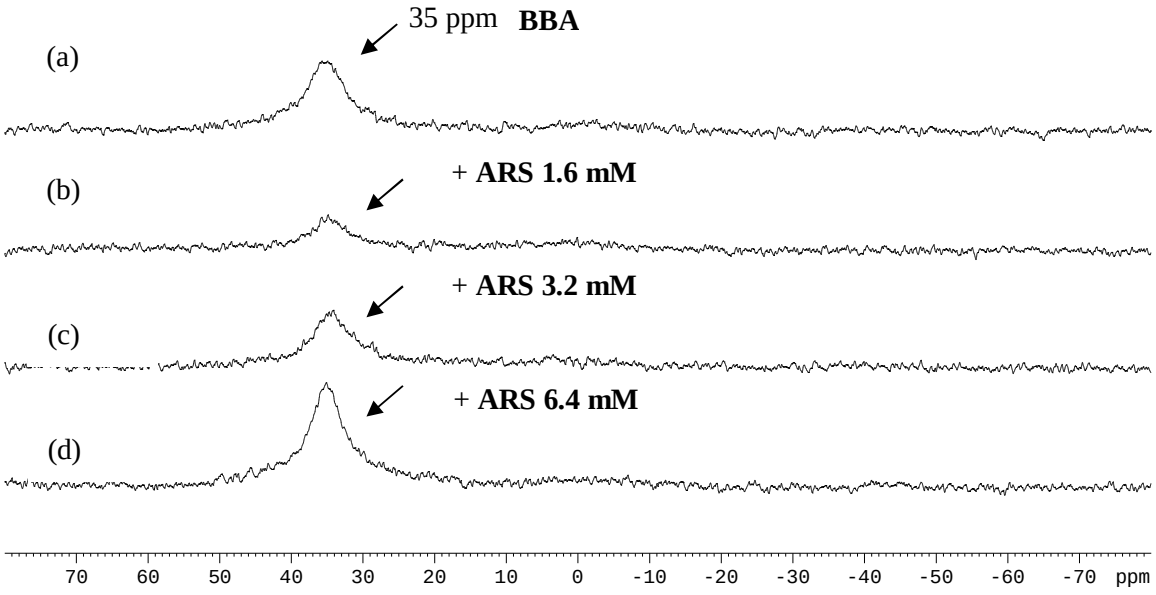

Figure 53. *^{11}B NMR for (a) BBA (20 mM); (b) in the presence of ARS (1.6 mM); (c) in the presence of ARS (3.2 mM); (d) in the presence of ARS (6.4 mM) in MeOH/D_2O = 1:4 mixture.*

4.3.4 ARS-NBA COMPLEX SYSTEM

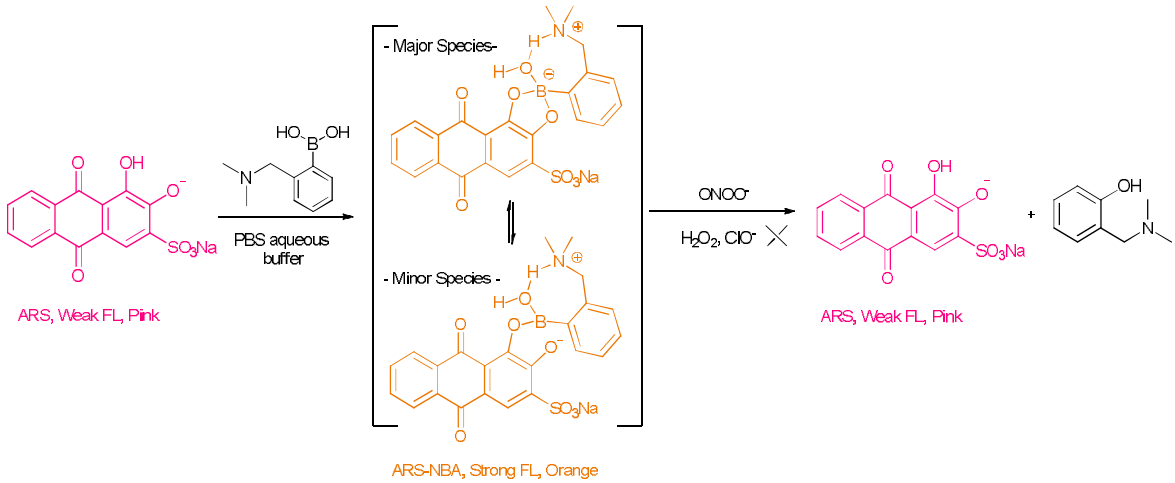

Scheme 55. *Sensing mechanism of ARS-NBA complex probe for peroxynitrite.*

Based on the explorations in the systems ARS-PBA and ARS-BBA for the detection of H_2O_2, it is reasoned that both of them are sensitive and reactive towards the common oxidants, e.g. H_2O_2, ClO^- and $ONOO^-$. Therefore, the previous two systems are not able to selectively recognise one of them under the condition of their co-existence. Since we have explored and confirmed the possibility of the enhanced interaction between the amine and boron to provide a protection method for the selective detection of $ONOO^-$ from H_2O_2 and ClO^-. Subsequently in the project, compound 2-(*N*, *N*-dimethylaminomethyl) phenylboronic acid with N-B structure to bind with ARS was determined to use and then we tested the ARS-NBA system in the sensing of H_2O_2, ClO^-, and $ONOO^-$.

When buffered at neutral pH, we found only small changes occur i.e. only a slight blue-shift was observed in the UV-Vis absorption and a very small fluorescence response due to binding of PBA (200 μM), BBA (200 μM), NBA (200 μM) with ARS (50 μM), respectively (Figure 54.). Whilst, the almost identical pink colours of the solutions clearly indicate weak binding between ARS and three boronic acid receptors at pH 7.30 (Figure 55).

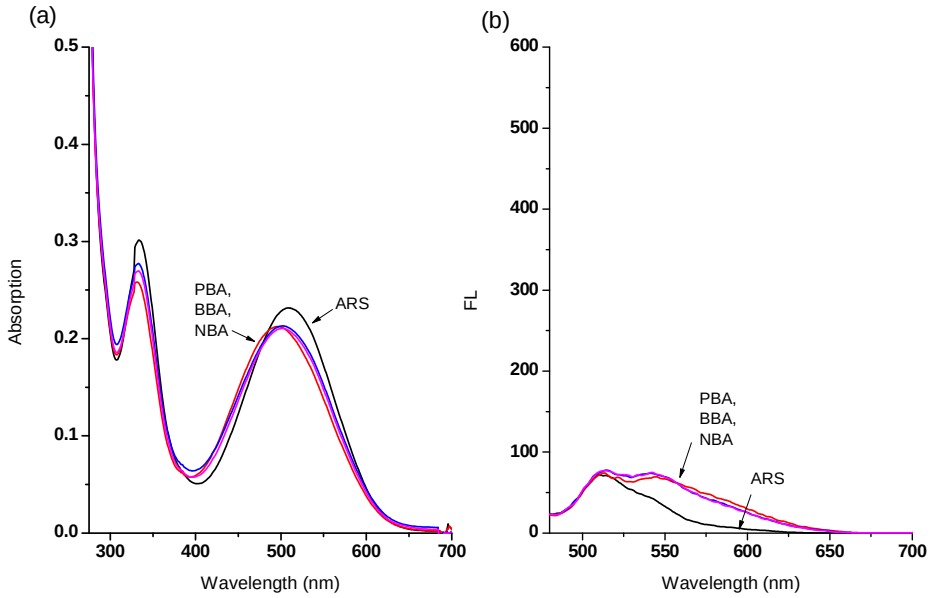

Figure 54. *(a) UV-Vis absorption spectra and (b) Fluorescence spectra (λex = 460 nm) of ARS only (50 μM), ARS-PBA (ARS, 50 μM; PBA, 200 μM), ARS-BBA (ARS, 50 μM; BBA, 200 μM), ARS-NBA (ARS, 50 μM; NBA, 200 μM). The data was obtained in 1/15 M PBS buffer (pH 7.30) without CTAB solution at 25 ºC.*

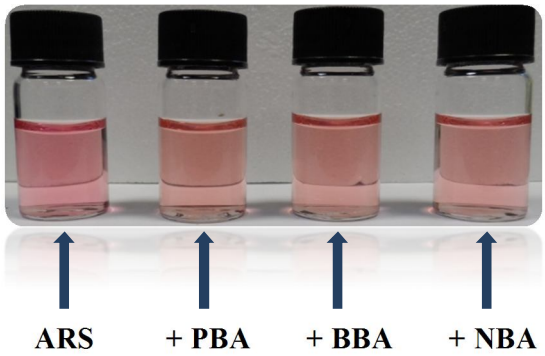

Figure 55. *Color images for ARS (50 μM), ARS-PBA (ARS, 50 μM; PBA, 200 μM), ARS-BBA (ARS, 50 μM; BBA, 200 μM) and ARS-NBA (ARS, 50 μM; NBA, 200 μM). The pictures were taken in 1/15 M PBS buffer (pH 7.33) without CTAB solution at 25 ºC.*

There is no wavelength change in the absorption and only 3-fold fluorescence increase for a longtime stirring even though by an assistance of CTAB (Figure 56). Apparantly, differing from PBA and BBA, incorparating 2-(*N*, *N*-dimethylaminomethyl) phenylboronic acid (NBA) with ARS in the hydrophobic core of micelles under neutral condition is not capable of greatly enhancing the absorption and emission signal due to their very low binding affinity so the system is not suitable to do further research in the sensing of ROS. Therefore, we decided that a higher pH working environment would be preferred to enhance the binding of

boronic acid with the catechol unit.

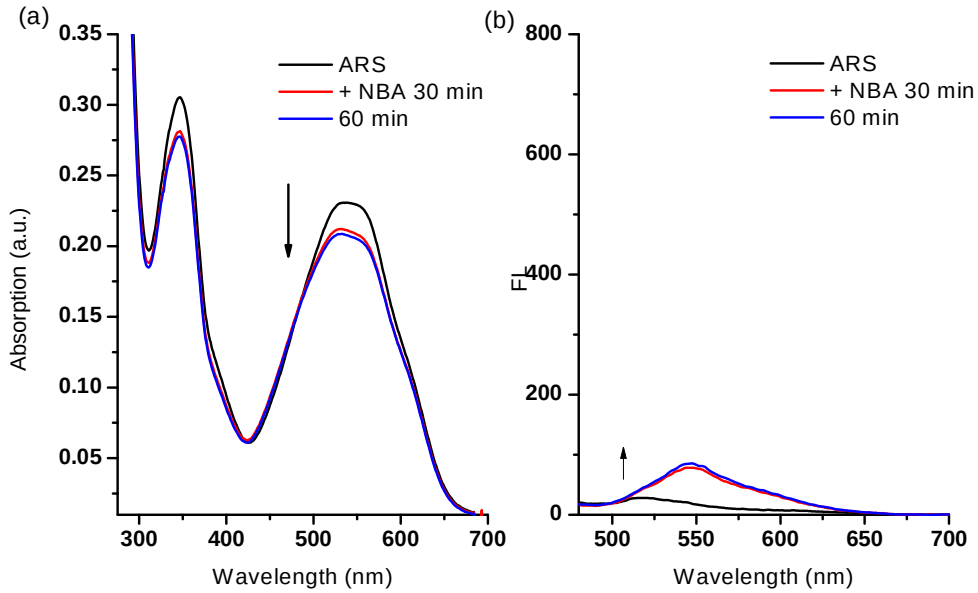

Figure 56. *(a) UV-Vis absorption spectra for ARS only (50 μM), ARS-NBA (ARS, 50 μM; NBA, 200 μM). (b) Fluorescence spectra (λ_{ex} = 460 nm) of ARS only (50 μM), ARS-NBA (ARS, 50 μM; NBA, 200 μM). The data was obtained in 1/15 M PBS buffer（pH 7.33）with 2.0 mM CTAB solution at 25 ºC.*

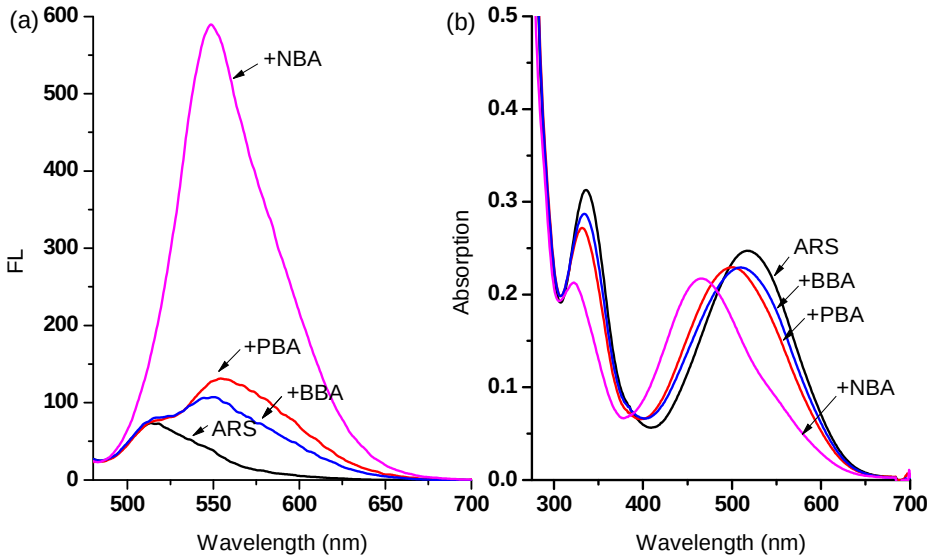

Figure 57. *Fluorescence spectra (λ_{ex} = 460 nm) (a) and Absorption spectra (b) for ARS only (50 μM), ARS-PBA (ARS, 50 μM; PBA, 200 μM), ARS-BBA (ARS, 50 μM; BBA, 200 μM), ARS-NBA (ARS, 50 μM; NBA, 200 μM). The complexes were formed in situ. The data was obtained in 52.1% MeOH/H_2O PBS buffer (pH 8.10) at 25 ºC.*

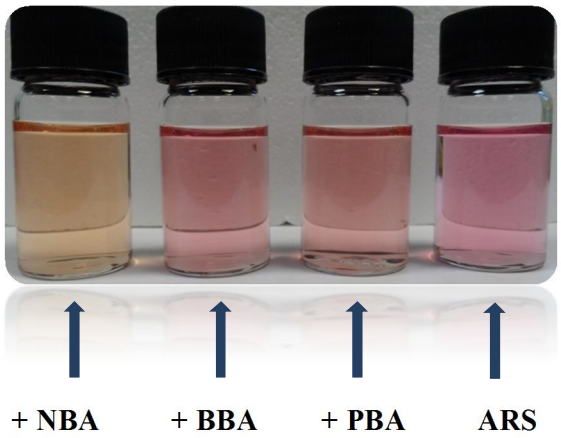

Figure 58. *Color images for ARS-NBA (ARS, 50 μM; NBA, 200 μM), ARS-BBA (ARS, 50 μM; BBA, 200 μM), ARS-PBA (ARS, 50 μM; PBA, 200 μM), ARS (50 μM). The pictures were taken in 52.1% MeOH/H_2O PBS buffer（pH 8.10）at 25 ºC.*

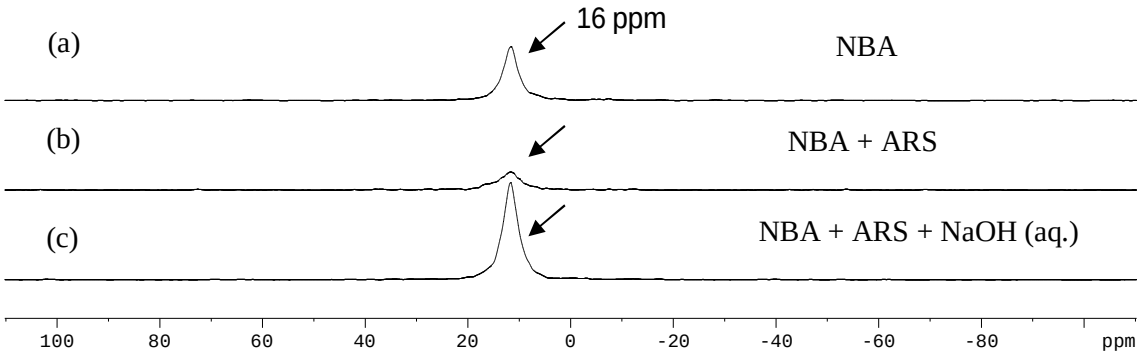

Figure 59. *^{11}B NMR for (a) NBA (10 mM); (b) in the presence of ARS (10 mM); (c) drop addition of NaOH (10 N) in MeOH/D_2O = 1:4.*

As can be seen from Figure 57 in 52.1% MeOH/H_2O PBS buffer (pH 8.10), compound NBA, PBA and BBA behaved differently with ARS and in particular for the fluorescence, there is *ca.* 15.0-fold fluorescence increase for NBA (F/F_0) while only a 3.4-fold increase is observed for PBA and a 2.8-fold increase with BBA, respectively. In terms of absorption, NBA (200 μM) induced the largest shift in wavelength from λ_{max} = 520 nm to λ_{max} = 465 nm (55 nm blue-shift) on binding with ARS in comparison for BBA a 10 nm blue-shift and for PBA a 20 nm blue-shift was observed. A significant colour change from pink to orange in the presence of NBA (200 μM) with ARS (50 μM) was observed (Figure 58), while BBA (200 μM) and PBA (200 μM) did not change significantly with one night of stirring. The binding between NBA and ARS is enhanced by the N-B interaction (N-B bond with solvent insertion). As we have previously demonstrated the N-B interaction provides protection for boronic acids towards common oxidants resulting in selectivity towards stronger reactive oxygen species such

as peroxynitrite ($ONOO^-$). From the boron NMR (Figure 59), the NBA boron is clearly sp^3 in nature and remains sp^3 with added ARS under neutral and alkaline conditions (16 ppm).

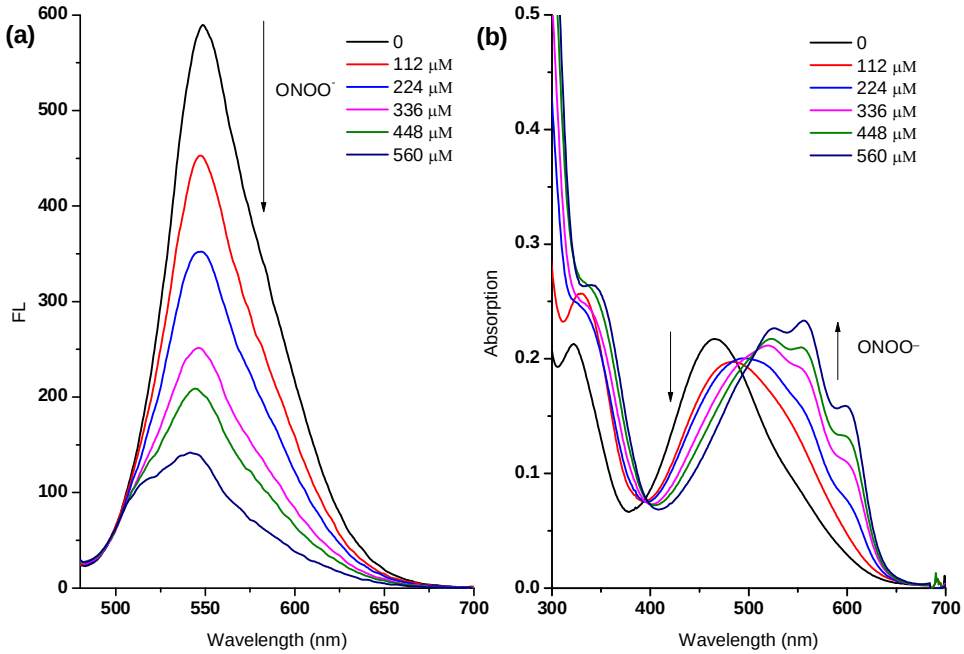

Figure 60. *(a) Fluorescence titration (λ_{ex} = 460 nm) and (b) UV-Vis titration for ARS-NBA (ARS, 50 μM; NBA, 200 μM) in the presence of various concentrations of $ONOO^-$ (0, 112 μM, 224 μM, 336 μM, 448 μM, 560 μM). The data was obtained in 52.1% MeOH/H_2O PBS buffer（pH 8.10）at 25 ºC.*

To the formed sensing system, peroxynitrite ($ONOO^-$) mediated oxidation of aryl boronates to phenols and subsequent decomposition of the complex releases ARS which leads to a fluorescence decrease and red-shift in the UV-Vis spectra.

As can be seen from dose-dependent titration curve in Figure 60a, the enhanced fluorescence of probe ARS-NBA complex was finally reduced to a *ca.* 0.22 (F (in the presence of $ONOO^-$) /F_0 (in the absence of $ONOO^-$)) over a concentration range of peroxynitrite $ONOO^-$ from 0 to 560 μM. A linear relationship is observed between the relative fluorescence ((F – F_0)/F at $\lambda_{550\ nm}$) and the peroxynitrite ($ONOO^-$) concentration (Figure 61a). In Figure 60b, when various concentrations of $ONOO^-$ (0 - 560 μM) were added to a solution of ARS-NBA (ARS, 50 μM; NBA, 200 μM), a significant decrease in the 465 nm absorption was observed with the appearance of a red-shifted band centred at 550 nm. A linear relationship between the absorption ratio (A_{550nm}/A_{465nm}) and the concentration of peroxynitrite ($ONOO^-$)

was observed (Figure 61b). These results indicate that the ARS-NBA system with assistance of N-B interaction displays high colorimetric and fluorimetric sensitivity towards peroxynitrite.

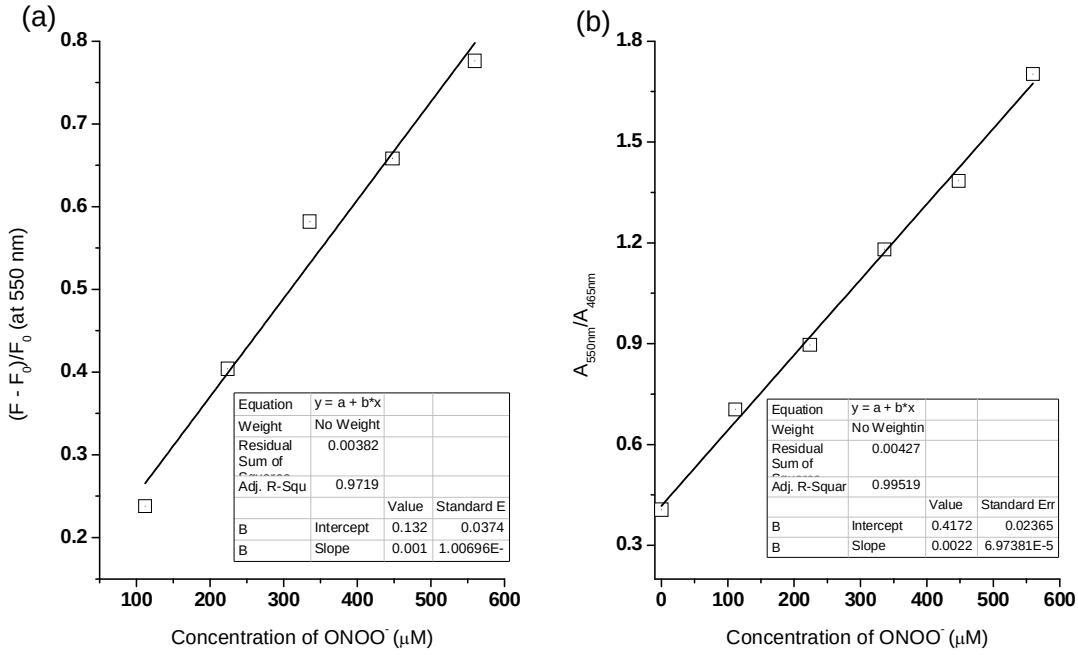

Figure 61. *(a) Linear relationship between $(F – F_0)/F$ at λ_{550nm} and concentration of $ONOO^-$ in fluorescence titration and (b) Linear relationship between A_{550nm}/A_{465nm} and concentration of $ONOO^-$ in UV-Vis titration for ARS-NBA (ARS, 50 μM; NBA, 200 μM) in the presence of various concentrations of $ONOO^-$ (0, 112 μM, 224 μM, 336 μM, 448 μM, 560 μM).*

As reported previously, hydrogen peroxide (H_2O_2), hypochlorite (ClO^-) and peroxynitrite ($ONOO^-$) react with boronate-based compounds to produce the phenol analogues.[243, 244] We have previously demonstrated that the interaction N-B between the amine and boron provides protection for the boronic acid towards oxidation and results in the selective detection of peroxynitrite ($ONOO^-$) over hydrogen peroxide (H_2O_2) and hypochlorite (ClO^-)[57, 58] With this research we use the NBA (2-(*N*, *N*-dimethylaminomethyl) phenylboronic acid) with ARS to provide a complex with strong N-B interaction for the selective sensing of peroxynitrite ($ONOO^-$) over hydrogen peroxide (H_2O_2) and hypochlorite (ClO^-).

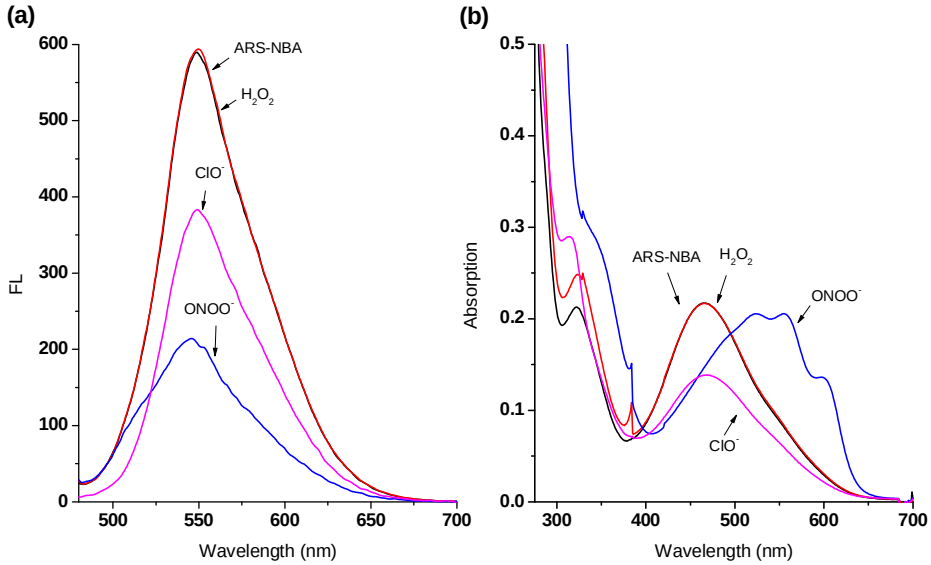

Figure 62. *Fluorescence spectra (λ_{ex} = 460 nm)* ***(a)*** *and Absorption spectra* ***(b)*** *for ARS-NBA (ARS, 50 μM; NBA, 200 μM) in the presence of H_2O_2 (1 mM) for 60 min, ClO^- (0.5 mM) for 30 min, $ONOO^-$ (0.5 mM) for 30 min. The data was obtained in 52.1% MeOH/H_2O PBS buffer（pH 8.10）at 25 ºC.*

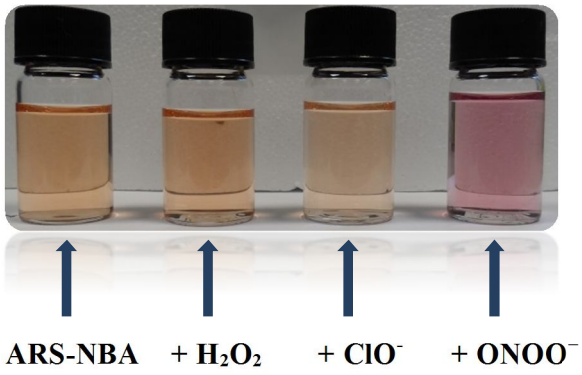

Figure 63. *Color images for ARS-NBA (ARS, 50 μM; NBA, 200 μM), addition of H_2O_2 (1 mM, 60 min), addition of ClO^- (500 μM, 60 min), addition of $ONOO^-$ (500 μM, 60 min). The pictures were taken in 52.1% MeOH/H_2O PBS buffer（pH 8.10）at 25 ºC.*

Both the absorption and emission spectra clearly demonstrate that we have achieved good selectivity for peroxynitrite ($ONOO^-$) since the addition of a high concentration of H_2O_2 (1 mM) was not able to change the fluorescence and absorption intensity of the ARS-NBA complex (ARS, 50 μM; NBA, 200 μM) over 60 min, therefore, the oxidation-reduction between boron and H_2O_2 has been prevented. Only hypochlorite (500 μM) caused a fluorescence decrease $(F - F_0)/F$ = *ca.* 0.35 over 30 min (Figure 62a), However, using the same concentration of ^-OCl (500 μM) and $ONOO^-$ (500 μM), peroxynitrite reacts significantly more with the ARS-NBA sensing system ($(F - F_0)/F$ = *ca.* 0.65). Remarkably, we observed there is

no absorption wavelength (i.e. colorimetric) change in the presence of $^{-}$OCl, yet a significant red-shift occured in the case of $ONOO^{-}$ (from λ_{max} = 465 nm to λ_{max} = 550 nm). The colour differences can be clearly observed *via* the naked-eye, the original ARS-NBA is orange, and on addition of hydrogen peroxide (1 mM H_2O_2, 60 min) and hypochlorite (0.5 mM ClO^{-}, 60 min) the solution remains orange. However on the addition of peroxynitrite (0.5 mM $ONOO^{-}$, 60 min) the color changes rapidly to pink (Figure 63).

4.3.5 ML-NBA COMPLEX SYSTEM

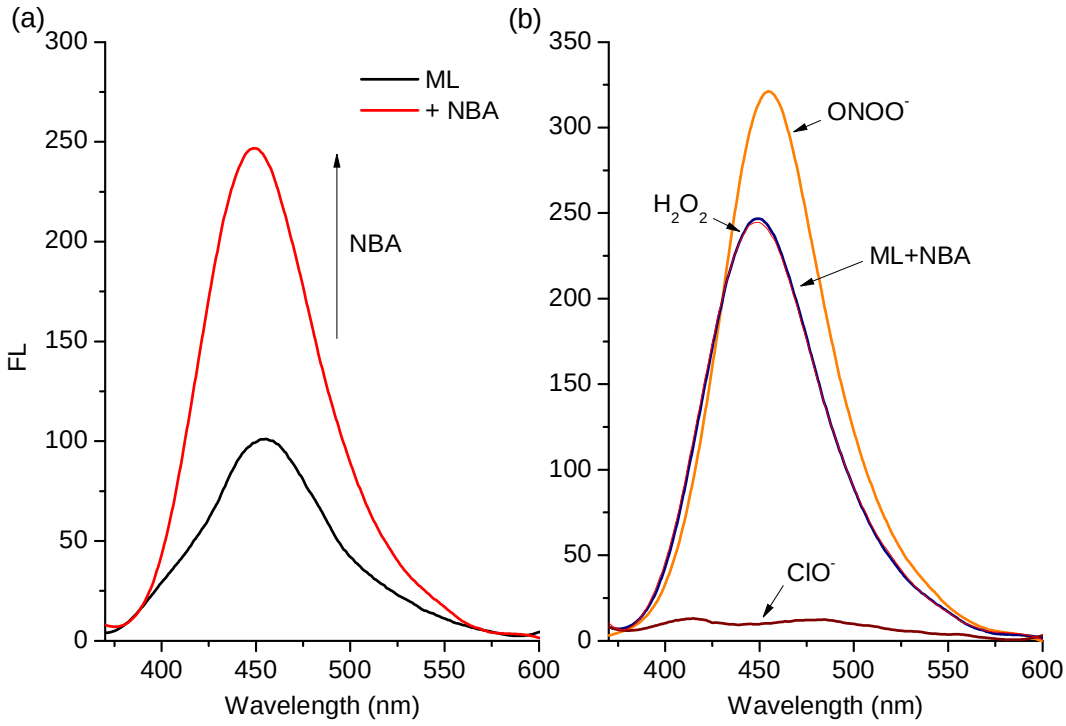

Figure 64. *Fluorescence titration (λ_{ex} = 362 nm) for (a) ML (1 μM) and addition of NBA (50 μM) (b) ML-NBA (ML, 1 μM; NBA, 50 μM) system in the presence of $ONOO^{-}$ (100 μM), ClO^{-} (100 μM) and H_2O_2 (1 mM). The data was obtained in 75%/25% MeOH/H_2O PBS buffer (pH 7.40) at 25 ºC.*

4-Methylesculetin (ML) in a neutral condition (75%/25% methanol/H_2O, pH 7.4 solution) showed a weak emission due to the proton-induced fluorescence quenching. Upon binding with boronic acid receptors, the active proton on hydroxyl groups was removed through dehydration and the electrons on oxygens compensated the electron deficient boron atom so as to suppress the PET process thermodynamically.[245] NBA was chosen as boronic acid receptor when binding with ARS, it showed both great colourimetric and fluorimetric responses towards

peroxynitrite rather than hydrogen peroxide. As can be revealed by Figure 64, after addition of NBA (200 μM) into the ML (50 μM) system at PBA buffered solution, nearly 2.5-fold fluorescence increase was observed. However, based on the ML-NBA, 100 μM $ONOO^-$ led to F/F_0 = *ca.* 1.3 fluorescence turn-on response while 1 mM H_2O_2 caused no disturbance to the fluorescence intensity and 100 μM ClO^- quenched the ML-NBA fluorescence completely.

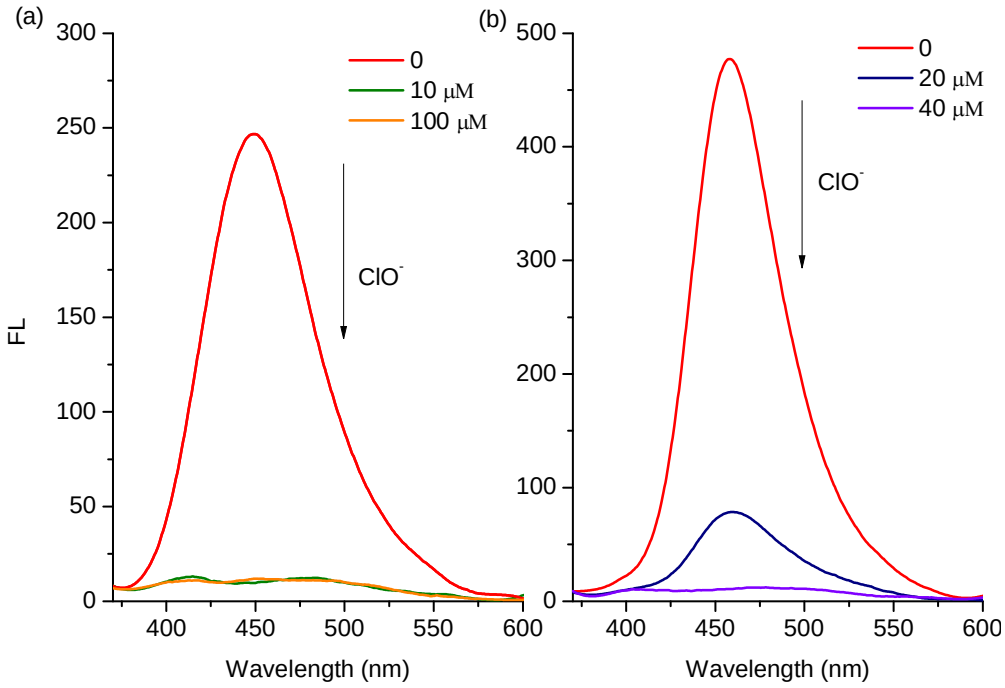

Figure 65. *(a) Fluorescence titration (λ_{ex} = 362 nm) for ML-NBA (ML, 1 μM; NBA, 50 μM) in the presence of ClO^- (10 μM and 100 μM) and (b) Fluorescence titration (λ_{ex} = 362 nm) for ML (2 μM) in the presence of ClO^- (20 μM and 40 μM). The data was obtained in 75%/25% MeOH/H_2O PBS buffer (pH 7.40) at 25 ºC.*

It is beyond the expectation that ClO^- made a difference to the ML-NBA system while $ONOO^-$ was not able to help release the free ML in the system. Thus, it is worth evaluating further the sensing ability of ML-NBA towards hypochlorite. In Figure 65, apparantly, both for the ML-NBA system and the ML itself, low concentrations of ClO^- induced a big fluorescence drop-down so we assume it is due to the damage of the ML structure in the presence of ClO^-. The strong reactivity between ML mother structure and hypochlorite lost its meaning in the fluorescence sensing of certain species.

4.4 CONCLUSION

Using a chemical reaction idea that induces indicator displacement, we designed and investigated new chemo/biosensors for the sensing of hydrogen peroxide and peroxynitrite, *via* the self-assembly of boronic acid derivatives (PBA, BBA and NBA) with different signalling reporters (ARS and ML).

Through observation, the sensing systems ARS-PBA and ARS-BBA displayed good electrochemical, colorimetric and fluorometric responses towards H_2O_2 in a neutral aqueous buffer. The ARS-NBA system displays minimal response towards hydrogen peroxide (H_2O_2) and hypochlorite (ClO^-) due to protection by the N-B interaction, but a large absorption and fluorescence response with peroxynitrite ($ONOO^-$) in an alkaline condition. The boronic acid receptor NBA is a good candidate for the selective detection of peroxynitrite as part of dye-displacement arrays and for biological applications, such as drug design and cell labelling experiments. The large initial change of fluorescence intensity indicates that the system might also be used as a temporal fluorescent probe to map intracellular $ONOO^-$. Systems that produce large visible colour changes are particular interesting since they could be incorporated into a diagnostic test paper for $ONOO^-$, similar to universal indicator papers for pH. Significantly, the ratiometric absorption wavelength shift is a reflection of colour change (from orange to pink) since this can be recorded by the camera and detected by naked-eye instantly. More importantly, ratiometric probes increase the dynamic range and permit signal-rationing, thus they provide built-in correction for monitoring environmental effects.[246, 247] Therefore, we believe that this simple but powerful system can be extended into new applications for the sensing of reactive oxygen and nitrogen species (ROS and RNS) both *in vitro* and *in vivo*.

Chapter Five:

RESULTS AND DISCUSSION IV

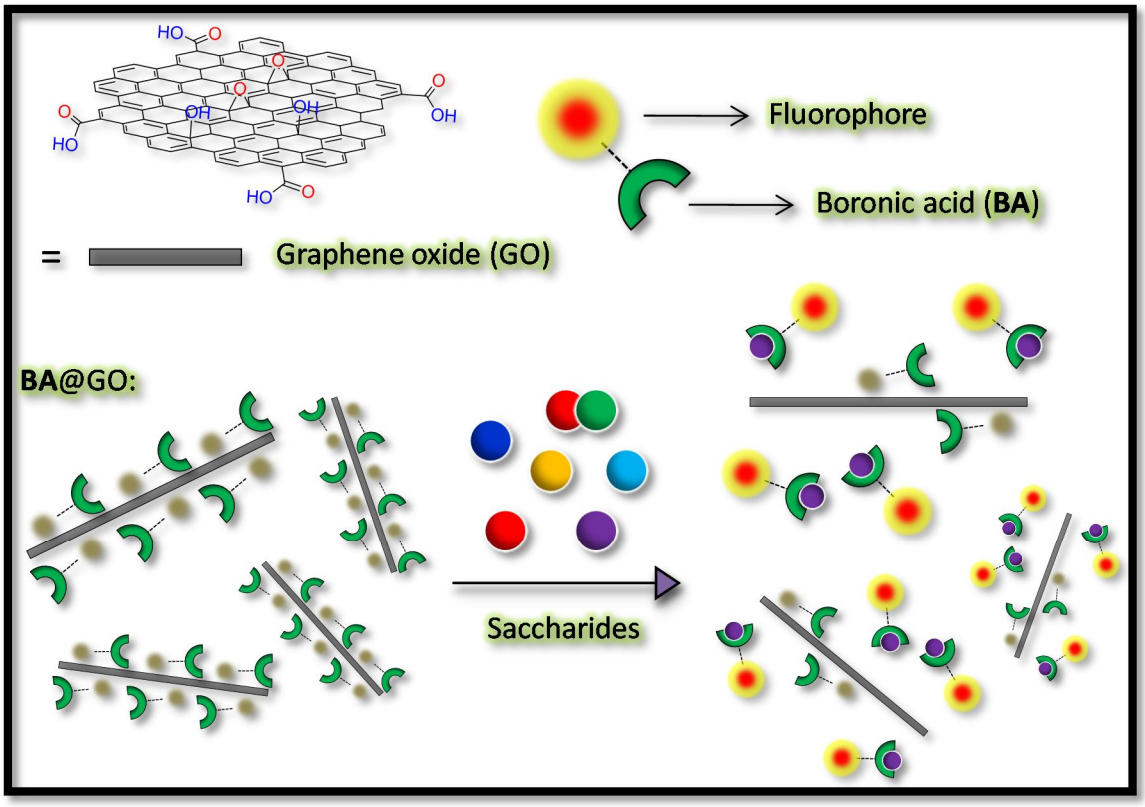

5. RESULTS AND DISCUSSION IV

5.1 BACKGROUND

Boronic acids have been exploited extensively as chemo/biosensors in the detection of saccharides, anion, and ROS/RNS through electrochemical, fluorescence, and colorimetric measurements.[62, 231, 246] Notably, boronic acid are an excellent molecular receptor for monosaccharides since boronic acid derivatives rapidly and reversibly interact with saccharides in aqueous media, and thus importantly the method does not consume the analyte. The chemical and biological significance of the interaction between boronic acid and saccharides has been extensively used for the study of saccharides detection *via* fluorescence methods.[194, 231]

However, limited work has been carried out in the development of fluorescent materials for the chemical sensing of sugars *via* boronic acid-saccharide interaction.[248-250] Among them, Strano *et al.* developed a series of boronic acid (BA) constructs using sodium cholate suspended SWNTs (SC/SWNTs) and have screened the resulting complexes for their ability to modulate fluorescence emission response to glucose (Scheme 56). However, the selectivity and sensitivity of BA-SWNT complexes towards saccharides were suboptimal and thus hampered their further development.[251] They also conjugated PBA with amphiphilic PEG polymers, and examined the interaction of these functionalized polymers with SWNTs using different spectroscopies, and finally evaluated the ability of these polymer−SWNTs to modulate fluorescence emission in the presence of different saccharides (Figure 66).[250] Through observation, they found the conformational variation of the aromatic boronic acids effected the quantum yield of the SWNTs. In addition, a novel signal transfer mechanism can be employed to control the binding selectivity of saccharides, which might open a new window to detect biomolecules which are otherwise difficult to recognize. However, this work was only a concept and they did discover good sensitivity and selectivity towards the target.

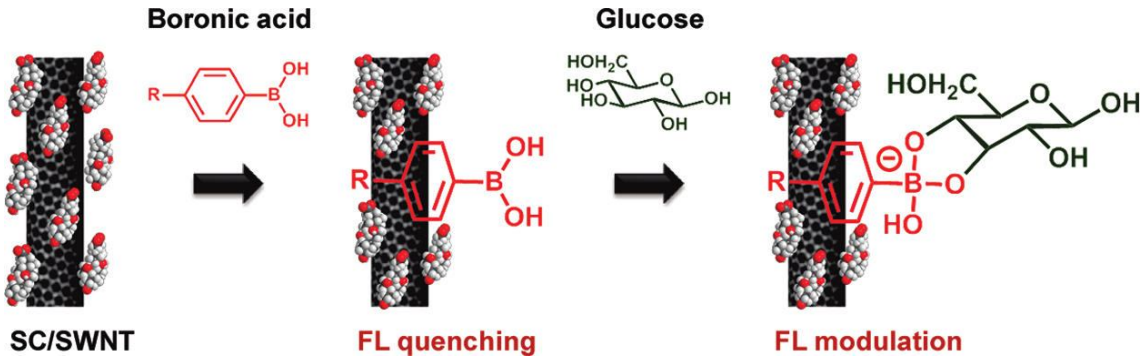

Scheme 56. *Schematic representation of boronic acid derivatives to form complexes with sodium cholate suspended single-walled carbon nanotubes (SWNTs) to reversibly report glucose binding via a change in SWNT fluorescence. Reproduced with permission from (ACS Nano, **2011**, 6, 819.) Copyright © 2011 American Chemical Society*

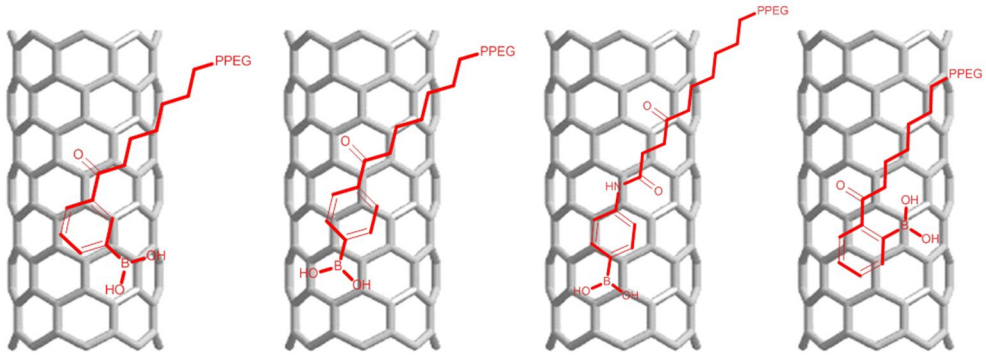

Figure 66. *Schematic representation of phenyl boronic acids conjugated to a polyethylene glycol polymer to disperse single-walled carbon nanotubes (SWNT).*

Graphene oxide (GO), due to its excellent optical and electrical properties, good water solubility and low toxicity to the human body, has become a material of choice for in the development of chemo- and biosensors.[252, 253] In particular, GO has been shown to be a universal quencher of nearly all fluorescent dyes, taking advantage of the fluorescence resonance energy transfer (FRET) mechanism.[254, 255] Merkoçi *et al.* indicated the FRET efficiency of this quenching process (E) depends on the inverse sixth distance between donor and acceptor (R): $E = 1/ [1 + (R/R_0)^6]$, where R_0 is the distance at which half of the energy is transferred, and depends on the spectra characteristics of the dyes and their relative orientation.[255, 256] Besides, GO exhibits strong stacking ability with an increased number of FRET acceptor molecules due to a high planar surface (~2620 m^2g^{-1}, theoretical specific surface area for completely exfoliated and isolated graphene).[257]

As a result, GO-based fluorogenic (fluorescence 'off-on') sensors that embody a fluorophore functionalized with biomolecules stacked to GO for detection of DNA,

proteins, enzymes, microbes and live cancer cells have been devised.[258-265] These GO composites are advantageous in that they are economic and simple to prepare, and a recent study reveals that the two-dimensional (2D) GO material is a better choice in DNA analysis than either SWNT (1D) or gold nanoparticles (0D).[266] Thus, it is of high interest to develop novel GO-based chemosensors for the recognition of various species.

5.2 DESIGN STRATEGY

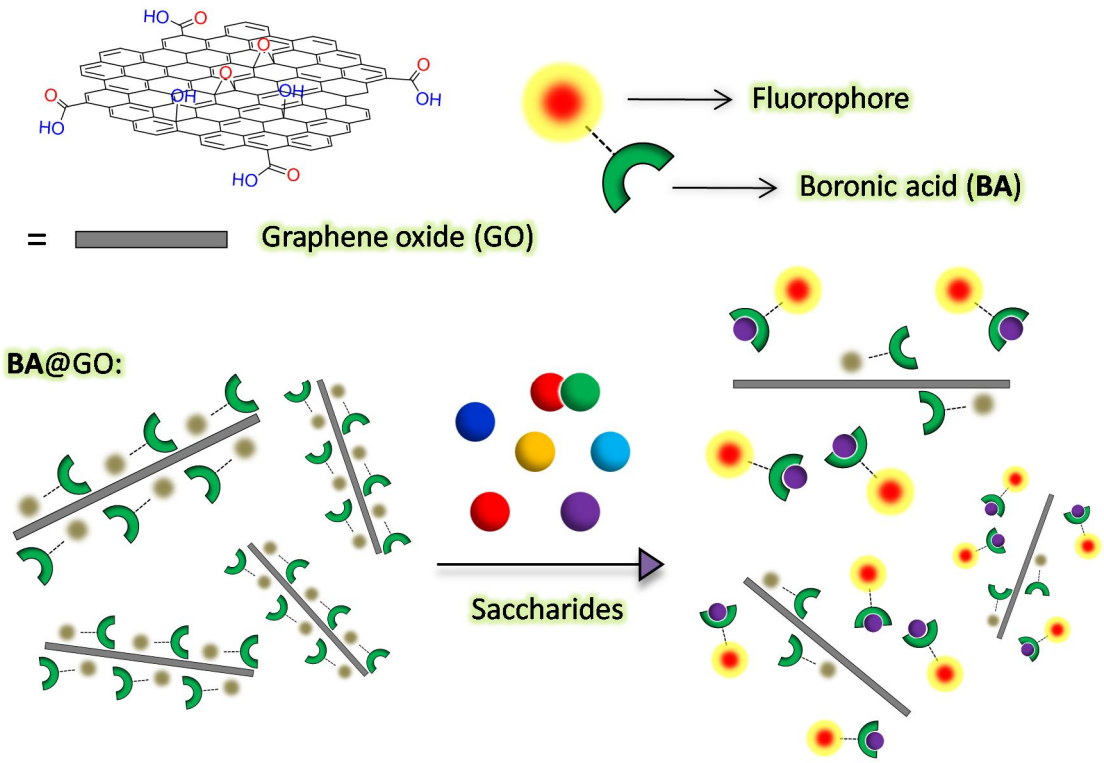

Figure 67. *Schematic representation of the designed fluorogenic BA@GO sensors for the selective detection of saccharides.*

To the best of our knowledge, GO fluorogenic sensors functionalized with boronic acid receptors for the sensing of saccharides have never been reported. By taking advantage of the good property of boronic acids in the sensing of monosaccharide, we assume GO should be one of good candidates among the various supporting materials for the development of fluorescence devices. Therefore, we hypothesized that the complexation of monosaccharides with an aromatic boronic acid probe conjugated on the surface of GO, presumably through stacking between the graphene plane and aromatic moiety of fluorescence probes, could modulate the fluorescence signal in response to the binding of saccharides (Figure 67).

Initially, it is very important to select suitable boronate-based fluorescent probes in this project since these stacking ability with GO and the binding strength with monosaccharide are key points in the design. We chose to use fluorescence probe **101** with *N*-substituted-1,8-naphthalimide as reporter and probe **108** with fluorescein as reporter which have been explored in our group and we observed in the previous

research that **101** showed excellent turn-on fluorescence response towards monosaccharides while **108** was a good protein labelling reagent in the biological systems.

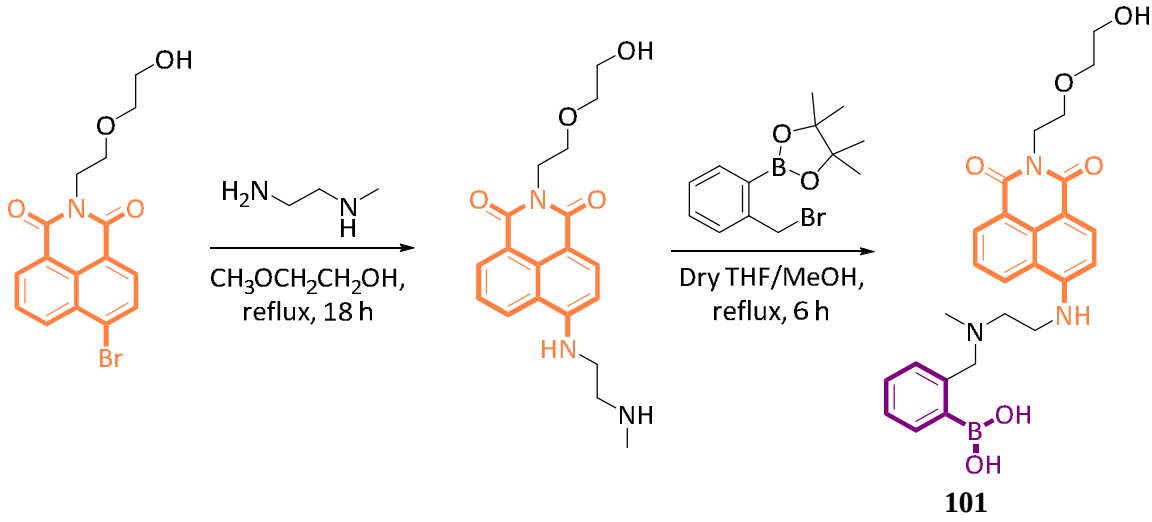

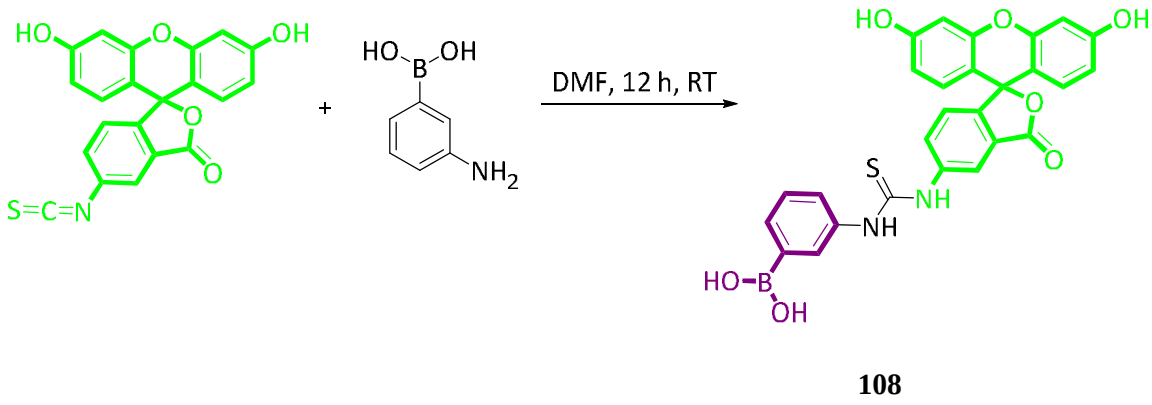

Scheme 57. *Synthetic route for **101** and **108**.*

Probe **101** (λ_{abs} = 440 nm, Ɛ = 9500 $M^{-1}cm^{-1}$, Scheme 57) was designed based on the PET mechanism.[227] *N*-substituted-1,8-naphthalimide is an excellent D-π-A chromophore with good photophysical and photochemical properties. The introduction of the hydroxyethoxyl side chain not only improves its water-solubility, but also makes the whole structure flexible. The system displays an "off-on" response towards monosaccharides due to the enhanced N-B interaction and has been used as a fluorescent water-soluble naphthalimide-based receptor for saccharides with highest sensitivity in the physiological pH range.[71, 227] Also, in our previous research, we reported that N-B bond formation with probe **101** allows for the selective detection of peroxynitrite among the various ROS/RNS species.

Probe **108** (λ_{abs} = 490 nm, Ɛ = 91900 $M^{-1}cm^{-1}$, Scheme 57) was synthesised by incorporating 3-aminophenylboronic acid with fluorescein isothiocyanate in nonaqueous DMF.[267] As known, fluorescein dye has been widely used in biological research and healthcare due to its good biocompability, bioorthogonality and non-toxicity. Similarly, **108** has been studied in the diol appended quenchers for fluorescein boronic acid due to the readily and reversibly interaction between boronic acids and 1,2- and 1,3-diols under basic conditions.[267] In addition, the entire compound is rigid from the perspective of molecule structure.

Therefore, it should be noted that compound **101** and **108** were selected as promising probes in the fluorescence detection of biomolecules. In both cases, fluorescence probe **101** and probe **108**, the boronic acid moiety is recognized as an excellent binding motif for saccharides.[268, 269]

Through experimental observation, we found that the fluorescence of BA@GO complex, quenched by the attachment of simple mono-boronic acid fluorophore to GO, can be recovered in the most significant response to binding of fructose, among the saccharides. With the potential to further develop novel BA-modified graphene oxides nanocomposites through taking advantages of boronic acid derivatives in the recognition of saccharides and good optical and physical properties of GO as the supporting holder. We believe that the simplicity of our method coupled with the possibility for extension towards a general sensing platform for other saccharides can provide new insight into developing advanced fluorogenic materials.

5.3 RESULTS AND DISCUSSION

5.3.1 FORMATION AND CHARACTERIZATION OF BA@GO

The **101**@GO and **108**@GO composites were formed by mixing boronic acids (**101** and **108**) with freshly prepared GO *in situ*.[265] The **101**@GO composite material was chosen as a model to be characterized by various techniques. Atomic force microscope was used to measure the height of the GO flakes. Whereas the height of unmodified GO measures 1.2 nm (Figure 68a), that of GO stacked with **101** grows to 1.8 nm (Figure 68b); the latter indicates composite formation of GO with **101**. Note that all intersected surface areas of **101**@GO showed a similar height increase of about 0.6 nm, indicating that the compound was densely distributed on the surface.

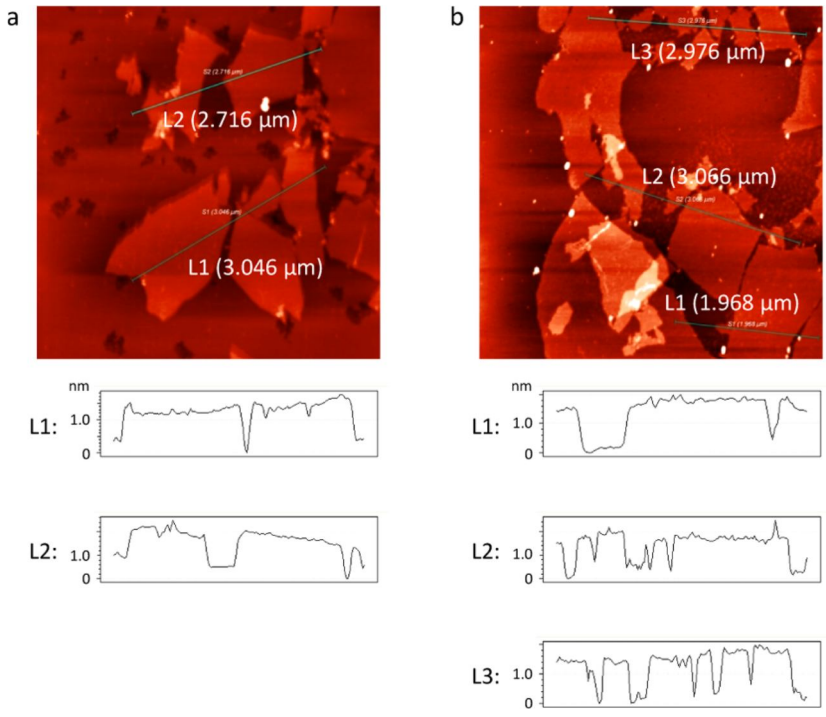

Figure 68. *AFM images of (a) GO and (b) **101**@GO.*

Raman spectroscopy additionally corroborated the composition of the composite (Figure 69a): the ratio of the intensity of D band (1355 cm^{-1}) to that of G band (1600 cm^{-1}) of **101**@GO (0.91) is greater than bare GO (0.86), which means that the carbon sp2-hybridization of the former is increased upon stacking with the aromatic compound.

[254, 255] In the meanwhile, through stacking with **101**, a new peak characteristic of GO appeared at 450 nm in the UV-Vis spectrum (Figure 69b), which also indicates the formation of **101**@GO composite. (*The work above was performed in Key Laboratory for Advanced Materials and Institute of Fine Chemicals, East China University of Science and Technology, China*)

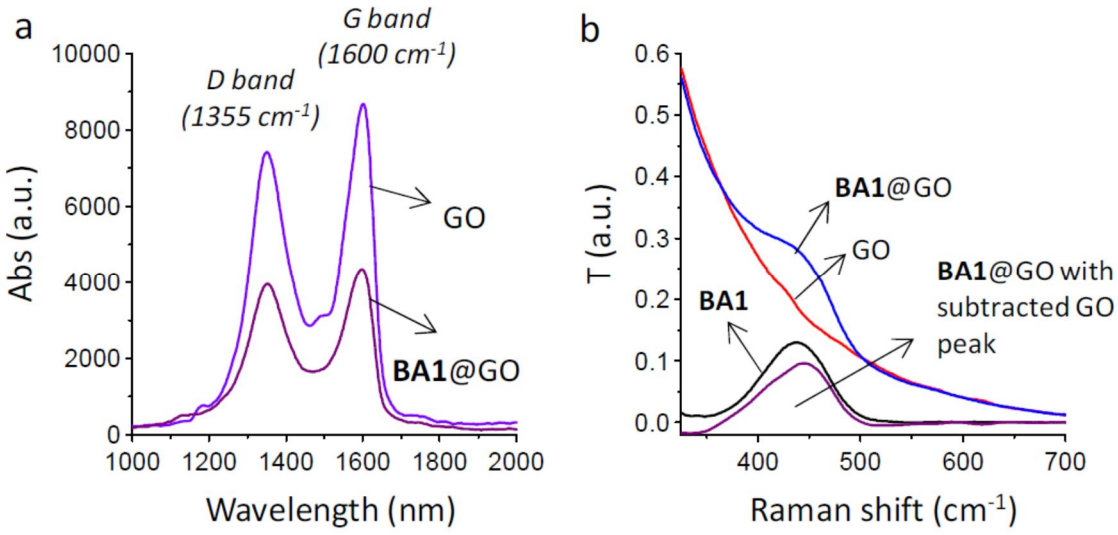

Figure 69. *(a) Raman spectra of GO and **101**@GO; (b) UV-Vis spectra of **101** (10 μM), GO (40 μg/mL) and **101**@GO.*

5.3.2 EMISSION SPECTRUM OF BAs@GO AND FRUCTOSE DETECTION

In the case of **101**, presence of 40 μg/mL of GO led to almost complete FL quenching of the probe [$(F_0\text{-}F)/F_0$ = 97.4%, where F is the FL of **101** with GO and F_0 that without GO] (Figure 70a). A good linear response in the presence of increasing GO (0 – 12 μg/mL) was observed (R^2 = 0.9955, Figure 70b). The quenching is probably due to the fact that, when the fluorescence probes are stacked to GO, the photoexcitated energy is transferred from the naphthalimide fluorophore to the GO acceptor.[8,9]

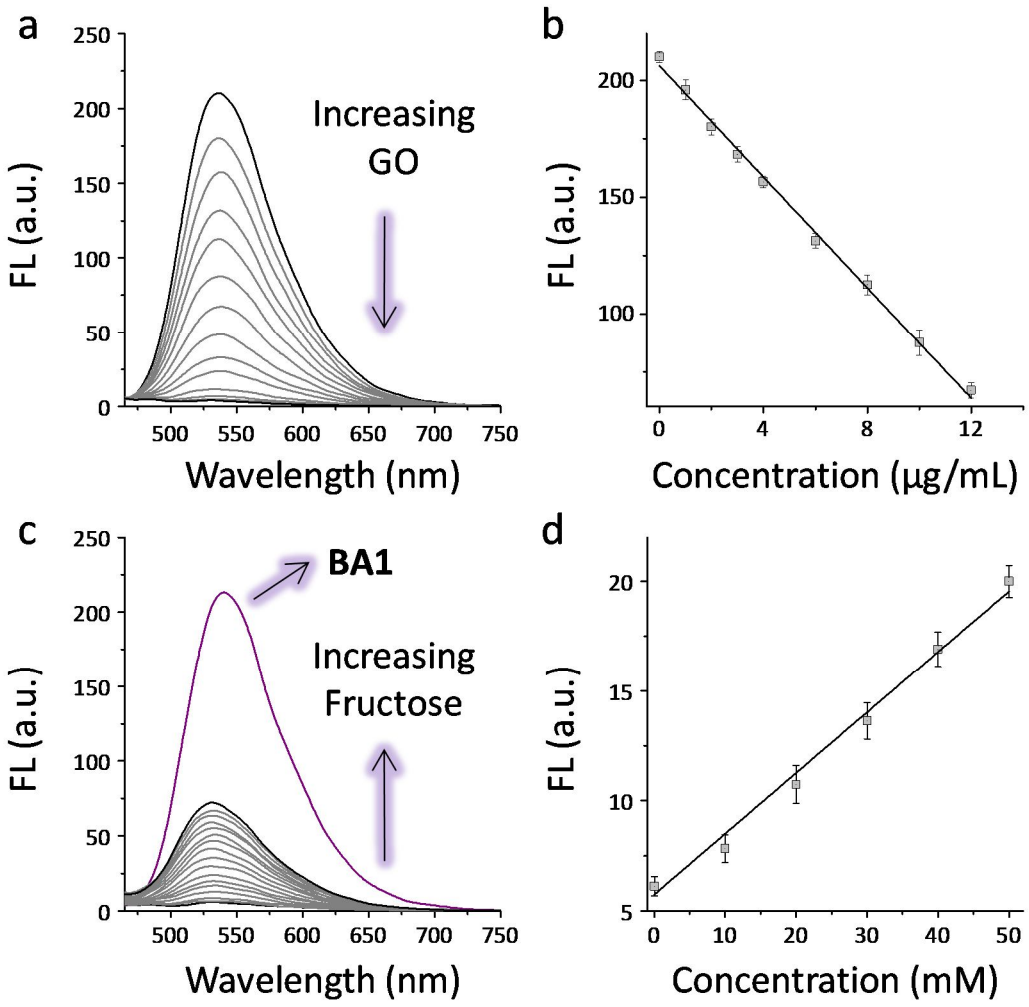

Figure 70. *(**a**) Fluorescence (FL) change of **101** (2μM) in the presence of increasing GO (graphene oxide, 0 – 45 μg/mL) in Tris-HCl (0.05 M, pH 7.3); (**b**) The linear range of FL change of **101** at 525 nm in the presence of increasing GO (0 – 12 μg/mL); (**c**) Fluorescence (FL) change of **101**@GO (2 μM) in the presence of increasing fructose (0 - 2 M, the yellow curve is the FL spectrum of **101**) in Tris-HCl (0.05 M, pH 9.0); (**d**) The linear range of FL change of **101** at 525 nm in the presence of increasing fructose. (λ_{ex} = 410 nm).*

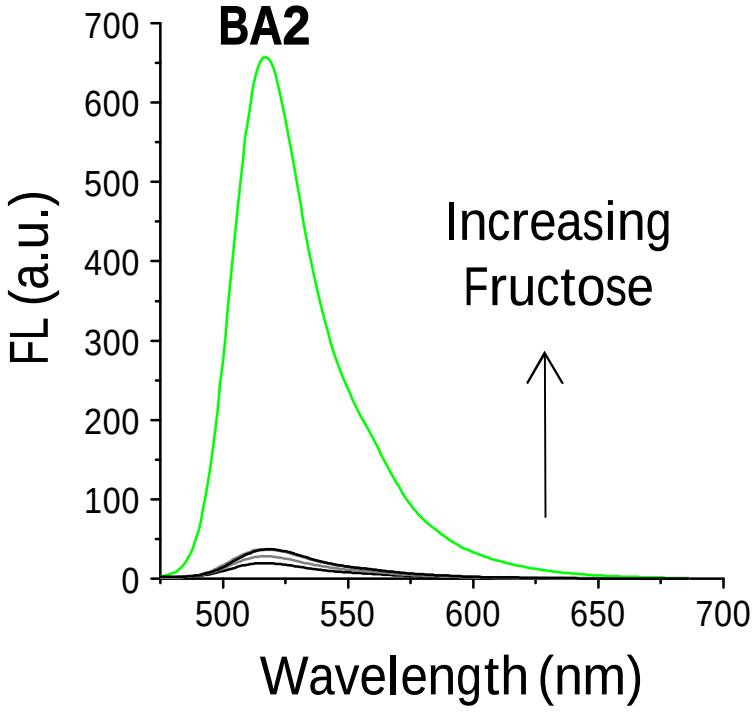

Figure 71. *Fluorescence (FL) change of **108** (2 μM) in the presence of increasing GO (graphene oxide, 0 – 45 μg/mL) in Tris-HCl (0.05 M, pH 7.3).*

Subsequently, in the presence of increasing fructose (0 – 2 M), the maximum FL of **101** at 525 nm was gradually recovered with a maximum recovery ratio[$(F_1-F)/(F_0-F)$, where F is the FL of **101** with GO, F_0 that without GO, and F_1 the FL of **101**@GO with fructose] of 32.2% (Figure 70c, the linear range of FL recovery is shown in Figure 70d, $R^2 = 0.9925$). The detection limit of **101**@GO for fructose was determined to be 2.7 mM (3σ/k). Meanwhile, we determined that, for the free **101** probe, the addition of fructose (0 – 1 M) led to 2.8-fold FL increase of the probe (2 μM) due to the enhanced N-B interaction in an aqueous solution (pH 9.0, Figure 72a). We ascribe the "turn-on" response of the **101**@GO composite to the specific covalent bonding of the boronic acid of **101** with fructose, leading to increase in hydrophilicity of the resulting **101**-saccharide complex which causes the complex to detach from the GO surface (i.e. weakened π-stacking). The release of the complex from the surface then leads to recovery of the fluorescence of the probe, since the surface quenching by FRET to the GO surface is now not possible. However, the incomplete FL recovery indicates that part of the small-molecule probe was still linked with GO likely due to strong stacking forces.

In contrast, while the maximum FL intensity of **108** could be similarly quenched adequately in the presence of 40 µg/mL of GO [$(F_0\text{-}F)/F_0$ = 97.4%, Figure 71], compared with **101**, the presence of excessive fructose (2 M) barely induced its FL recovery (recovery rate = 2.7 %). This is probably due to stronger stacking forces between the fluorescein-based probe and the GO surface. Furthermore, for the free **108** probe, the addition of fructose (0 – 1 M) led to only slight FL decrease of the probe **108** (0.5 µM) in an aqueous solution (pH 9.0, Figure 72b).

As a result, the minimum FL recovery of **108** towards fructose could be due to a stronger interaction of the more rigid fluorophore receptor system of **108** with the GO surface (*cf.* **101** has a more flexible linkage between the fluorophore and boronic acid receptor)**.** But, it could also be due to the inherent quenching and low sensitivity of the **108** system towards fructose. Consequently, **101** was selected for further detailed analyses.

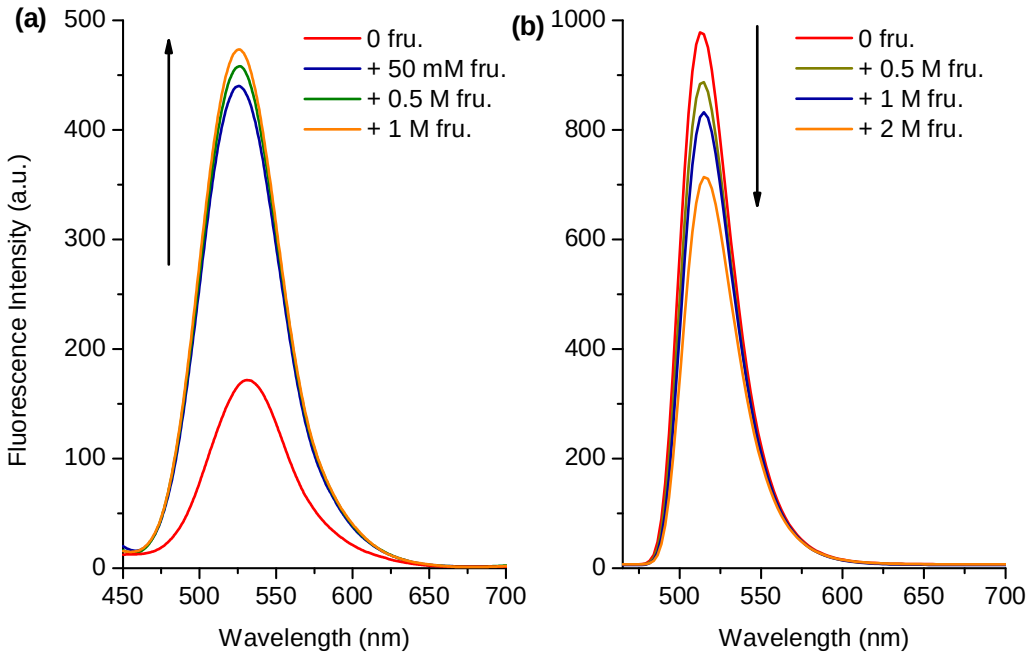

Figure 72. *(a) Fluorescence spectra of probe **101** (2 µM) with various monosaccharides (0, 0.05 M, 0.5 M, 1 M) in pH 9.0 Tris-HCl buffer; Fluorescence intensities were measured with excitation at 410 nm. Ex slit: 5.0 and Em slit: 5.0. (b) Fluorescence spectra of probe **108** (0.5 µM) with various monosaccharides (0, 0.5 M, 1 M, 2 M) in pH 9.0 Tris-HCl buffer; Fluorescence intensities were measured with excitation at 450 nm. Ex slit: 5.0 and Em slit: 5.0.*

5.3.3 SENSITIVITY AND SELECTIVITY OF 96@GO

By varying the pH from 7 to 11, we determined that the sensitivity of **101**@GO increased to a maximum at pH 9, but weakened with further increase of the pH (Figure 73a, Figure 74). The selectivity of **101**@GO was investigated with a range of different saccharides that are important cell-membrane components of mamanlian cells. As shown in Figure 73b, in the presence of 50 mM of different saccharides including fructose, galactose, *N*-acetyl galactosamine, mannose, lactose, glucose and *N*-acetyl gluctosamine, the sensor only showed a significant fluorogenic response to fructose (Figure 75). This is the expected selectivity for a simple monoboronic acid based system.[4] Our approach suggests that saccharide-selective optical off-on sensors can be simply developed based on stacking fluorescent boronic acids to GO. Since, in order to develop BA@GO systems with appropriate saccharide selectivity, composite materials constructed using boronic acid based receptors with the required saccharide selectivity must be prepared.

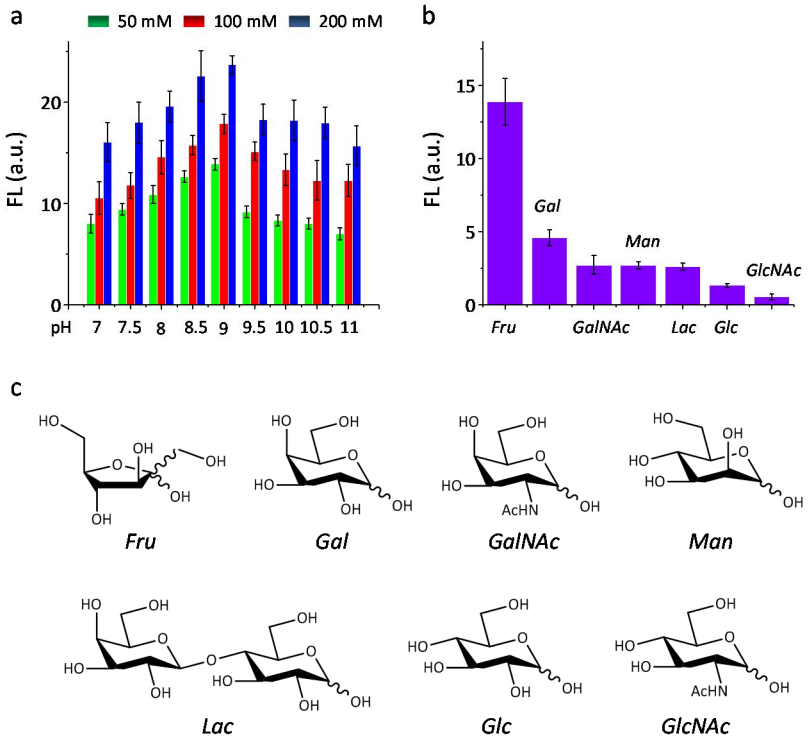

Figure 73. *(a) Fluorescence (FL) change of **101**@GO in the presence of fructose in 0.05 M Tris-HCl with different pH values; (b) Fluorescence (FL) change of **101**@GO in the presence of 50 mM of different saccharides (where Fru. is fructose, Gal. is galactose, GalNAc. is N-acetyl galactosamine, Man. is mannose, Lac. is lactose, Glc. is glucose, and GlcNAc. is N-acetyl gluctosamine) in Tris-HCl (0.05 M, pH 9.0). (λ_{ex} = 410 nm)*

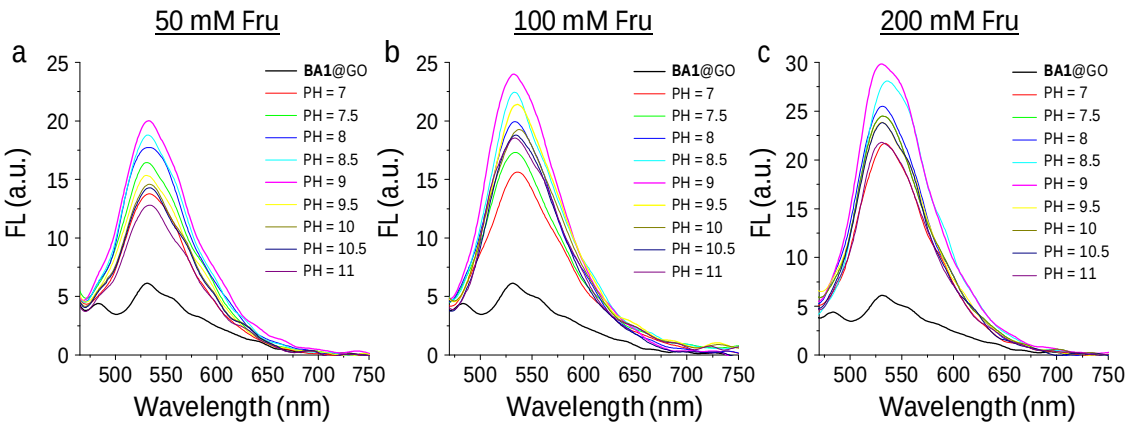

Figure 74. *Fluorescence (FL) change of **101**@GO (2 μM **101** with 40 μg/mL GO) in the presence of (a) 50 mM, (b) 100 mM, and (c) 200 mM of fructose (Fru) in Tris-HCl (0.05 M, different pH as indicated in each diagram).*

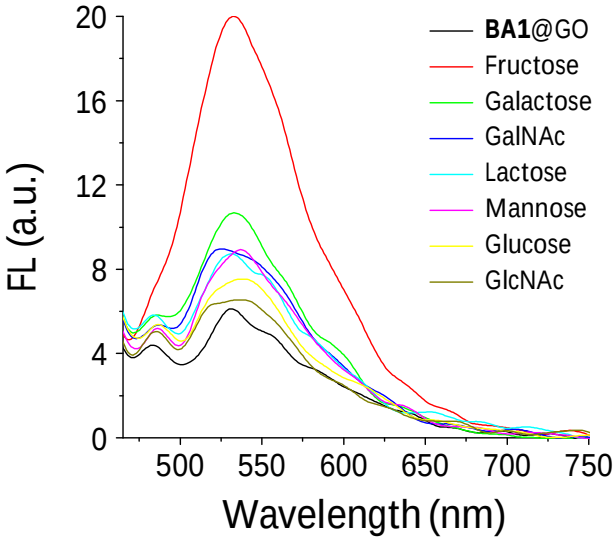

Figure 75. *Fluorescence (FL) change of **101**@GO (2 μM **101** with 40 μg/mL GO) in the presence of 50 mM of different saccharides in Tris-HCl (0.05 M, pH 9.0).*

5.4 CONCLUSION

In summary, we have developed a BA@GO composite material for the detection of saccharides. The stacking of a fluorescent BA onto the surface of GO, produced a quenched optical material. The sensor was found to be selective for fructose among a panel of biologically important saccharides producing a fluorogenic signal response. This study sets the basis for the development of a new generation of boronate-based saccharide sensors using simple and economic graphene oxide composite materials. We believe that our model BA@GO composite sensor represents a unique sensing strategy for the detection of the biologically important sugars. Fabrication of BA@GO systems with improved sensitivity and selectivity are currently underway.

This work has been published: *Sun, X.; Zhu, B.; Ji, D.-K.; Chen, Q.; He, X.-P.; Chen, G. R.; James, T. D., Selective Fluorescence Detection of Monosaccharides Using a Material Composite Formed Between Graphene Oxide and Boronate-based Receptors. ACS Appl. Mater. Interfaces. 2014, **6**, 10078–10082;*

Chapter Six:

RESULTS AND DISCUSSION V

6. RESULTS AND DISCUSSION V

6.1 BACKGROUND

ROS and RNS are both physiologically necessary and potentially cytotoxic. Under physiological conditions, specific ROS/RNS act as very important intracellular signal transducers in a variety of molecular effectors, such as growth factors, vasoactive modulators and biomechanical forces.[120] Recent evidence suggests that ROS/RNS play a key role in the activation and regulation of muscle remodelling.[270] Among them, nitric oxide (NO) and nitroxyl (HNO) have been acknowledged as very important species in various organisms and pathological activities. In many intra- and intercellular signalling functions, NO is known to play a key role in the process, such as regulation of growth, defence signalling against microbial pathogens and vascular smooth muscle relaxation. In addition, NO also has been indicated involving in many common diseases, including Parkinson's disease (PD), Alzheimer's disease (AD), amyotrophic lateral sclerosis (ALS), Huntington's disease (HD), and ischemic brain injury (stroke).[271]

While, nitroxyl (HNO, pK_a = 11.4) – one-electron reduced analogue of $^{\cdot}$NO – has recently been of interest due to its regulation of cellular function and therapeutic potential, especially as a potential alternative to current treatments of cardiovascular disease.[272] Thus, the importance of nitric oxide and nitroxyl has led to researchers seeking effective and applicable approaches for its detection. Synthetic fluorescence probes are among the powerful tools for the detection since they can measure intracellular NO and HNO directly.

In the past decade, numerous fluorescent probes for NO have been developed, which mainly fall into the following two types: *ortho* aromatic diamines (Scheme 58) and transition-metal complexes (Scheme 59).[150, 273] However, in the case of *ortho* diamine fluorescent probes, they are susceptible to the oxidants and antioxidants, also they can be interfered with by light, Mg (II) and Ca (II).[274-276] Lippard *et al.* reported copper complex-based probes for monitoring nitric oxide which have many advantages over other transitional metal NO probes, such as cobalt, ruthenium and dirhodium, in the improvement of low sensitivity and water-incompatibility.[162, 163] In other types of NO fluorescence probes, Anslyn *et al.* reported a new fluorescent

probe for NO on the basis of a *N*-nitrosation reaction.[166]

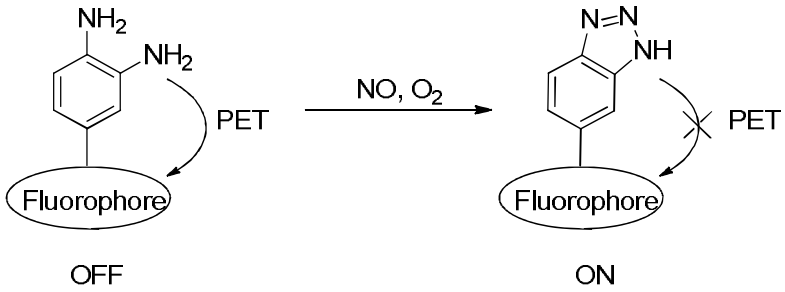

Scheme 58. *Reaction mechanism of ortho aromatic diamines with NO.*

Fluorescence detection of HNO has been explored using metal complex and the oxidation-reduction between copper and nitroxyl.[175, 277] However, the sensitivity of these copper complexes towards HNO was suboptimal and thus hampered its further applications. Recently, Nakagawa *et al.* demonstrated a fluorogenic HNO probe by utilizing the combination of aza-ylide formation *via* reaction of triarylphosphine with HNO.[183]

Over the last decade, many groups developed different fluorescent probes for the detection of nitric oxide and nitroxyl. Significantly, transition metal based probes were employed since NO and HNO could interact with the central metal atom and switch the paramagnetic effect.[273, 278]

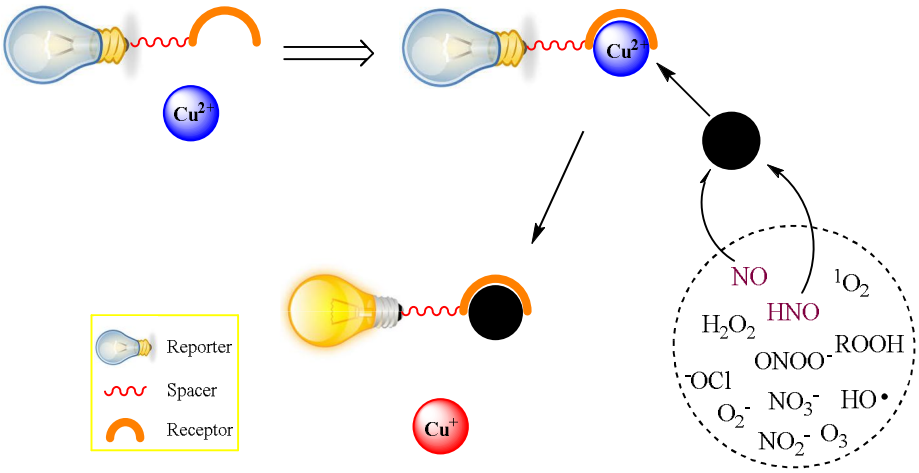

Scheme 59. *Design strategy of fluorescent probes for NO and HNO.*

Lippard and co-workers are pioneering in the developmet of fluorescence probes based on metal complexes, such as Fe (III),[159] Cu (II),[160-162, 164, 279] Eu (III),[280] Co (II),[153, 157]

Ru (II),[158] Rh (II).[156] Among them, copper (II) complexes were widely used due to their high bio-capability and excellent selectivity towards the target. Notably, Cu^{2+}[Fluorescein], Cu^{2+}[Benzoresorufin], Cu^{2+}[BODIPY] and Cu^{2+}[Coumarin] has been successfully applied for cellular imaging experiments.[163, 175, 176, 277]

However, to the best of our knowledge, the sensitivity of the reported copper complexes probes was suboptimal toward the substrate and the cell imaging experiments need to be done *via* external simulation. For example, the endogenous production of NO in the corresponding biological experiments was stimulated by iNOS following treatment with LPS and INF-γ or cNOS which was activated by simultaneous administration of 17β-estradiol.[163, 277] For the intracellular HNO fluorescent detection, researchers investigated the emission response by incubation of the probe with cells *via* addition of Angeli's salt (HNO donor).[175, 176, 277] Therefore, the importance of these kind of ROS/RNS and previous systems with many disadvantages have led to scientists to seek better and more powerful tools for the selective detection.

6.2 RESULTS AND DISCUSSION FOR COPPER COMPLEX PROBE

6.2.1 DESIGN STRATEGY

Bearing this in mind, we evaluate novel copper complex systems **104**, **105**, with the dual-analytes recognition characteristics both for NO and HNO and that might be employed for intracellular imaging. The fluorescent probes were easy to prepare (Scheme 60) and the introduction of hydroxyl group not only improved water-solubility, but could also provide a group to allow incorporation into a polymeric support, such as silicon mesoporous materials. The *N*-substituted-1, 8-naphthalimide is an excellent D-π-A chromophore with excellent photophysical and photochemical properties. As reported previously, 8-aminoquinoline was a good receptor for the coordination of copper (II).[162, 277] Thus, the fluorescence probe was designed by incorporating the three parts, *N*-substituted-1, 8-naphthalimide as reporter, 8-aminoquinolin as receptor and the hydroxyl chain as an auxiliary group.

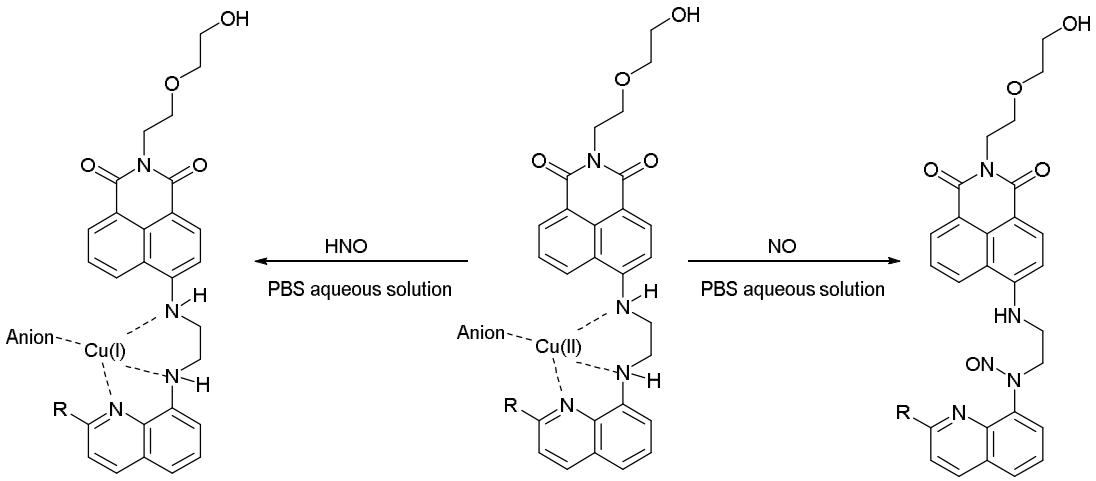

109. R = H
110. R = CH_3

Scheme 60. *Proposed strategy for NO and HNO sensing based on copper (II) complex.*

6.2.2 pH TITRATION

The pH titration of probe **109** is shown in Figure 76, the fluorescence intensity of the probe increases at below pH 7.0. There are two steps for the increase of the fluorescence intensity due to the two types of amine. However, between pH 7.0 and 10.0, the pH

change had hardly any effect on the fluorescence intensity. Thus, the probe can be expected to work under biological conditions (pH 7.3, aqueous PBS buffer).

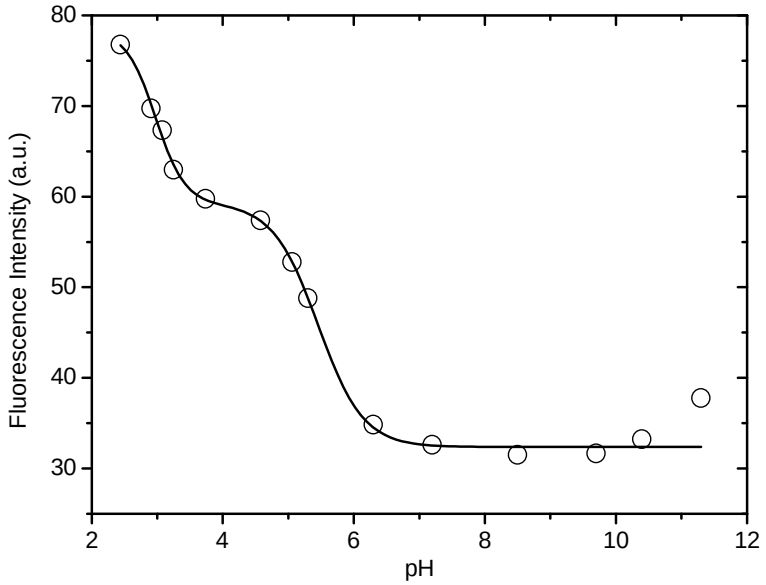

Figure 76. *pH titration of probe **109** in pure water.*

6.2.3 PROPERTIES OF NITRIC OXIDE SENSING

The fluorescence of the **109**-copper (II) complex was turned on by adding saturated NO aqueous solution. Nitric oxide transforms into NO^+ after the oxidation-reduction reaction with copper (II). The oxidized NO^+ links to the amine and the copper (I) detached from the molecule. Thus, the probe demonstrated an “off-on” response since both the paramagnetic effect and PET effect were stoped due to the added NO.

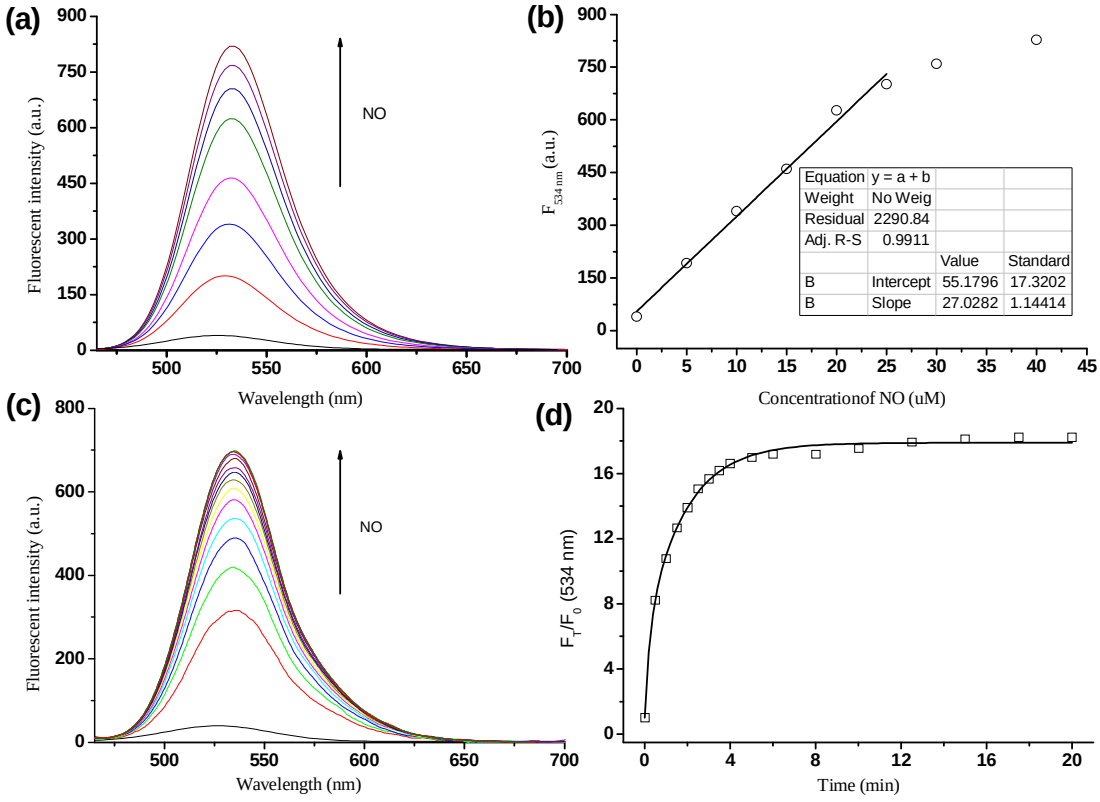

Figure 77. *(a) Fluorescence spectra of probe **109**-copper (II) (20 µM) after incubation with nitric oxide. Data were collected after incubation of probe with NO at 25 ˚C for 10 min; (b) Correlation between fluorescence intensity at 534 nm and the corresponding nitric oxide (0 – 40 µM). A linear correlation with concentrations of NO below 25 µM; (c) Time-course kinetic measurement of the fluorescence response of probe **109**-copper (II) (20 µM) to NO (45 µM); (d) Relationship between fluorescence intensity ratio F_T/F_0 at 534 nm and time (0 – 20 min). Spectra were acquired in PBS buffer (10 mM KCl, pH 7.30) at 25 ºC (λ_{exc} = 450 nm, slit width 5.0 nm).*

To investigate the interaction between the complex probe and NO, we carried out the corresponding experiments of dose-dependent titration and strength-duration curve through adding saturated NO aqueous solution (about 2.0 mM) to **109**-copper (II) probe (20 µM) in pH 7.30 PBS buffer.

In the concentration titration of **109**-copper (II) complex (20 µM), the *in situ* mixtures were stirred for 10 min after adding various concentrations of NO at 25 ˚C. As can be seen from Figure 77a, the initial fluorescence of **109**-copper (II) probe (20 µM) was very weak and then increases remarkably with the addition of NO in a dose-dependent manner. Upon addition of NO (40 µM) to the **109**-copper (II) complex (20 µM) a nearly 21-fold fluorescent enhancement was measured. Significantly, a good linear relationship was observed between fluorescence intensity at λ_{max} = 534 nm and concentration of NO

(0 – 25 μM) (R = 0.9911, Figure 77b). When higher doses of nitric oxide (25 – 40 μM) were added into the system, the reaction speed decreased which was attributed to nearly saturation of the probe.

In terms of strength-duration curve, **109**-copper (II) complex (20 μM) displayed a quick response towards NO initially, as indicated in Figure 77c, fluorescence spectra of the copper complex probe in the presence of 45 μM NO was collected (0 – 20 min). The sensing process reached to saturated state at 10 min after NO (45 μM) was added into the system (Figure 77d) producing a nearly 18-fold fluorescence increase.

6.2.4 PROPERTIES OF NITROXYL SENSING

Due to the similarity in properties between NO and HNO, the fluorescent probe **109**-copper (II) complex also showed an "off-on" response in the presence of HNO which results from AS decomposition. The oxidation-reduction reaction between HNO and copper (II) then results in the production of NO and copper (I), which leads to the fluorescence enhancement, and leads to a different mechanism to explain the off-on fluorescence increase between HNO and the copper (II)-complex.

To investigate the interaction between the complex probe and HNO, we carried out a dose-dependent titration by adding AS alkaline aqueous solution to **109**-copper (II) probe (20 μM) in pH 7.30 PBS buffer. The **109**-copper (II) complex (20 μM) mixtures were stirred for 20 min after different concentration of AS were added at 25 ˚C. As can be seen from Figure 78a, the fluorescence intensity of **109**-copper (II) probe (20 μM) increases with the titration of AS in a dose-dependent manner. Eventually, upon addition of AS (50 μM) the reaction reached F/F_0 = *ca.* 22-fold enhancement at λ_{em} = 534 nm with the **109**-copper (II) complex (20 μM)

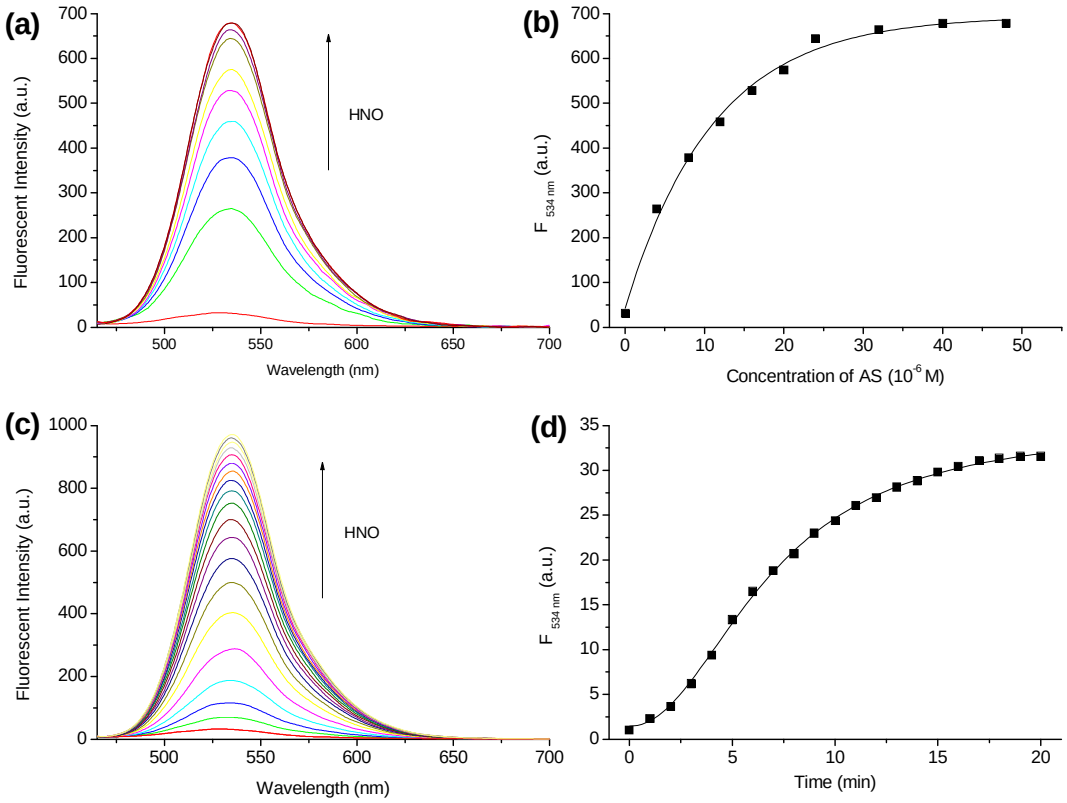

Figure 78. *(a) Fluorescence spectra of probe **109**-copper (II) complex (20 µM) after incubation with Angeli's salt. Data were collected after incubation of probe with AS at 25 ˚C for 20 min; (b) Correlation between fluorescence intensity at 534 nm and the corresponding AS (0 – 50 µM); (c) Time-course kinetic measurement of the fluorescence response of probe **109**-copper (II) complex (20 µM) to AS (50 µM); (d) Relationship between fluorescence intensity ratio F_T/F_0 at 534 nm and time (0 – 20 min). Spectra were acquired in PBS buffer (10 mM KCl, pH 7.30), at 25 ºC (λ_{exc} = 450 nm, slit width 5.0 nm).*

In terms of strength-duration curve, **109**-copper (II) complex (20 µM) displayed a gradual increase in the presence of AS (50 µM), as indicated in Figure 78c, fluorescence spectra of the copper complex probe in the presence of AS was collected over (0 – 20 min). The sensing process reached saturation at *ca.* 20 min after AS (50 µM) was added into the system (Figure 78d).

The paramagnetic effect disappears when copper (II) is reduced to copper (I), and the photo-induced electron transfer was stoped when the copper (I) metal interacts with the ligand (i.e. amines). Thus, the probe demonstrated an "off-on" response since both the paramagnetic effect and PET effect was hampered through interaction with HNO.

6.2.5 SELECTIVITY TEST FOR NO AND HNO

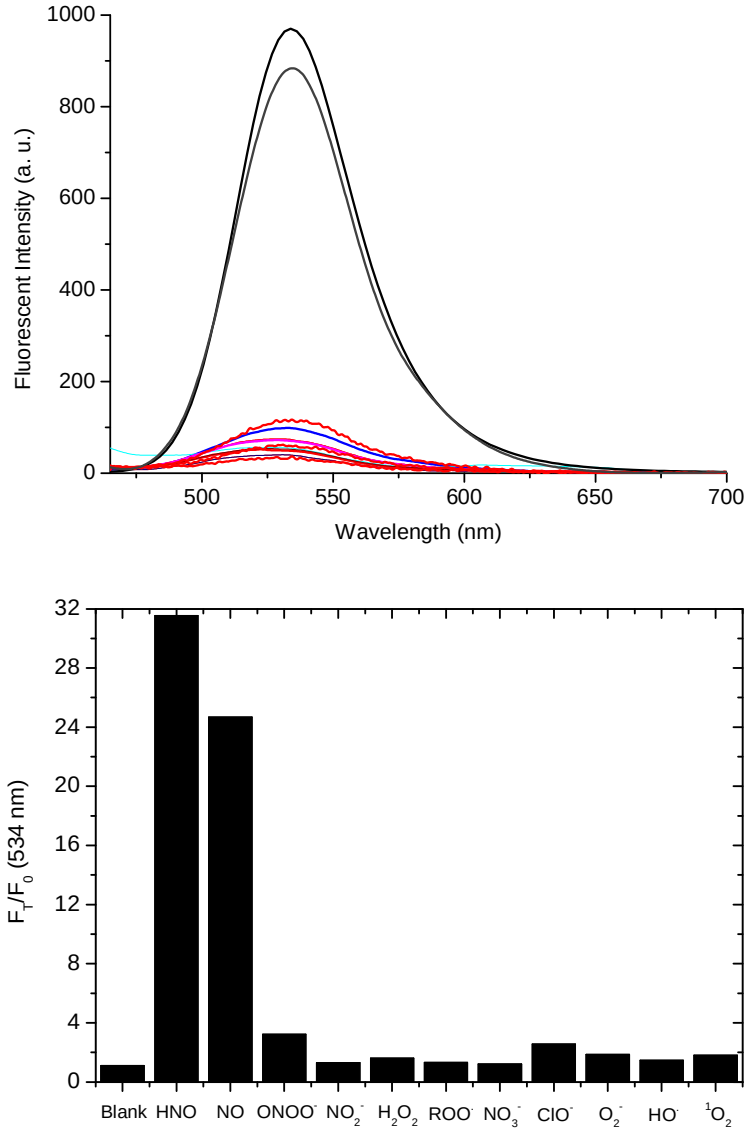

Figure 79. *Fluorescence responses of probe **109** (20 µM) to various ROS and RNS. Data were shown in NO (45 µM, 20 min), Angeli's salt (50 µM, 20 min) and other species (100 µM) for 1 h. Spectra were acquired in PBS buffer (KCl, 10 mM, pH 7.30), at 25 ºC (λ_{exc} = 450 nm, slit width 5.0 nm).*

While copper (II) complex was highly sensitive to HNO and NO, it is worthwhile investigating its selectivity with all kinds of ROS and RNS species under the same conditions. Figure 79 summarises the response of the copper-based sensor **109**-assembled by treatment with 1 equiv. $CuCl_2$ - to various ROS and RNS in neutral PBS buffer (pH 7.30).

The **109**-copper (II) probe was then treated with 2.25 equiv. NO for 10 min, 2.5 equiv.

Angeli's salt for 20 min, and 5.0 equiv. other species for 60 min, respectively. The fluorescence intensity ratio (F_T/F_0, F_T = in the presence of substrates, F_0 = in the absence of substrates) at emission maxima 534 nm was recorded. From Figure 79, the probe displayed high sensitivity and selectivity toward HNO and NO with 32-fold growth for HNO (AS, 50 µM) over 20 min and 25-fold growth for NO (45 µM) over 10 min. while $ONOO^-$ (100 µM) and ClO^- (100 µM) caused only 3-fold and 2-fold fluorescence increase after 1 h. Other species did not induce a remarkable change to fluorescent emission of the probe.

The dual-analyte response of the probe demonstrated a high sensitivity and selectivity toward HNO and NO over other ROS/RNS in biological conditions. In addition, a significant "off-on" switch can be turned on through the reaction between the copper complexes and the substrates (HNO and NO). It is worth noting that the naphthalimide-based probe showed a better response for HNO than NO over a short time period. Therefore, we believe our copper complex probe should be a good candidate to map both intracellular HNO and NO concentrations as imaging agent and sensor.

6.2.6 PROPOSED MECHANISM

To do further investigation of the interaction between the copper (II) complex and NO/HNO, we performed more relevant experiments. Interestingly, we observed that the free probe showed weak fluorescence intensity and the incorporation of copper (II) did not cause any effect on the fluorescence under neutral conditions. Therefore, we carried out a pH titration with the probe in pure water. A significant "off-on" response can be seen at low pH values (2.5 – 6.5). Hence, the fluorescence of probe **109** was reduced at pH 7.30 due to the PET from the amines of the 8-aminoquinolin. When copper (II) coordinates with the three types of amine the PET is hampered, however, the paramagnetic effect of copper (II) maintains the low fluorescence. Both NO and HNO reduce with copper (II) (switching off the paramagnetic effect) and also react with the amines (reducing the PET effect).

As can be seen from Figure 80, the coordination of copper (II) with the ligand caused reduction in the absorption intensity of free probe **109** (20 µM) from 0.07 to 0.04 with one equiv. of $CuCl_2$ in aqueous solution (λ_{abs} = 450 nm). This is because the conjugated ICT system is disturbed since the electron-donating ability of the amine is weakened

when it coordinates with the copper (II). In the absence of copper (II), the fluorescence of probe **109** (20 µM) displays only a small increase towards NO (50 µM, F/F_0 = 7.0) and HNO (50 µM, F/F_0 = 5.8), respectively, in the same buffer systems (Figure 81, Figure 82). Therefore, the metal is essential and strengthens the recognition ability of the probe towards the targets, which is essential for a sensing system capable of the detection of NO and HNO in cellular imaging applications.

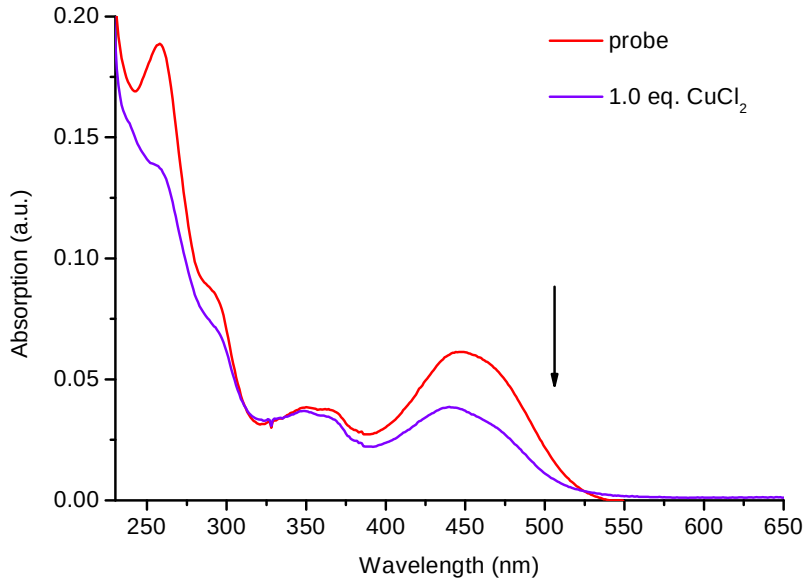

Figure 80. *UV-visible spectrum for probe **109** (20 µM) with titration of $CuCl_2$ (20 µM).*

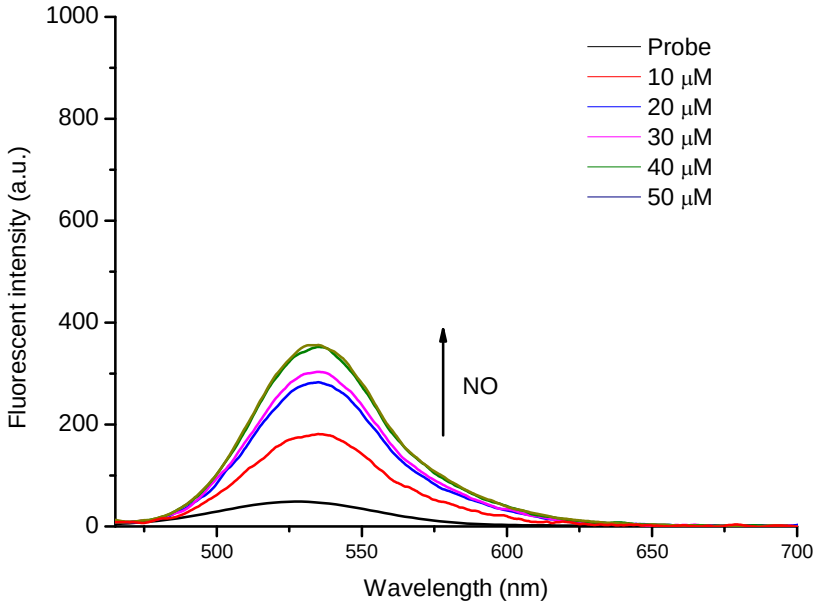

Figure 81. *Fluorescence spectra of free probe **109** (20 µM) upon addition of NO.*

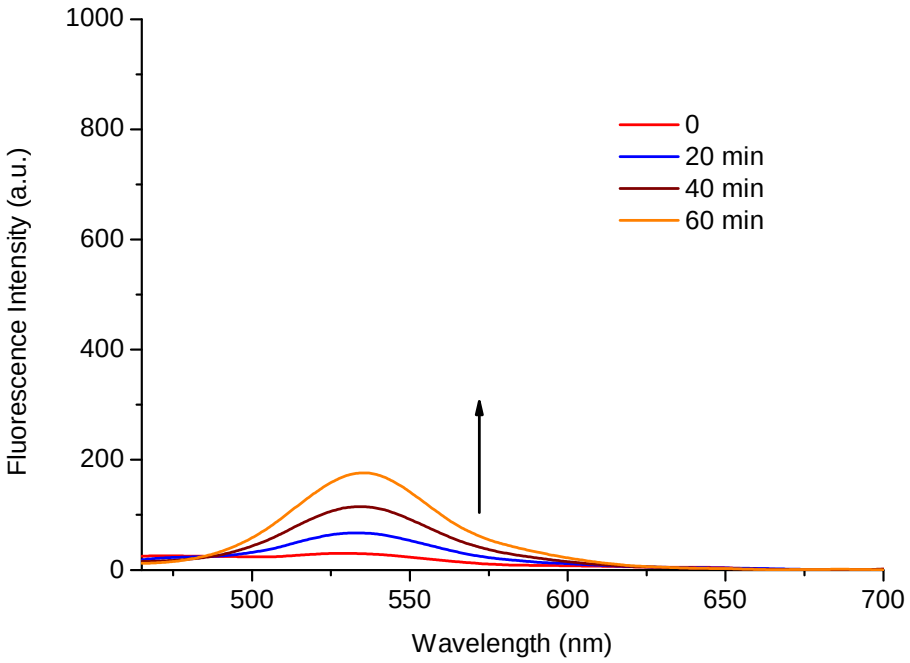

Figure 82. *Fluorescence spectra of probe **109** (20 µM) in the presence of AS (50 µM). The data was collected in 0, 20, 40 and 60 min after addition of AS at pH 7.30 PBS buffer solution.*

6.3 RESULTS AND DISCUSSION FOR PHOSPHOROUS-BASED PROBE

6.3.1 DESIGN STRATEGY

In the research work reported by King and co-workers,[176, 182, 281] the phosphine-based compound they developed used the reaction with HNO through Staudinger Ligation. The colorimetric change upon reaction with HNO was used for the detection of HNO *in vitro*. However, the short emission wavelength of the reporter and easy hydrolysis of the compound in aqueous buffer hampered its further application for the biological analysis and quantification of HNO *in vivo*.

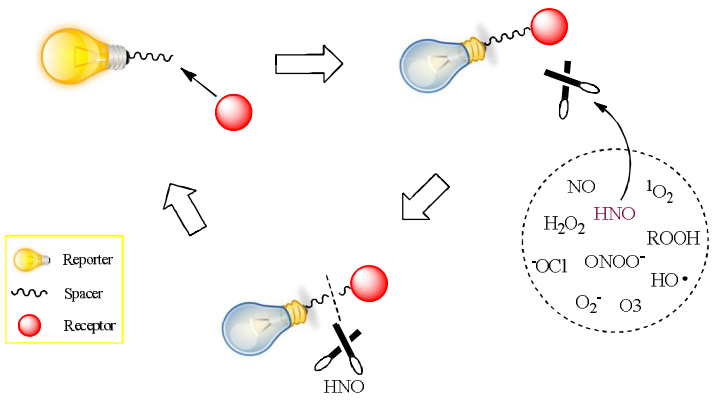

Scheme 61. *Schematic representation of the designed HNO fluorescent probes for the selective detection of HNO.*

We surmised that it is possible to develop a series of small-molecule fluorescent probes for the evaluation of intracellular HNO and imaging experiments based on the Staudinger Ligation above. Scheme 61 schematically represents the construction of target fluorescent probes and the reaction mechanism of selectivity toward HNO over other various ROS species. Initially, the fluorescence was quenched dramatically by linkage of 2-(diphenylphosphino) ethylamine with the fluorophore due to disturbance of the conjugated system and then the introduction of nitroxyl radical led to the recovery of the fluorescence by cleavage of spacer using “scissor” HNO through Staudinger Ligation.

Therefore, the fluorophores with phenol as the part of the emission moiety were employed to link with 2-(diphenylphosphino) ethylamine through 1,1'-

carbonyldiimidazole (CDI reagent, Scheme 62). These fluorophore candidates, such as coumarin, resorufin and fluorescein, were selected as potential signal groups due to their longer wavelength fluorescence emission, good biocompatibility, bioorthogonal, and nontoxicity (Figure 83).

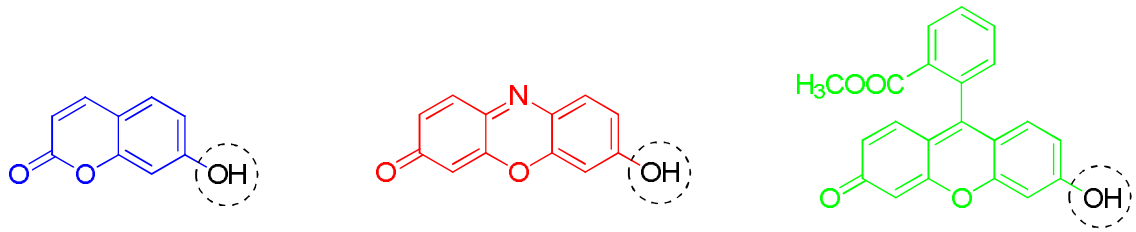

111. Coumarin **112.** Resorufin **113.** Fluorescein

Figure 83. *Structures of the chosen fluorophores.*

Noticeably, the novel phosphine-based fluorescent probe **116** has been synthesised successfully and evaluated for the selective and real-time detection and identification of HNO over other physiologically relevant reactive oxygen species.

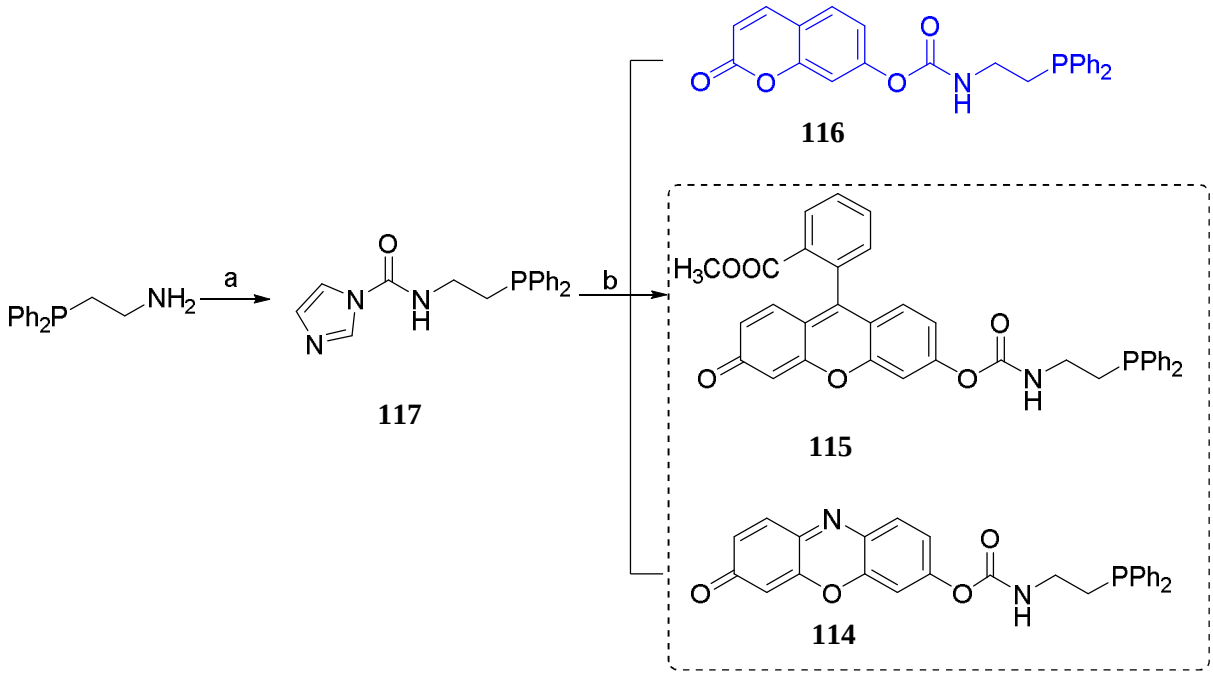

Scheme 62. *Reagents and conditions: (a) CDI, DMAP, CH_3CN, reflux, 20 h; (b) Fluorophore, Et_3N, CH_3CN, reflux, 24 h.*

7-Hydroxycoumarin dyes have stable photophysical and photochemical properties which was used for assays of phosphatases, β-galactosidases and β-lactamases.[282]

Therefore, the first synthetic fluorescent probe was developed by incorporating coumarin as the reporter with phosphine derivative as receptor (Scheme 62). In the synthetic work, the CDI reagent was employed to react with 2-(diphenylphosphino) ethylamine to form the key intermediate *N*-(2-(diphenylphosphino)ethyl)-1*H*-imidazole-1-carboxamide with a high yield (98%). The target molecule **116** was acquired after umbelliferone was introduced to remove the imidazole group through reaction between hydroxyl and acyl (Scheme 62).

Of the various HNO donors, Angeli's salt (AS, $Na_2N_2O_3$) has been studied extensively in terms of simple structure, thermodynamics and decomposition mechanism.[173, 283-287] Research indicates that the reagent can decompose at pH 4 - 8 ($K = 4.6 \times 10^{-4}\ S^{-1}$) to provide equivalent HNO and nitrite (Scheme 63). The half-life of Angeli's salt in 0.1 M phosphate buffer (pH 7.4), is 2.3 minutes at 37 ˚C.

$$N_2O_3^{2-} + H^+ \longrightarrow HNO + NO_2^-$$

Scheme 63. *Mechanism of decomposition of Angeli's salt (Sodium trioxodinitrate) at physiological pH*

Therefore, in our research work, Angeli's salt was utilized as the source of HNO. The production of AS followed that reported.[283] Furthermore, UV-Vis experiments were carried out to determine the purity of the AS (Figure 84). When adding purified product AS (6.00 mg) into sodium hydroxide solution (500 mL, 0.1 N), the absorption value was 0.76 at a wavelength λ_{max} = 248 nm. Using the Beer-Lambert equation $A = \varepsilon bc$ where ε is 8000 $M^{-1}cm^{-1}$ for AS, the accurate mass of AS in solution was calculated to be 5.795 g. Thus, the purity of the final AS was > 95% and as such could be employed as a source of HNO.

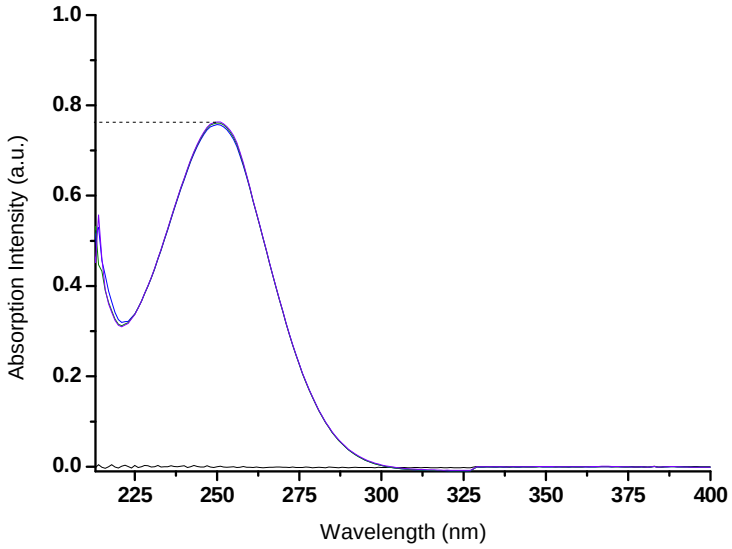

Figure 84. *Absorption spectra of AS (6.00 mg in 500 mL 0.1 N NaOH aqueous solution).*

6.3.2 pH TITRATION

Initially, the pH effect on the fluorescence of probe **116** was evaluated. As can be seen from Figure 85, the fluorescence intensity of the probe decreased at above pH 8.0. While, pH changes between 4.0 and 8.0, had hardly any effect on the fluorescence intensity (Figure 85). Thus, the probe can be expected to work well under biological conditions (pH 7.3, PBS buffer).

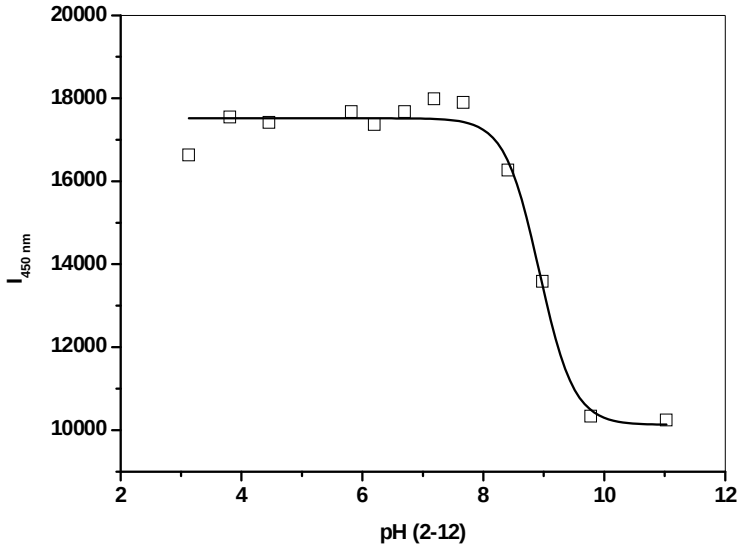

Figure 85. *Effect of pH on the fluorescence emission of probe **116** (2 μM) in water (20% methanol). The pH was adjusted by adding HCl or NaOH aqueous solution.*

6.3.3 CONCENTRATION TITRATION

The fluorescence titrations of probe **116** with Angeli's salt were carried out in pH 7.20 PBS buffer (52.1% methanol in water with KCl, 10 mM; KH_2PO_4, 2.752 mM; Na_2HPO_4, 2.757 mM) at 25 ˚C.[288] Specifically, the reactivity of **116** toward HNO (generating from AS) was investigated in an abiotic system. To initiate the release of HNO, various amounts of AS (0.2 – 1.0 mM) in sodium hydroxide solutions (0.01 N) were added into neutral PBS buffer solutions of probe **116** (2 μM) and then the mixtures were stirred in the dark for 10 min. With excitation at 370 nm, data was collected in a fluorescence spectrometer between 400 – 600 nm. Significantly, HNO led to the increase of the fluorescence intensity maxima at 450 nm in a dose-dependent manner (Figure 86). The reaction between probe **116 (**2 μM) and Angeli's salt (1 mM) triggered a 6-fold "off-on" fluorescent response (I_F/I_0, in the presence of HNO/in the absence of HNO) due to HNO induced release of 7-hydroxycoumarin. Also, a good linear relationship was observed between the fluorescent intensity and concentration of Angeli's salt (R = 0.99758).

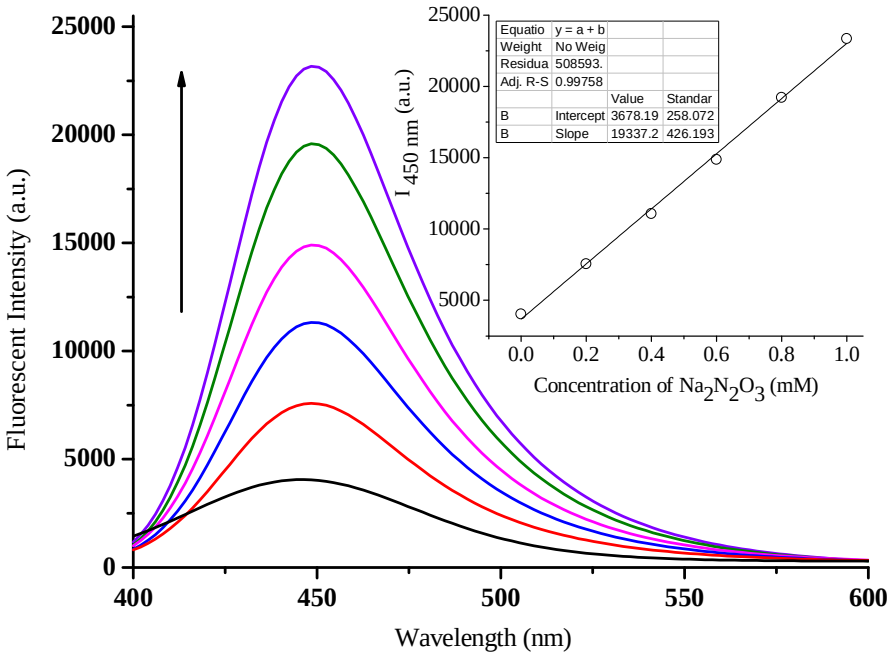

Figure 86. *HNO-induced fluorescence spectra (λ_{ex} = 370 nm) of probe **116** (2 μM) with varied concentrations of AS in PBS buffer solution. Inset shows the changes at 450 nm as a function of AS concentration.*

6.3.4 SELECTIVITY DETECTION

To evaluate the selectivity, various reactive oxygen species were selecteted to react with probe **116** (2 μM) in a neutral buffer solution, such as nitrate, nitrite, hydrogen peroxide, hypochlorite, singlet oxygen, nitric oxide, hydroxyl radical and AAPH. (Figure 87) Whereas, a nearly 6-fold fluorescence increase was observed when probe **116** (2 μM) was allowed to react with AS (1 mM), all the other reagents did not cause any fluoresence increase over 20 min. Especially, NO_2^- (5.0 mM), which is another product from decomposition of Angeli's salt along with HNO, led to fluorecence decrease (I_F/I_0 = *ca*. 0.89) when added it into the system independently. Notably, nitric oxide (1.9 mM), product of HNO oxidation by oxygen, reduced the fluorescence I_F/I_0 = *ca*. 0.16. That is to say, the probe **116** can successfully distinguish HNO from NO under neutral buffer conditions. Therefore, the probe has excellent selectivity towards HNO over other ROS and can therefore be employed as a fluorescent indicator for HNO.

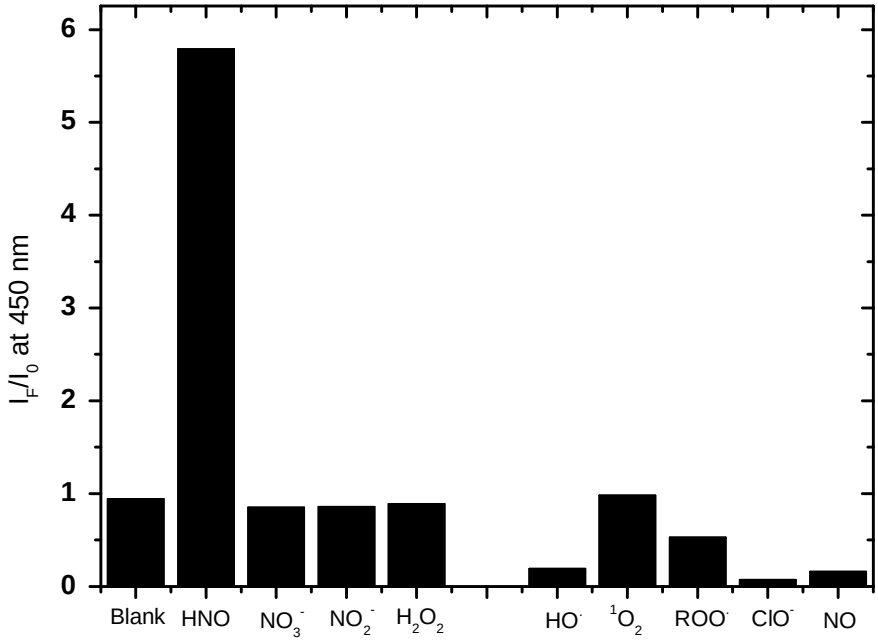

Figure 87. *Fluorescence responses of probe **116** (2 μM) to AS (1 mM) in sodium hydroxide solution (0.01 N) and other various ROS and RNS species. Spectra were acquired in PBS buffer solution (pH 7.30), at 25 ºC.*

6.3.5 PROPOSED MECHANISM

The fluorescence of probe **116** is weak due to the inhibited ICT effect when the phenolic hydroxyl group was linked with the phosphine derivative. On release of HNO when Angeli's salt was exposed to the neutral buffer solution, it reacts with the fluorescence probe to form the $(R)_2P$ = NH intermediate. Subsequently, the carbon–oxygen bond is cleaved through an internal Staudinger Ligation reaction (Scheme 64) and the fluorescence increases dramatically when 7-hydroxylcoumarin is released from the system.

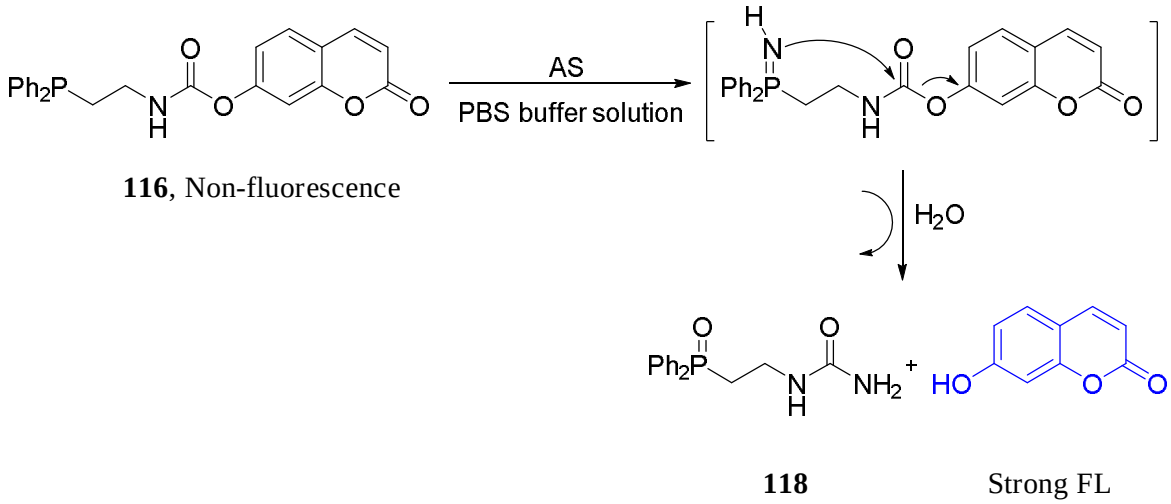

116, Non-fluorescence

118 Strong FL

Scheme 64. *Proposed mechanism for the reaction between probe **116** and HNO*

In order to explain the sensing mechanism further, we synthesized the by-product **118** independently to acquire more evidence.[182] HPLC and mass spectra were used to confirm the final products (Figure 88, 89). In HPLC analysis, we observed that the residence time for probe **116** was at 17.0 min and shifted to 6.0 min after reaction with AS, which was in accordance with the prepared by-product. Moreover, the m/z ion peak at 161.0252 in the negative ESI demonstrated the expected compound 7-hydroxylcoumarin (m/z = 161.0317 calculated) after reaction with AS (Figure 89). Hence, demonstrating that the phosphorous-based fluorescent probe breaks into two parts and results in a fluorescence enhancement.

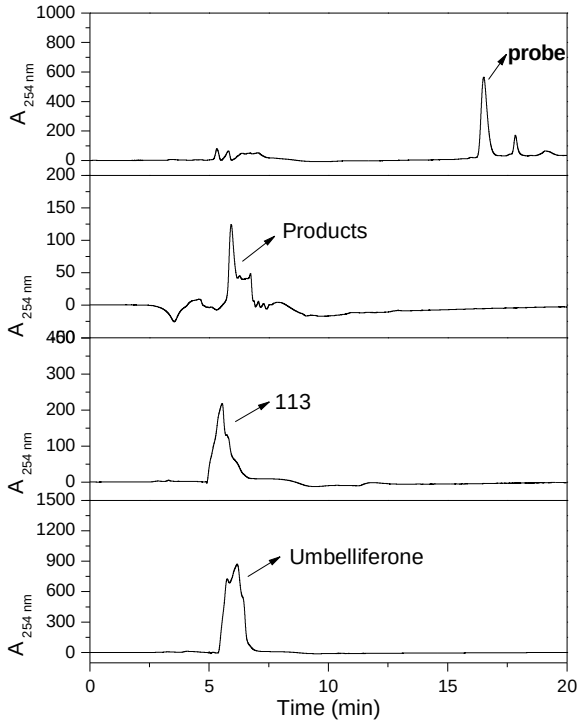

Figure 88. *HPLC analysis of the reaction between probe **116** and HNO.*

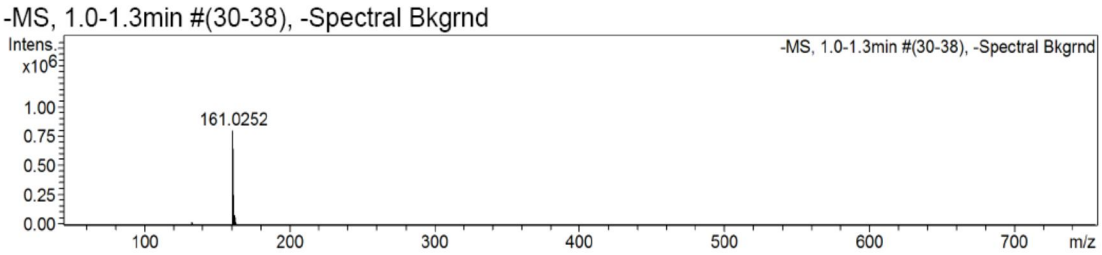

Figure 89. *ESI-MS analysis to confirm the product of the reaction between probe **116** and HNO.*

6.4 CELL CULTURE

We then evaluated the ability of the probe **109**-copper (II) complex and probe **116** to sense nitric oxide and nitroxyl in cell experiments (*Work was performed in Department of Cardiovascular Medicine, University of Oxford, United Kindom*). The TET cells contain all the cofactors for NOS to produce nitric oxide. We then added either eNOS (by transfection) or Angeli's salts.

Nitric oxide synthases (NOSs) are a family of enzymes catalyzing the production of nitric oxide (NO) from L-arginine. eNOS plays a critical role in embryonic heart development and morphogenesis of coronary arteries and cardiac valves.[289] Under physiological conditions, it is usually accepted that the aerobic decomposition of Angeli's salt produces nitrite (NO_2^-) and nitroxyl (HNO), which dimerizes and leads to N_2O.[290] In experiment, these data were obtained through detecting the fluorescence intensity of probe **109**-copper (II) complex and **116** *via* stimulating the cells with eNOS and Angeli's salt, respectively. As can be seen from Figure 91a, probe **109**-copper (II) complex showed a weak fluorescence in TET cells probably due to a tiny concentration of NO while a strong intensity can be observed when adding eNOS. The production of NO in the presence of eNOS enlarged the fluorescence signal of probe **109**-copper (II) complex after chemical reaction. However, there is only a slight fluorescence increase towards HNO in Figure 91b which is difficult to interpret.

In the case of probe **109**-copper (II) complex, we used sEnd.1 cells as model, sEnd.1 cells are mouse endothelial cells that are routinely used as an *in vitro* model of eNOS function. We knocked out eNOS with siRNA (Dharmacon 72h) and show a decrease in NO production as detected using compound **109**-copper (II) complex Figure 91c. Apparently, the knock-out of eNOS led to the fluorescence decrease of the **109**-copper (II) complex due to the decrease of NO generation which clearly demonstrates the sensing of nitric oxide *in vivo*.

In the case of probe **116**, we observe selective detection of HNO over NO *in vivo*. The weak fluorescence towards NO and very strong fluorescence towards HNO of probe **116** indicated in Figure 91a and 91b proved the good selectivity between them. Therefore, **116** is an excellent small-molecular fluorescence probe which can be used as powerful tool for both *in vivo* and *in vitro* sensing of HNO.

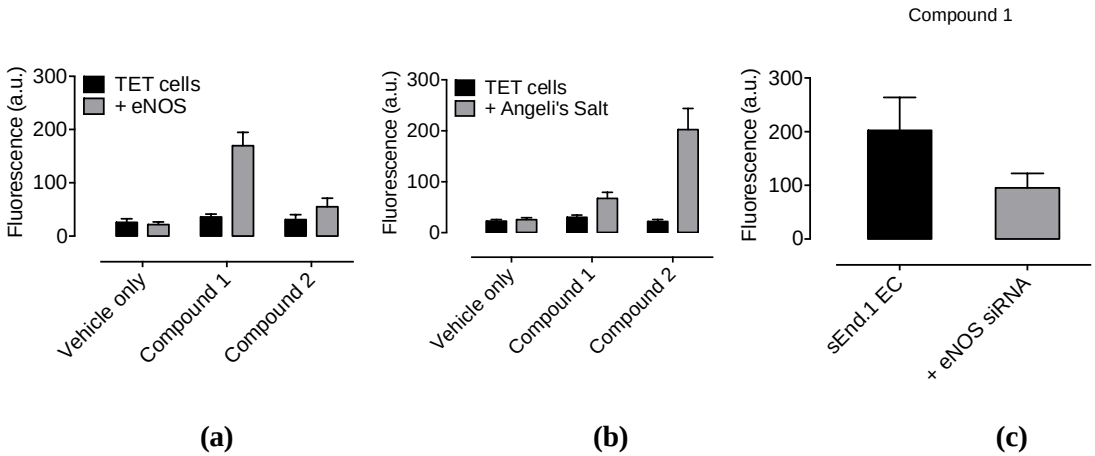

(a) **(b)** **(c)**

Figure 90. *Fluorescence detection of NO and HNO for probes **109** and **116** in cells. (a) probes **104** and **111** for the detection of NO (eNOS as donor) in TET cells; (b) probes **109** and **116** for the detection of nitroxyl (AS as donor) in TET cells; (c) "knock-out" experiment in sEnd.1 cells*

6.5 CONCLUSION

In this chapter, water-soluble copper (II) complex fluorescence probes were developed and evaluated for the detection of nitric oxide and nitroxyl under physiological conditions. A significant fluorescence “off-on” response was observed using the copper (II) complex for the detection of NO and HNO ($Na_2N_2O_3$ as a donor). The oxidation-reduction reaction between the probe and NO removes the copper from the system and nitrites the amine which hampers the PET mechanism. While HNO led to the reduction of copper which is still coordinated with the ligand. Under pathological conditions generating various ROS/RNS, the copper (II) complex fluorescent probe preferentially reacts with NO/HNO over other reactive oxygen species. The dual-analyte recognitions of the simple, sensitive probe were further applied in TET and sEnd.1 living cell test for the exogenous NO.

Also, we, prepared a phosphorous-based compound for the detection of HNO derived from Angeli’s salt under biological conditions. The probe displayed a high sensitivity and selectivity toward HNO over other various ROS species, especially NO. The underlying mechanism was attributed to the cleavage of C-O bond induced by Staudinger Ligation. The success of the coumarin-based chemsensor has inspired us to develop other benzoresorufin and fluorescein-based fluorescent probes in the future. We also evaluated the fluorescent probe in response to HNO in TET living cells.

We believe that our probe systems will enable the investigation of diseases states (such as inflamation) in biological systems involving the production of NO and HNO.

Chapter Seven:

CONCLUSIONS AND FUTURE WORK

7. OVERALL CONCLUSIONS AND FUTURE WORK

7.1 OVERALL CONCLUSIONS

Our general contribution in the thesis lies on the design, synthesis and evaluation of different fluorescent sensors for the detection of saccharide and ROS/RNS. In detail, we studied the regulation of monosaccharides on the reaction of "integrated" and "insulated" boronate-based fluorescent probes 2-naphthylboronic acid and *N*-methyl-*o*-(aminomethyl)phenylboronic acid with hydrogen peroxide, respectively. Based on the observation of the N-B interaction in the protection of boron oxidation, we developed a water-soluble boronate-based fluorescence probe for the selective detection of peroxynitrite and imaging in living cells. Furthermore, using the self-assembly of aromatic boronic acids with Alizarin Red S, we develped a new sensing strategy for the selective colorimetric and fluorimetric detection of peroxynitrite, referred to herein as RIA (Reaction-based Indicator displacement Assay). Meanwhile, a novel class of simple materials for the selective sensing D-fructose by the functionalization of graphene oxide (GO) with boronate-based fluorescence probes were devised which set the basis for the development of a new generation of boronate-based saccharide sensors using simple and economic composite materials. Also, copper (II) complex fluorescence probes and phosphorous-based probe were designed and synthesized for the detection of nitric oxide and nitroxyl in a physiological condition.

7.2 FUTURE WORK

In the process of all kinds of sensors design, researchers, especially biologists prefer the application of fluorescent probes (high QE, brightness and life time) with "turn-on" sensing response which can result in a much higher contrast imaging, quantitative and high specificity toward the target in biological and physiological processes. Herein, we proposed a new boronate-based fluorescence structure **119** with 4-amino-1,8-naphthalimide as the reporter and B-N interaction as the reaction site towards peroxynitrite. In the design, it is predicated that the probe would show a ratiomatric signal response towards peroxynitrite due to the modulation of the electron-donating 4-amino donor in the ICT system and nitrogen-boron protection to against hydrogen peroxide, also other ROS/RNS species. Reaction of probe with $ONOO^-$ will trigger

chemoselective cleavage of the boronate-based carbamate protecting group to deliver the green fluorescence aminonaphthalimide.

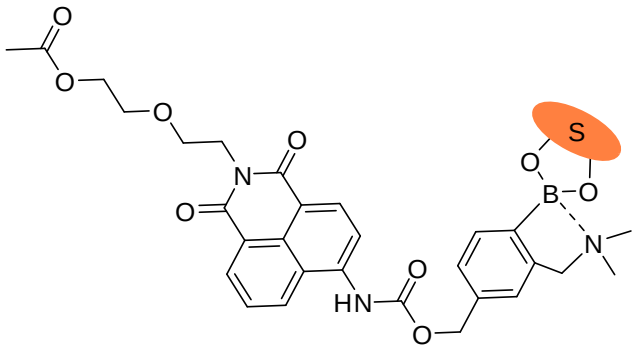

119

It is also very attractive for people to explore new fluorophores with longer emission wavelength and high quantum yield, coupling with non-toxicity and bio-compability, which would be promising application in the super-resolution fluorescence microscopy.

The new strategy of RIA (Reaction-based Indicator displacement Assay) can be extended in the application of ROS/RNS sensing. The schematic illustration displays the sensing mechanism, which the receptor and reporter are separate initially and the binding of them can be selectively cleaved in the presence of the species (Scheme 1S).

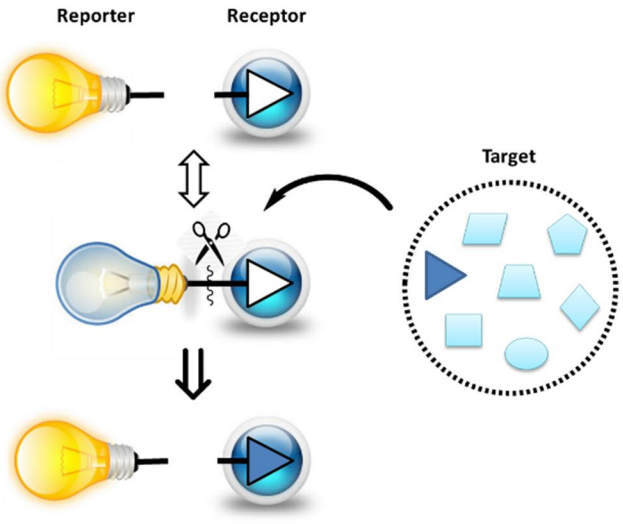

Scheme 1S. *Schematic illustration of the proposed RIA: "Reaction-based Indicator displacement Assay".*

In terms of the BA@GO nanomaterials, the selectivity and sensitivity towards the D-fructose were suboptimal, thus we are studying and modifying the structural effect (GO

of different lateral size) on the sensing properties and observed new promising results which we will extend the application to glucose/fructose detection in real serum samples. More importantly, based on the work above, we are developing new diboronic acids derivatives **120** to stack with GO or SWNT to form novel sensing systems for the selective detection of D-glucose.

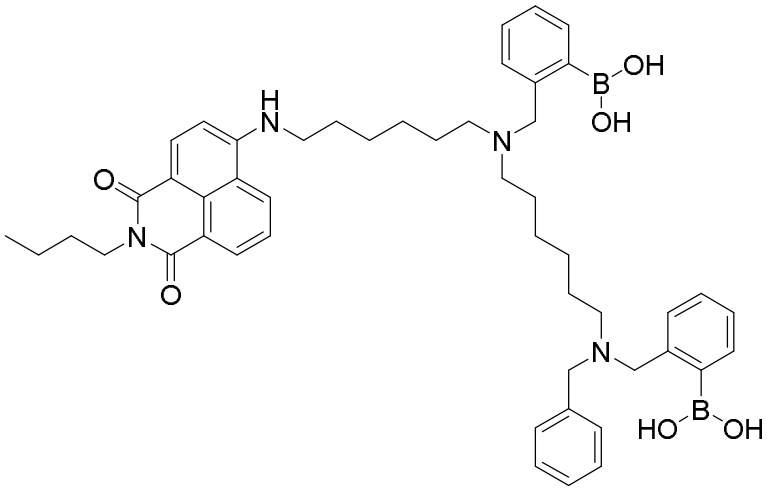

120

The success of the coumarin-based chemsensor **116** has inspired us to develop other benzoresorufin and fluorescein-based fluorescent probes **114** and **115** in the future for the chemoselective detection of nitroxyl *in vitro* and *in vivo*.

Chapter Eight:

EXPERIMENTAL

8. EXPERIMENTAL

8.1 GENERAL METHODS

Solvents and Reagents

Solvents and reagents were reagent grade unless stated otherwise and were purchased from Fisher Scientific UK, Frontier Scientific Europe Ltd, TCI UK, Alfa Aesar and Sigma-Aldrich Company Ltd and were used without further purification.

Thin Layer Chromatography (TLC)

Thin layer chromatography was performed using commercially available Macherey-Nagel aluminium backed plates coated with a 0.20 mm layer of silica gel 60 Å with fluorescent indicator UV254. These plates were visualised using either ultraviolet light of 254 nm or 365 nm wavelength, or by staining the plates with vanillin or ninhydrin solution. Silica gel column chromatography was carried out using Fisher or Sigma-Aldrich 60 Å silica gel (35-70 μm).

Nuclear Magnetic Resonance (NMR) Spectra

Nuclear magnetic resonance (NMR) spectra were run in chloroform-D, methanol-D_4, and dimethyl sulfoxide-d_6. Where a Bruker AVANCE 300 was used, ^{1}H spectra were recorded at 300 MHz, ^{11}B spectra at 96 MHz and ^{13}C at 75 MHz where a Bruker AVANCE 250 was used. Chemical shifts (δ) are expressed in parts per million and are reported relative to the residual solvent peak as an internal standard in ^{1}H and ^{13}C spectra. The multiplicities and general assignments of the spectroscopic data are denoted as: singlet (s), doublet (d), triplet (t), double of doublets (dd), unresolved multiplet (m), broad (br) and aryl (Ar). All ^{13}C spectra is proton decoupled, and the boron attached carbon is not visible due to ^{11}B quadrupolar rapid relaxation.

Mass Spectra

A micrOTOF electrospray time-of-flight (ESI-TOF) mass spectrometer (Bruker Daltonik GmbH, Bremen, Germany) was used; this was coupled to an Agilent 1200 LC system (Agilent Technologies, Waldbronn, Germany) as an autosampler. 10 μL of

sample was injected into a 30:70 flow of water: methanol at 0.4 mL/min to the mass spectrometer. 10 μL of 5 mM sodium formate was injected after the sample. This acted as a calibrant over the mass range 50-1500 m/z. The observed mass and isotope pattern matched the corresponding theoretical values as calculated from the expected elemental formula.

Melting Points (MP)

Capillary melting points were determined using Stuart MDP10. Compounds were purified and dried before melting points were determined.

Fluorescence Measurements

Fluorescence measurements were performed on a Perkin-Elmer Luminescence Spectrophotometer LS 50B and Gilden Photonics Ltd. FluoroSENS, utilising Starna Silica (quartz) cuvette with 10 mm path length, four faces polished. Data were collected *via* the Perkin-Elmer FL Winlab software package or GPL FluorSENS as appropriate. All solvents used in fluorescence measurements were HPLC or fluorescence grade and the water was Milli-Q. All saccharides used in fluorescence measurements were certified as ≥ 99% pure.

pH Measurement

All pH measurements taken during fluorescence/absorption experiments were recorded on a Hanna Instruments HI 9321 Microprocessor pH meter which was routinely calibrated using Fisher Chemicals standard buffer solutions (pH 4.0 - phthalate, 7.0 – phosphate, and 10.0 - borate).

UV-Vis Measurement

UV-Vis measurements were performed on a Perkin-Elmer Lambda20 Spectrophotometer,utilising Starna Silica (quartz) cuvette with 10 mm path lengths, two faces polished. Data was collected *via* the Perkin-Elmer UVWinlab software package. Further reprocessing of the data was carried in OriginPro 8.0 graph software.

High Performance Liquid Chromatography (HPLC)

HPLC was carried out using a Dionex UltiMate 3000 HPLC systems, samples were injected and passed through Symmetry® C-18 column (4.6 × 260 mm), using a UltiMate 3000 Diode Array Detector with UV/visible detection measured at λ_{obs} = 200 nm, 300 nm, 400 nm, 450 nm, 500 nm, 600 nm, 700 nm and 800 nm. The flow speed was 0.8 mL/min and the flow mixed with two solvents, solvent A was made of 0.1% TFA with MilliQ and 0.1% TFA in MeCN as solvent B.

The HPLC system was switched on 60 minutes prior the initial measurement, the flow was set at 0.2 mL/min under UV/Vis detection in order to wash all residuals in the column. Samples were injected and examined with following method: Start 95% A reverse gradient until 5% A at 7.5 minutes, retaining gradient until 15 minutes, reverse gradient until 17.5 minutes 95% A, then hold to 21 minutes.

The UltiMate 3000 pump was maintained by the solution made of 80% MilliQ water, 15% MeCN and 5% Isopropanol. All solvent used in HPLC measurements were HPLC grade and the water was deionised.

Atomic Force Microscope (AFM)

Morphology study was performed with an AFM (AJ-III, Aijian nanotechnology Inc., China) in air under tapping mode at room temperature. The samples used were dispersed on freshly cleaved mica and then dried at room temperature.

Raman spectroscopy

Raman spectra were performed on a RenishawInVia Reflex Raman system (Renishaw plc, Wotton-under-Edge, UK) employing a grating spectrometer with a Peltier-cooled charge-coupled device (CCD) detector coupled to a confocal microscope, which were then processed with RenishawWiRE 3.2 software. The Raman scattering was excited by an argon ion laser (I = 514.5 nm).

8.2 PREPARATION OF ROS/RNS

Preparation of NO

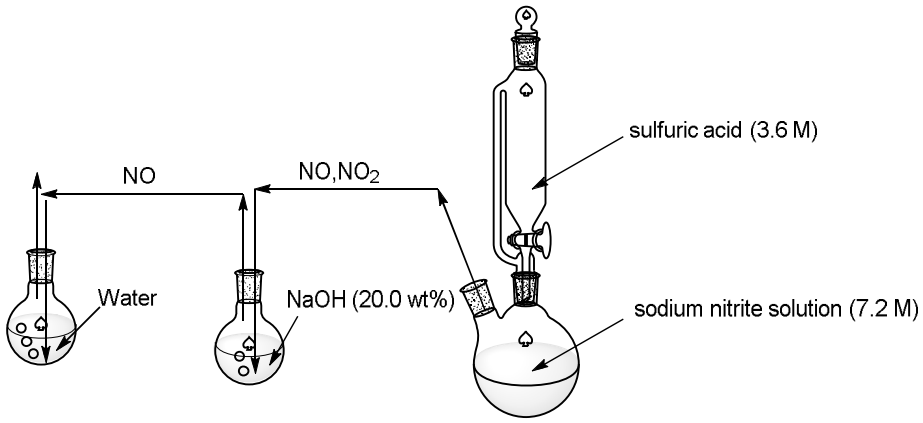

Scheme 65. *Preparation of saturated NO aqueous solution.*

Nitric oxide (NO) was prepared by treating a sodium nitrite solution (7.3 M) with sulfuric acid (3.6 M) and its stock solution (2.0 mM) was prepared by bubbling NO into deoxygenated de-ionized water for 30 min (Scheme 65).[166] Before the operation of the reaction, nitrogen gas was inlet into the system for 15 min. The aqueous sulfuric acid drop speed was carefully controlled and the reaction would run smoothly under stirring. The produced NO and NO_2 gas flowed along the outlet tube and the NO_2 was absorbed through reaction with the alkaline in the middle of aqueous sodium hydroxide solution. In the final flask, the saturated NO solution can be formed through prolonged bubbling.

Preparation of $^1O_2$

$^1O_2$ was generated by the reaction of H_2O_2 (10 M) with NaClO (10 M). Drop the solution of H_2O_2 into the aqueous NaClO and stir for 2 min.

Preparation of ROO•

ROO• was generated from 2, 2'-azobis (2-amidinopropane) dihydrochloride. AAPH (2, 2'-azobis (2-amidinopropane) dihydrochloride, 10 M) was added in de-ionized water, and then stirred at 37 ºC for 30 min.

Preparation of O_2^-

Superoxide was generated from KO_2 with a saturated solution of KO_2 in DMSO (~1

mM).

Preparation of HO•

Hydroxyl radical was generated by Fenton reaction. To prepare •OH solution, ferrous chloride (1 M) was added in the presence of 10 equiv of H_2O_2 (37.0 wt%).[128]

Preparation of $ONOO^-$

Peroxynitrite stock solution was prepared by the reaction of hydrogen peroxide with sodium nitrite and stabilized in basic solution (Scheme 31), which is frequently used for the *in vitro* experiments.[184]

Owing to I being a short-lived oxidant species, especially in the physiological pH (half-life, 10 ms), the preparation of peroxynitrite was carried out in the sodium hydroxide solution by chemical synthesis with a quenched flow reactor: using equal flow rates of the following solutions at 0 ºC: 0.6 M $NaNO_2$, 0.6 M in HC1, 0.7 M in H_2O_2, and 3 M NaOH.[184] The product solution was analyzed spectrophotometrically. The stock solution of peroxynitrite was fresh-made and reanalysed each time in the detection experiments. The concentration of peroxynitrite was estimated by using an extinction coefficient of 1670 ± 50 cm^{-1} M^{-1} at 302 nm in 0.1 N sodium hydroxide (aq.)

Preparation of ^-OCl and H_2O_2.

The concentration of ^-OCl was determined from the absorption at 292 nm (Ɛ = 350 $M^{-1}cm^{-1}$).[128] The concentration of H_2O_2 was determined from the absorption at 240 nm (Ɛ = 43.6 $M^{-1}cm^{-1}$).

Preparation of Angeli's salt (HNO donor).

The preparation of Angeli's salt was following the procedure reported. [291]

All other chemicals were from commercial sources and of analytical reagent grade, unless indicated otherwise.

8.3 GENERAL PROCEDURE

A. In the "integrated" and "insulated" system, probe **100** was prepared according to described methods.[71] The fluorescence titrations with H_2O_2 were carried out at 25 ºC in a pH 7.20 buffer (52.1% methanol in water with KCl, 10 mM; KH_2PO_4, 2.752 mM; Na_2HPO_4, 2.757 mM, modulated by aq. HCl)[288] and pH 9.70 buffer (10.0% methanol in water with Na_2CO_3, 50 mM; $NaHCO_3$, 50 mM). Photographs were taken using a Canon camera and images were processed with Bitmap Image.

B. In the water-soluble boronate-based fluorescent probe for the selective detection of peroxynitrite. The UV-Vis and fluorescent titrations with peroxynitrite were carried out at 25 ºC in pH 7.30 PBS buffer (KH_2PO_4, 1/15 M; Na_2HPO_4, 1/15 M) and pH 5.00 buffer (NaOAc/HOAc, 50 mM). The probe-D-fructose complex was formed by mixing free probe (2 μM) with D-fructose (100 mM) *in situ*.

Cell culture. HeLa cells (human epithelial adenocarcinoma) and RAW 264.7 cells (mouse macrophage cell) were obtained from Korean Cell Line Bank (Seoul, Korea). Cells were cultured in RPMI 1640 (Roswell Park Memorial Institute, without HEPES) supplemented with heat-inactivated 10% fetal bovine serum, 100 U/ml penicillin and 100 U/ml streptomycin. All cells were kept in 5% CO_2 at 37 ºC.

Confocal microscopy imaging. Cells were seeded in a 35-mm glass bottomed dishes at a density of 3×10^5 cells per dish in culture media. After 24 h, 5 μM sensor (final 0.25% DMF, *N, N*-dimethylformamide), 250 mM D-fructose were added to the cells and the cells were incubated for 30 min at 37 ºC. For HeLa cells, the 5, 30 μM peroxynitrite/PBS solutions added to the cells for 10 min at 37 ºC. For RAW 264.7 cells, 1 μg/ml LPS (lipopolysaccharide) treated to the media for 16 h, 50 ng/ml IFN-γ (interferon-gamma) for 4 h and 2.5 ng/ml PMA (phorbol 12-myristate 13-acetate) for 30 min then incubated with 5 μM sensor for 30 min. For the inhibition test, 100 μM TEMPO and 0.5 mM amino guanidine pre-treated to the media for 4 h. After washing with the DPBS twice to remove the residual probe, the cells were imaged by confocal laser scanning microscopy (FV1200, Olympus, Japan). Cells were excited by a 405 nm diode laser and detected at BA 490–590 nm.

C. In the ARS-BAs complex systems, ARS-PBA and ARS-BBA in UV-Vis absorption and fluorescence titrations with H_2O_2 were carried out at 25 ºC in pH 7.30 PBS buffer

(KH_2PO4, 1/15 M; Na_2HPO_4, 1/15 M) and electrochemical data was obtained in pH 7.30 buffer (KCl, 0.1 M, KH_2PO_4, 1/15 M; Na_2HPO_4, 1/15 M) with 2.0 mM cetyl trimethylammonium bromide (CTAB). Probe ARS-NBA complex for the selective detection of peroxynitrite were tested in 52.1% methanol/aqueous PBS buffer solution at pH 8.10.

D. In the selective fluorescence detection of monosaccharides using a material composite formed between graphene oxide and boronate-based receptors, the **101**@GO and **108**@GO composites were formed by mixing boronic acids (**101** and **108**) with fresh-made GO *in situ.* The UV-Vis and fluorescent titrations were running in a buffer solution - Tris-HCl (0.05 M, pH 9.0).

E. In a water-soluble copper (II) complex fluorescence probe for the selective detection of nitric oxide/nitroxyl and imaging in living cells, *in vitro* fluorescence titrations with NO/HNO and other ROS/RNS were carried out at 25 ºC in a pH 7.30 buffer (KCl, 10 mM; KH_2PO_4, 2.752 mM; Na_2HPO_4, 2.757 M). The pH titration was modulated by utilizing aqueous hydrogen chloride (1.2 N) and sodium hydrogen solution (1 N) at 25 ºC. The probe **109**-copper (II) complex was formed by mixing free probe **109** (20 µM) with $CuCl_2$ (20 µM) *in situ* at 25 ºC in a pH 7.30 buffer.[162, 277] While in phosphine-based florescent probe for HNO, the fluorescence titrations of probe **109** with Angeli's salt were carried out in a pH 7.20 PBS buffer (52.1% methanol in water with KCl, 10 mM; KH_2PO_4, 2.752 mM; Na_2HPO_4, 2.757 mM, modulated by HCl) at 25 ºC.

8.4 STRUCTURE OF COMPOUNDS

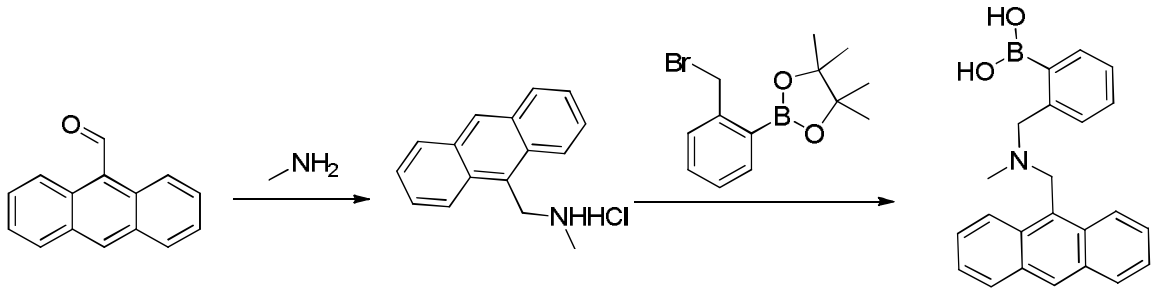

Scheme 66. *Synthetic route for probe **100.***

Anthracen-9-ylmethyl-methyl-ammonium chloride[292]

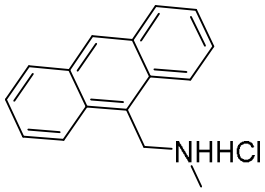

121

A solution of the required 9-anthraldehyde (1.85 g, 8.98 mmol) and methylamine (33.0 wt% in methanol, 2.16 g, 23.0 mmol) in tetrahydrofuran (90 mL) and methanol (30 mL) was heated under reflux for 7 hours. The system was allowed to cool to room temperature, placed in an ice bath and sodium borohydride (1.96 g, 51.8 mmol) was added in portions. Stirring continued at room temperature for 2 hours before the careful addition of hydrochloric acid (1 M, 10 mL). The resulting residue was then extracted in dichloromethane (3 × 30 mL) from sodium hydroxide (0.5 M, 30 mL). The organic phases were recombined, washed with water (≥ 5 × 30 cm^3) until neutral pH was obtained, dried over magnesium sulfate and filtered. An excess of gaseous hydrogen chloride was bubbled through the filtrate, which was subsequently purged with nitrogen gas and condensed under reduced pressure. Dichloromethane (25 mL) was added. The suspension was then filtered and washed with dichloromethane (3 × 30 mL) prior to the removal of all solvent from it *in vacuo* to afford a light yellow powder **121** (1.87 g). Yield: 81%. Mp: 275 - 276 ºC, lit 248 ºC. ^{1}H NMR (300 MHz, MeOD) δ 8.46 (s, 1H), 8.33 (d, *J* = 8.6 Hz, 2H), 8.04 (d, *J* = 8.6 Hz, 2H), 7.53 – 7.59 (m, 2H), 7.45 – 7.50 (m, 2H), 4.73 (s, 2H), 2.59 (s, 3H); ^{13}C NMR (75 MHz, MeOD) δ 132.8, 132.2, 131.7,

130.6, 128.8, 126.6, 124.1, 122.8, 45.3, 33.9. HRMS (ES+) Calcd for $([M+H])^+$, 222.3030; Found, 222.1300.

Anthracene-9-ylmethyl-(2-borono-benzyl)-methyl-amine[71]

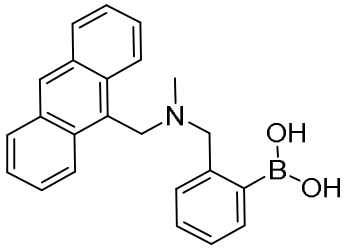

To a solution of the required ammonium hydrochloride salt anthracen-9-ylmethyl-methyl-ammonium chloride (506 mg, 1.96 mmol) in tetrahydrofuran (80 mL) and acetonitrile (80 mL) was added potassium carbonate (1.35 g, 9.74 mmol). The solution was stirred for 10 minutes before 2-(2-bromobenzyl)-1, 3-dioxaborinane (735 mg, 2.47 mmol) was added and the system heated under reflux for 6 hours. The solvent was removed under reduced pressure. The residue was slurried in water (50 mL) and adjusted to pH ~ 7 with hydrochloric acid (2 M). The suspension was extracted in dichloromethane (3 × 50 mL). The organic phases were recombined and the solvent removed under reduced pressure. The resulting oil was purified by flash column chromatography on silica gel (methanol/dichloromethane, gradient elution: loading with a 5:95 ratio initially to 90:10 finally). The desired fractions were re-condensed, filtered in dichloromethane and dried *in vacuo* to afford a yellow powder **100** (536 mg). Yield: 77%. Mp: 150-152 ºC, lit 128 ºC. ^{1}H NMR (300 MHz, MeOD) δ 8.58 (s, 1H), 8.14 (d, J = 9.0 Hz, 2H), 8.04 – 8.07 (m, 2H), 7.73 (d, J = 7.4 Hz, 1H), 7.47 - 7.55 (m, 4H), 7.36 – 7.42 (m, 2H), 7.32 (dd, J_1 = 7.4 Hz, J_2 = 1.6 Hz, 1H), 5.01 (s, 2H), 4.43 (s, 2H), 2.43 (s, 3H); ^{13}C NMR (75 MHz, MeOD) δ 135.6, 132.8, 132.7, 132.0, 131.4, 130.5, 129.0, 128.4, 127.7, 126.3, 124.7, 64.2, 39.9. Note: the quarternary carbons with no H atoms within four bonds would be missing or very weak signal; HRMS (ES+) Calcd for $([M+H])^+$, 356.1821; Found, 356.1828.

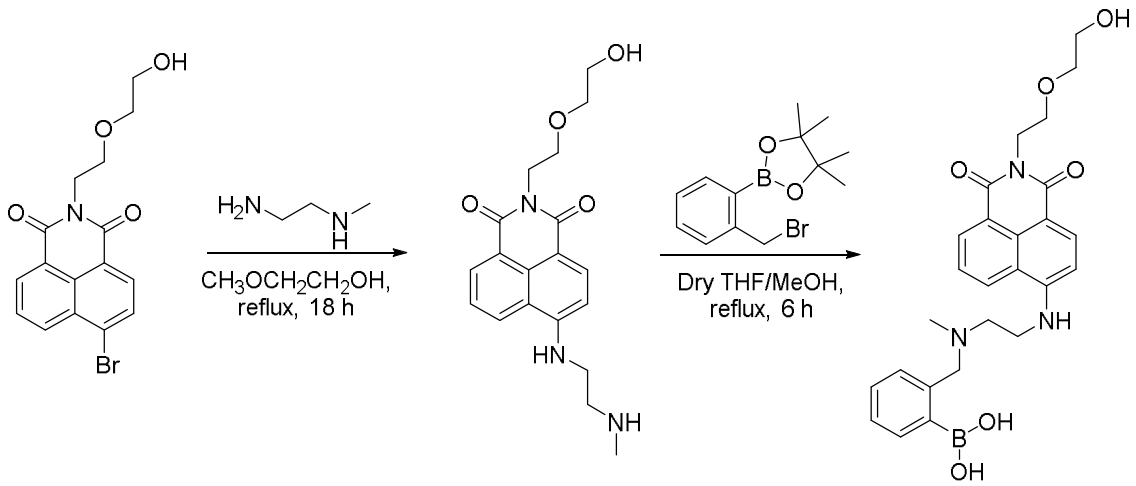

Scheme 67. *Synthetic route for probe **101.***

2-(2-(2-hydroxyethoxy)ethyl)-6-((2-(methylamino)ethyl)amino)-1*H*-benzo[de] isoquinoline-1,3 (2*H*)-dione[227]

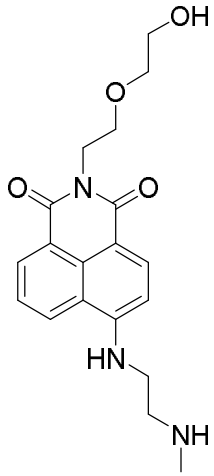

122

A solution of 2-bromoethylamine hydrobromide (1.5 g, 4.12 mmol) and *N*-methylethylene-diamine (0.322 g, 95.0 wt%, 4.12 mmol) in 2-methoxyethanol was refluxed overnight under a nitrogen atmosphere. The mixture was concentrated under reduced pressure to obtain a purple oil product. Column chromatography on silica gel (CH_2Cl_2 : CH_3OH, 3 : 1, v/v) was employed to purify the crude product as yellow solid **122** (0.8 g). Yield: 55%. Mp: 198 - 200 ºC. ^{1}H NMR (300 MHz, $CDCl_3$) δ 8.49 (dd, J_1 = 7.5 Hz, J_2 = 0.9 Hz 1H), 8.39 (d, J = 8.4 Hz, 1H), 8.19 (dd, J_1 = 8.4 Hz, J_2 = 0.9 Hz 1H), 7.55 (dd, J_1 = 8.4 Hz, J_2 = 7.5 Hz, 1H), 6.59 (d, J = 8.4 Hz, 1H), 6.39 (br s, 1H), 4.41 (t, J = 5.4 Hz, 2H), 3.87 (t, J = 5.4 Hz, 2H), 3.68 - 3.72 (m, 4H), 3.48 (overlapped, 2H), 3.07 (t, J = 6.0 Hz, 2H), 2.54 (s, 3H); ^{13}C NMR (75 MHz, $CDCl_3$), δ 165.0, 164.5, 150.0,

134.6, 131.2, 129.6, 126.9, 124.4, 122.3, 120.2, 109.4, 104.1, 72.4, 68.8, 61.7, 50.8, 42.1, 39.3, 35.9; HRMS (ES+) Calcd for $([M+H])^+$, 358.1766; Found, 358.1772.

(2-(((2-((2-(2-(2-hydroxyethoxy)ethyl)-1,3-dioxo-2,3-dihydro-1*H*-benzo[de]isoquinolin-6-yl)amino)ethyl)(methyl)amino)methyl)phenyl)boronic acid

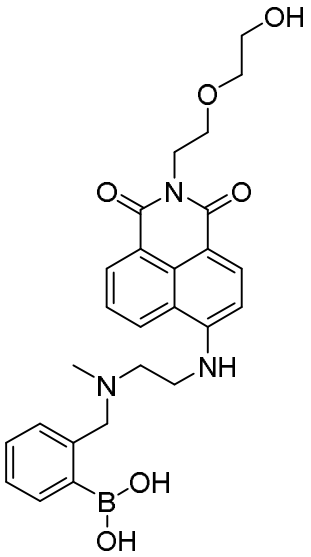

The product compound **101** was synthesised by refluxing compound **122** with 2-bromomethylphenylboronic acid pinacol ester (0.28 g, 0.94 mmol) in dry tetrahydrofuran (20 mL) for 6 hours. The product was purified on silica gel, using dichloromethane/methanol 5:1 to afford **101** as yellow solid (0.15 g). Yield: 50%. Mp: 119 – 121 °C. ^{1}H NMR (300 MHz, CD_3OD) δ 8.62 (d, *J* = 8.4 Hz, 1H), 8.44 (d, *J* = 7.2 Hz, 1H), 8.28 (d, *J* = 8.4 Hz, 1H), 7.58 (t, *J* = 7.8 Hz, 2H), 7.17 – 7.23 (m, 3H), 6.80 (d, *J* = 8.7 Hz, 1H), 4.32 (t, *J* = 6.3 Hz, 2H), 4.17 (s, 2H), 3.74 - 3.84 (m, 4H), 3.57 - 3.62 (m, 4H); 3.31 - 3.34 (overlapped, 2H), 2.59 (s, 3H); ^{13}C NMR (75 MHz, CD_3OD), δ 166.6, 166.1, 152.4, 136.2, 134.6, 132.6, 131.5, 130.3, 128.8, 128.6, 128.5, 125.9, 123.6, 122.4, 110.5, 105.5, 73.8, 69.6, 64.7, 62.6, 56.3, 41.7, 40.5, 39.8; HRMS (ES+) m/z calcd for $[M + H]^+$, 492.2305; found, 492.2326.

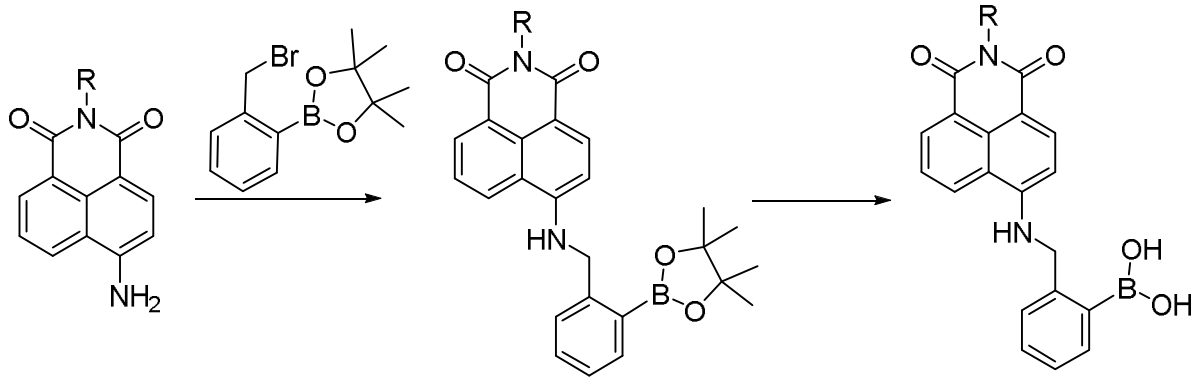

Scheme 68. *Synthetic route for probe **102***

4-Amino-*N*-(2-(2-acetoxyethoxy)ethyl)naphthalimide.[293]

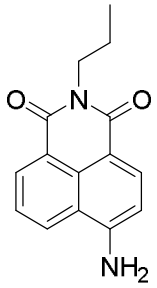

123

4-Amino-1,8-napthalic anhydride (0.40 g, 1.88 mmol) was dissolved in 50 mL ethanol under a nitrogen atmosphere and brought to reflux. To this solution was added propylamine (0.63 mL, 7.51 mmol), after which the reaction was left to reflux for 14 h. Upon cooling to room temperature, the solvent was removed under reduced pressure, and the crude product was collected, added into methanol and filtered. Product was collected and dried to afford a yellow solid (0.20 g). Yield: 42%. Mp: 250-253 ºC, lit 258 ºC. ^{1}H NMR (300 MHz, DMSO-d_6) δ 8.61 (dd, J_1 = 8.4 Hz, J_2 = 1.2 Hz, 1H), 8.43 (dd, J_1 = 7.4 Hz, J_2 = 1.2 Hz, 1H), 8.20 (d, J = 8.4 Hz, 1H), 7.67 (dd, J_1 = 8.4 Hz, J_2 = 7.4 Hz, 1H), 7.42 (s, 2H), 6.85 (d, J = 8.4 Hz, 1H), 3.99 (t, J = 7.4 Hz, 2H), 1.55 – 1.65 (m, 2H), 0.92 (t, J = 7.4 Hz, 3H).

(2-(((2-(2-(2-hydroxyethoxy)ethyl)-1,3-dioxo-2,3-dihydro-1*H*-benzo[de]isoquinolin-6-yl)amino)methyl)phenyl)boronic acid

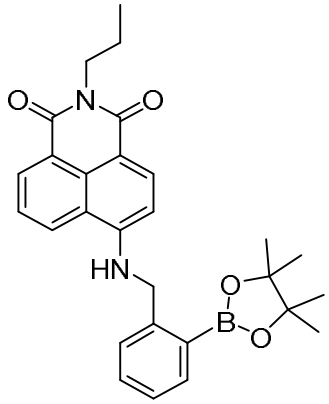

124

A mixture of **123** (70 mg, 0.27 mmol) and sodium hydride (12 mg, 60.0 wt%, 0.28 mmol) was stirred at room temperature in dry DMF (2 mL) for 20 min. A solution of 2-bromomethylphenylboronic acid pinacol ester (98 mg, 0.33 mmol) in dry DMF (2 mL) was added into the system dropwise under N_2. The mixture was stirred in room temperature overnight, poured into $KHSO_4$ (aq. 5 mL, 5.0 wt%) and filtered to afford a crude solid. Purify it by column chromatography on silica gel (CH_2Cl_2 : CH_3OH, 100 : 1, v/v) to afford a yellow solid as product **124** (25 mg). Yield: 24%. ^{1}H NMR (300 MHz, $CDCl_3$) δ 8.57 (dd, J_1 = 7.4 Hz, J_2 = 0.9 Hz, 1H), 8.45 (d, J = 8.4 Hz, 1H), 8.08 (d, J = 8.4 Hz, 1H), 7.91 (d, J = 7.3 Hz, 1H), 7.59 (dd, J_1 = 8.4 Hz, J_2 = 7.4 Hz, 1H), 7.44 – 7.46 (m, 2H), 7.32 – 7.35 (m, 1H), 6.89 (d, J = 8.5 Hz, 1H), 4.77 (d, J = 5.7 Hz, 2H), 4.14 (t, J = 7.6 Hz , 2H), 1.70 – 1.78 (m, 2H), 1.58 (s, 1H), 1.32 (s, 12H), 0.99 (t, J = 7.5 Hz, 3H). ^{13}C NMR (75 MHz, MeOD), δ 166.5, 166.0, 152.7, 145.8, 138.0, 136.0, 132.8, 132.5, 129.5, 128.9, 128.1, 125.8, 123.7, 122.2, 110.0, 106.3, 85.6, 55.1, 42.9, 25.6, 22.8, 12.1; HRMS (ES-) m/z calcd for $[M - H]^-$, 469.2298; found, 469.2320.

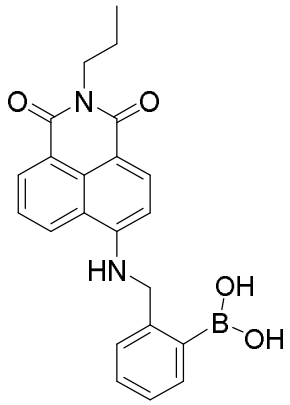

102b

A mixture of **124** (140 mg, 0.30 mmol) and potassium hydrogenfluoride (130 mg, 1.34 mmol) was stirred in methanol (5 mL) at room temperature overnight. The suspension was filtered to afford the yellow salt powder.

The powder (34 mg, 0.07 mmol) obtained above together with lithium hydroxide (13 mg, 0.54 mmol) were put into acetonitrile (4 mL) and water (2 mL). The mixture was stirred at room temperature for 4 hours. The solution was concentrated under vacuum to yellow solid. Then water (10 mL) was input and then extracts the mixture with dichloromethane (2 × 20 mL). To remove the solvent from the mixture solution and obtain the final yellow compound **102b**. Mp: 139-141 ºC. ^{1}H NMR (300 MHz, MeOD) δ 8.64 (dd, J_1 = 8.5 Hz, J_2 = 1.1 Hz, 1H), 8.50 (dd, J_1 = 7.4 Hz, J_2 = 1.1 Hz, 1H), 8.30 (d, J = 8.8 Hz, 1H), 7.90 (d, J = 7.4 Hz, 1H), 7.58 – 7.67 (m, 2H), 7.23 (dd, J_1 = 7.4 Hz, J_2 = 1.1 Hz, 1H), 7.00 – 7.12 (m, 2H), 6.92 (d, J = 8.8 Hz, 1H), 4.83 (s, 2H), 4.07 (t, J = 7.51, 2H), 1.68 – 1.75 (m, 2H), 0.99 (t, J = 7.6 Hz, 3H). ^{13}C NMR (75 MHz, MeOD), δ 166.9, 166.3, 154.0, 142.5, 136.7, 136.3, 132.5, 132.0, 130.7, 128.8, 126.9, 126.8, 125.4, 123.4, 122.6, 108.0, 105.9, 42.9, 24.6, 22.9, 12.2; HRMS (ES-) m/z calcd for $[M - H]^-$, 387.1516; found, 387.1540.

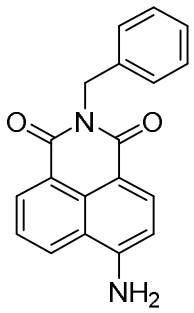

125

4-Amino-1,8-napthalic anhydride (0.50 g, 2.35 mmol) was dissolved in 150 mL ethanol under a nitrogen atmosphere and brought to reflux. To this solution was added benzylamine (1.01 mL, 9.35 mmol), after which the reaction was left to reflux for 18 h. Upon cooling to room temperature, the solvent was removed under reduced pressure, and the crude product was purified by column chromatography (DCM : MeOH = 50 : 1) and dried to afford a yellow solid **125** (0.64 g). Yield: 91%. Mp: 247 - 249 ºC. ^{1}H NMR (300 MHz, DMSO-d_6) δ 8.64 (dd, J_1 = 8.4 Hz, J_2 = 1.0 Hz, 1H), 8.45 (dd, J_1 = 7.4 Hz, J_2 = 1.1 Hz, 1H), 8.22 (d, J = 8.5 Hz, 1H), 7.68 (dd, J_1 = 8.4 Hz, J_2 = 7.4 Hz, 1H), 7.51 (s, 2H), 7.21 – 7.33 (m, 5H), 6.87 (d, J = 8.5 Hz, 1H), 5.21 (s, 2H); ^{13}C NMR (75 MHz, DMSO-d_6) δ 164.2, 163.2, 153.3, 138.3, 134.6, 131.6, 130.1, 129.9, 128.6, 127.8, 127.2, 124.4, 121.9, 119.7, 108.6, 107.6, 42.8; HRMS (ES+) m/z calcd for $[M + Na]^+$, 325.0952; found, 325.0946.

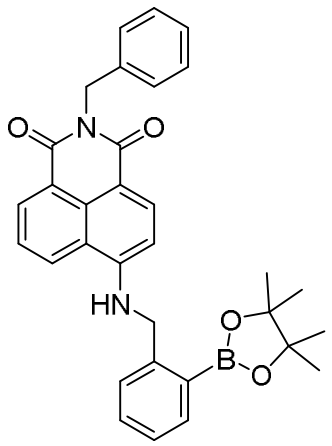

126

A mixture of **125** (200 mg, 0.66 mmol) and sodium hydride (35 mg, 60.0 wt%, 0.86 mmol) was stirred at room temperature in dry DMF (5 mL) for 40 min. A solution of 2-bromomethylphenylboronic acid pinacol ester (254 mg, 0.86 mmol) in dry DMF (1.5

mL) was added into the system dropwise under N_2. The mixture was stirred at room temperature overnight, poured into $KHSO_4$ (aq. 10 mL, 5.0 wt%) and filtered to afford a crude solid. Purify it by column chromatography on silica gel (CH_2Cl_2 : CH_3OH, 100: 1, v/v) to afford a yellow solid as product **126** (120 mg). Yield: 35%. Mp: 216 - 218 ºC. ^{1}H NMR (300 MHz, DMSO-d_6) δ 8.78 (d, J = 8.1 Hz, 1H), 8.48 (d, J = 7.8 Hz, 1H), 8.43 (d, J = 6.9 Hz, 1H), 8.22 (d, J = 8.6 Hz, 1H), 7.66 – 7.76 (m, 2H), 7.51 (s, 1H), 7.20 – 7.40 (m, 10H), 6.69 (d, J = 8.7 Hz, 1H), 5.20 (s, 2H), 4.89 (d, J = 5.7 Hz, 2H), 1.30 (s, 12H); ^{13}C NMR (75 MHz, DMSO-d_6), δ 164.1, 163.2, 151.2, 144.6, 138.2, 136.3, 134.7, 131.7, 131.3, 129.8, 129.1, 128.6, 127.8, 127.2, 126.7, 124.9, 122.1, 120.5, 108.1, 104.8, 84.0, 46.1, 42.8, 25.0; HRMS (ES-) m/z calcd for $[M - H]^-$, 517.2298; found, 517.2317.

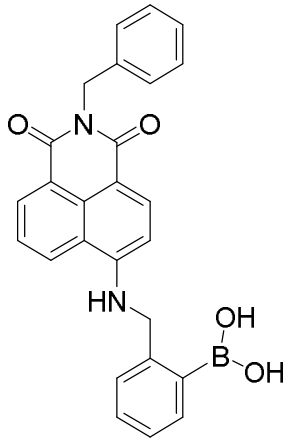

102a

A mixture of **126** (100 mg, 0.19 mmol) and potassium hydrogen fluoride (94 mg, 0.97 mmol) was stirred in methanol (5 mL) at room temperature overnight. The suspension was filtered to afford the yellow salt powder.

The powder (65 mg, 0.13 mmol) obtained above together with lithium hydroxide (9 mg, 0.37 mmol) were put into acetonitrile (4 mL) and water (2 mL). The mixture was stirred at room temperature for 4 hours. The solution was concentrated under vacuum to yellow solid. Then water (10 mL) was input and then extracts the mixture with dichloromethane (2 × 20 mL). Remove the solvent from the mixture solution and obtain the final yellow compound **102a** (41 mg). Yield: 49%. ^{1}H NMR (300 MHz, MeOD) δ 8.59 (d, J = 8.1 Hz 1H), 8.56 (d, J = 6.5 Hz, 1H), 8.27 (d, J = 8.6 Hz, 1H), 7.73 (t, J = 8.1 Hz, 1H), 7.19 – 7.41 (m, 9H), 6.72 (d, J = 8.6 Hz, 1H), 5.30 (s, 2H), 4.70 (s, 1H), 4.62 (s, 1H); ^{13}C NMR (75 MHz, MeOD), δ 166.7, 166.1, 153.4, 142.2,

139.6, 136.6, 132.6, 129.9, 129.7, 129.5, 129.4, 128.5, 128.4, 127.9, 127.3, 125.6, 123.5, 122.2, 108.8, 106.5, 44.5; HRMS (ES-) m/z calcd for $[M - H]^-$, 459.1492; found, 459.1504.

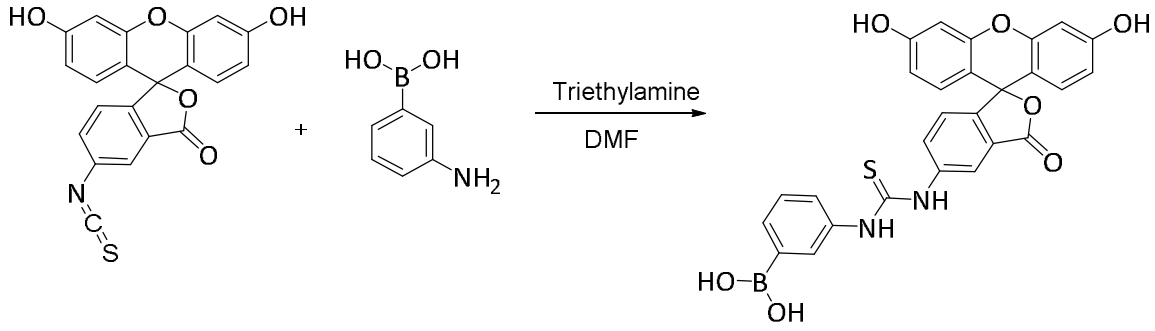

127 **108**

3-Aminophenylboronic acid monohydrate **127** (0.2865 g, 1.85 mmol) and fluorescein isothiocyanate (0.72 g, 1.85 mmol) were dissolved in DMF (20 mL). Triethylamine (0.5 mL) was added into the solution and stirred at room temperature overnight. Solvents were evaporated under reduced pressure and the residue was purified by flash column chromatography using DCM / MeOH as eluent to give the FITC based boronic acid **108** (0.70 g). Yield: 72 %. ^{1}H NMR (300 MHz, MeOD) δ 8.10 (d, J = 2.0 Hz, 1H), 7.96 (s, 1H), 7.78 (dd, J_1 = 8.2 Hz, J_2 = 2.0 Hz, 1H), 7.68 (s, 1H), 7.48 (d, J = 8.2 Hz, 1H), 7.35 (t, J = 7.6 Hz, 1H), 7.10 (d, J = 8.2 Hz, 1H), 6.63 - 6.67 (m, 4H), 6.52 – 6.55 (m, 2H); ^{13}C NMR (75 MHz, MeOD), δ 182.6, 171.5, 165.2, 161.8, 154.6, 142.9, 133.1, 130.7, 129.8, 129.3, 125.9, 121.2, 114.0, 111.8, 103.9; HRMS (ES+) m/z calcd for $[M + H]^+$, 527.1084; found, 527.1091.

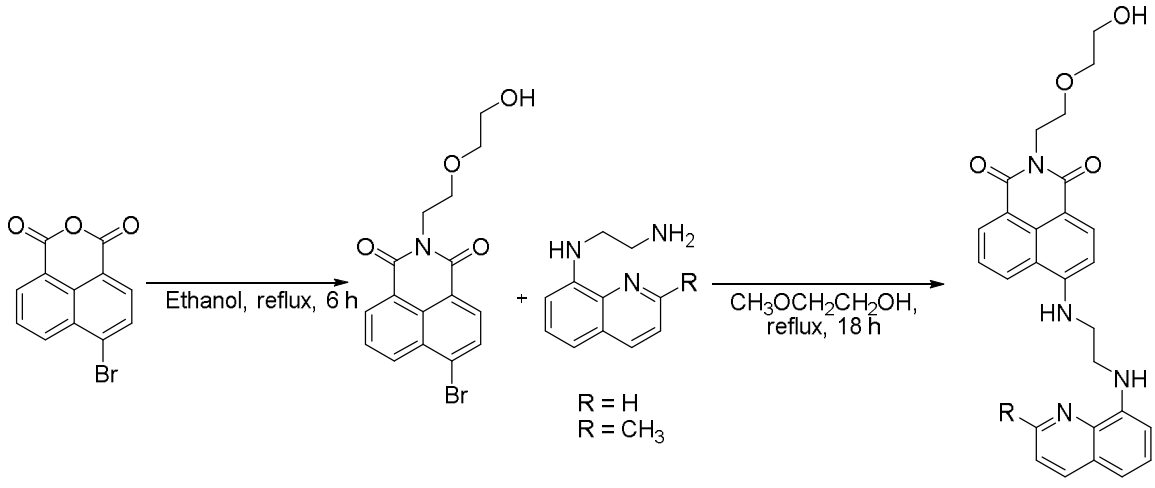

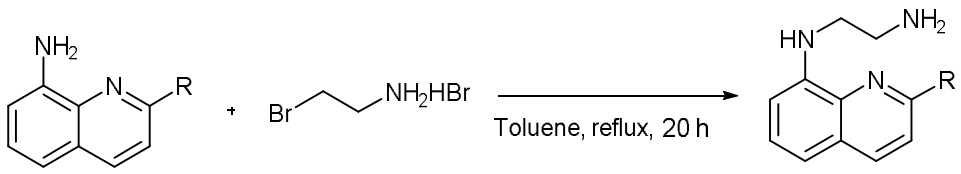

Scheme 69. *Synthetic route for probe **109** and probe **110**.*

6-Bromo-2-(2-(2-hydroxyethoxy)ethyl)-1*H*-benzo[de]isoquinoline-1,3(2*H*)-dione

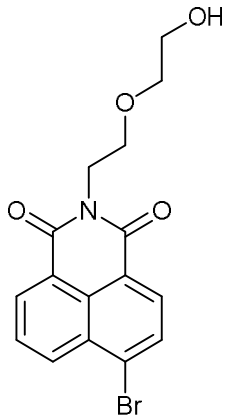

128

Under a nitrogen atmosphere, to a solution of 4-bromo-1, 8-naphthalic anhydride (0.30 g, 1.08 mmol) in anhydrous ethanol (20 mL) was added 2-(2-aminoethoxy) ethanol (0.12 g, 1.19 mmol). The mixture was heated at reflux for 3 h and concentrated under reduced pressure. Purified by flash chromatography (CH_2Cl_2:CH_3OH, 50:1, v/v) afforded a yellow powder (0.35 g). Yield: 88%. Mp: 136 - 138 ºC. lit 141 - 142 ºC. ^{1}H NMR (300 MHz, $CDCl_3$) δ 8.60 (dd, J_1 = 7.2 Hz, J_2 = 1.1 Hz, 1H), 8.53 (dd, J_1 = 8.4 Hz, J_2 = 1.1 Hz, 1H), 8.36 (d, J = 7.9 Hz, 1H), 7.99 (d, J = 7.9 Hz, 1H), 7.79 (dd, J_1 = 8.4 Hz, J_2 = 7.2 Hz, 1H), 4.38 (t, J = 5.6 Hz, 2H), 3.79 (t, J = 5.6 Hz, 2H), 3.59 - 3.63 (m, 4H); ^{13}C NMR (75 MHz, $CDCl_3$), δ 163.9, 163.8, 133.4, 132.2, 131.4, 131.1, 130.54, 130.52, 128.9, 128.1, 122.8, 121.9, 72.3, 68.3, 61.8, 39.6; HRMS (ES+) m/z calcd for $[M + Na]^+$, 386.0004; found, 386.0028.

***N*1-(quinolin-8-yl)ethane-1,2-diamine/*N*1-(2-methylquinolin-8-yl)ethane-1,2-diamine[294]**

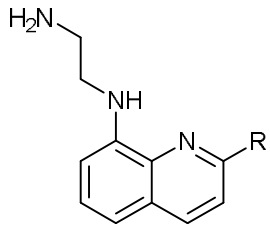

129: R = H

130: R = CH_3

General Procedure for the Synthesis of compound 129 and 130,

A solution of 2-bromoethylamine hydrobromide (1.0 g, 4.48 mmol) and quinolin-8-amine (0.5 g, 3.47 mmol) was refluxed in dry toluene (30 ml) for 24 h under a nitrogen atmosphere. The mixture was concentrated under reduced pressure and treated with a 20% aqueous NaOH solution (50 mL) and extracted with dichloromethane (50 mL × 3). The organic phase was dried over anhydrous Na_2SO_4, filtered out and the solvent was distilled. The crude product was further purified by column chromatography on silica gel (CH_2Cl_2 : CH_3OH : Et_3N, 50 : 1 : 0.5, v/v/v) to afford a yellow oil for compound *N*1-(quinolin-8-yl)ethane-1, 2-diamine **129** and a black solid for compound *N*1-(2-methylquinolin-8-yl)ethane-1, 2-diamine **130**.

***N*1-(quinolin-8-yl)ethane-1, 2-diamine 129**. 0.30 g. Yield: 46%. ^{1}H NMR (300 MHz, $CDCl_3$) δ 8.72 (dd, J_1 = 4.2 Hz, J_2 = 1.8 Hz, 1H), 8.07 (dd, J_1 = 8.4 Hz, J_2 = 1.8 Hz, 1H), 7.34 - 7.40 (m, 2H), 7.06 (dd, J_1 = 8.1 Hz, J_2 = 1.1 Hz, 1H), 6.72 (d, J = 7.6 Hz, 1H), 6.34 (br s, 1H), 3.45 (t, J = 6.2 Hz, 2H), 2.97 (t, J = 6.2 Hz, 2H); ^{13}C NMR (75 MHz, $CDCl_3$) δ 146.9, 144.8, 138.3, 136.0, 128.7, 127.7, 121.4, 113.9, 104.7, 46.4, 41.2; HRMS (ES+) m/z calcd for $[M + Na]^+$, 210.1007; found, 210.0992.

***N*1-(2-methylquinolin-8-yl)ethane-1, 2-diamine 130.** 0.31 g. Yield: 31%. Mp: 100 – 102 ºC. ^{1}H NMR (300 MHz, $CDCl_3$) δ 7.87 (d, J = 8.4 Hz, 1H), 7.22 - 7.27 (m, 1H), 7.16 (d, J = 8.4 Hz, 1H), 7.00 (dd, J_1 = 8.1 Hz, J_2 = 0.9 Hz, 1H), 6.64 (d, J = 7.5 Hz, 1H), 6.61 (br s, 1H), 5.13 (br s, 1H), 3.50 (t, J = 8.2 Hz, 2H), 3.14 (t, J = 8.2, 2H), 2.64 (s, 3H); ^{13}C NMR (75 MHz, $CDCl_3$) δ 155.9, 143.8, 137.5, 136.2, 126.6, 122.2, 114.4,

105.2, 44.6, 40.5, 25.1; HRMS (ES+) m/z calcd for $[M + H]^+$, 202.1266; found, 202.1445.

2-(2-(2-hydroxyethoxy)ethyl)-6-((2-(quinolin-8-ylamino)ethyl)amino)-1*H*benzo[de]isoquinoline-1,3(2*H*)-dione/2-(2-(2-hydroxyethoxy)ethyl)-6-((2-((2-methylquinolin-8-yl)amino)ethyl)amino)-1*H*-benzo[de]isoquinoline-1,3(2*H*)-dione

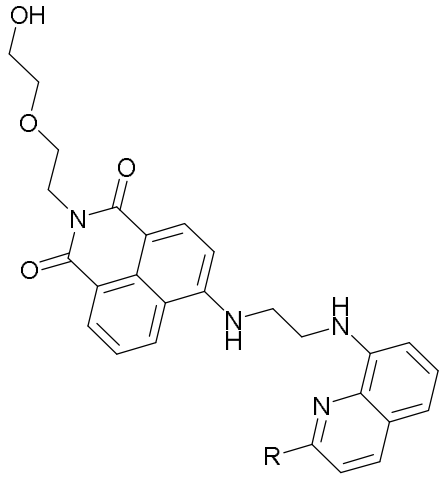

109: R = H

110: R = CH_3

General Procedure for the Synthesis of compound 109 and 110,

A solution of compound **129** (50 mg, 0.14 mmol) and quinolin-8-amine (64 mg, 0.34 mmol) was refluxed in 2-methoxylethanol (5 mL) overnight under a nitrogen atmosphere. The mixture was concentrated under vacuum to obtain a red crude oil. The crude product was further purified by column chromatography on silica gel (CH_2Cl_2 : CH_3OH, 30 : 1, v/v) to afford a yellow solid.

Synthesis of compound 109, 0.04 g. Yield: 62%. Mp: 187 – 189 ºC. ^{1}H NMR (300 MHz, $CDCl_3$) δ 8.74 (dd, J_1 = 4.5 Hz, J_2 = 1.8 Hz, 1H), 8.52 (dd, J_1 = 7.2 Hz, J_2 = 0.9 Hz, 1H), 8.43 (d, J = 8.4 Hz, 1H), 8.21 - 8.26 (m, 2 H), 7.44 - 7.57 (m, 3 H), 7.18 (d, J = 7.5 Hz, 1H), 6.88 (d, J = 7.8 Hz, 1H), 6.75 (d, J = 8.4 Hz, 1H), 6.28 (br, 1H), 4.41 (t, J = 5.4 Hz, 2H), 3.68 - 3.88 (m, 11H), 3.49 (s, 1 H); ^{13}C NMR (75 MHz, $CDCl_3$) δ 165.08, 164.53, 149.64, 145.62, 143.41, 134.63, 131.46, 129.91, 129.20, 128.62, 127.10, 124.84, 122.63, 121.43, 120.52, 115,14, 106.73, 104.22, 72.23, 68.70, 61.89, 42.57, 42.30, 39.27; HRMS (ES+) m/z calcd for $[M + Na]^+$, 493.1851; found, 493.1866.

Synthesis of compound 110, 0.007 g, Yield: 5%. Mp: 194 – 196 ºC. ^{1}H NMR (300 MHz, $CDCl_3$) δ 8.48 (d, *J* = 7.8 Hz, 1H), 8.41 (d, *J* = 8.4 Hz 1H), 8.04 (br, 1H), 7.50 (t, *J* = 7.8 Hz, 1H), 7.28 - 7.36 (m, 4H), 7.10 (d, *J* = 8.4 Hz, 1H), 6.83 (d, *J* = 7.8 Hz, 1H), 6.72 (d, *J* = 8.4 Hz, 1H), 4.41 (t, *J* = 5.7 Hz, 2H), 3.68 - 3.88 (m, 11H), 2.74 (br s, 1H), 2.73 (s, 3H); ^{13}C NMR (75 MHz, $CDCl_3$) δ 165.0, 164.5, 156.1, 149.7, 134.6, 131.4, 129.8, 124.7, 122.6, 122.5, 120.4, 115.1, 77.2, 72.1, 68.7, 61.9, 42.3, 39.2; HRMS (ES+) m/z calcd for $[M + Na]^+$, 507.2008; found, 507.2013.

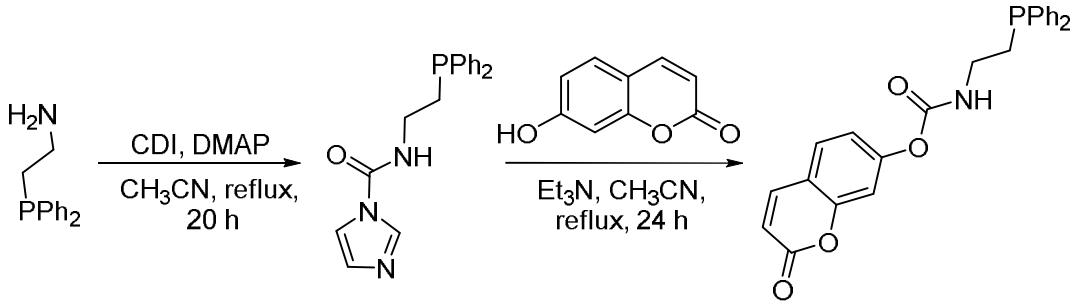

Scheme 70. *Synthetic route for probe **116***

***N*-(2-(diphenylphosphino) ethyl)-1*H*-imidazole-1-carboxamide[295]**

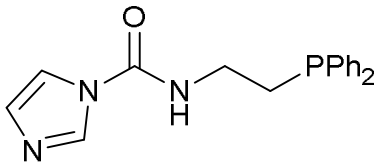

117

To a stirred solution of 2-(diphenylphosphino) ethylamine (0.50 g, 2.18 mmol) and 1,1'-carbonyldiimidazole (0.53 mg, 3.27 mmol) in anhydrous CH_3CN (10 mL), DMAP (0.08g, 0.65 mmol) was added, and the mixture was refluxed under a nitrogen atmosphere for 18 h. Then the solution was concentrated in vacuum and purified by column chromatography on silica gel (CH_2Cl_2 : MeOH, 50 : 1, v/v) to obtain a light yellow solid **117** (0.537 g). Yield: 76%. Mp: 103 – 105 ºC. ^{1}H NMR (300 MHz, $CDCl_3$) δ 8.08 (s, 1H), 7.41 - 7.47 (m, 4H), 7.31 - 7.34 (m, 6H), 7.21 (d, *J* = 1.5 Hz, 1H), 7.00 (d, *J* = 1.5 Hz, 1H), 6.73 (br s, 1H), 3.56 - 3.66 (td, 2H), 2.46 (t, *J* = 7.2 Hz, 2H), note: The phosphorous split the nearly proton into triplet-doublet; ^{13}C NMR (75 MHz, $CDCl_3$), δ 148.9, 137.5, 137.3, 135.8, (C_1 = 132.8, 132.5), (C_2 = 129.4, 129.0), (C_3 = 128.7, 128.6), 116.7, (C_4 = 38.6, 38.4), (C_5 = 28.3, 28.2), note: The phosphorous split the nearly

carbon into doublet with J_{C1P} = 22.5 Hz, J_{C2P} = 30.0 Hz, J_{C3P} = 7.5 Hz, J_{C4P} = 15.0 Hz, J_{C5P} = 7.5 Hz; HRMS (ES+) m/z calcd for $[M + H]^+$, 322.1109; found, 322.1110.

2-oxo-2*H*-chromen-7-yl (2-(diphenylphosphino)ethyl)carbamate

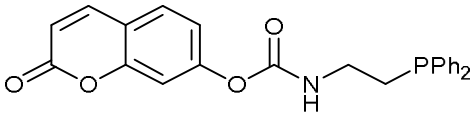

116

To a solution of **117** (0.20 g, 0.62 mmol) and umbelliferone (0.10 g, 0.62 mmol) was added Et_3N (0.125 g, 1.24 mmol). The solution was stirred at reflux for 18 h and concentrated under reduced pressure. Purified by flash chromatography on silica gel (CH_2Cl_2 : MeOH, 100 : 1, v/v) afforded a slight yellow solid **116** (0.070 g). Yield: 27%, Mp: 131 -133 ºC. ^{1}H NMR (300 MHz, $CDCl_3$) δ 7.68 (d, *J* = 9.7 Hz, 1H), 7.34 - 7.46 (m, 11H), 7.04 - 7.10 (m, 2H), 6.38 (d, *J* = 9.6 Hz, 1H), 5.39 (br s, 1H), 3.41 - 3.46 (m, 2H), 2.39 (t, *J* = 7.4 Hz, 2H), note: The phosphorous split the nearly proton into triplet-doublet; ^{13}C NMR (75 MHz, $CDCl_3$), δ 160.6, 154.6, 153.6, 153.3, 143.0, 137.4, 137.3, 132.8, 132.6, 129.0, (C1 = 128.8, 128.7), (C2 = 128.6, 128.5), (C3 =128.4, 118.3, 116.1, 115.6, 110.1, 38.8, 38.5, 28.8, 28.7, note: The phosphorous split the nearly carbon into doublet with J_{C1P} = 22.5 Hz, J_{C2P} = 30.0 Hz, J_{C3P} = 7.5 Hz, J_{C4P} = 15.0 Hz, J_{C5P} = 7.5 Hz; HRMS (ES+) m/z calcd for $[M + H]^+$, 418.1208; found, 418.1195.

9. BIBLIOGRAPHY

1. B. Breiten, M. R. Lockett, W. Sherman, S. Fujita, M. Al-Sayah, H. Lange, C. M. Bowers, A. Heroux, G. Krilov and G. M. Whitesides, *J. Am. Chem. Soc.*, 2013, **135**, 15579-15584.
2. R. Y. Tsien, *Biochemistry*, 1980, **19**, 2396-2404.
3. G. Grynkiewicz, M. Poenie and R. Y. Tsien, *J. Biol. Chem.*, 1985, **260**, 3440-3450.
4. R. Y. Tsien, T. Pozzan and T. J. Rink, *J. Cell Biol.*, 1982, **94**, 325-334.
5. K. J. Albert and D. R. Walt, *Anal. Chem.*, 2000, **72**, 1947-1955.
6. D. R. Goud, A. K. Purohit, V. Tak, D. K. Dubey, P. Kumar and D. Pardasani, *Chem. Commun.*, 2014.
7. T. L. Andrew and T. M. Swager, *J. Am. Chem. Soc.*, 2007, **129**, 7254-7255.
8. L. Basabe-Desmonts, D. N. Reinhoudt and M. Crego-Calama, *Chem. Soc. Rev.*, 2007, **36**, 993-1017.
9. R. Jelinek and S. Kolusheva, *Chem. Rev.*, 2004, **104**, 5987-6015.
10. J. Chan, S. C. Dodani and C. J. Chang, *Nat. Chem.*, 2012, **4**, 973-984.
11. T. D. James, P. Linnane and S. Shinkai, *Chem. Commun.*, 1996, 281-288.
12. S. Arimori, M. L. Bell, C. S. Oh, K. A. Frimat and T. D. James, *J. Chem. Soc., Perkin Trans. 1*, 2002, 803-808.
13. S. Shinkai and M. Takeuchi, *Bull. Chem. Soc. Jpn.*, 2005, **78**, 40-51.
14. J. Yan, H. Fang and B. Wang, *Med. Res. Rev.*, 2005, **25**, 490-520.
15. A. P. Davis and T. D. James, in *Functional Synthetic Receptors*, eds. T. Schrader and A. Hamilton, Wiley-VCH, 2005, pp. 45-109.
16. T. D. James, in *Boronic Acids*, ed. D. G. Hall, Wiley-VCH, 2005, pp. 441-480.
17. T. D. James, M. D. Phillips and S. Shinkai, *Boronic Acids in Saccharide Recognition*, RSC, Cambridge, 2006.
18. T. D. James, *Top. Curr. Chem.*, 2007, **277**, 107-152
19. H. S. Mader and O. S. Wolfbeis, *Microchim. Acta*, 2008, **162**, 1-34.
20. S. Jin, Y. F. Cheng, S. Reid, M. Y. Li and B. H. Wang, *Med. Res. Rev.*, 2010, **30**, 171-257.
21. C. J. Musto and K. S. Suslick, *Curr. Opin. Chem. Biol.*, 2010, **14**, 758-766.
22. M. S. Steiner, A. Duerkop and O. S. Wolfbeis, *Chem. Soc. Rev.*, 2011, **40**, 4805-4839.
23. S. Huang, M. Jia, Y. Xie, J. Wang, W. Xu and H. Fang, *Curr. Med. Chem.*, 2012, **19**, 2621-2637.

24. J. S. Fossey, F. D'Hooge, J. M. H. van den Elsen, M. P. P. Morais, S. I. Pascu, S. D. Bull, F. Marken, A. T. A. Jenkins, Y. B. Jiang and T. D. James, *Chem. Rec.*, 2012, **12**, 464-478.
25. J. S. Hansen, J. B. Christensen, J. F. Petersen, T. Hoeg-Jensen and J. C. Norrild, *Sens. Actuator B-Chem.*, 2012, **161**, 45-79.
26. S. D. Bull, M. G. Davidson, J. M. H. Van den Elsen, J. S. Fossey, A. T. A. Jenkins, Y.-B. Jiang, Y. Kubo, F. Marken, K. Sakurai, J. Zhao and T. D. James, *Acc. Chem. Res.*, 2013, **46**, 312-326.
27. X. Wu, Z. Li, X.-X. Chen, J. S. Fossey, T. D. James and Y.-B. Jiang, *Chem. Soc. Rev.*, 2013, **42**, 8032-8048.
28. G. F. Whyte, R. Vilar and R. Woscholski, *J. Biol. Chem.*, 2013, **6**, 161-174.
29. L. F. Wang, C. F. Dai, S. K. Burroughs, S. M. L. Wang and B. H. Wang, *Chem. Eur. J.*, 2013, **19**, 7587-7594.
30. Y. Guan and Y. Zhang, *Chem. Soc. Rev.*, 2013, **42**, 8106-8121.
31. J. Hansen and J. Christensen, *Biosensors*, 2013, **3**, 400-418.
32. K. Yum, T. P. McNicholas, B. Mu and M. S. Strano, *J. Diabetes Sci. Technol.*, 2013, **7**, 72-87.
33. Y. J. Heo and S. Takeuchi, *Adv. Healthc. Mater.*, 2013, **2**, 43-56.
34. K. Tohda, *Bunseki Kagaku*, 2013, **62**, 903-914.
35. C. A. McClary and M. S. Taylor, *Carbohydr. Res.*, 2013, **381**, 112-122.
36. R. Ma and L. Shi, *Polym. Chem.*, 2014, **5**, 1503-1518.
37. R. Nishiyabu, Y. Kubo, T. D. James and J. S. Fossey, *Chem. Commun.*, 2011, **47**, 1106-1123.
38. Z. Q. Guo, I. Shin and J. Yoon, *Chem. Commun.*, 2012, **48**, 5956-5967.
39. T. W. Hudnall, C.-W. Chiu and F. P. Gabbai, *Acc. Chem. Res.*, 2009, **42**, 388-397.
40. E. Galbraith and T. D. James, *Chem. Soc. Rev.*, 2010, **39**, 3831-3842.
41. C. R. Wade, A. E. J. Broomsgrove, S. Aldridge and F. P. Gabbai, *Chem. Rev.*, 2010, **110**, 3958-3984.
42. Y. Zhou, J. F. Zhang and J. Yoon, *Chem. Rev.*, 2014, **114**, 5511-5571.
43. A. M. Kelly, Y. Pérez-Fuertes, J. S. Fossey, S. L. Yeste, S. D. Bull and T. D. James, *Nat. Protoc.*, 2008, **3**, 215-219.
44. A. M. Kelly, Y. Perez-Fuertes, S. Arimori, S. D. Bull and T. D. James, *Org. Lett.*, 2006, **8**, 1971-1974.
45. M. E. Powell, C. D. Evans, S. D. Bull, T. D. James and P. S. Fordred, in *Comprehensive Chirality*, eds. E. M. Carreira and H. Yamamoto, Elsevier, Amsterdam, 2012, pp. 571-599.

46. D. A. Tickell, M. F. Mahon, S. D. Bull and T. D. James, *Org. Lett.*, 2013, **15**, 860-863.
47. T. R. Jackson, J. S. Springall, D. Rogalle, N. Masumoto, H. C. Li, F. D'Hooge, S. P. Perera, A. T. A. Jenkins, T. D. James, J. S. Fossey and J. M. H. van den Elsen, *Electrophoresis*, 2008, **29**, 4185-4191.
48. M. P. Pereira Morais, J. D. Mackay, S. K. Bhamra, J. G. Buchanan, T. D. James, J. S. Fossey and J. M. van den Elsen, *Proteomics*, 2010, **10**, 48-58.
49. M. P. P. Morais, D. Marshall, S. E. Flower, C. J. Caunt, T. D. James, R. J. Williams, N. R. Waterfield and J. M. H. van den Elsen, *Sci. Rep.*, 2013, **3**.
50. M. P. Pereira Morais, J. S. Fossey, T. D. James and J. M. H. van den Elsen, in *Protein Electrophoresis: Methods and Protocols, Methods in Molecular Biology*, ed. B. T. K. a. R. H. Schofield, Humana Press, 2012, vol. 869.
51. K. Severin, *Dalton Trans.*, 2009, 5254-5264.
52. K. Kataoka, S. Okuyama, T. Minami, T. D. James and Y. Kubo, *Chem. Commun.*, 2009, 1682-1684.
53. K. Kataoka, T. D. James and Y. Kubo, *J. Am. Chem. Soc.*, 2007, **129**, 15126-15127.
54. N. Fujita, S. Shinkai and T. D. James, *Chem. Asian J.*, 2008, **3**, 1076-1091.
55. R. Nishiyabu, Y. Kubo, T. D. James and J. S. Fossey, *Chem. Commun.*, 2011, **47**, 1124-1150.
56. A. Wilson, G. Gasparini and S. Matile, *Chem. Soc. Rev.*, 2014, **43**, 1948-1962.
57. X. L. Sun, S. Y. Xu, S. E. Flower, J. S. Fossey, X. H. Qian and T. D. James, *Chem. Commun.*, 2013, **49**, 8311-8313.
58. X. Sun, Q. Xu, G. Kim, S. E. Flower, J. P. Lowe, J. Yoon, J. S. Fossey, X. Qian, S. D. Bull and T. D. James, *Chem. Sci.*, 2014, **5**, 3368-3373.
59. B. C. Dickinson and C. J. Chang, *Nat. Chem. Biol.*, 2011, **7**, 504-511.
60. B. C. Dickinson, C. Huynh and C. J. Chang, *J. Am. Chem. Soc.*, 2010, **132**, 5906-5915.
61. Bryan C. Dickinson, Y. Tang, Z. Chang and Christopher J. Chang, *Chem. Biol.*, 2011, **18**, 943-948.
62. A. R. Lippert, G. C. Van de Bittner and C. J. Chang, *Acc. Chem. Res.*, 2011, **44**, 793-804.
63. D. Srikun, A. E. Albers, C. I. Nam, A. T. Iavarone and C. J. Chang, *J. Am. Chem. Soc.*, 2010, **132**, 4455-4465.
64. G. C. Van de Bittner, C. R. Bertozzi and C. J. Chang, *J. Am. Chem. Soc.*, 2013, **135**, 1783-1795.
65. G. C. Van de Bittner, E. A. Dubikovskaya, C. R. Bertozzi and C. J. Chang, *P. Natl. Acad. Sci.*, 2010, **107**, 21316-21321.
66. J. P. Lorand and J. O. Edwards, *J. Org. Chem.*, 1959, **24**, 769-774.

67. L. I. Bosch, T. M. Fyles and T. D. James, *Tetrahedron*, 2004, **60**, 11175-11190.
68. J. D. Larkin, J. S. Fossey, T. D. James, B. R. Brooks and C. W. Bock, *J. Phys. Chem. A*, 2010, **114**, 12531-12539.
69. L. Zhu, S. H. Shabbir, M. Gray, V. M. Lynch, S. Sorey and E. V. Anslyn, *J. Am. Chem. Soc.*, 2006, **128**, 1222-1232.
70. T. D. James, K. R. A. S. Sandanayake and S. Shinkai, *J. Chem. Soc, Chem. Commun.*, 1994, 477.
71. T. D. James, K. R. A. S. Sandanayake, R. Iguchi and S. Shinkai, *J. Am. Chem. Soc.*, 1995, **117**, 8982-8987.
72. J. Zhao, M. G. Davidson, M. F. Mahon, G. Kociok-Köhn and T. D. James, *J. Am. Chem. Soc.*, 2004, **126**, 16179-16186.
73. C. R. Cooper, N. Spencer and T. D. James, *Chem. Commun.*, 1998, 1365-1366.
74. G. Wulff, *Pure Appl. Chem.*, 1982, **54**, 2093-2102.
75. S. L. Wiskur, J. J. Lavigne, H. Ait-Haddou, V. Lynch, Y. H. Chiu, J. W. Canary and E. V. Anslyn, *Org. Lett.*, 2001, **3**, 1311-1314.
76. S. Franzen, W. Ni and B. Wang, *J. Phys. Chem. B.*, 2003, **107**, 12942-12948.
77. S. L. Wiskur, H. Ait-Haddou, J. J. Lavigne and E. V. Anslyn, *Acc. Chem. Res.*, 2001, **34**, 963-972.
78. S. C. McCleskey, P. N. Floriano, S. L. Wiskur, E. V. Anslyn and J. T. McDevitt, *Tetrahedron*, 2003, **59**, 10089-10092.
79. A. Goodey, J. J. Lavigne, S. M. Savoy, M. D. Rodriguez, T. Curey, A. Tsao, G. Simmons, J. Wright, S. J. Yoo, Y. Sohn, E. V. Anslyn, J. B. Shear, D. P. Neikirk and J. T. McDevitt, *J. Am. Chem. Soc.*, 2001, **123**, 2559-2570.
80. Y. S. Sohn, A. Goodey, E. V. Anslyn, J. T. McDevitt, J. B. Shear and D. P. Neikirk, *Biosens. Bioelectron.*, 2005, **21**, 303-312.
81. A. P. Umali, E. V. Anslyn, A. T. Wright, C. R. Blieden, C. K. Smith, T. Tian, J. A. Truong, C. E. Crumm, J. E. Garcia, S. Lee, M. Mosier and C. P. Nguyen, *J. Chem. Educ.*, 2010.
82. B. T. Nguyen and E. V. Anslyn, *Coord. Chem. Rev.*, 2006, **250**, 3118-3127.
83. A. P. Umali and E. V. Anslyn, *Curr. Opin. Chem. Biol.*, 2010, **14**, 685-692.
84. A. Buryak and K. Severin, *Angew. Chemie. Int. Ed.*, 2004, **43**, 4771-4774.
85. B. Vilozny, A. Schiller, R. A. Wessling and B. Singaram, *Anal. Chim. Acta*, 2009, **649**, 246-251.
86. S. Gamsey, A. Miller, M. M. Olmstead, C. M. Beavers, L. C. Hirayama, S. Pradhan, R. A. Wessling and B. Singaram, *J. Am. Chem. Soc.*, 2007, **129**, 1278-1286.

87. A. Schiller, R. A. Wessling and B. Singaram, *Angew. Chemie. Int. Ed.*, 2007, **46**, 6457-6459.

88. Z. Sharrett, S. Gamsey, J. Fat, D. Cunningham-Bryant, R. A. Wessling and B. Singaram, *Tetrahedron Lett.*, 2007, **48**, 5125-5129.

89. J. N. Camara, J. T. Suri, F. E. Cappuccio, R. A. Wessling and B. Singaram, *Tetrahedron Lett.*, 2002, **43**, 1139-1141.

90. D. B. Cordes, A. Miller, S. Gamsey and B. Singaram, *Anal. Bioanal. Chem.*, 2007, **387**, 2767-2773.

91. A. Schiller, B. Vilozny, R. A. Wessling and B. Singaram, in *Reviews in Fluorescence 2009*, ed. C. D. Geddes, 2011, vol. 6, pp. 155-191.

92. D. B. Cordes and B. Singaram, *Pure Appl. Chem.*, 2012, **84**, 2183-2202.

93. E. V. Anslyn, *J. Org. Chem.*, 2007, **72**, 687-699.

94. G. Springsteen and B. Wang, *Chem. Commun.*, 2001, 1608-1609.

95. G. Springsteen and B. Wang, *Tetrahedron*, 2002, **58**, 5291-5300.

96. J. Yan, G. Springsteen, S. Deeter and B. Wang, *Tetrahedron*, 2004, **60**, 11205-11209.

97. S. Arimori, C. J. Ward and T. D. James, *Chem. Commun.*, 2001, 2018-2019.

98. S. Boduroglu, J. M. El Khoury, D. Venkat Reddy, P. L. Rinaldi and J. Hu, *Bioorg. Med. Chem. Lett.*, 2005, **15**, 3974-3977.

99. K. Ngamdee, T. Noipa, S. Martwiset, T. Tuntulani and W. Ngeontae, *Sens. Actuator B-Chem.*, 2011, **160**, 129-138.

100. S. Arimori, C. J. Ward and T. D. James, *Tetrahedron Lett.*, 2002, **43**, 303-305.

101. H. R. Mulla, N. J. Agard and A. Basu, *Bioorg. Med. Chem. Lett.*, 2004, **14**, 25-27.

102. L. A. Cabell, M. K. Monahan and E. V. Anslyn, *Tetrahedron Lett.*, 1999, **40**, 7753-7756.

103. Z. Zhong and E. V. Anslyn, *J. Am. Chem. Soc.*, 2002, **124**, 9014-9015.

104. A. M. Piatek, Y. J. Bomble, S. L. Wiskur and E. V. Anslyn, *J. Am. Chem. Soc.*, 2004, **126**, 6072-6077.

105. S. L. Wiskur and E. V. Anslyn, *J. Am. Chem. Soc.*, 2001, **123**, 10109-10110.

106. S. L. Wiskur, P. N. Floriano, E. V. Anslyn and J. T. McDevitt, *Angew. Chemie. Int. Ed.*, 2003, **42**, 2070-2072.

107. B. T. Nguyen, S. L. Wiskur and E. V. Anslyn, *Org. Lett.*, 2004, **6**, 2499-2501.

108. L. Zhu and E. V. Anslyn, *J. Am. Chem. Soc.*, 2004, **126**, 3676-3677.

109. L. Zhu, Z. Zhong and E. V. Anslyn, *J. Am. Chem. Soc.*, 2005, **127**, 4260-4269.

110. J. Zielonka, A. Sikora, M. Hardy, J. Joseph, B. P. Dranka and B. Kalyanaraman, *Chem. Res. Toxicol.*, 2012, **25**, 1793-1799.

111. M. C. Y. Chang, A. Pralle, E. Y. Isacoff and C. J. Chang, *J. Am. Chem. Soc.*, 2004, **126**, 15392-15393.
112. E. W. Miller, A. E. Albers, A. Pralle, E. Y. Isacoff and C. J. Chang, *J. Am. Chem. Soc.*, 2005, **127**, 16652-16659.
113. A. E. Albers, V. S. Okreglak and C. J. Chang, *J. Am. Chem. Soc.*, 2006, **128**, 9640-9641.
114. E. W. Miller, O. Tulyathan, E. Y. Isacoff and C. J. Chang, *Nat. Chem. Biol.*, 2007, **3**, 263-267.
115. D. Srikun, E. W. Miller, D. W. Domaille and C. J. Chang, *J. Am. Chem. Soc.*, 2008, **130**, 4596-4597.
116. H. G. K. a. A. G. Armour, *J. Am. Chem. Soc.*, 1957, **79**, 5659–5662.
117. A. Sikora, J. Zielonka, M. Lopez, J. Joseph and B. Kalyanaraman, *Free Radical Biol. Med.*, 2009, **47**, 1401-1407.
118. G. E. Conner, M. Salathe and R. Forteza, *Am. J. Respir. Crit. Care Med.*, 2002, **166**, S57-S61.
119. B. R. T. Leto., *Oxidative Innate Immune Defenses by Nox/Duox Family NADPH Oxidases, Trends in Innate Immunity. Contrib Microbiol. Basel, Karger*, 2008.
120. A. Bachi, I. Dalle-Donne and A. Scaloni, *Chem. Rev.*, 2012, **113**, 596-698.
121. X. Chen, X. Tian, I. Shin and J. Yoon, *Chem. Soc. Rev.*, 2011, **40**, 4783-4804.
122. Biochemical oxygen demand (BOD) is the amount of dissolved oxygen needed by aerobic biological organisms in a body of water to break down organic material present in a given water sample at certain temperature over a specific time period.
123. In environmental chemistry, the chemical oxygen demand (COD) test is commonly used to indirectly measure the amount of organic compounds in water.
124. J. P. Fruehauf and F. L. Meyskens, *Clin. Cancer Res.*, 2007, **13**, 789-794.
125. M. P. Mattson, *Nature*, 2004, **430**, 631-639.
126. H. Ohshima, M. Tatemichi and T. Sawa, *Arch. Biochem. Biophys.*, 2003, **417**, 3-11.
127. K. Wannajuk, M. Jamkatoke, T. Tuntulani and B. Tomapatanaget, *Tetrahedron*, 2012, **68**, 8899-8904.
128. M. Abo, Y. Urano, K. Hanaoka, T. Terai, T. Komatsu and T. Nagano, *J. Am. Chem. Soc.*, 2011, **133**, 10629-10637.
129. S. Weinreb, A. H. Barrett, M. L. Meeks and J. C. Henry, *Nature*, 1963, **200**, 829-831.
130. D. J. Kieber and N. V. Blough, *Anal. Chem.*, 1990, **62**, 2275-2283.
131. S. Pou, Y. I. Huang, A. Bhan, V. S. Bhadti, R. S. Hosmane, S. Y. Wu, G. L. Cao and G. M. Rosen, *Anal. Biochem.*, 1993, **212**, 85-90.
132. X.-F. Yang and X.-Q. Guo, *Anal. Chim. Acta*, 2001, **434**, 169-177.

133. P. Li, T. Xie, X. Duan, F. Yu, X. Wang and B. Tang, *Chem. Eur. J.*, 2010, **16**, 1834-1840.

134. T. Maki, N. Soh, T. Fukaminato, H. Nakajima, K. Nakano and T. Imato, *Anal. Chim. Acta*, 2009, **639**, 78-82.

135. N. Soh, K. Makihara, E. Sakoda and T. Imato, *Chem. Commun.*, 2004, 496-497.

136. B. Tang, N. Zhang, Z. Chen, K. Xu, L. Zhuo, L. An and G. Yang, *Chem. Eur. J.*, 2008, **14**, 522-528.

137. N. Umezawa, K. Tanaka, Y. Urano, K. Kikuchi, T. Higuchi and T. Nagano, *Angew. Chemie. Int. Ed.*, 1999, **38**, 2899-2901.

138. K. Tanaka, T. Miura, N. Umezawa, Y. Urano, K. Kikuchi, T. Higuchi and T. Nagano, *J. Am. Chem. Soc.*, 2001, **123**, 2530-2536.

139. C. Flors, M. J. Fryer, J. Waring, B. Reeder, U. Bechtold, P. M. Mullineaux, S. Nonell, M. T. Wilson and N. R. Baker, *J. Exp. Bot.*, 2006, **57**, 1725-1734.

140. T. Guo, L. Cui, J. Shen, R. Wang, W. Zhu, Y. Xu and X. Qian, *Chem. Commun.*, 2013, **49**, 1862-1864.

141. N. Pauly, C. Pucciariello, K. Mandon, G. Innocent, A. Jamet, E. Baudouin, D. Hérouart, P. Frendo and A. Puppo, *J. Exp. Bot.*, 2006, **57**, 1769-1776.

142. T. Nagano and T. Yoshimura, *Chem. Rev.*, 2002, **102**, 1235-1270.

143. F. Bedioui and N. Villeneuve, *Electroanalysis*, 2003, **15**, 5-18.

144. S. Fujii and T. Yoshimura, *Coord. Chem. Rev.*, 2000, **198**, 89-99.

145. J. F. Brien, B. E. McLaughlin, K. Nakatsu and G. S. Marks, in *Meth. Enzymol.*, ed. P. Lester, Academic Press, 1996, vol. 268, pp. 83-92.

146. E. M. Hetrick and M. H. Schoenfisch, *Annu. Rev. Anal. Chem.*, 2009, **2**, 409-433.

147. H. Kojima, N. Nakatsubo, K. Kikuchi, S. Kawahara, Y. Kirino, H. Nagoshi, Y. Hirata and T. Nagano, *Anal. Chem.*, 1998, **70**, 2446-2453.

148. H. Kojima, Y. Urano, K. Kikuchi, T. Higuchi, Y. Hirata and T. Nagano, *Angew. Chemie. Int. Ed.*, 1999, **38**, 3209-3212.

149. H. Kojima, M. Hirotani, N. Nakatsubo, K. Kikuchi, Y. Urano, T. Higuchi, Y. Hirata and T. Nagano, *Anal. Chem.*, 2001, **73**, 1967-1973.

150. Y. Gabe, Y. Urano, K. Kikuchi, H. Kojima and T. Nagano, *J. Am. Chem. Soc.*, 2004, **126**, 3357-3367.

151. E. Sasaki, H. Kojima, H. Nishimatsu, Y. Urano, K. Kikuchi, Y. Hirata and T. Nagano, *J. Am. Chem. Soc.*, 2005, **127**, 3684-3685.

152. T. Nagano, *P. Jpn. Acad. B-phys.*, 2010, **86**, 837-847.

153. K. J. Franz, N. Singh and S. J. Lippard, *Angew. Chemie. Int. Ed.*, 2000, **39**, 2120-2122.

154. N. Soh, T. Imato, K. Kawamura, M. Maeda and Y. Katayama, *Chem. Commun.*, 2002, 2650-2651.
155. M. H. Lim and S. J. Lippard, *Abstr. Pap. Am. Chem. S.*, 2007, **234**.
156. S. A. Hilderbrand, M. H. Lim and S. J. Lippard, *J. Am. Chem. Soc.*, 2004, **126**, 4972-4978.
157. S. A. Hilderbrand and S. J. Lippard, *Inorg. Chem.*, 2004, **43**, 5294-5301.
158. M. H. Lim and S. J. Lippard, *Inorg. Chem.*, 2004, **43**, 6366-6370.
159. M. D. Pluth and S. J. Lippard, *Chem. Commun. (Camb.)*, 2012, **48**, 11981-11983.
160. M. H. Lim and S. J. Lippard, *J. Am. Chem. Soc.*, 2005, **127**, 12170-12171.
161. M. H. Lim and S. J. Lippard, *Inorg. Chem.*, 2006, **45**, 8980-8989.
162. M. H. Lim, B. A. Wong, W. H. Pitcock, D. Mokshagundam, M. H. Baik and S. J. Lippard, *J. Am. Chem. Soc.*, 2006, **128**, 14364-14373.
163. M. H. Lim, D. Xu and S. J. Lippard, *Nat. Chem. Biol.*, 2006, **2**, 375-380.
164. M. Sarma and B. Mondal, *Inorg. Chem.*, 2011, **50**, 3206-3212.
165. X. L. Sun, Y. F. Xu, W. P. Zhu, C. S. He, L. Xu, Y. J. Yang and X. H. Qian, *Anal. Methods*, 2012, **4**, 919-922.
166. Y. Yang, S. K. Seidlits, M. M. Adams, V. M. Lynch, C. E. Schmidt, E. V. Anslyn and J. B. Shear, *J. Am. Chem. Soc.*, 2010, **132**, 13114-13116.
167. A. Angeli, *Chem. Zentralbl.*, 1902, **33**, 691.
168. A. Angeli, *Gazz. Chim. Ital.*, 1903, **33**, 245.
169. N. Paolocci, M. I. Jackson, B. E. Lopez, K. Miranda, C. G. Tocchetti, D. A. Wink, A. J. Hobbs and J. M. Fukuto, *Pharmacol. Therapeut.*, 2007, **113**, 442-458.
170. N. Paolocci, W. F. Saavedra, K. M. Miranda, C. Martignani, T. Isoda, J. M. Hare, M. G. Espey, J. M. Fukuto, M. Feelisch, D. A. Wink and D. A. Kass, *Proc. Natl. Acad. Sci. U.S.A.*, 2001, **98**, 10463-10468.
171. N. Paolocci, T. Katori, H. C. Champion, M. E. St. John, K. M. Miranda, J. M. Fukuto, D. A. Wink and D. A. Kass, *Proc. Natl. Acad. Sci.*, 2003, **100**, 5537-5542.
172. C. G. Tocchetti, W. Wang, J. P. Froehlich, S. Huke, M. A. Aon, G. M. Wilson, G. Di Benedetto, B. O'Rourke, W. D. Gao, D. A. Wink, J. P. Toscano, M. Zaccolo, D. M. Bers, H. H. Valdivia, H. Cheng, D. A. Kass and N. Paolocci, *Circ. Res.*, 2007, **100**, 96-104.
173. J. C. Irvine, R. H. Ritchie, J. L. Favaloro, K. L. Andrews, R. E. Widdop and B. K. Kemp-Harper, *Trends Pharmacol. Sci.*, 2008, **29**, 601-608.
174. R. Z. Pino and M. Feelisch, *Biochem. Biophys. Res. Commun.*, 1994, **201**, 54-62.
175. J. Rosenthal and S. J. Lippard, *J. Am. Chem. Soc.*, 2010, **132**, 5536-5537.

176. Y. Zhou, K. Liu, J.-Y. Li, Y. Fang, T.-C. Zhao and C. Yao, *Org. Lett.*, 2011, **13**, 1290-1293.
177. G. M. Rosen and B. A. Freeman, *Proc. Natl. Acad. Sci.*, 1984, **81**, 7269-7273.
178. A. A. Bobko, A. Ivanov and V. V. Khramtsov, *Free Radical Res.*, 2013, **47**, 74-81.
179. M. A. Martí, S. E. Bari, D. A. Estrin and F. Doctorovich, *J. Am. Chem. Soc.*, 2005, **127**, 4680-4684.
180. M. R. Cline, C. Tu, D. N. Silverman and J. P. Toscano, *Free Radical Biol. Med.*, 2011, **50**, 1274-1279.
181. M. R. Cline and J. P. Toscano, *J. Phys. Org. Chem.*, 2011, **24**, 993-998.
182. J. A. Reisz, C. N. Zink and S. B. King, *J. Am. Chem. Soc.*, 2011, **133**, 11675-11685.
183. K. Kawai, N. Ieda, K. Aizawa, T. Suzuki, N. Miyata and H. Nakagawa, *J. Am. Chem. Soc.*, 2013, **135**, 12690-12696.
184. J. W. Reed, H. H. Ho and W. L. Jolly, *J. Am. Chem. Soc.*, 1974, **96**, 1248-1249.
185. D. Yang, H.-L. Wang, Z.-N. Sun, N.-W. Chung and J.-G. Shen, *J. Am. Chem. Soc.*, 2006, **128**, 6004-6005.
186. Z.-N. Sun, H.-L. Wang, F.-Q. Liu, Y. Chen, P. K. H. Tam and D. Yang, *Org. Lett.*, 2009, **11**, 1887-1890.
187. T. Peng and D. Yang, *Org. Lett.*, 2010, **12**, 4932-4935.
188. Q. Zhang, Z. Zhu, Y. Zheng, J. Cheng, N. Zhang, Y. T. Long, J. Zheng, X. Qian and Y. Yang, *J. Am. Chem. Soc.*, 2012, **134**, 18479-18482.
189. F. Yu, P. Li, G. Li, G. Zhao, T. Chu and K. Han, *J. Am. Chem. Soc.*, 2011, **133**, 11030-11033.
190. F. Yu, P. Li, B. Wang and K. Han, *J. Am. Chem. Soc.*, 2013, **135**, 7674-7680.
191. Z. J. Chen, W. Ren, Q. E. Wright and H. W. Ai, *J. Am. Chem. Soc.*, 2013, **135**, 14940-14943.
192. L. J. Thénard, *Annales de chimie et de physique, 2nd series*, 1818, **8**, 306-312.
193. R. Nishiyabu, Y. Kubo, T. D. James and J. S. Fossey, *Chem. Commun.*, 2012, **47**, 1106-1123.
194. S. D. Bull, M. G. Davidson, J. M. van den Elsen, J. S. Fossey, A. T. Jenkins, Y. B. Jiang, Y. Kubo, F. Marken, K. Sakurai, J. Zhao and T. D. James, *Acc. Chem. Res.*, 2013, **46**, 312-326.
195. K. Tsukagoshi and S. Shinkai, *J. Org. Chem.*, 1991, **56**, 4089-4091.
196. T. D. James, K. R. A. S. Sandanayake and S. Shinkai, *J. Chem. Soc., Chem. Commun.*, 1994, 477.
197. Y. Wu, H. Guo, T. D. James and J. Zhao, *J. Org. Chem.*, 2011, **76**, 5685-5695.

198. W. M. J. Ma, M. P. Pereira Morais, F. D'Hooge, J. M. H. van den Elsen, J. P. L. Cox, T. D. James and J. S. Fossey, *Chem. Commun.*, 2009, **5**, 532-534.

199. W. Chen, S. A. Elfeky, Y. Nonne, L. Male, K. Ahmed, C. Amiable, P. Axe, S. Yamada, T. D. James and S. D. Bull, *Chem. Commun.*, 2011, **47**, 253-255.

200. Y. Egawa, T. Seki, S. Takahashi and J.-i. Anzai, *Mater. Sci. Eng. C*, 2011, **31**, 1257-1264.

201. H. Suenaga, M. Mikami, K. R. A. S. Sandanayake and S. Shinkai, *Tetrahedron Lett.*, 1995, **36**, 4825-4828.

202. T. D. James, K. R. A. Samankumara Sandanayake and S. Shinkai, *Nature*, 1995, **374**, 345-347.

203. J. Yoon and A. W. Czarnik, *J. Am. Chem. Soc.*, 1992, **114**, 5874-5875.

204. C. M. Harris and B. K. Selinger, *J. Phys. Chem. B*, 1980, **84**, 891-898.

205. Given that the reactions take time to reach completion we confirmed that H_2O_2 is stable in pH 9.70 buffer at 25 ˚C for two hours.

206. S. Uchiyama, N. Kawai, A. P. de Silva and K. Iwai, *J. Am. Chem. Soc.*, 2004, **126**, 3032-3033.

207. The NOR gate is a combination OR gate followed by an inverter. Its output is "true" if both inputs are "false." Otherwise, the output is "false."

208. J. S. Beckman, T. W. Beckman, J. Chen, P. A. Marshall and B. A. Freeman, *P. Natl. Acad. Sci.*, 1990, **87**, 1620-1624.

209. P. Pacher, J. S. Beckman and L. Liaudet, *Physiol. Rev.*, 2007, **87**, 315-424.

210. K.-T. Lin, J.-Y. Xue, M. C. Lin, E. G. Spokas, F. F. Sun and P. Y.-K. Wong, *Am. J. Physiol - Cell. Ph.*, 1998, **274**, C855-C860.

211. A. G. Estévez, R. Radi, L. Barbeito, J. T. Shin, J. A. Thompson and J. S. Beckman, *J. Neurochem.*, 1995, **65**, 1543-1550.

212. C. Szabo, H. Ischiropoulos and R. Radi, *Nat. Rev. Drug. Discov.*, 2007, **6**, 662-680.

213. Michael J. Mihm and John A. Bauer, *Biochimie*, 2002, **84**, 1013-1019.

214. J. Li, J. Su, W. Li, W. Liu, B. T. Altura and B. M. Altura, *Neurosci. Lett.*, 2003, **350**, 173-177.

215. C. Szabó, A. L. Salzman and H. Ischiropoulos, *FEBS Lett.*, 1995, **372**, 229-232.

216. J. G. Mabley, L. Liaudet, P. Pacher, G. J. Southan, J. T. Groves, A. L. Salzman and C. Szabo, *Mol. Med.*, 2002, **8**, 581-590.

217. J. C. Niles, J. S. Wishnok and S. R. Tannenbaum, *Nitric Oxide*, 2006, **14**, 109-121.

218. S. Takizawa, Y. Aratani, N. Fukuyama, N. Maeda, H. Hirabayashi, H. Koyama, Y. Shinohara and H. Nakazawa, *J. Cerebr. Blood F. Met.*, 2002, **22**, 50-54.

219. F. Torreilles, S. d. Salman-Tabcheh, M.-C. Guérin and J. Torreilles, *Brain Res. Rev.*, 1999, **30**, 153-163.
220. M.-H. Zou, C. Shi and R. A. Cohen, *Diabetes*, 2002, **51**, 198-203.
221. H. Ischiropoulos and J. S. Beckman, *J. Clin. Invest.*, 2003, **111**, 163-169.
222. P. Sarchielli, F. Galli, A. Floridi, A. Floridi and V. Gallai, *Amino Acids*, 2003, **25**, 427-436.
223. N. Ito, U. T. Ruegg, A. Kudo, Y. Miyagoe-Suzuki and S. i. Takeda, *Nat. Med.*, 2013, **19**, 101-106.
224. D. Srikun, A. E. Albers, C. I. Nam, A. T. Iavarone and C. J. Chang, *J. Am . Chem. Soc.*, 2010, **132**, 4455-4465.
225. X. Sun, S. Y. Xu, S. E. Flower, J. S. Fossey, X. Qian and T. D. James, *Chem. Commun. (Camb.)*, 2013, **49**, 8311-8313.
226. Q. Xu, K.-A. Lee, S. Lee, K. M. Lee, W.-J. Lee and J. Yoon, *J. Am. Chem. Soc.*, 2013, **135**, 9944-9949.
227. S. Trupp, A. Schweitzer and G. J. Mohr, *Org. Biomol. Chem.*, 2006, **4**, 2965-2968.
228. S. Banerjee, E. B. Veale, C. M. Phelan, S. A. Murphy, G. M. Tocci, L. J. Gillespie, D. O. Frimannsson, J. M. Kelly and T. Gunnlaugsson, *Chem. Soc. Rev.*, 2013, **42**, 1601-1618.
229. R. M. Duke, E. B. Veale, F. M. Pfeffer, P. E. Kruger and T. Gunnlaugsson, *Chem. Soc. Rev.*, 2010, **39**, 3936-3953.
230. X. Qian, Y. Xiao, Y. Xu, X. Guo, J. Qian and W. Zhu, *Chem. Commun.*, 2010, **46**, 6418-6436.
231. X. Wu, Z. Li, X. X. Chen, J. S. Fossey, T. D. James and Y. B. Jiang, *Chem. Soc. Rev.*, 2013, **42**, 8032-8048.
232. M. Pekarova, L. Kubala, H. Martiskova, L. Bino, M. Twarogova, A. Klinke, T. K. Rudolph, Z. Kuchtova, H. Kolarova, G. Ambrozova, R. Kuchta, J. Kadlec and A. Lojek, *Eur. J. Pharmacol.*, 2013, **713**, 68-77.
233. S. Pfeiffer, A. Lass, K. Schmidt and B. Mayer, *FASEB J.*, 2001, **15**, 2355-2364.
234. J. C. Sullivan and J. S. Pollock, *Circ. Res.*, 2006, **98**, 717-719.
235. L. Zhu, S. H. Shabbir, M. Gray, V. M. Lynch, S. Sorey and E. V. Anslyn, *J. Am. Chem. Soc.*, 2006, **128**, 1222-1232.
236. J. W. Tomsho and S. J. Benkovic, *J. Org. Chem.*, 2012, **77**, 2098-2106.
237. M. Dowlut and D. G. Hall, *J. Am. Chem. Soc.*, 2006, **128**, 4226-4227.
238. M. Berube, M. Dowlut and D. G. Hall, *J. Org. Chem.*, 2008, **73**, 6471-6479.
239. Square Wave Voltammetry (SWV) only the homogeneous effects were evaluated as the electrode was polished before each scan.

240. A. Adamczyk-Wozniak, K. M. Borys, I. D. Madura, A. Pawelko, E. Tomecka and K. Zukowski, *New J. Chem.*, 2013, **37**, 188-194.
241. M. Bérubé, M. Dowlut and D. G. Hall, *J. Org. Chem.*, 2008, **73**, 6471-6479.
242. M. Dowlut and D. G. Hall, *J. Am. Chem. Soc.*, 2006, **128**, 4226-4227.
243. A. Sikora, J. Zielonka, M. Lopez, J. Joseph and B. Kalyanaraman, *Free Radical Bio. Med.*, 2009, **47**, 1401-1407.
244. J. Zielonka, A. Sikora, M. Hardy, J. Joseph, B. P. Dranka and B. Kalyanaraman, *Chem. Res. Toxicol*, 2012, **25**, 1793-1799.
245. A. P. de Silva, H. Q. N. Gunaratne, T. Gunnlaugsson, A. J. M. Huxley, C. P. McCoy, J. T. Rademacher and T. E. Rice, *Chem. Rev.*, 1997, **97**, 1515-1566.
246. Z. Xu, S. K. Kim, S. J. Han, C. Lee, G. Kociok-Kohn, T. D. James and J. Yoon, *Eur. J. Org. Chem.*, 2009, **2009**, 3058-3065.
247. Y. Kubo, M. Yamamoto, M. Ikeda, M. Takeuchi, S. Shinkai, S. Yamaguchi and K. Tamao, *Angew. Chemie. Int. Ed.*, 2003, **42**, 2036-2040.
248. Y.-H. Li, L. Zhang, J. Huang, R.-P. Liang and J.-D. Qiu, *Chem. Commun.*, 2013, **49**, 5180-5182.
249. Z.-b. Qu, X. Zhou, L. Gu, R. Lan, D. Sun, D. Yu and G. Shi, *Chem. Commun.*, 2013, **49**, 9830-9832.
250. B. Mu, T. P. McNicholas, J. Zhang, A. J. Hilmer, Z. Jin, N. F. Reuel, J.-H. Kim, K. Yum and M. S. Strano, *J. Am. Chem. Soc.*, 2012, **134**, 17620-17627.
251. K. Yum, J.-H. Ahn, T. P. McNicholas, P. W. Barone, B. Mu, J.-H. Kim, R. M. Jain and M. S. Strano, *ACS Nano*, 2011, **6**, 819-830.
252. K. S. Novoselov, A. K. Geim, S. V. Morozov, D. Jiang, Y. Zhang, S. V. Dubonos, I. V. Grigorieva and A. A. Firsov, *Science*, 2004, **306**, 666-669.
253. K.-H. Liao, Y.-S. Lin, C. W. Macosko and C. L. Haynes, *ACS Appl. Mater. Interfaces*, 2011, **3**, 2607-2615.
254. J. Kim, L. J. Cote, F. Kim and J. Huang, *J. Am. Chem. Soc.*, 2010, **132**, 260-267.
255. E. Morales-Narváez and A. Merkoçi, *Adv. Mater.*, 2012, **24**, 3298-3308.
256. P. R. Selvin, *Nat. Struct. Biol.*, 2000, **7**, 730-734.
257. S. Stankovich, D. A. Dikin, G. H. B. Dommett, K. M. Kohlhaas, E. J. Zimney, E. A. Stach, R. D. Piner, S. T. Nguyen and R. S. Ruoff, *Nature*, 2006, **442**, 282-286.
258. A. K. Geim and K. S. Novoselov, *Nat. Mater.*, 2007, **6**, 183-191.
259. A. K. Geim, *Science*, 2009, **324**, 1530-1534.
260. J. H. Jung, D. S. Cheon, F. Liu, K. B. Lee and T. S. Seo, *Angew. Chemie. Int. Ed.*, 2010, **49**, 5708-5711.

261. L. Wang, K.-Y. Pu, J. Li, X. Qi, H. Li, H. Zhang, C. Fan and B. Liu, *Adv. Mater.*, 2011, **23**, 4386-4391.
262. Y. Liu, X. Dong and P. Chen, *Chem. Soc. Rev.*, 2012, **41**, 2283-2307.
263. L. Feng, L. Wu and X. Qu, *Adv. Mater.*, 2013, **25**, 168-186.
264. Z. Li, S. S. Deng, Y. Zang, Z. Gu, X. P. He, G. R. Chen, K. Chen, T. D. James, J. Li and Y. T. Long, *Sci. Rep.*, 2013, **3**, 2293.
265. H.-L. Zhang, X.-L. Wei, Y. Zang, J.-Y. Cao, S. Liu, X.-P. He, Q. Chen, Y.-T. Long, J. Li, G.-R. Chen and K. Chen, *Adv. Mater. (Weinheim, Ger.)*, 2013, **25**, 4097-4101.
266. F. Li, H. Pei, L. Wang, J. Lu, J. Gao, B. Jiang, X. Zhao and C. Fan, *Adv. Funct. Mater.*, 2013, **23**, 4140-4148.
267. S. A. Elfeky, S. E. Flower, N. Masumoto, F. D'Hooge, L. Labarthe, W. Chen, C. Len, T. D. James and J. S. Fossey, *Chem. Asian J.*, 2010, **5**, 581-588.
268. A. Stephenson-Brown, H.-C. Wang, P. Iqbal, J. A. Preece, Y. Long, J. S. Fossey, T. D. James and P. M. Mendes, *Analyst*, 2013, **138**, 7140-7145.
269. H.-C. Wang, H. Zhou, B. Chen, P. M. Mendes, J. S. Fossey, T. D. James and Y.-T. Long, *Analyst*, 2013, **138**, 7146-7151.
270. S. K. Powers, E. E. Talbert and P. J. Adhihetty, *J. Physiol.*, 2011, **589**, 2129-2138.
271. A. B. Knott and E. Bossy-Wetzel, *Antioxid. Redox Signaling*, 2009, **11**, 541-553.
272. B. K. Kemp-Harper, *Antioxid. Redox Signaling*, 2011, **14**, 1609-1613.
273. M. H. Lim and S. J. Lippard, *Acc. Chem. Res.*, 2006, **40**, 41-51.
274. X. Zhang, W.-S. Kim, N. Hatcher, K. Potgieter, L. L. Moroz, R. Gillette and J. V. Sweedler, *J. Biol. Chem.*, 2002, **277**, 48472-48478.
275. X. Ye, S. S. Rubakhin and J. V. Sweedler, *J. Neurosci. Methods*, 2008, **168**, 373-382.
276. J.-Y. Chatton and M.-C. Broillet, in *Meth. Enzymol.*, ed. L. P. Enrique Cadenas, Academic Press, 2002, vol. Volume 359, pp. 134-148.
277. U.-P. Apfel, D. Buccella, J. J. Wilson and S. J. Lippard, *Inorg. Chem.*, 2013, **52**, 3285-3294.
278. S. A. Hilderbrand and S. J. Lippard, *Abstr. Pap. Am. Chem. S.*, 2003, **225**, U160-U160.
279. B. Mondal, P. Kumar, P. Ghosh and A. Kalita, *Chem. Commun.*, 2011, **47**, 2964-2966.
280. Y. Chen, W. Guo, Z. Ye, G. Wang and J. Yuan, *Chem. Commun.*, 2011, **47**, 6266-6268.
281. J. A. Reisz, E. B. Klorig, M. W. Wright and S. B. King, *Org. Lett.*, 2009, **11**, 2719-2721.
282. P. R. C. Aleksandr Petrovich Demchenko, *Springer Ser. Fluoresc.*, 2010, **8**, 389.
283. J. A. Reisz, E. Bechtold and S. B. King, *Dalton Trans.*, 2010, **39**, 5203-5212.
284. P. J. Farmer and F. Sulc, *J. Org. Chem.*, 2005, **99**, 166-184.
285. C. M. Maragos, D. Morley, D. A. Wink, T. M. Dunams, J. E. Saavedra, A. Hoffman, A. A. Bove, L. Isaac, J. A. Hrabie and L. K. Keefer, *J. Med. Chem.*, 1991, **34**, 3242-3247.

286. K. M. Miranda, A. S. Dutton, L. A. Ridnour, C. A. Foreman, E. Ford, N. Paolocci, T. Katori, C. G. Tocchetti, D. Mancardi, D. D. Thomas, M. G. Espey, K. N. Houk, J. M. Fukuto and D. A. Wink, *J. Am. Chem. Soc.*, 2004, **127**, 722-731.

287. M. D. Bartberger, J. M. Fukuto and K. N. Houk, *Proc. Natl. Acad. Sci.*, 2001, **98**, 2194-2198.

288. D. D. Perrin and B. Dempsey, in *Chapman and Hall: London*, 1974.

289. Y. Liu and Q. Feng, *Differentiation*, 2012, **84**, 54-61.

290. C. Amatore, S. Arbault, C. Ducrocq, S. Hu and I. Tapsoba, *ChemMedChem*, 2007, **2**, 898-903.

291. S. B. King and H. T. Nagasawa, *Nitric Oxide, Pt C*, 1999, **301**, 211-220.

292. M. D. Phillips, (2005), *Synthetic strategies in the design and construction of saccharide selective fluorescent sensors / Marcus Damian Phillips*, PhD thesis, University of bath.

293. W. C. Silvers, B. Prasai, D. H. Burk, M. L. Brown and R. L. McCarley, *J. Am. Chem. Soc.*, 2012, **135**, 309-314.

294. I. Perillo, M. C. Caterina, J. López and A. Salerno, *Synthesis*, 2004, **2004**, 851-856.

295. M. Mor, A. Lodola, S. Rivara, F. Vacondio, A. Duranti, A. Tontini, S. Sanchini, G. Piersanti, J. R. Clapper, A. R. King, G. Tarzia and D. Piomelli, *J. Med. Chem.*, 2008, **51**, 3487-3498.

10. APPENDICES

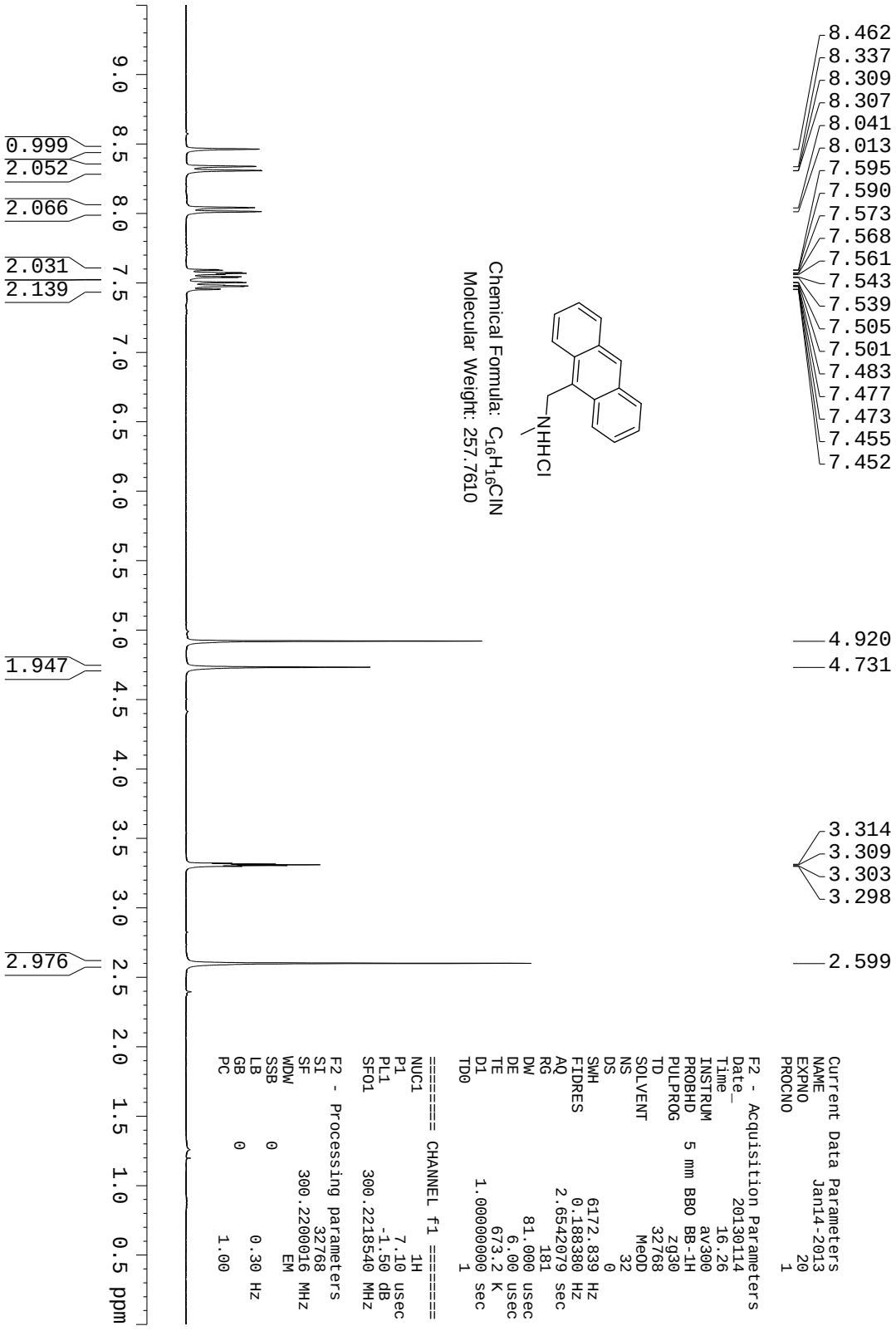

Figure 91. *[1]H NMR for compound **121** in MeOD.*

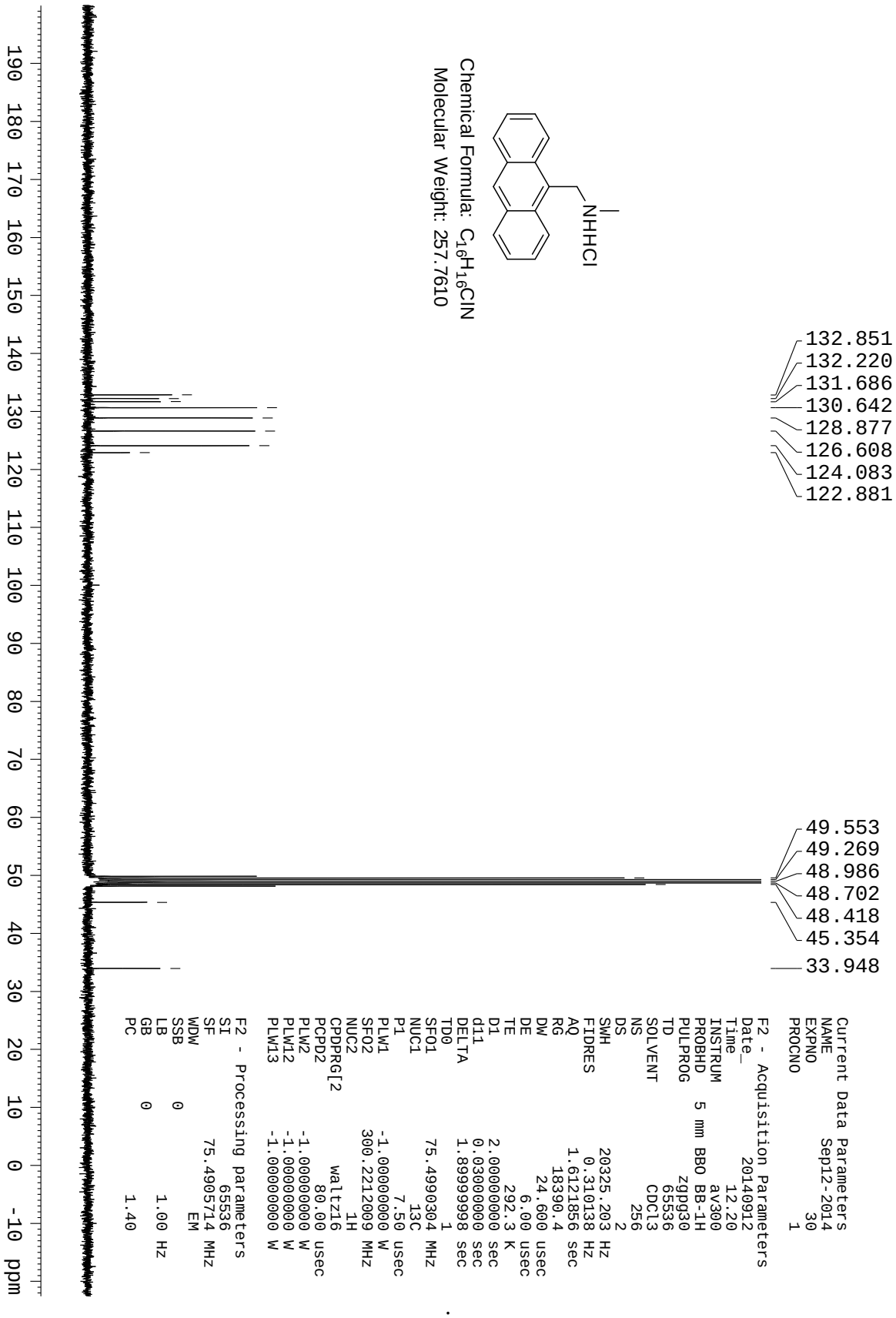

Figure 92. *^{13}C NMR for compound **121** in MeOD.*

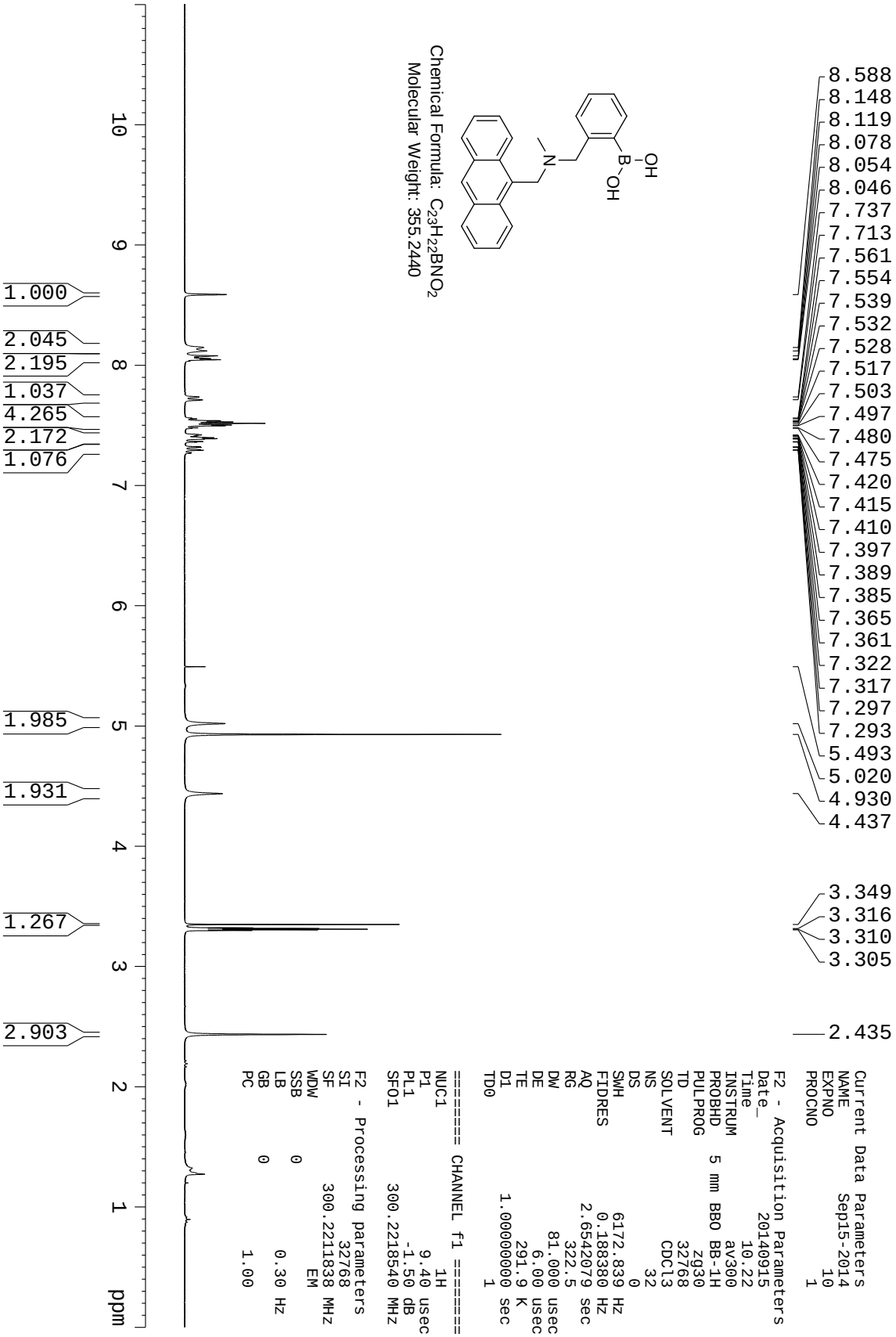

Figure 93. *^{1}H NMR for compound **100** in MeOD.*

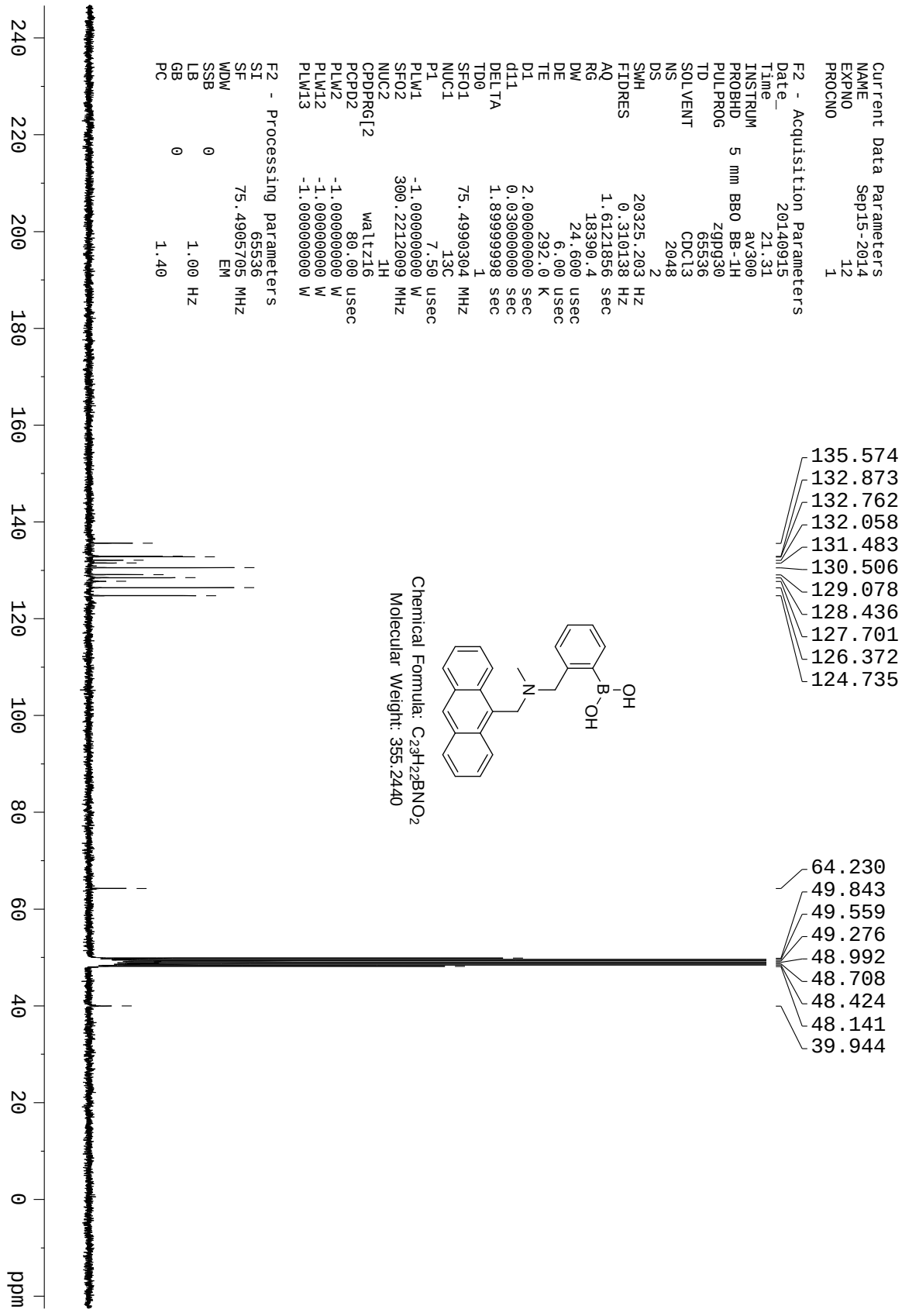

Figure 94. *^{13}C NMR for compound **100** in MeOD.*

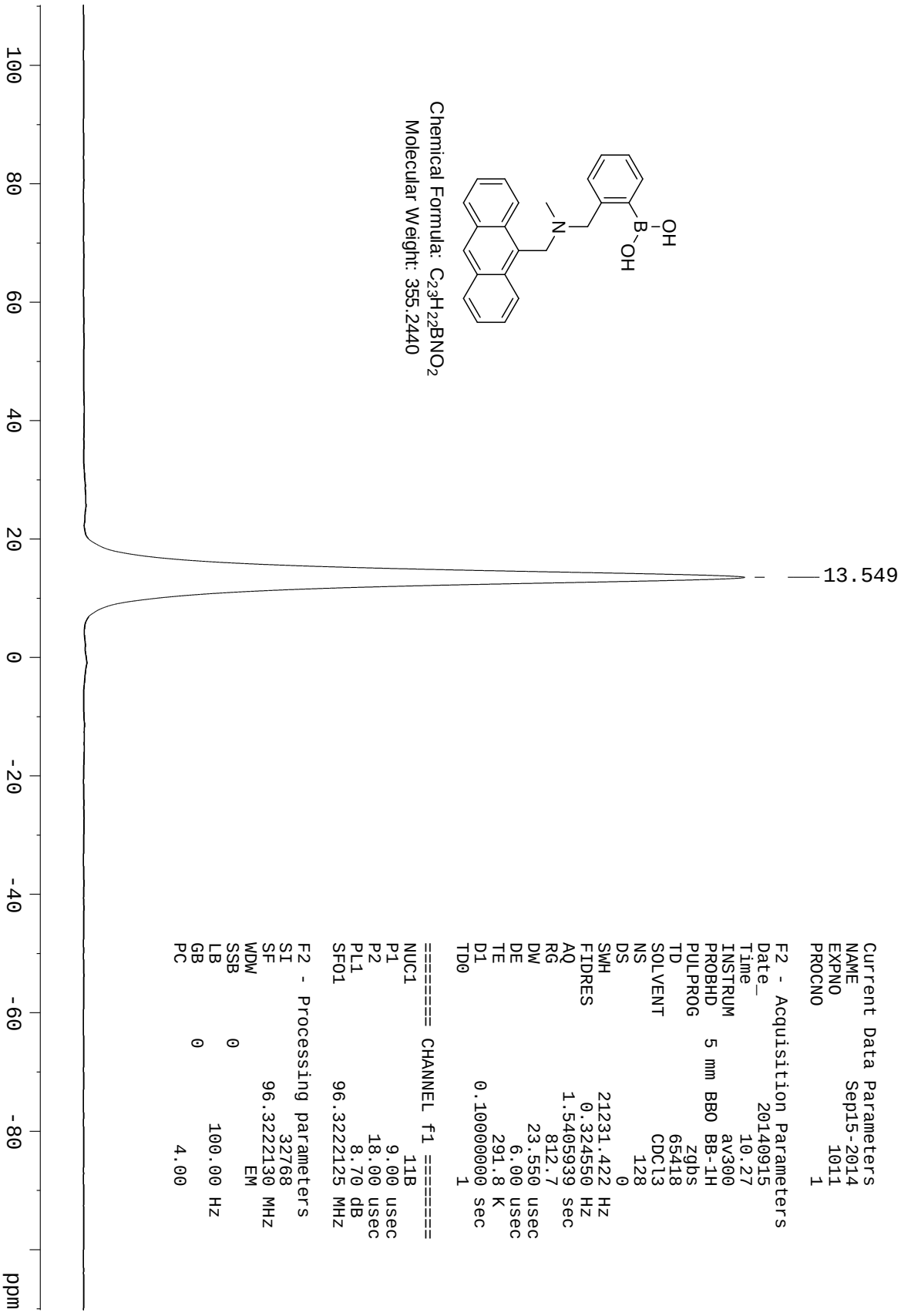

Figure 95. *[11]B NMR for compound **100** in MeOD.*

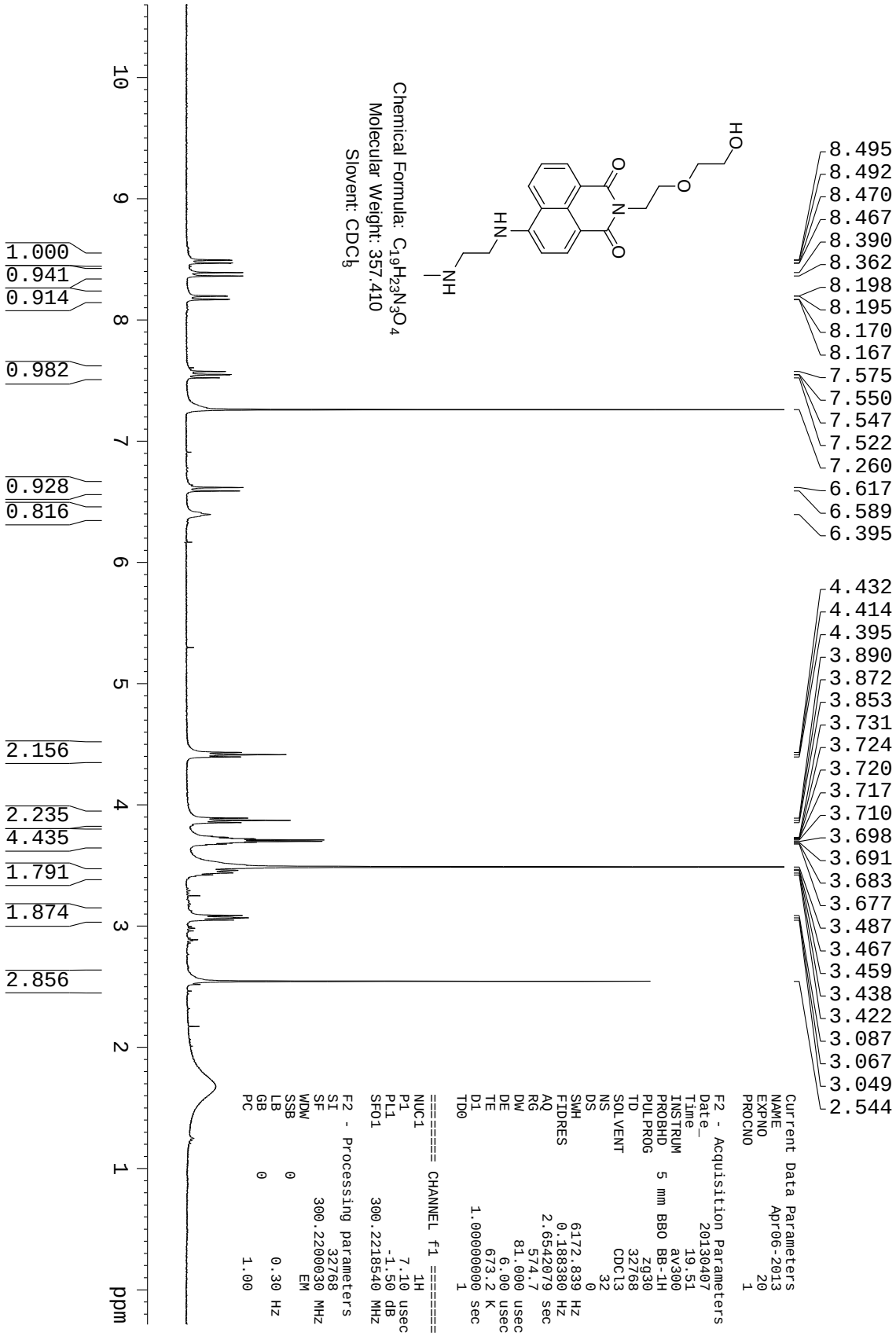

Figure 96. *^{1}H NMR for compound **122** in $CDCl_3$.*

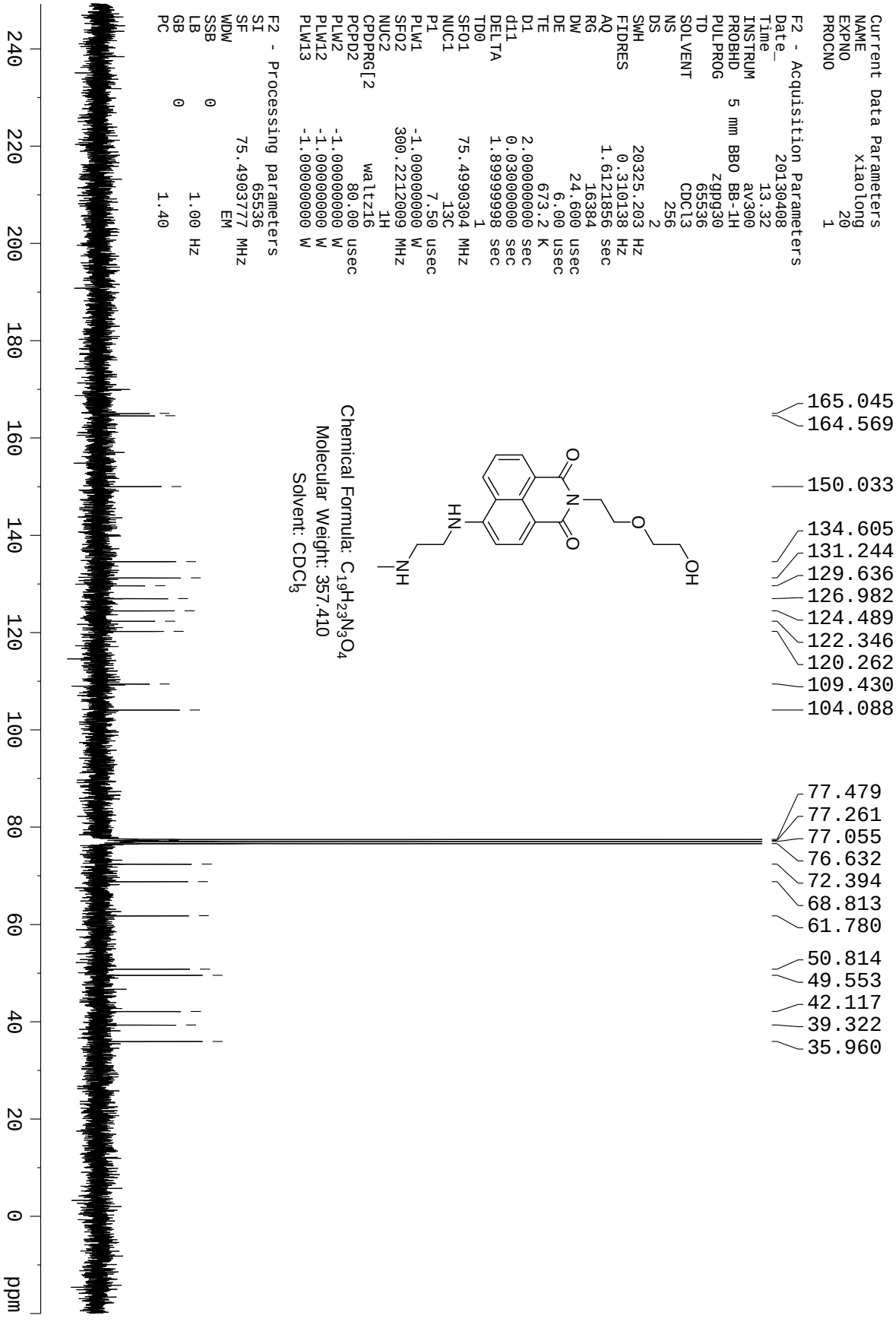

Figure 97. *^{13}C NMR for compound **122** in $CDCl_3$*

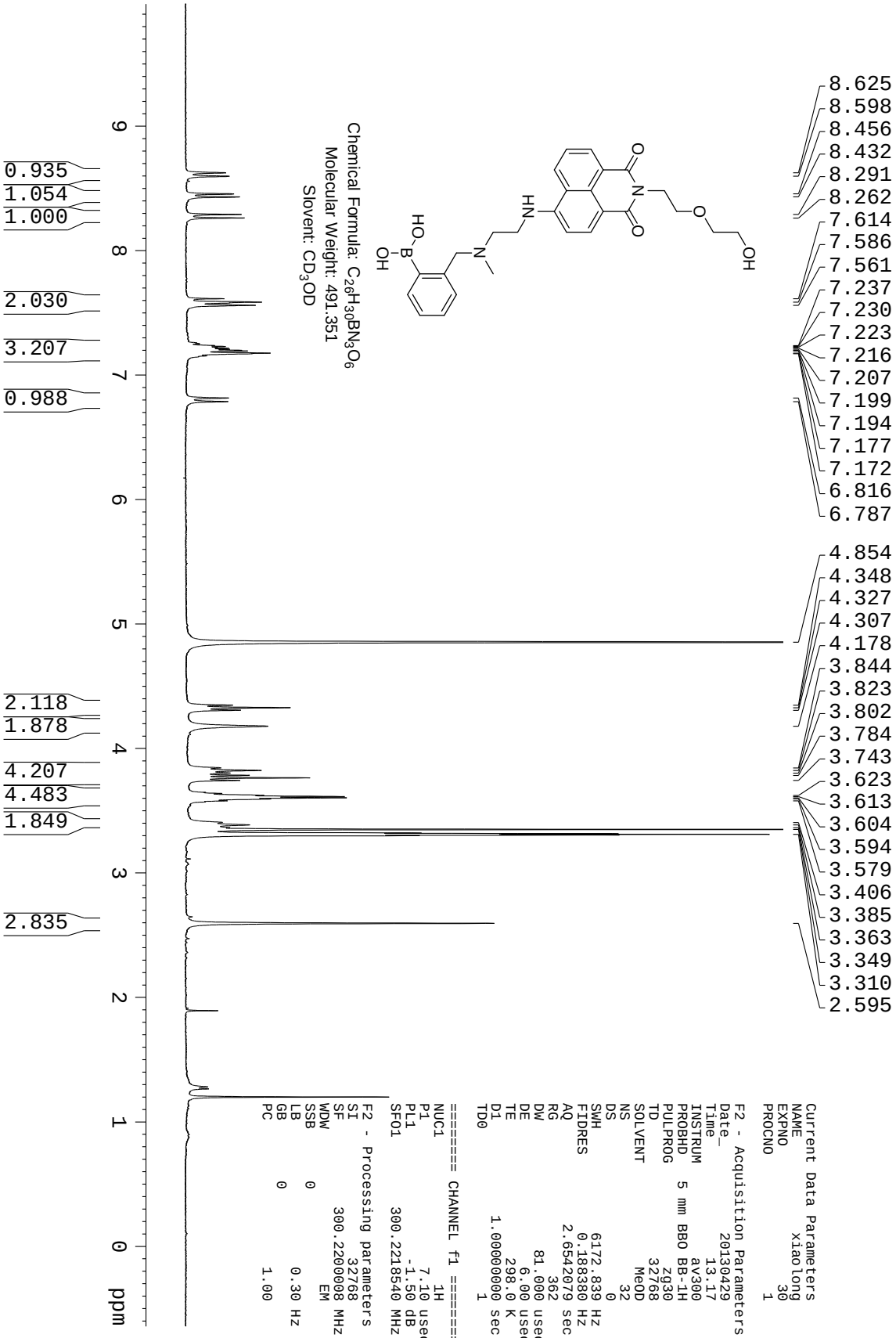

Figure 98. *^{1}H NMR for compound **101** in MeOD.*

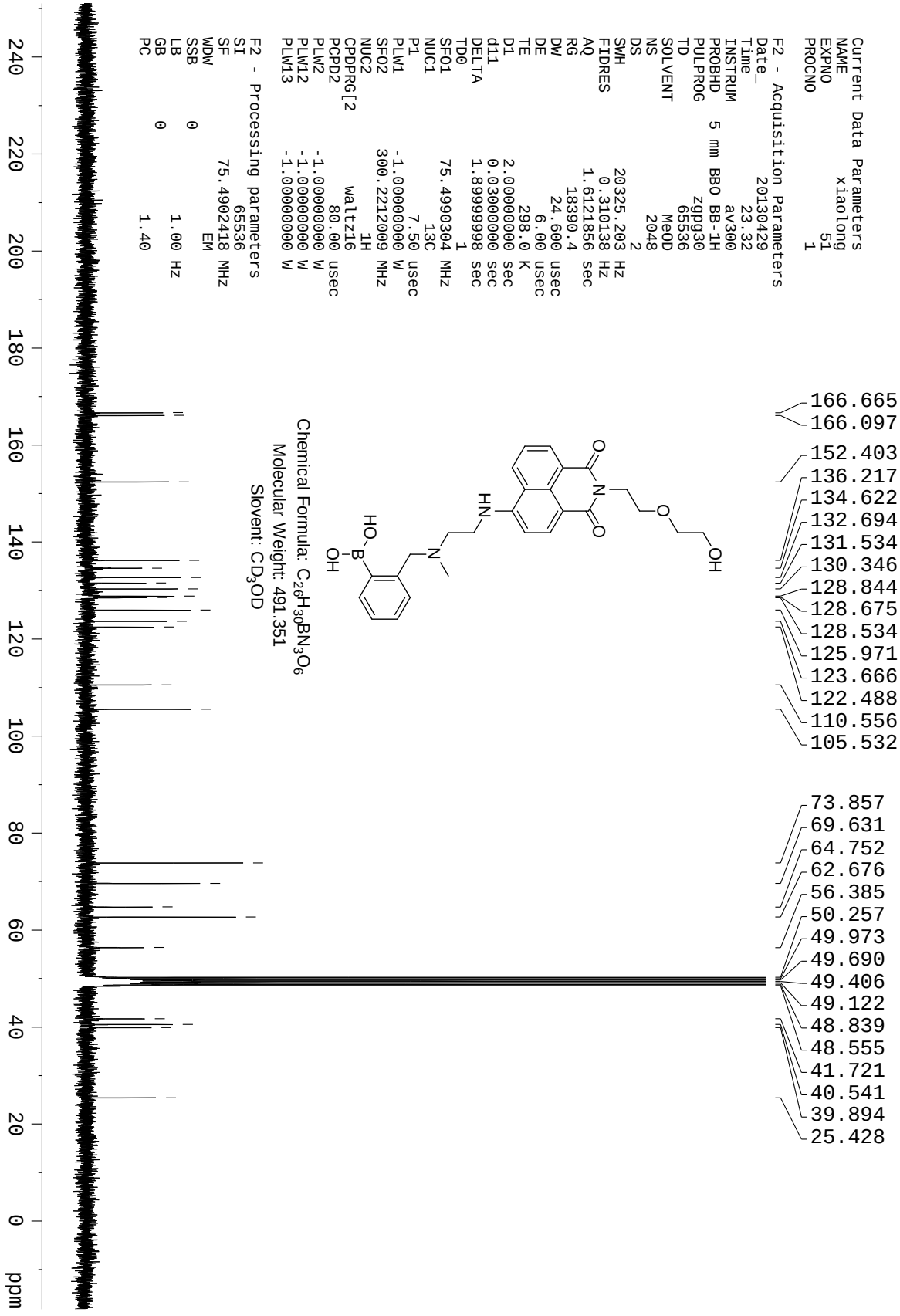

Figure 99. *^{13}C NMR for compound **101** in MeOD.*

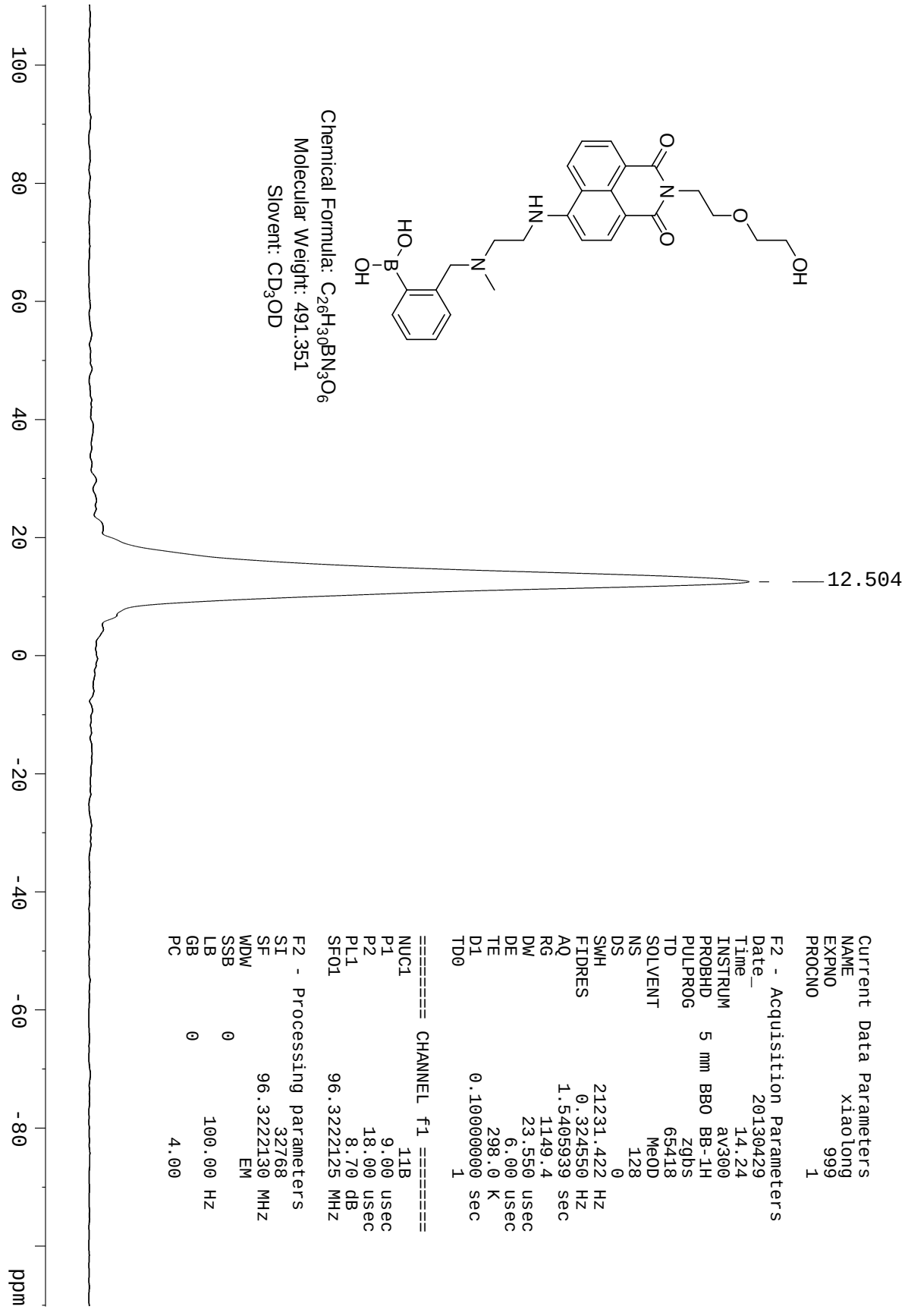

Figure 100. *^{11}B NMR for compound **101** in MeOD.*

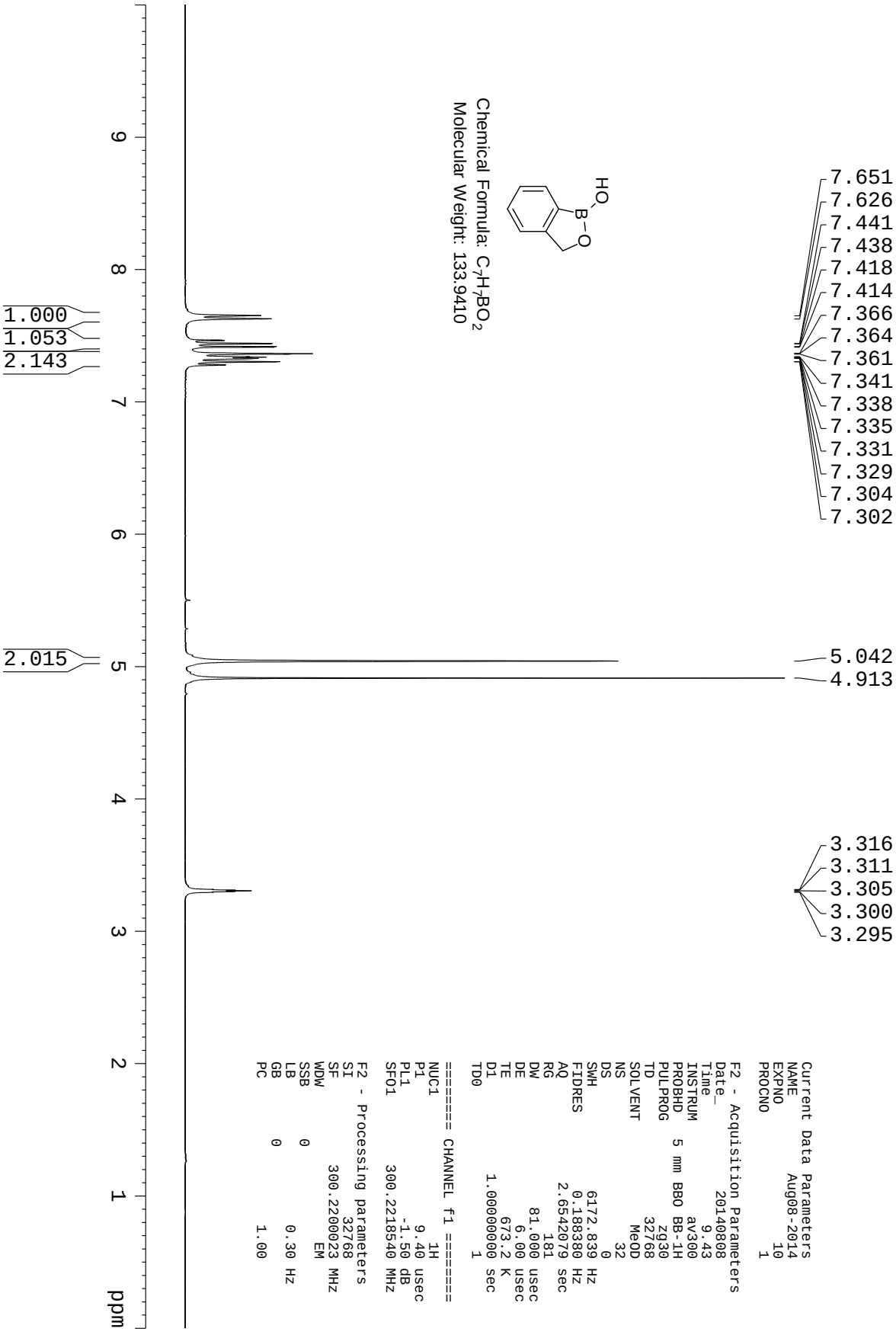

Figure 101. *^{1}H NMR for compound benzoboroxole **104** in MeOD.*

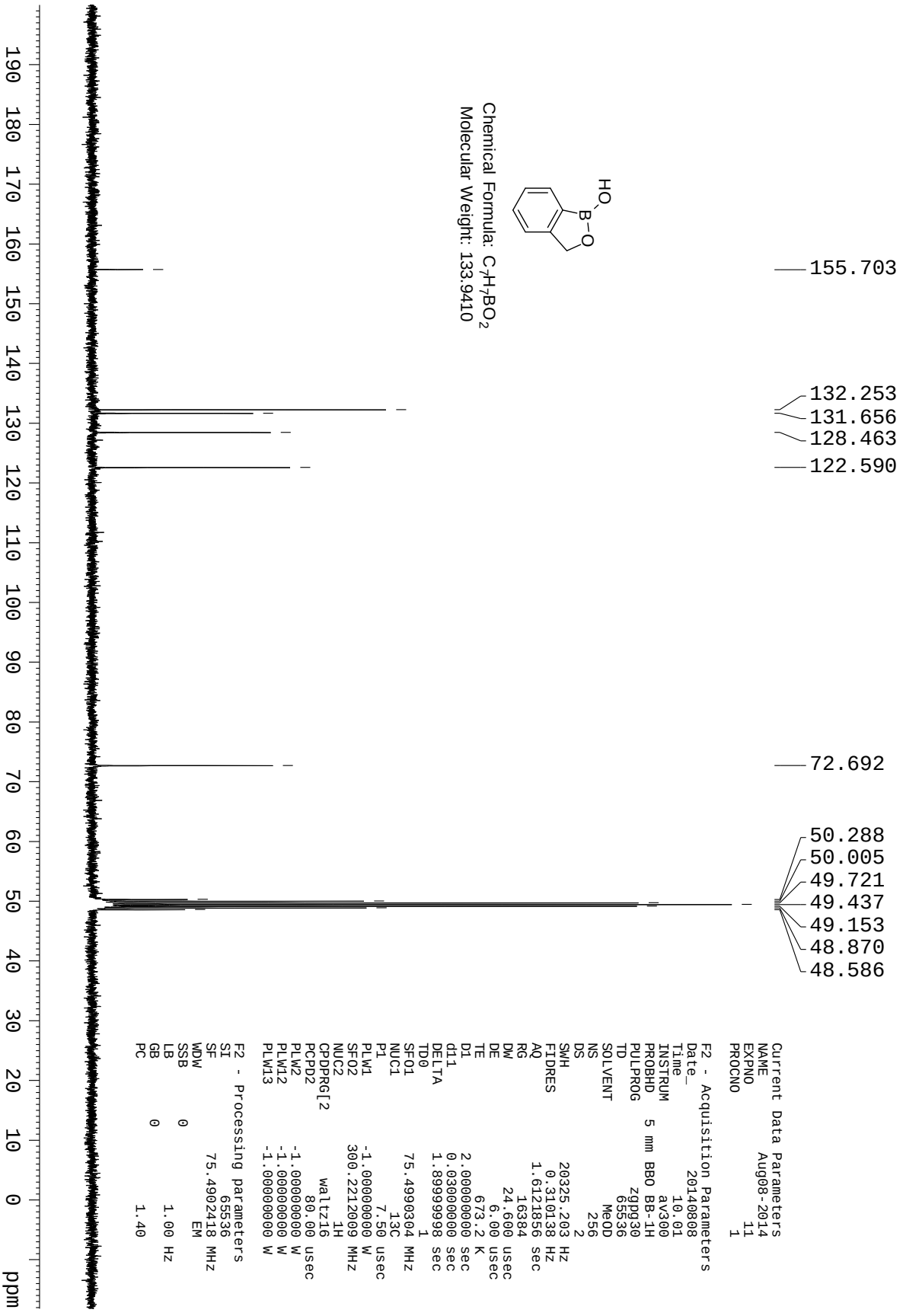

Figure 102. *^{13}C NMR for compound benzoboroxole in MeOD.*

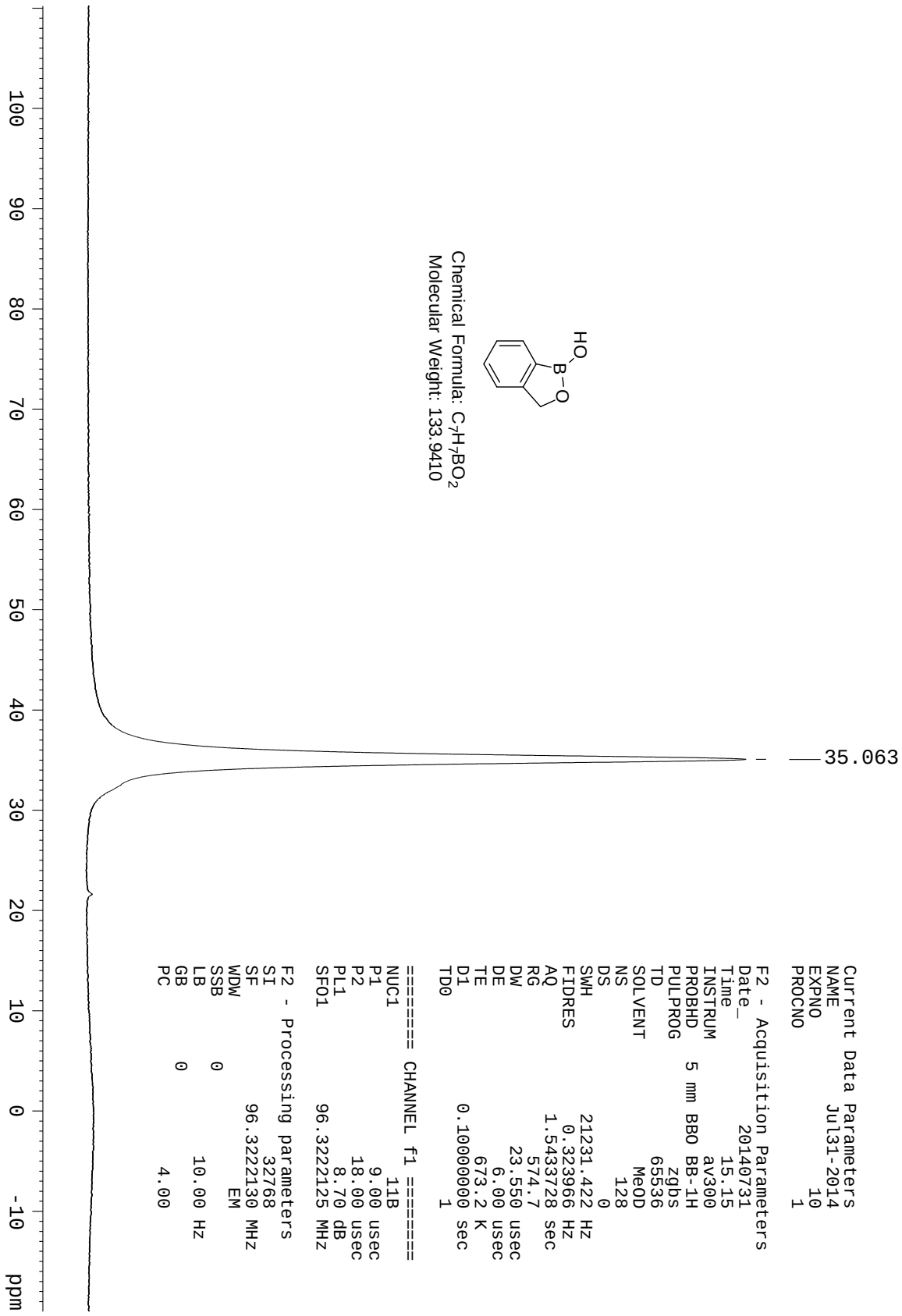

Figure 103. *^{11}B NMR for compound benzoboroxole in MeOD*

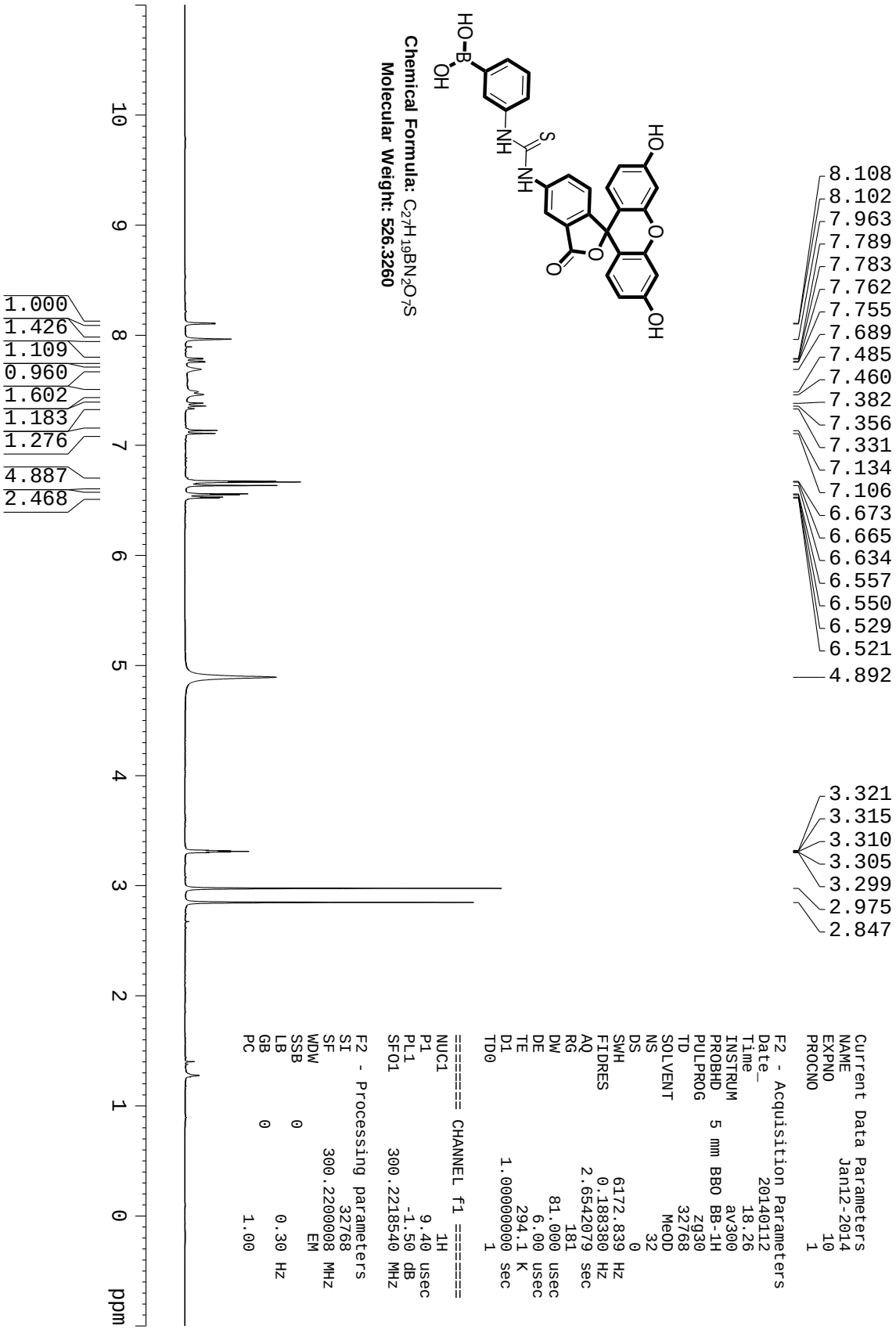

Figure 104. *[1]H NMR for compound **108** in MeOD*

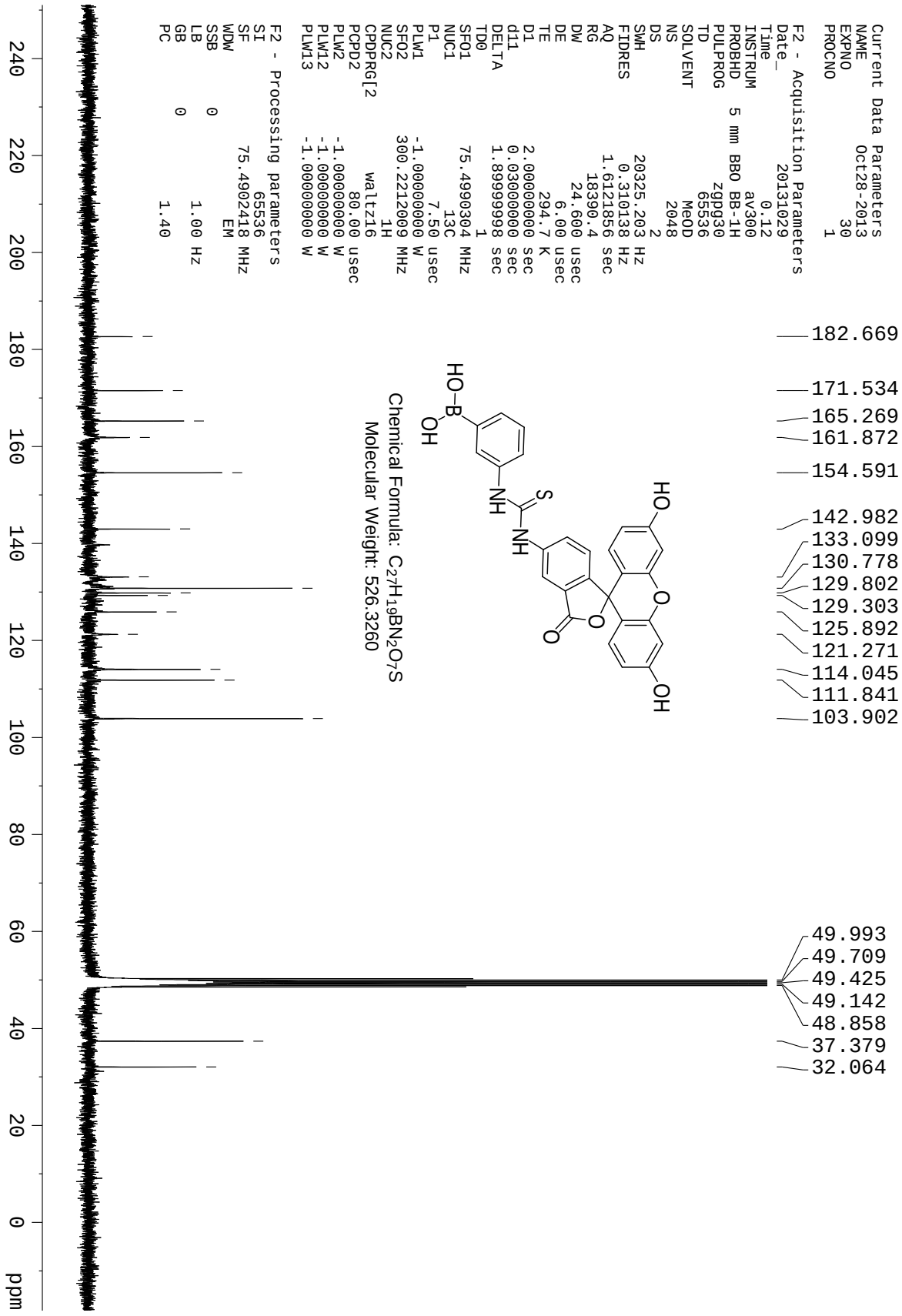

Figure 105. *[1]H NMR for compound **108** in MeOD*

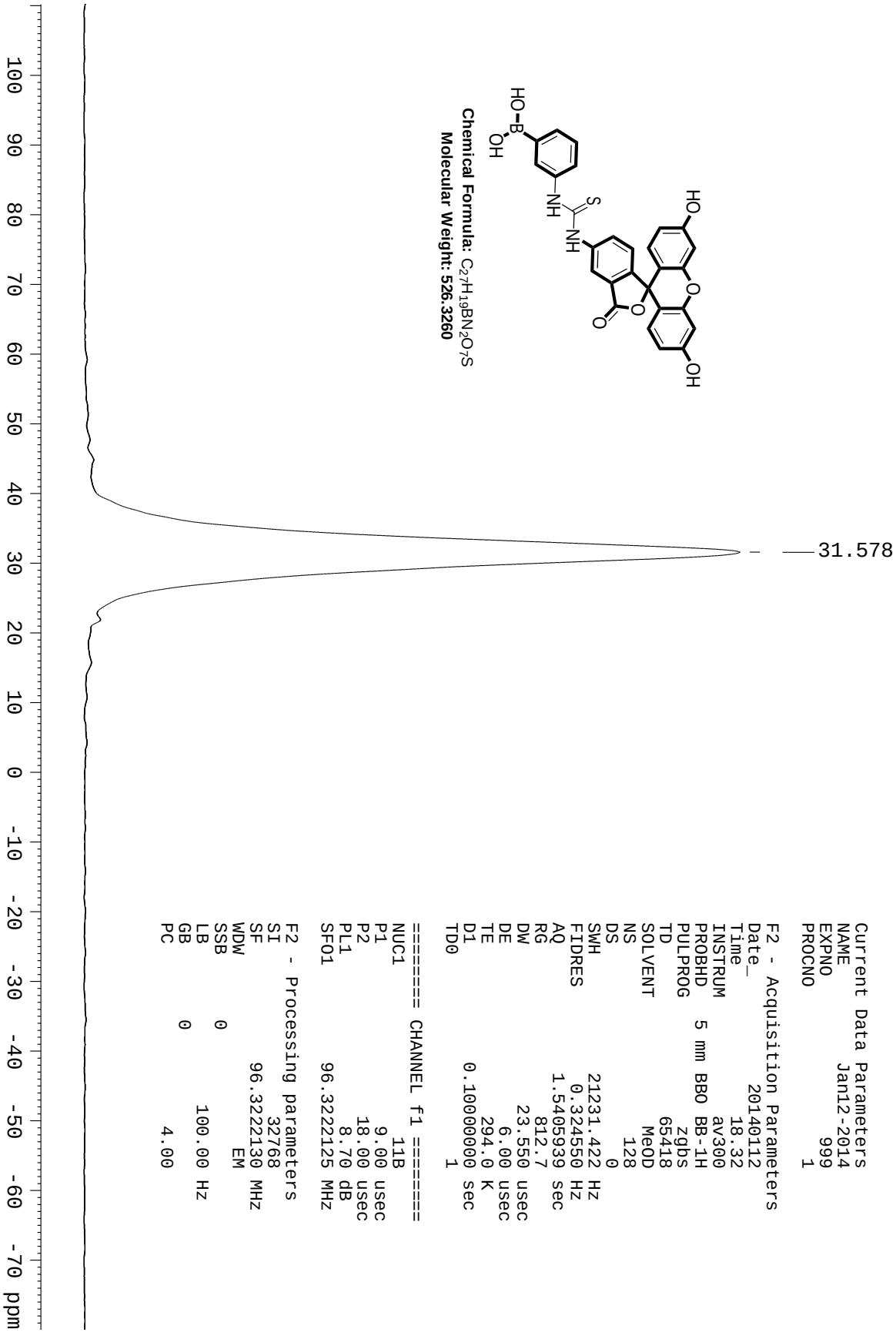


```
Current Data Parameters
NAME                  Jan12-2014
EXPNO                        999
PROCNO                         1

F2 - Acquisition Parameters
Date_                   20140112
Time                       18.32
INSTRUM                    av300
PROBHD     5 mm BBO BB-1H
PULPROG                     zgbs
TD                         65418
SOLVENT                     MeOD
NS                           128
DS                             0
SWH                    21231.422 Hz
FIDRES                  0.324550 Hz
AQ                      1.5405939 sec
RG                         812.7
DW                        23.550 usec
DE                         6.00 usec
TE                        294.0 K
D1                     0.10000000 sec
TD0                            1

======== CHANNEL f1 ========
NUC1                         11B
P1                          9.00 usec
P2                         18.00 usec
PL1                         8.70 dB
SFO1                   96.3222125 MHz

F2 - Processing parameters
SI                         32768
SF                     96.3222130 MHz
WDW                           EM
SSB                            0
LB                        100.00 Hz
GB                             0
PC                          4.00
```

Figure 106. *^{11}B NMR for compound **108** in MeOD*

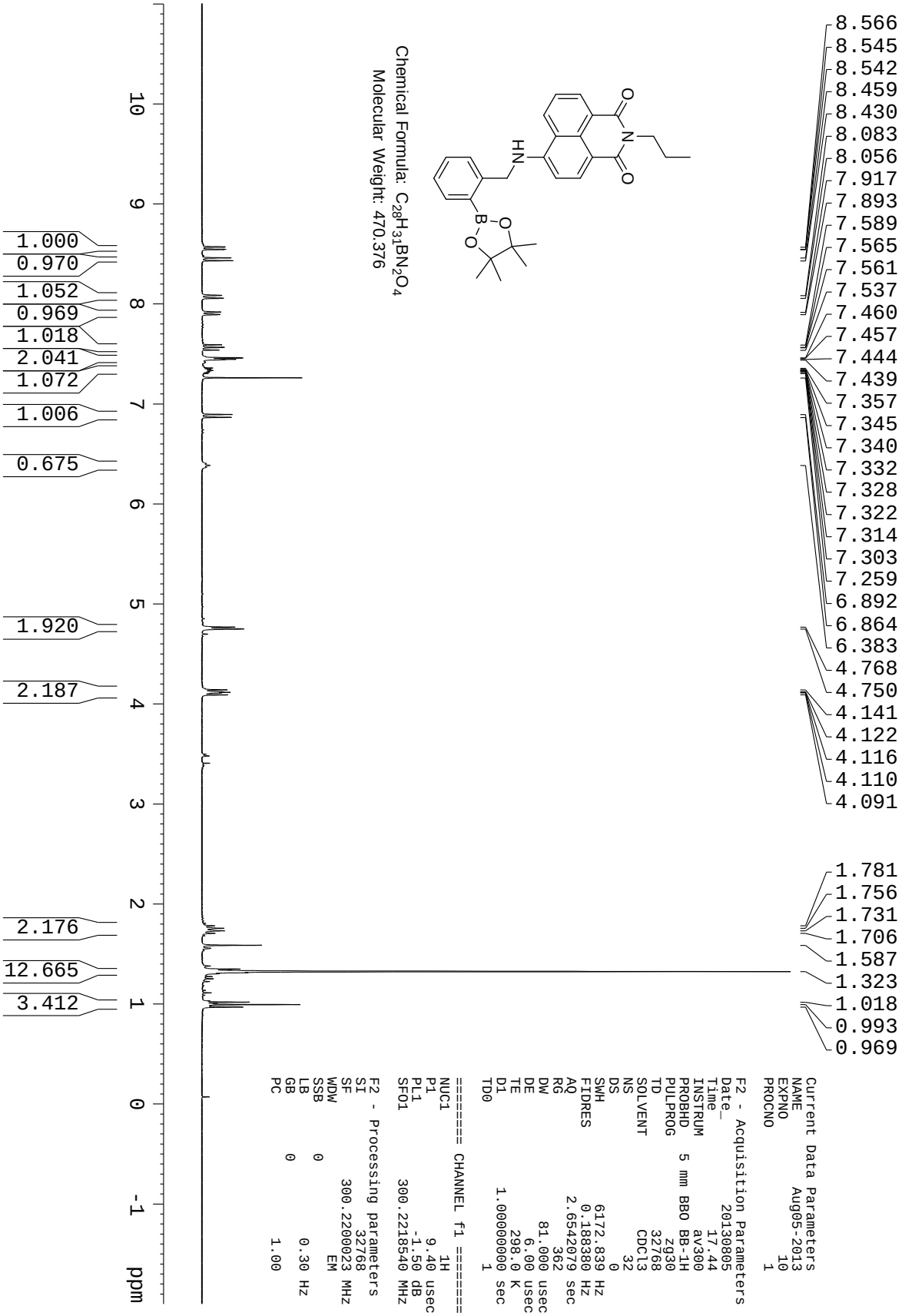

Figure 107. *^{1}H NMR for compound **123** in $CDCl_3$*

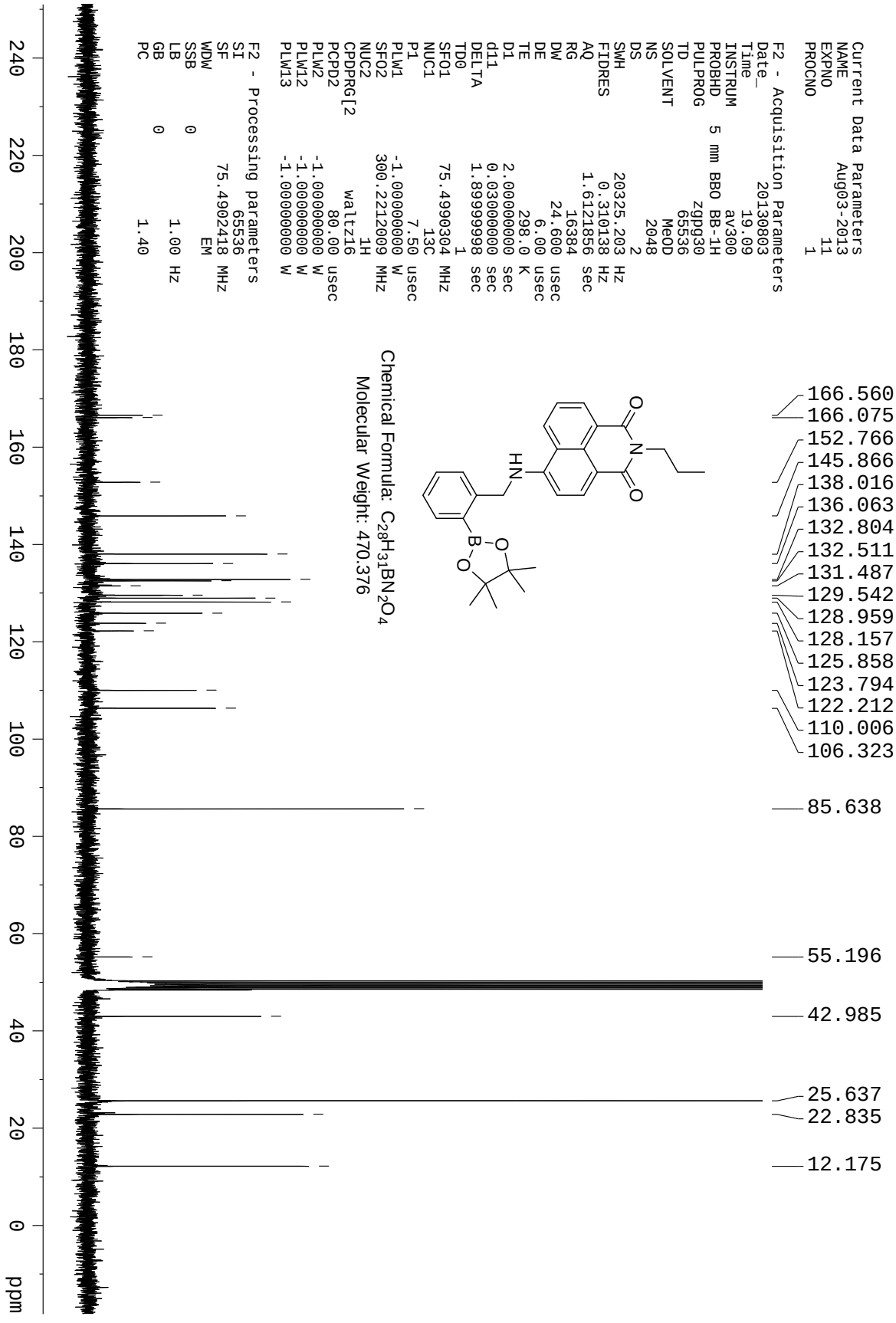

Figure 108. *^{13}C NMR for compound **124** in MeOD*

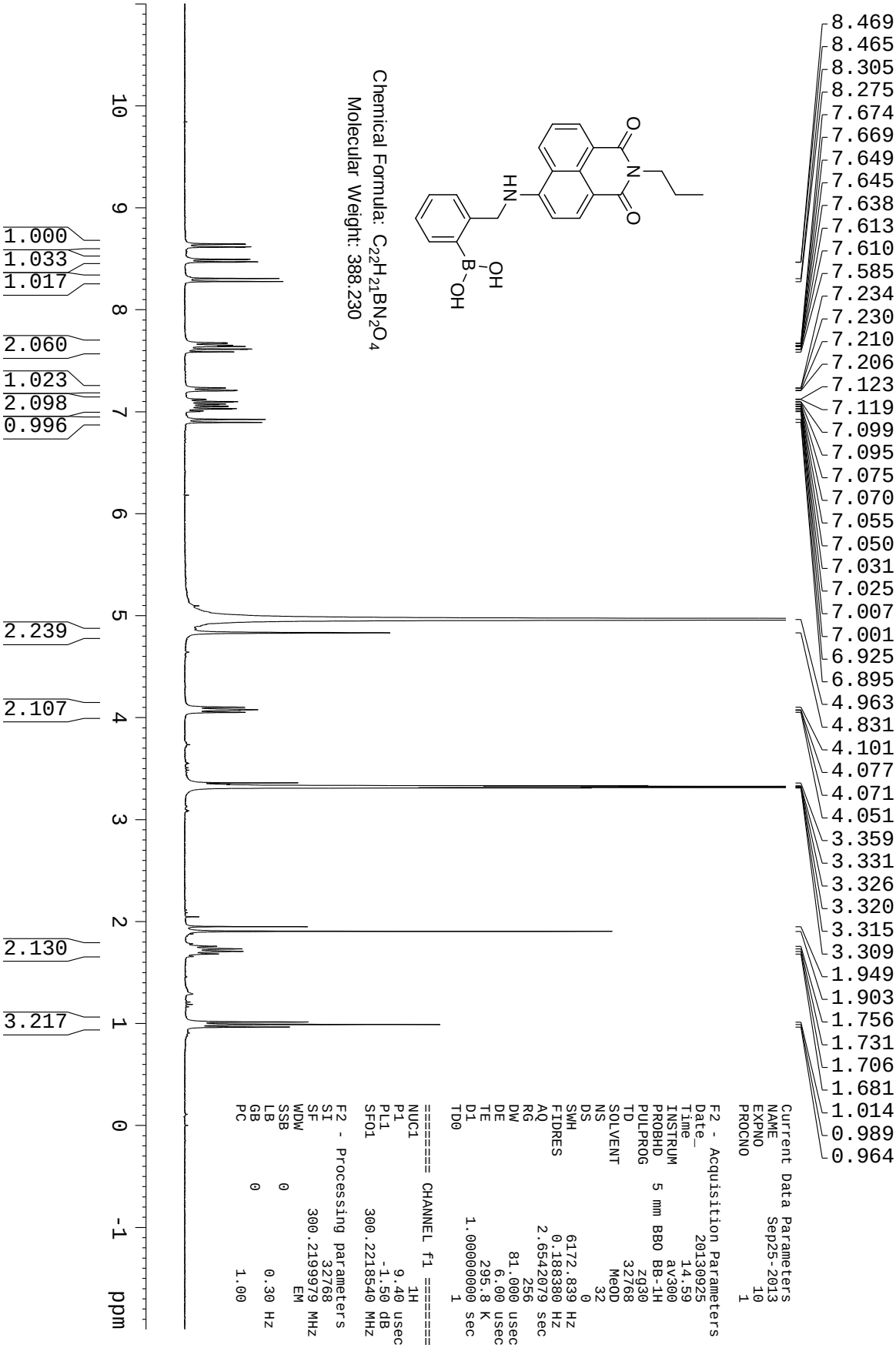

Figure 109. *^{1}H NMR for compound **102b** in MeOD*

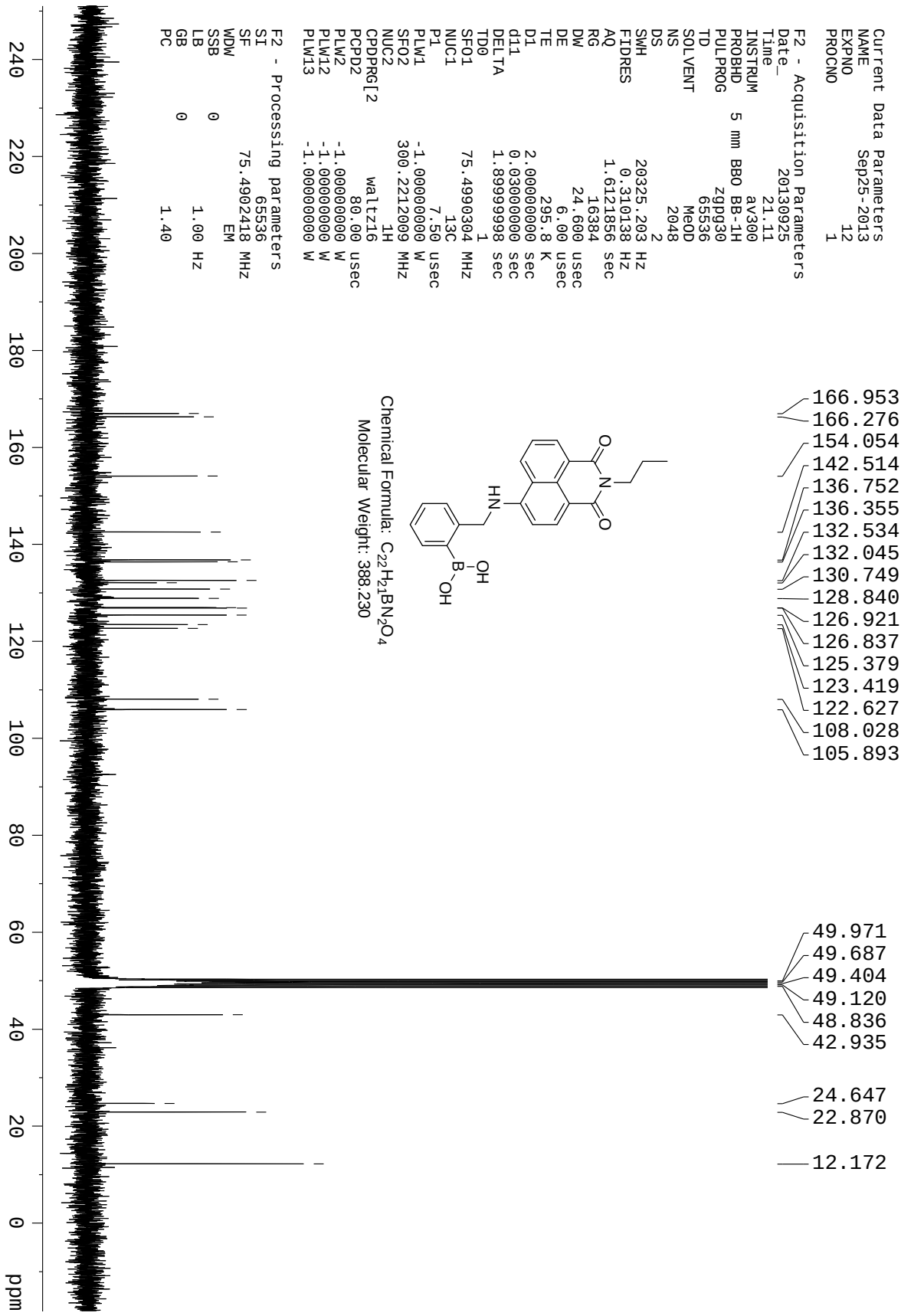

Figure 110. *^{13}C NMR for compound **102b** in MeOD*

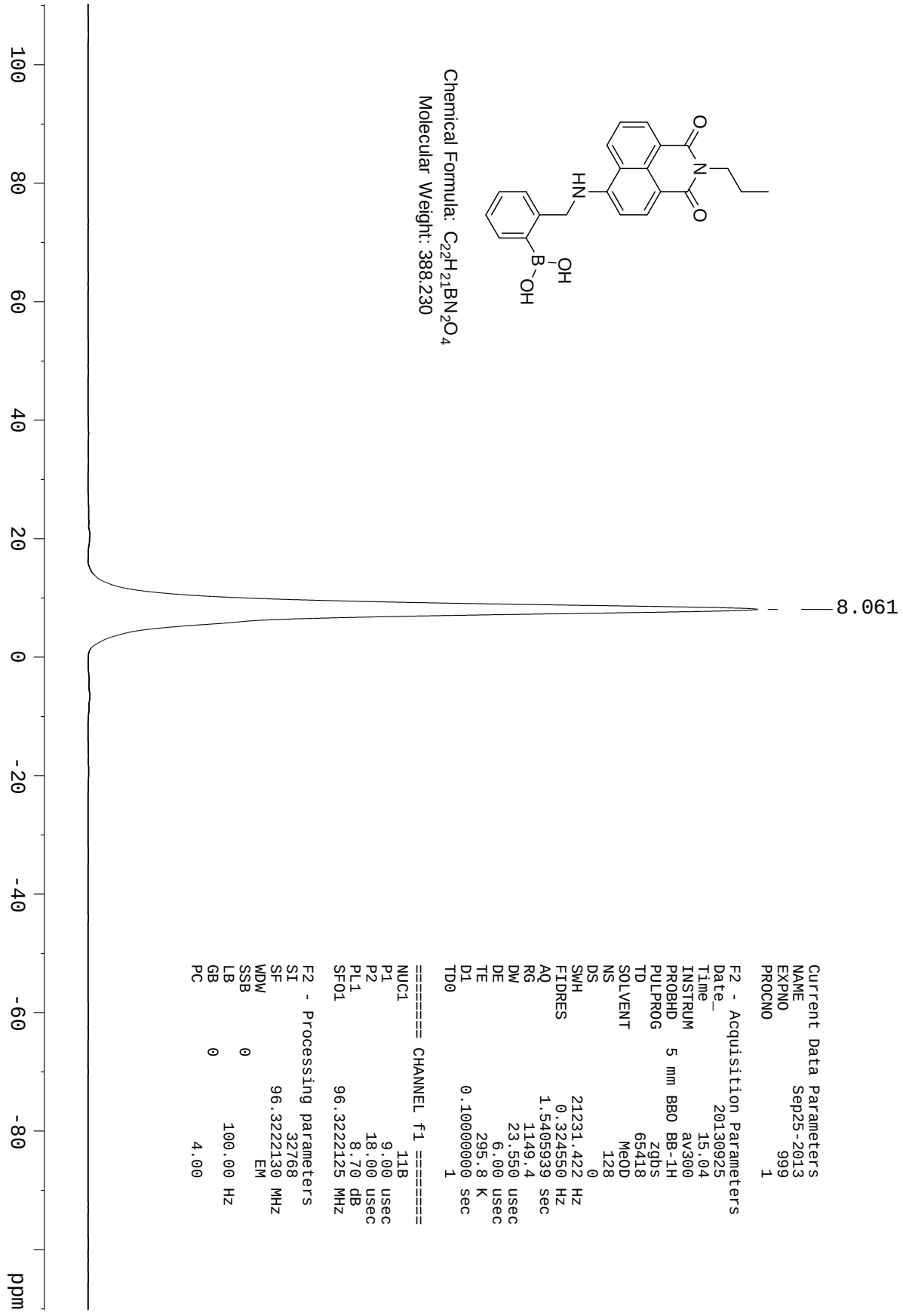

Figure 111. *^{11}B NMR for compound **102b** in MeOD*

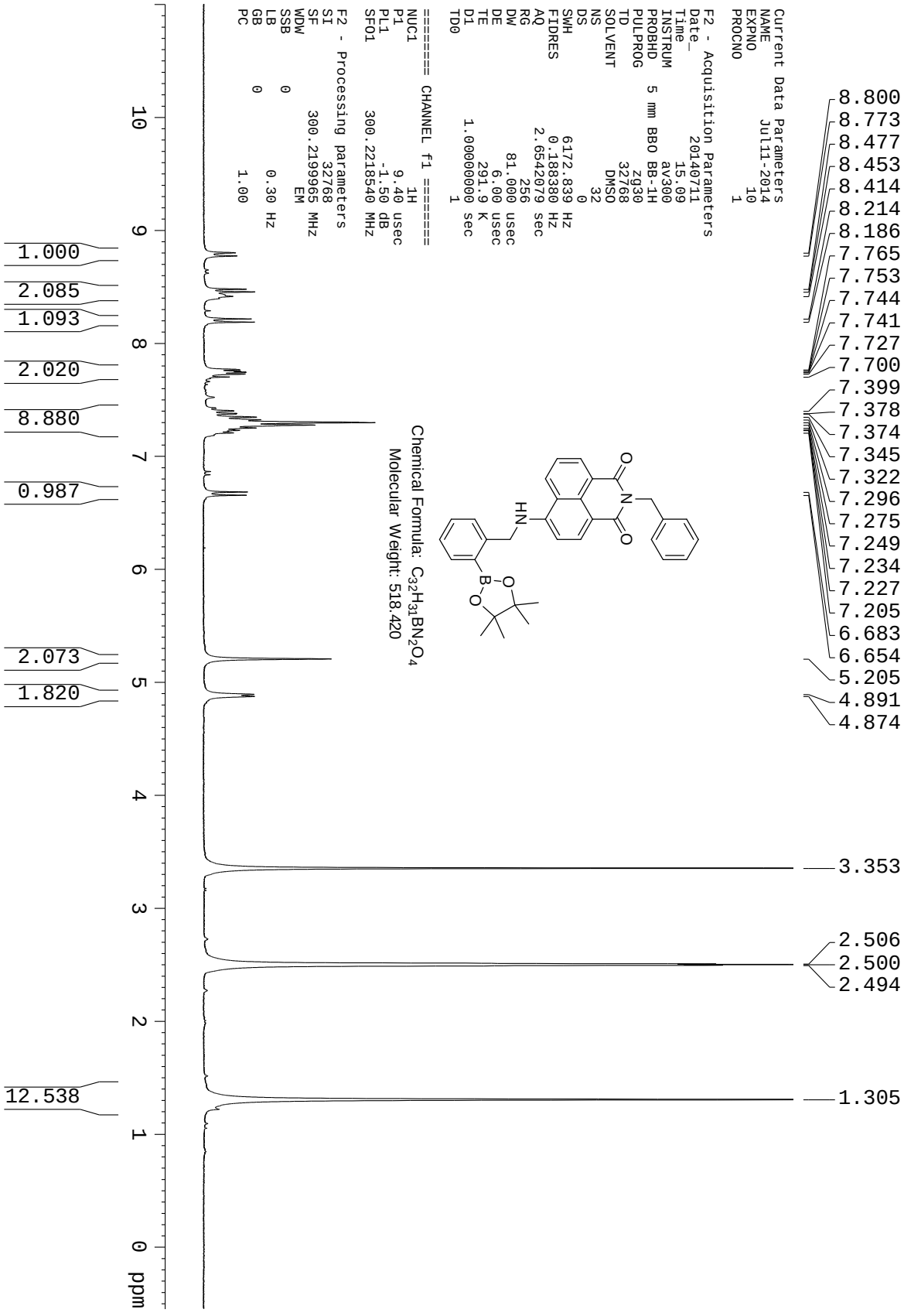

Figure 112. *[1]H NMR for compound **126** in DMSO.*

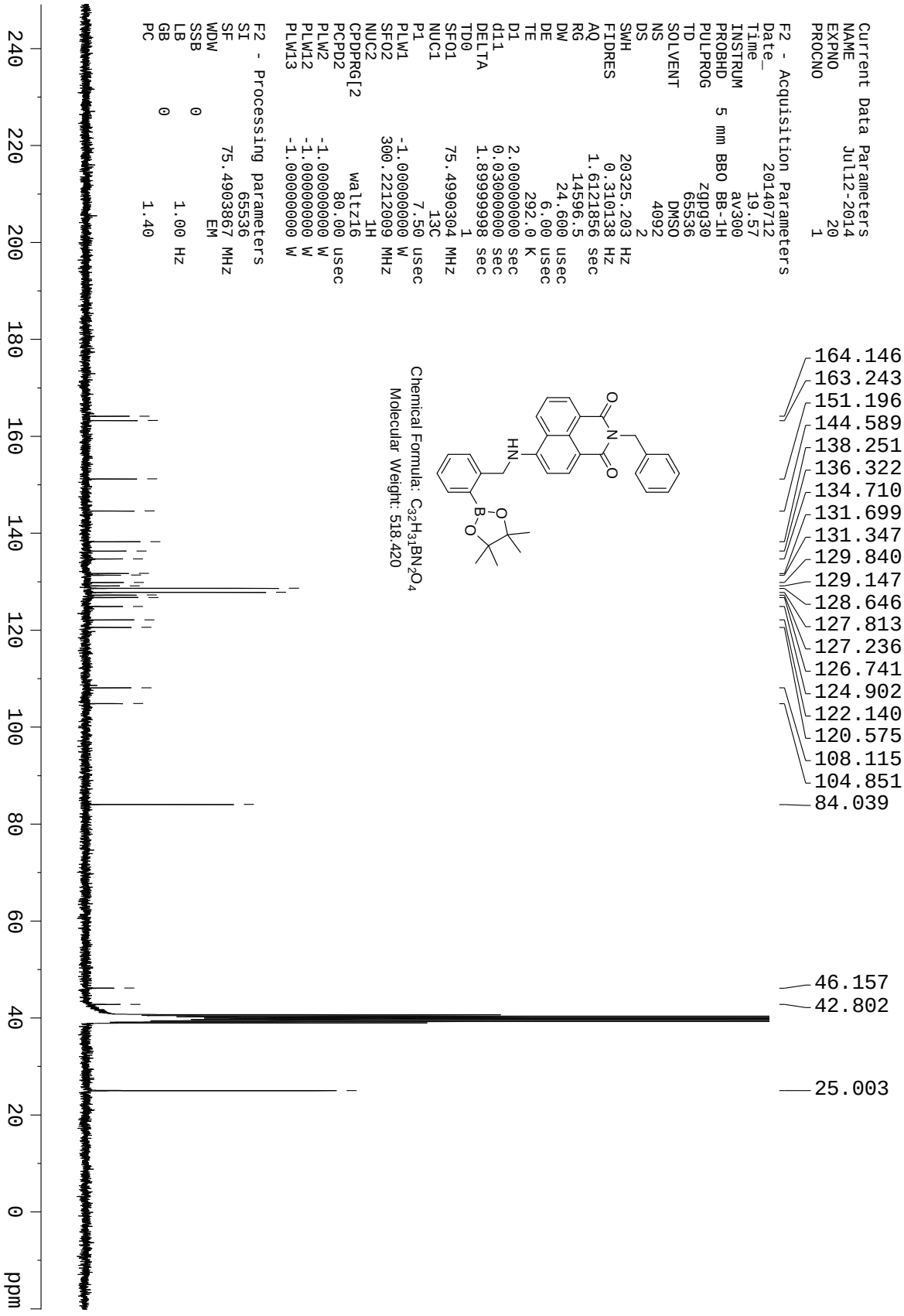

Figure 113. *^{13}C NMR for compound **126** in DMSO*

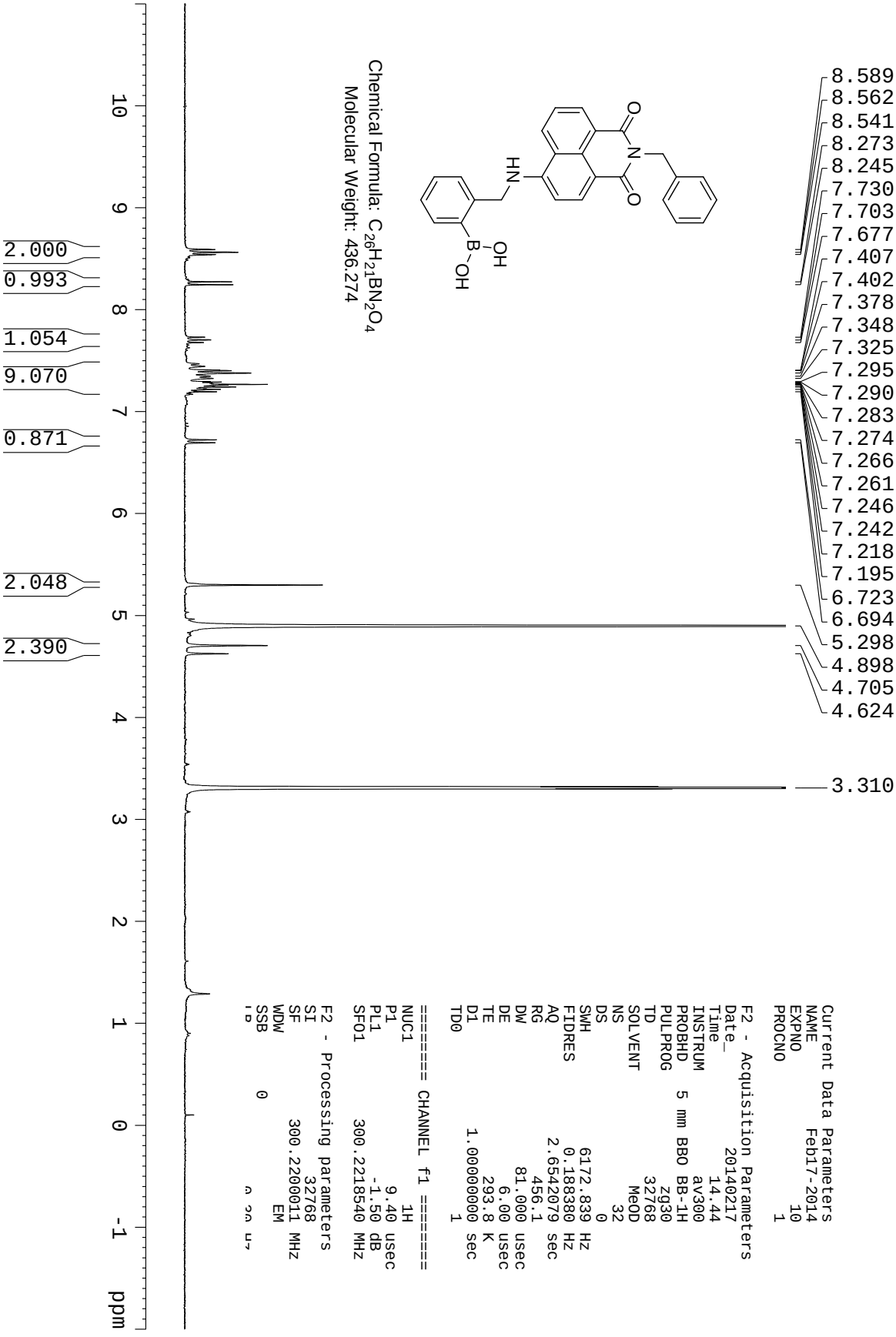

Figure 114. *[1]H NMR for compound **102a** in MeOD*

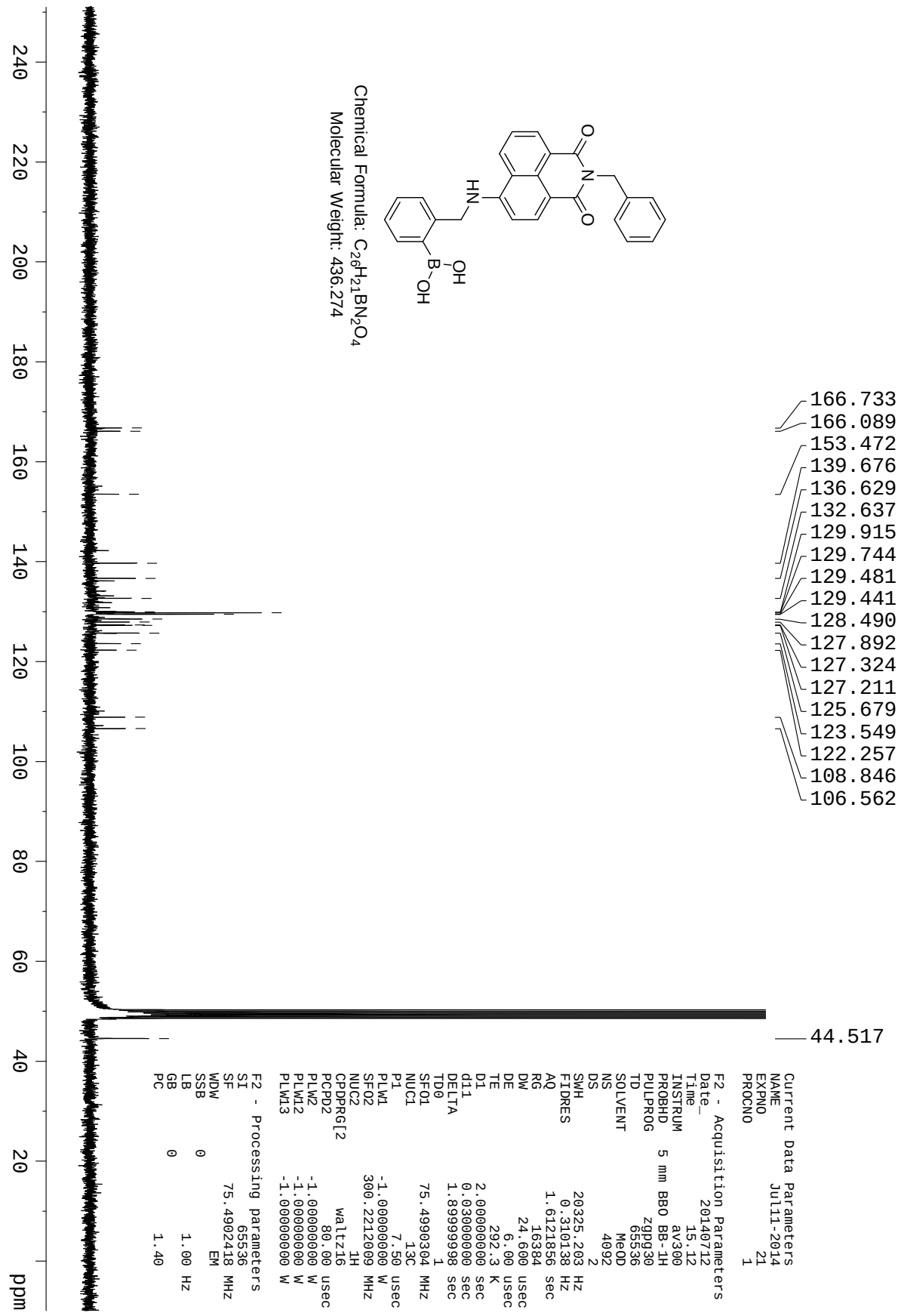

Figure 115. *^{13}C NMR for compound **102a** in MeOD*

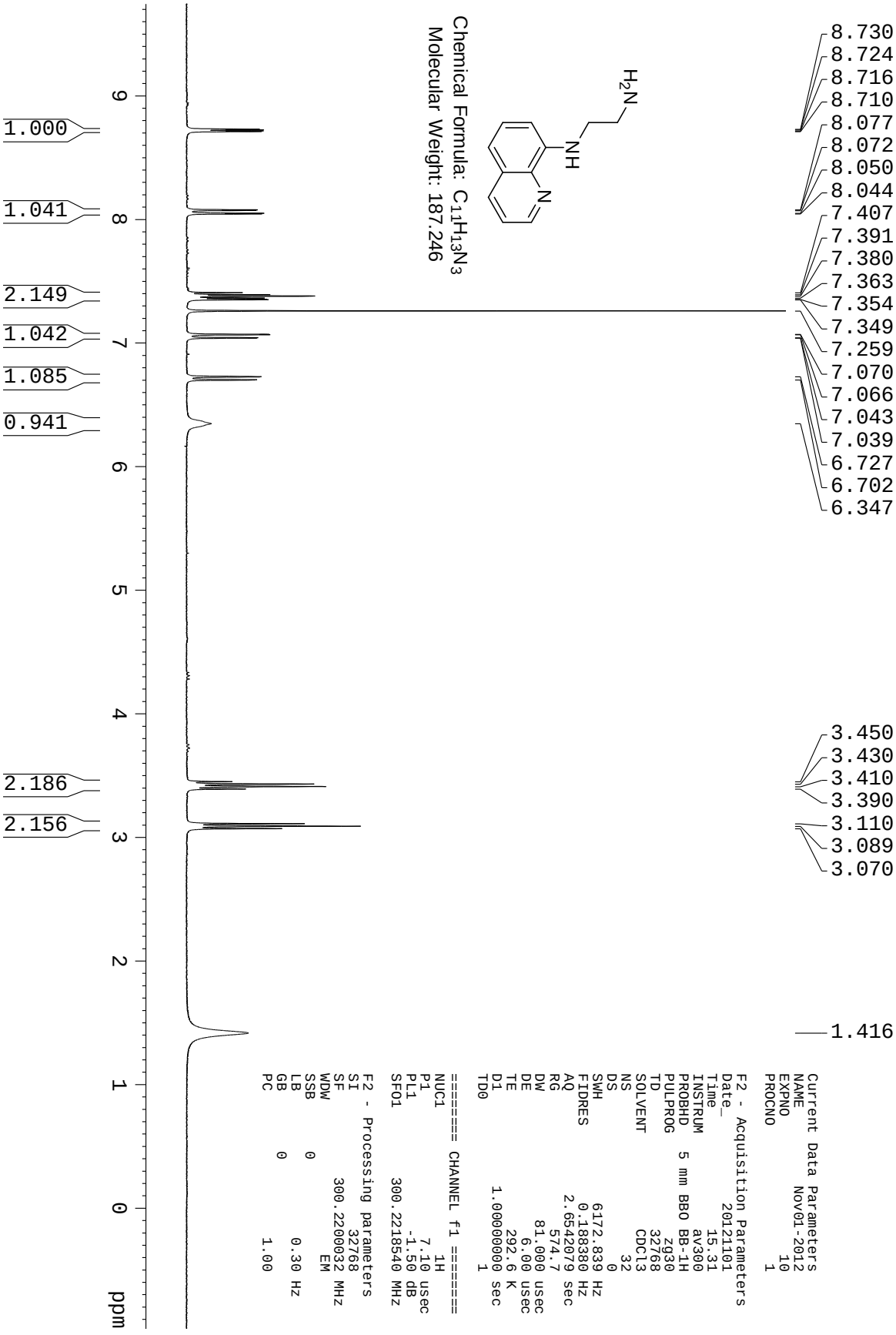

Figure 116. *^{1}H NMR for compound **129** in $CDCl_3$*

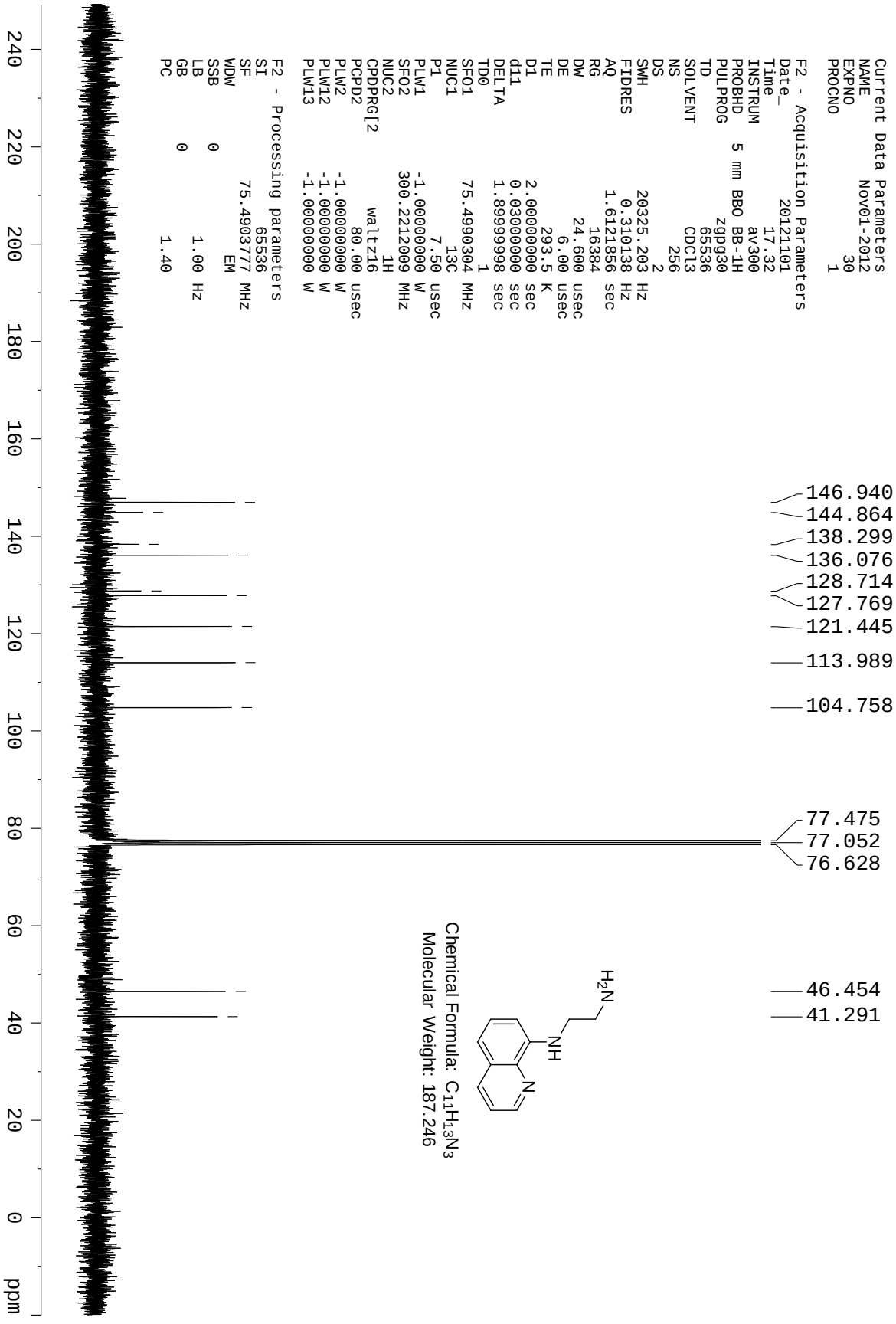

Figure 117. *^{13}C NMR for compound **129** in $CDCl_3$*

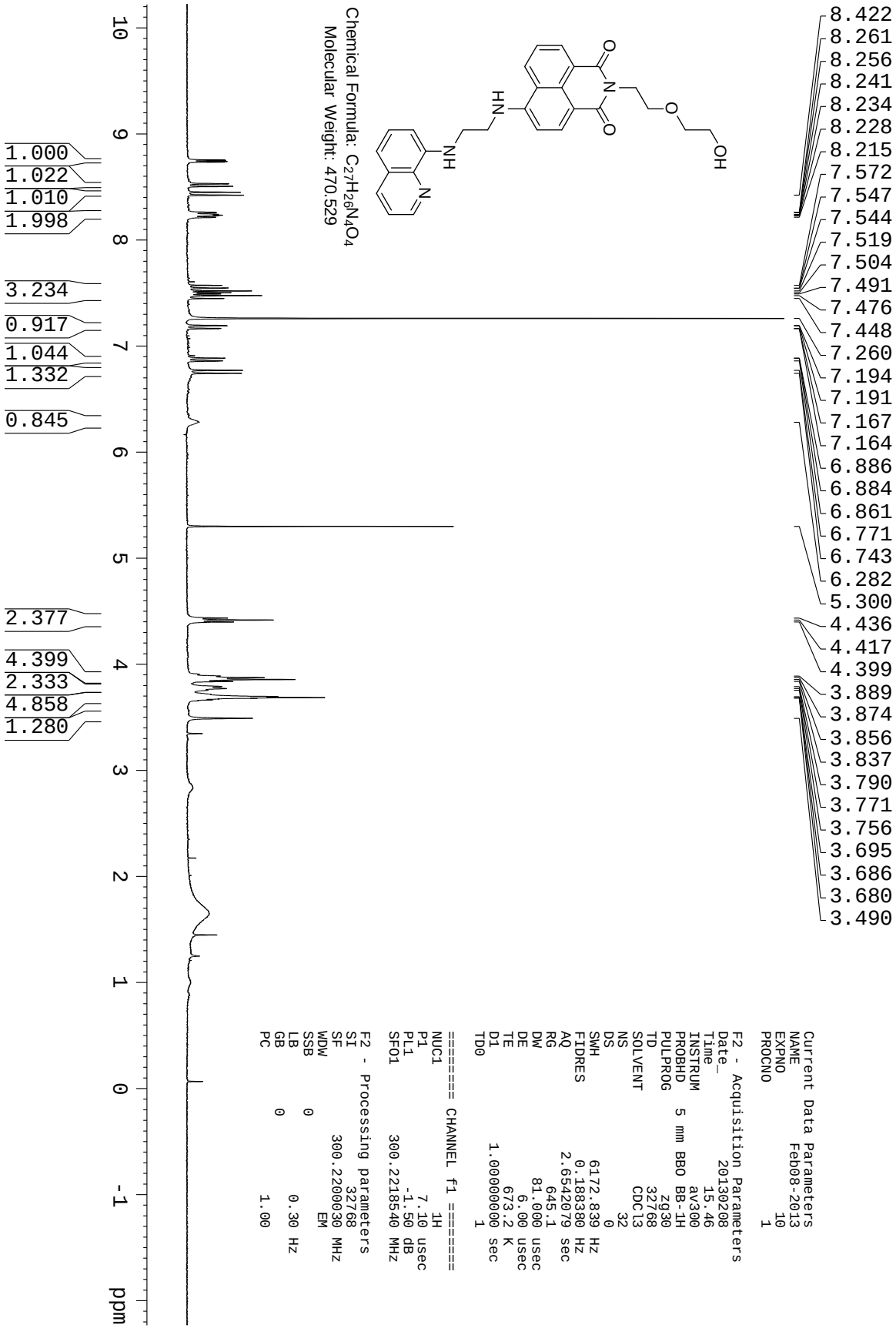

Figure 118. *^{1}H NMR for compound **109** in $CDCl_3$*

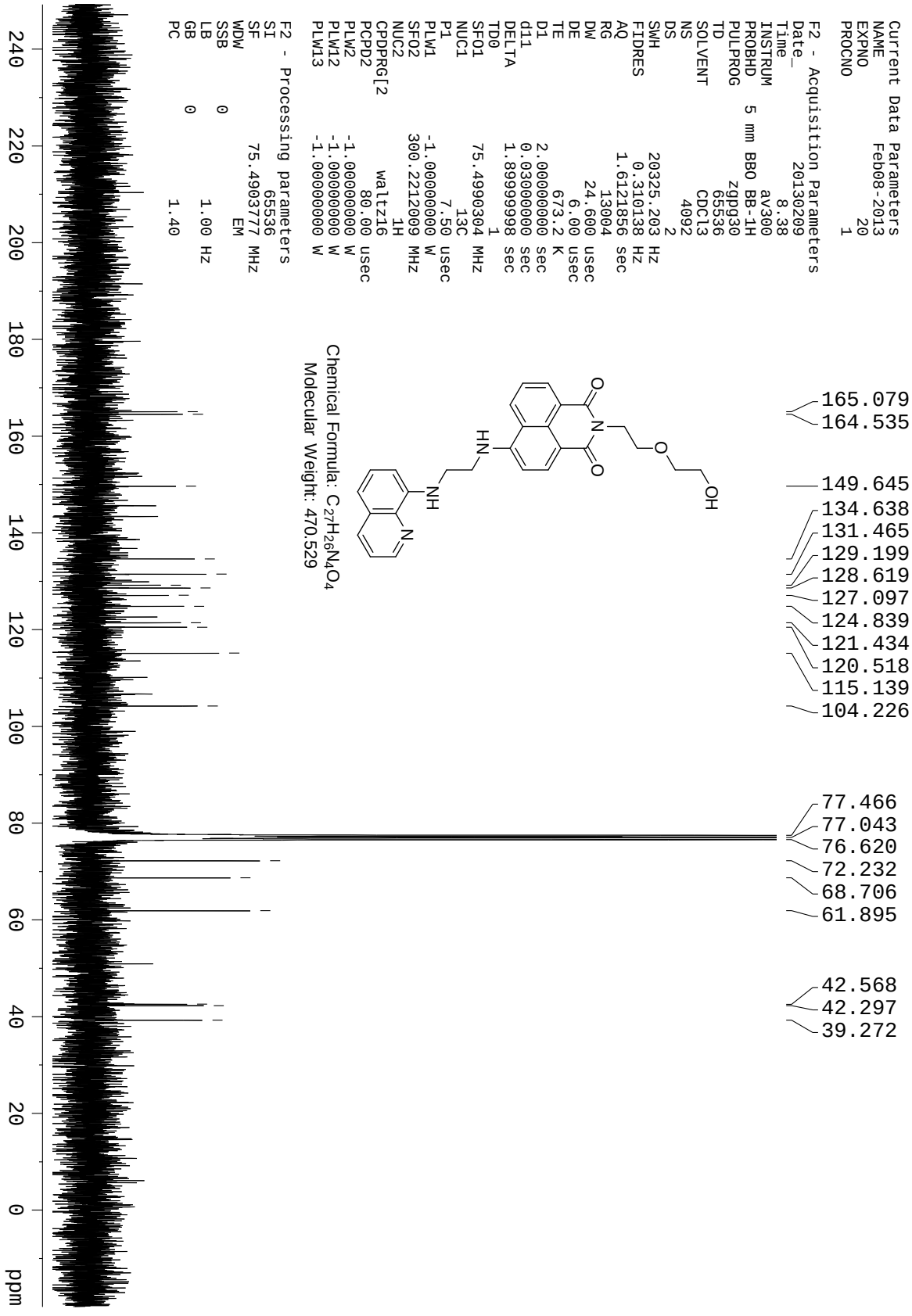

Figure 119. *^{13}C NMR for compound **109** in $CDCl_3$*

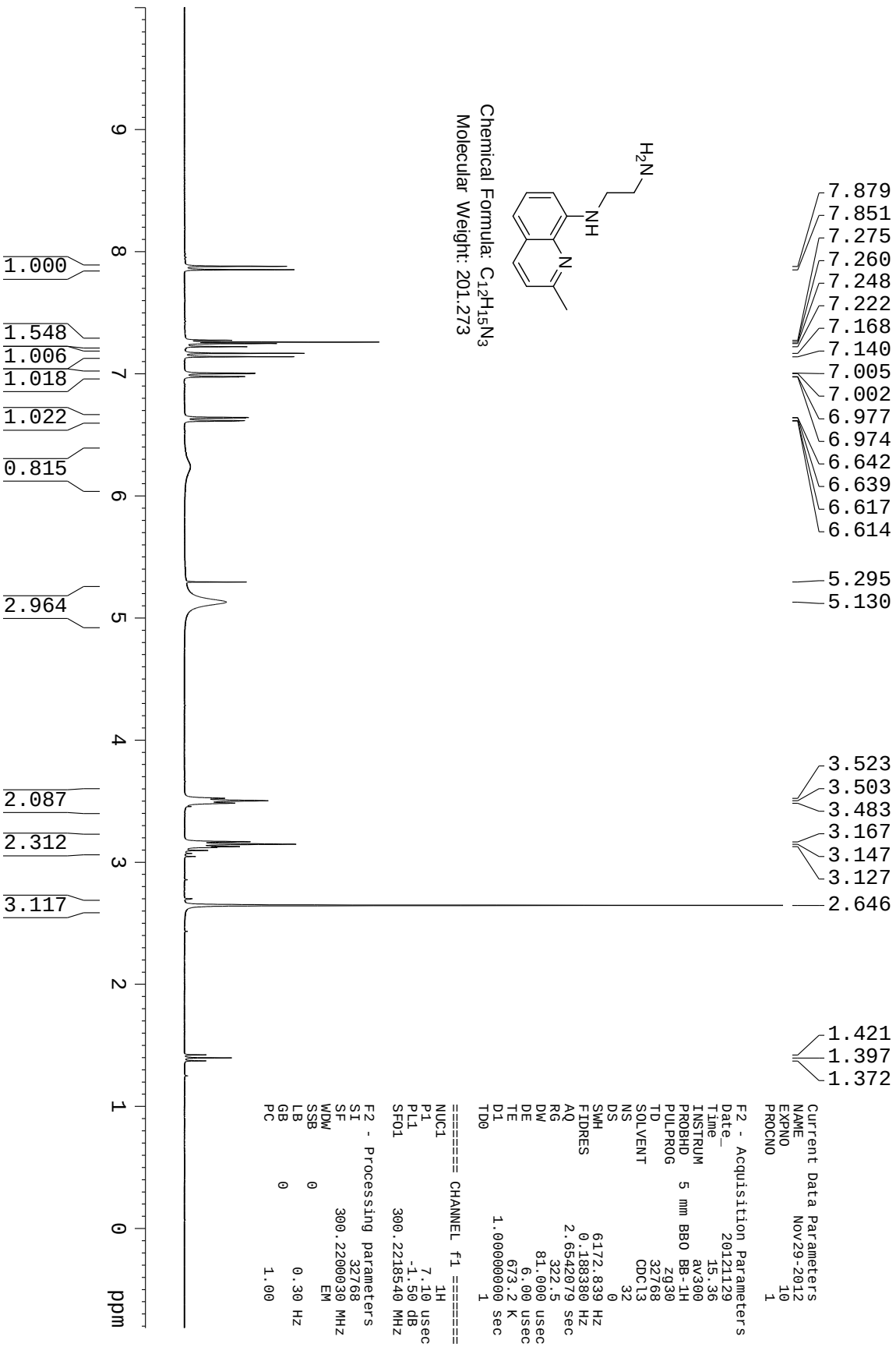

Figure 120. *^{1}H NMR for compound **130** in $CDCl_3$*

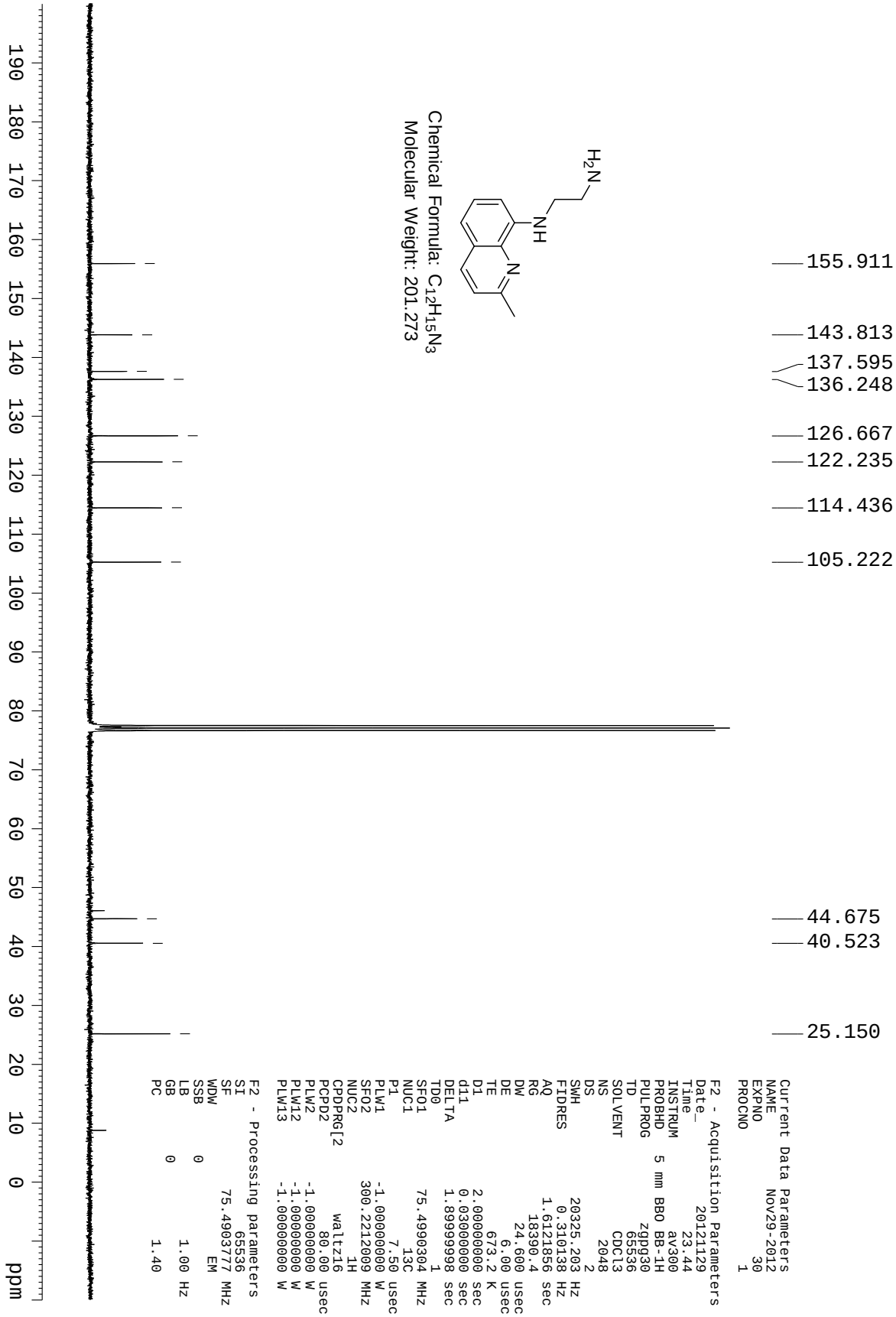

Figure 121. *^{13}C NMR for compound **130** in $CDCl_3$*

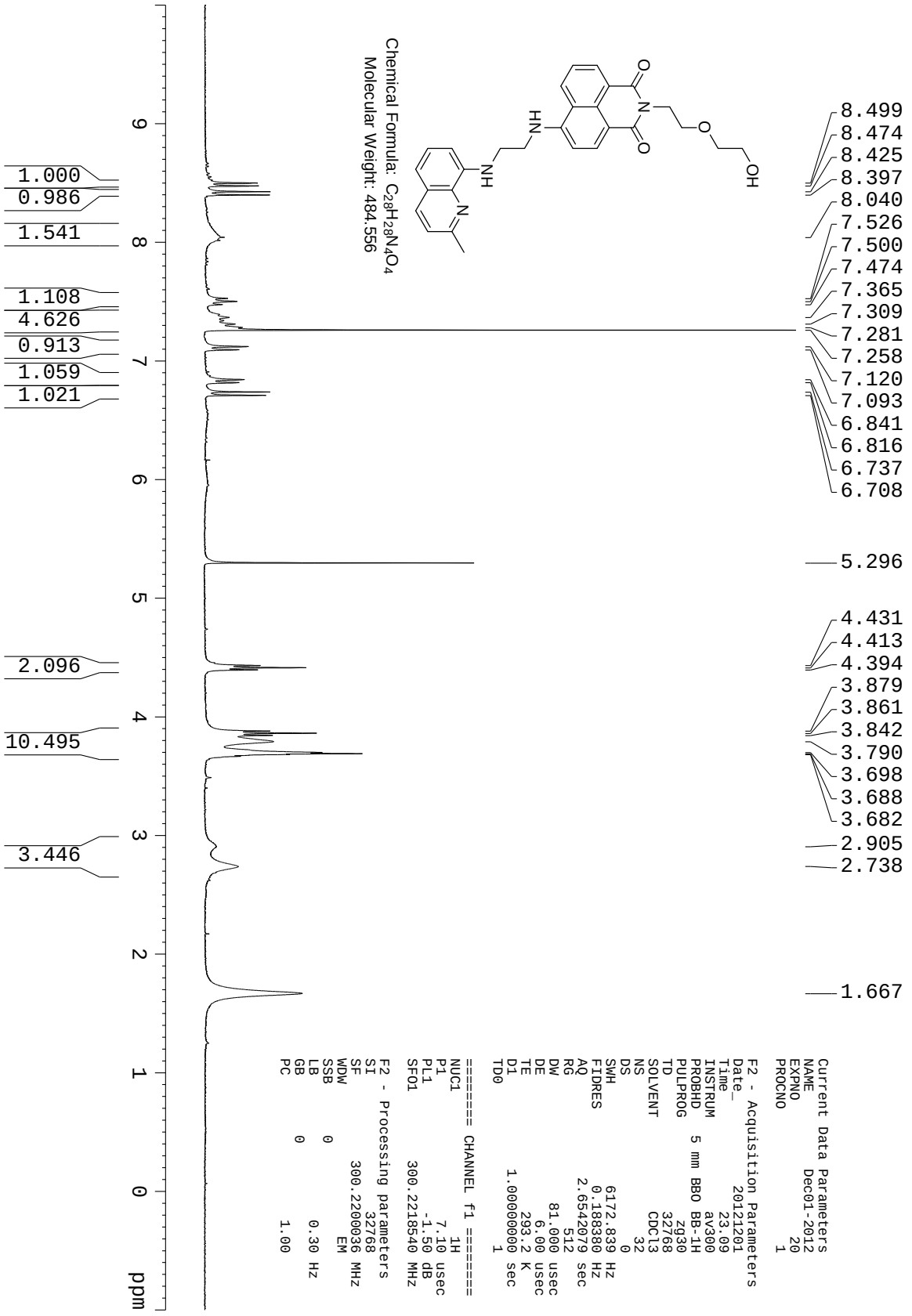

Figure 122. *^{1}H NMR for compound **110** in $CDCl_3$*

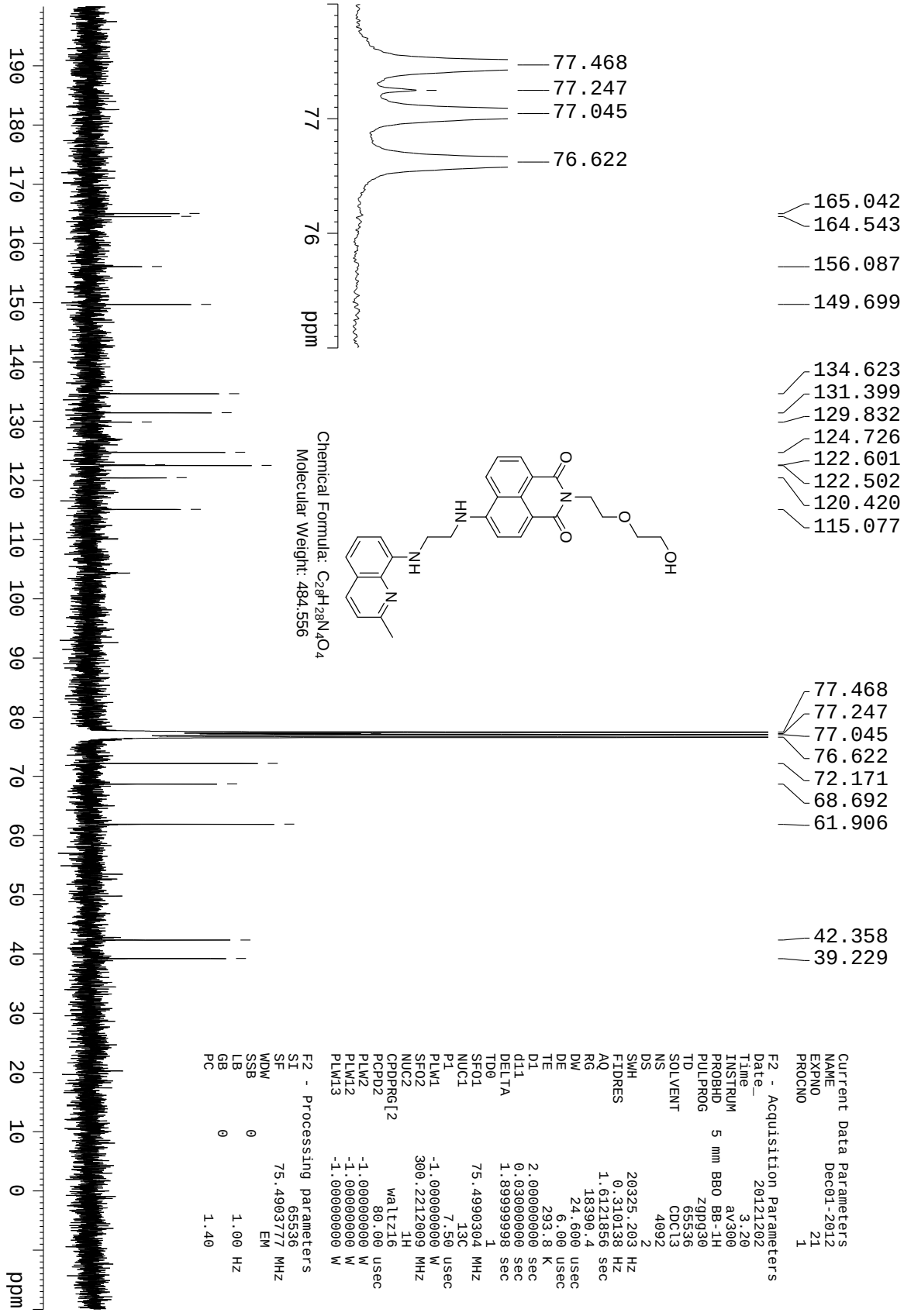

Figure 123. *^{1}H NMR for compound **110** in $CDCl_3$*

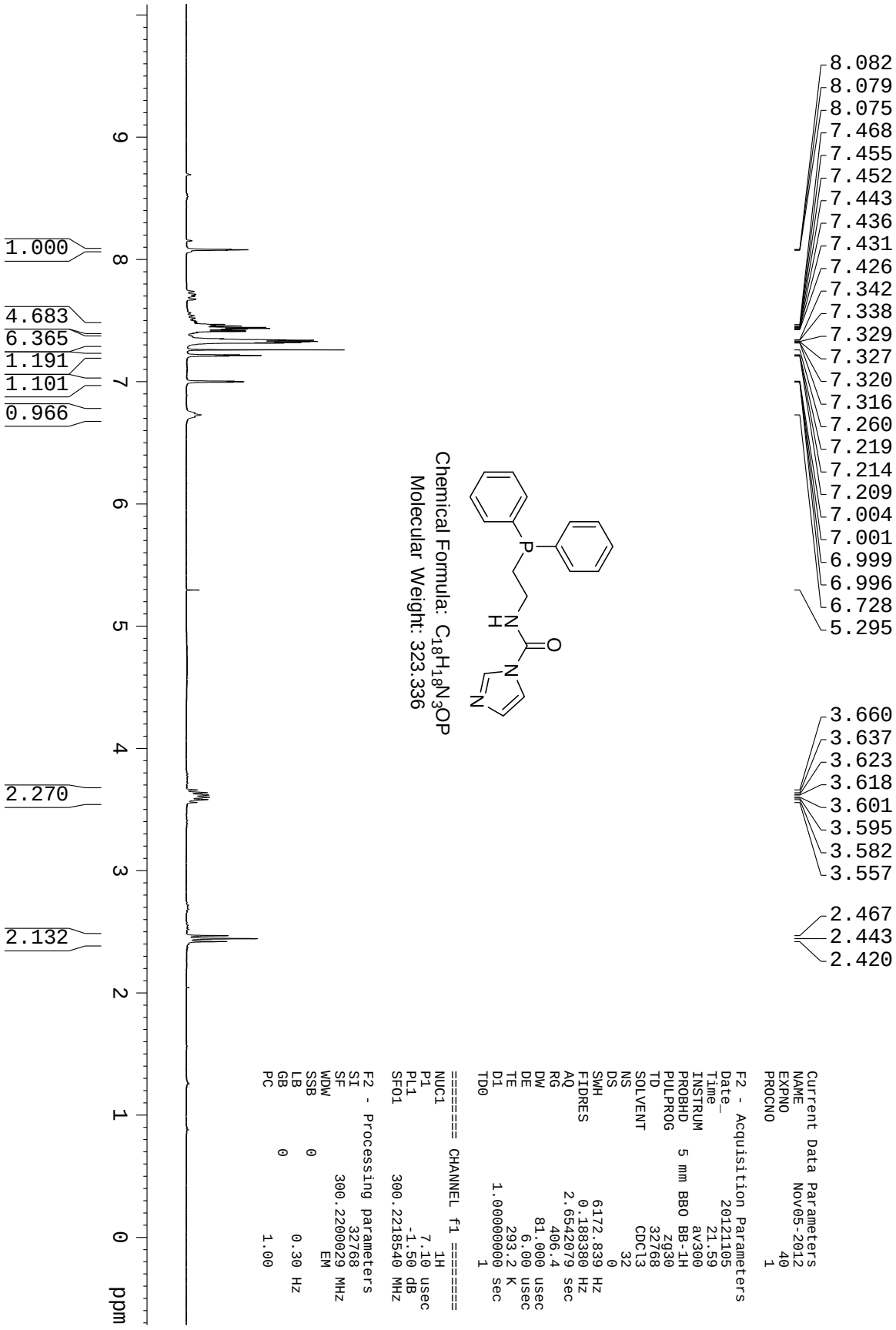

Figure 124. *^{1}H NMR for compound **117** in $CDCl_3$*

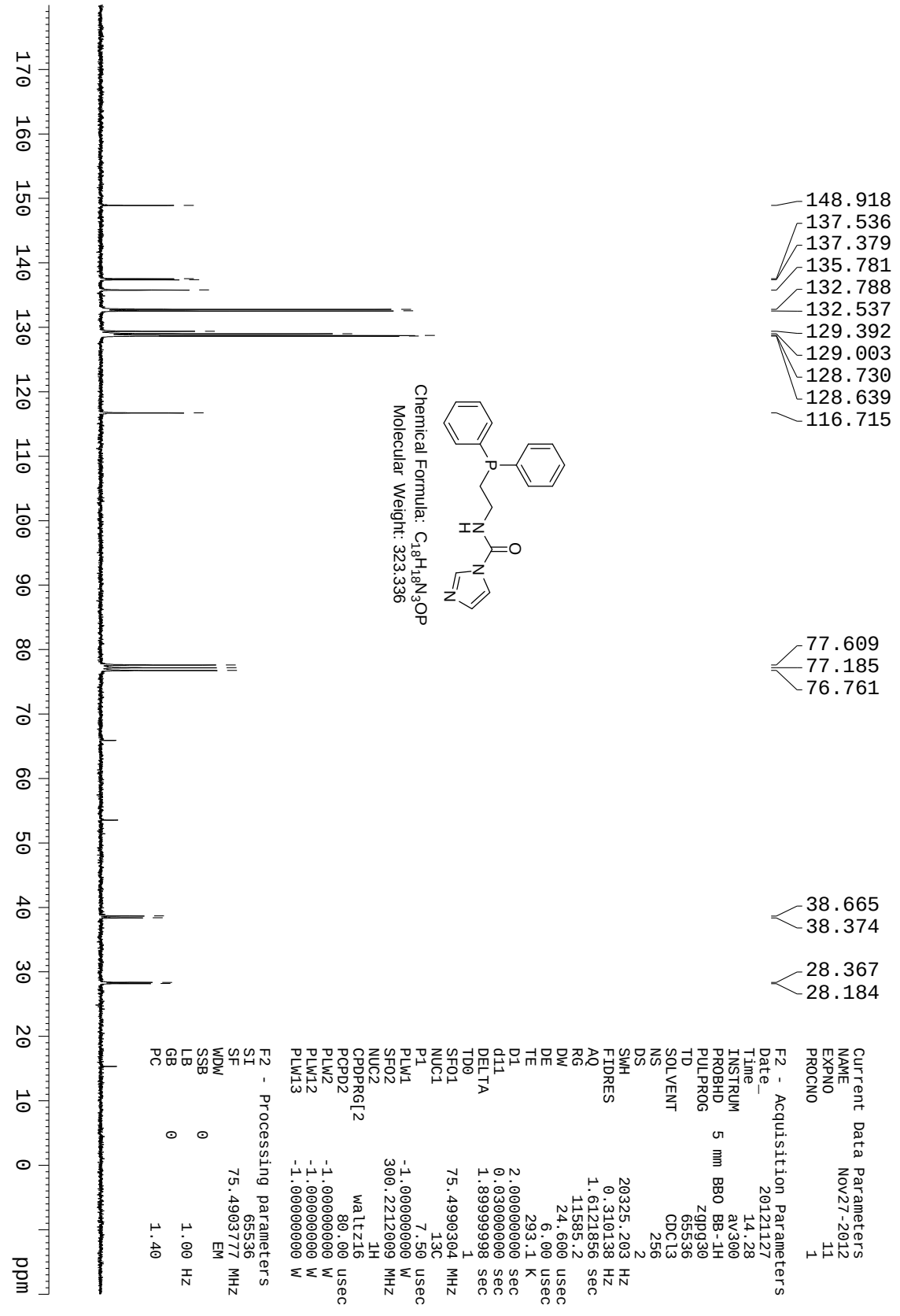

Figure 125. *^{13}C NMR for compound **117** in $CDCl_3$*

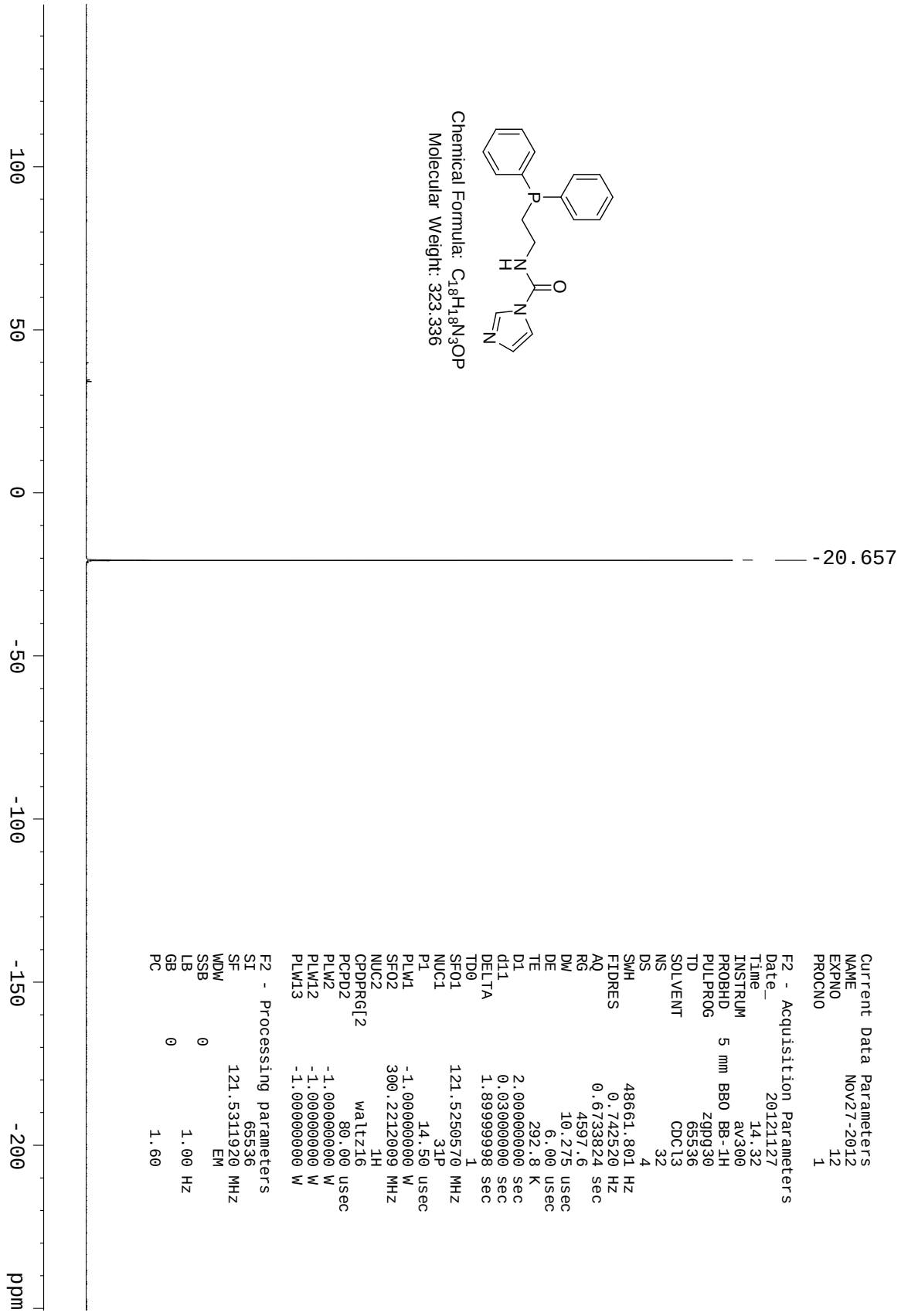

Figure 126. *^{15}P NMR for compound **117** in $CDCl_3$*

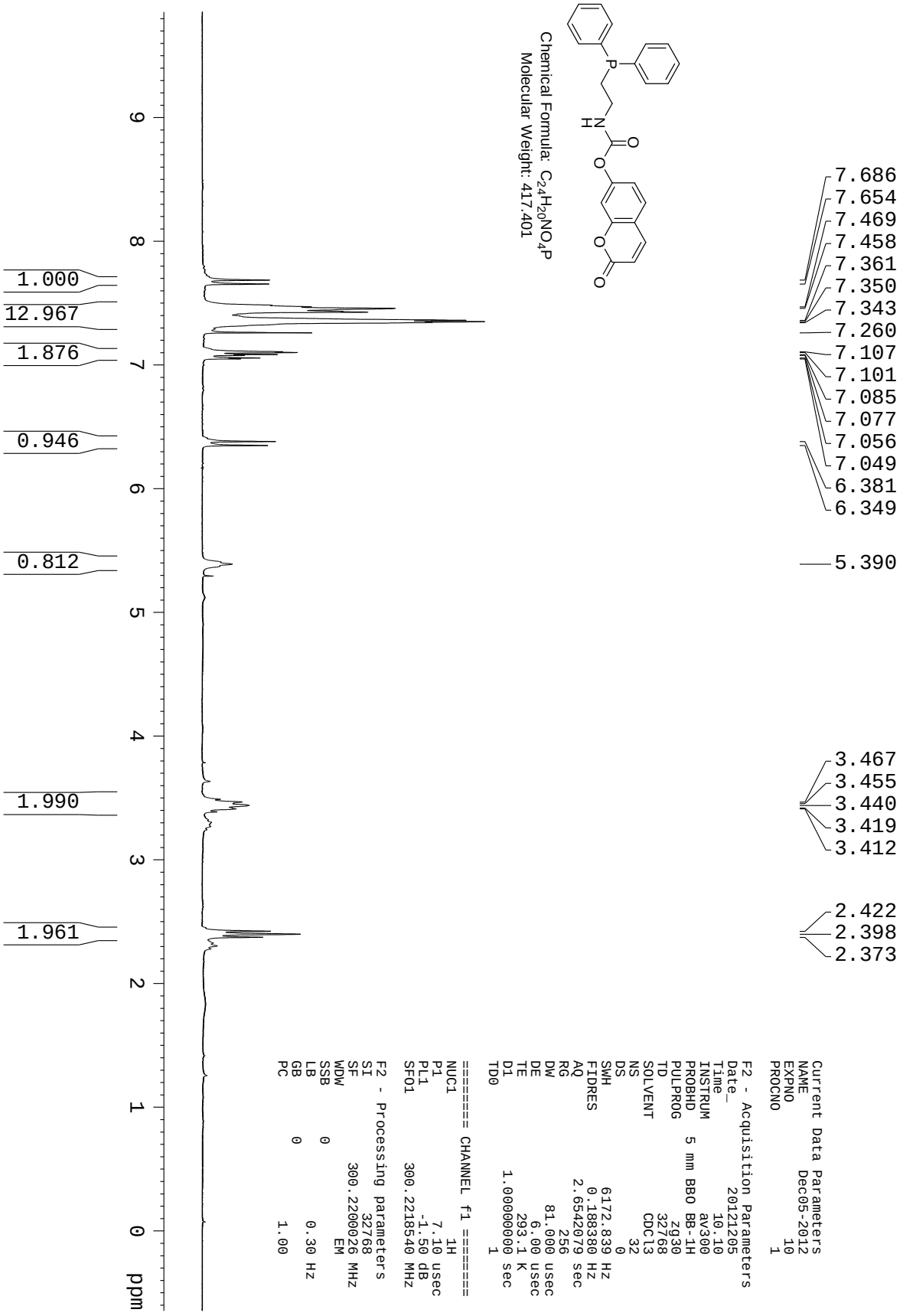

Figure 127. *^{1}H NMR for compound **116** in $CDCl_3$*

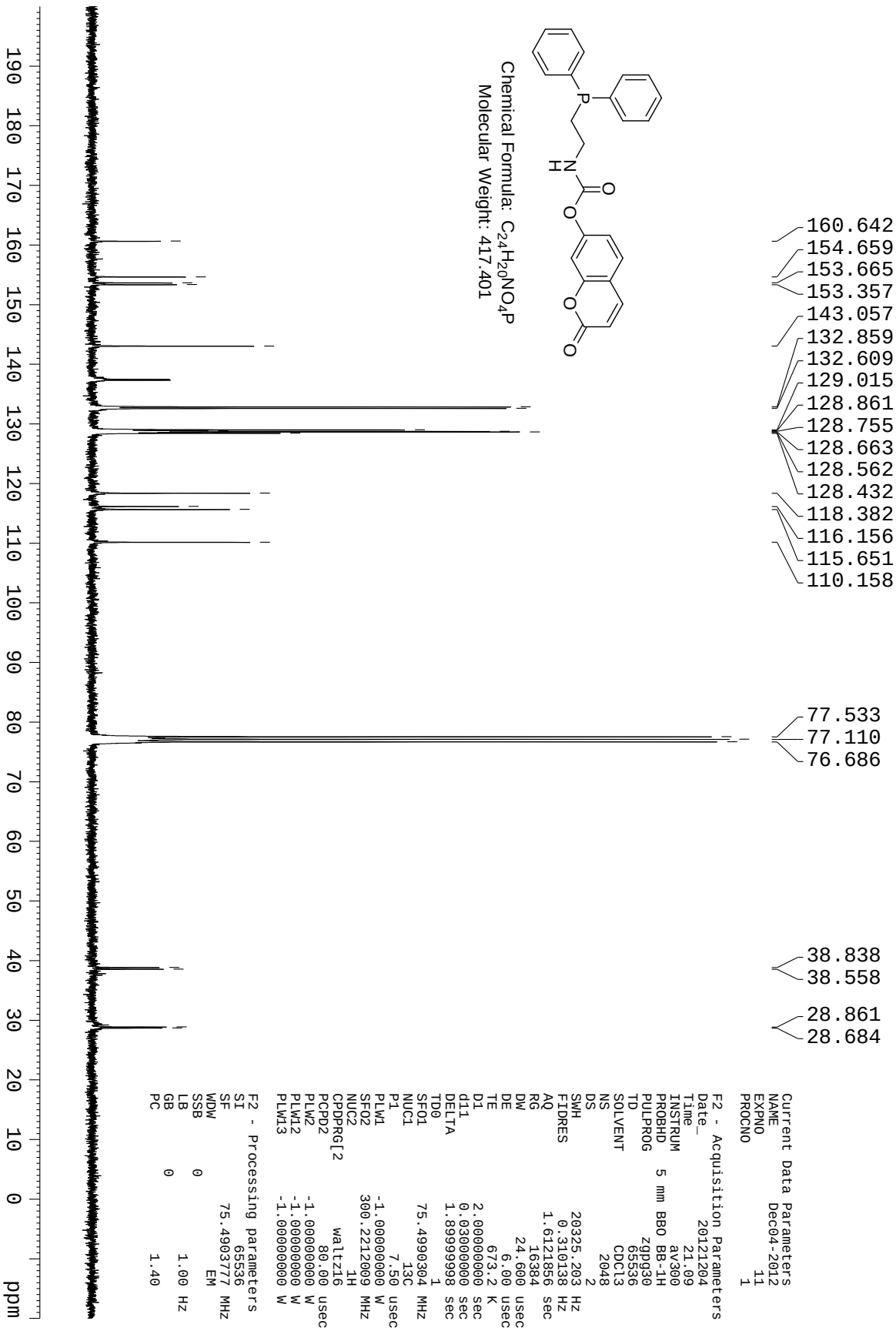

Figure 128. *^{13}C NMR for compound **116** in $CDCl_3$*

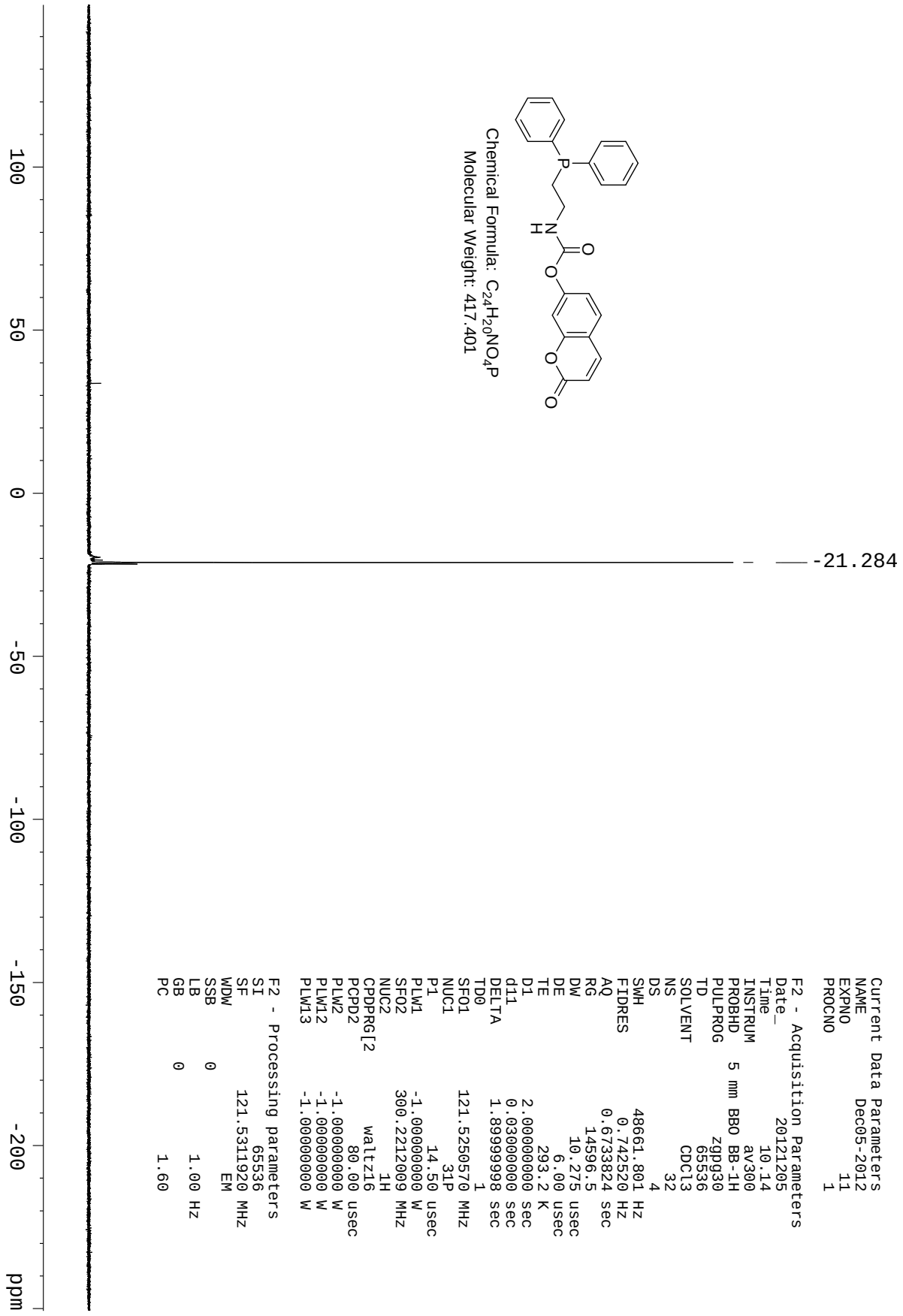

Figure 129. *^{15}P NMR for compound **116** in $CDCl_3$*